SODIUM METAL AEROSOL CHARACTERIZATION IN COVER GAS REGION

By
AMIT KUMAR
PHYS02201004019

Indira Gandhi Centre for Atomic Research, Kalpakkam

A thesis submitted to the
Board of Studies in Physical Sciences

In partial fulfillment of requirements
for the Degree of
DOCTOR OF PHILOSOPHY
of
HOMI BHABHA NATIONAL INSTITUTE

September, 2016

Homi Bhabha National Institute

Recommendations of the Viva Voce Committee

As members of the viva voce committee, we certify that we have read the dissertation prepared by Amit Kumar entitled "Sodium metal aerosol characterization in cover gas region" and recommend that it may be accepted as fulfilling the thesis requirement for the award of degree of Doctor of Philosophy.

Chairman - Dr. B. Venkatraman		Date: 9/2/17
Guide/Convener - Dr. R. Baskaran		Date: 9/2/17
Examiner - Dr. K. Krishnamoorthy		Date: 09/02/2017
Member 1- Dr. V. Jayaraman	V. Jayaraman	Date: 09/02/2017.
Member 2 - Dr. D. Ponraju	D. Pon	Date: 9/2/2017

Final approval and acceptance of this thesis is contingent upon the candidate's submission of the final copies of the thesis to HBNI.

I/We hereby certify that I/We have read this thesis prepared under my/our direction and recommended that it may be accepted as fulfilling the thesis requirement.

Date: 09/02/2017

Place: KALPAKKAM

Guide

STATEMENT BY AUTHOR

This dissertation has been submitted in partial fulfillment of requirements for an advanced degree at Homi Bhabha National Institute (HBNI) and is deposited in the Library to be made available to borrowers under rules of the HBNI.

Brief quotations from this dissertation are allowable without special permission, provided that accurate acknowledgement of source is made. Requests for permission for extended quotation from or reproduction of this manuscript in whole or in part may be granted by the Competent Authority of HBNI when in his or her judgment the proposed use of the material is in the interests of scholarship. In all other instances, however, permission must be obtained from the author.

Amit

Amit Kumar

DECLARATION

I, hereby declare that the investigation presented in the thesis has been carried out by me. The work is original and has not been submitted earlier as a whole or in part for a degree/diploma at this or any other Institution/University.

Amit

Amit Kumar

List of Publications arising from the thesis

Journal

1. "An experimental study on the charging of non-radioactive aerosols with and without the presence of gamma radiation", V. Subramanian, **Amit Kumar,** R. Baskaran, J. Misra and B. Venkatraman, Journal of Aerosol Science, **2012** Vol. 52, 98-108.

2. "Development and validation of methodology for characterization of sodium aerosols in cover gas region", **Amit Kumar**, Subramanian V., Baskaran R., Krishnakumar S., Chandramouli S. and Venkatraman B., Aerosol and Air Quality Research, **2014**, Vol. 14, 1534-1541.

3. "Characterization of Sodium Aerosol in Cover Gas Region of SILVERINA Loop", **Amit Kumar,** Subramanian V., Krishnakumar S., Baskaran R., Chandramouli S. and Venkatraman B., Aerosol and Air Quality Research, **2015**, Vol.15, 1813-1822.

4. "Size Evolution of sodium combustion aerosol with various RH%", **Amit Kumar,** Subramanian V., Baskaran R., and Venkatraman B., Aerosol and Air Quality Research, **2015**, Vol.15, 2270-2276.

5. "Studies on Geometrical effect on sodium aerosol characteristics in cover gas region", **Amit Kumar,** Subramanian V., Baskaran R., Krishnakumar S., Chandramouli S. and Venkatraman B., Aerosol and Air Quality Research, **2016**, Vol.16, 1832-1840.

Conferences

1. "Standardization of sodium aerosols characterisation techniqes", **Amit Kumar**, V. Subramanian, J. Misra, R. Baskaran, & B. Venkataraman, IASTA-**2012**, Vol. 20 No 1&2, 441-445 .

2. "Characterization of Sodium Aerosol (Metal Vapor) from cover gas region of Sodium Cooled Fast Reactor", Baskaran R., **Amit Kumar**, V. Subramanian, Krishnakumar S., Chandramouli S., Nashine B. K., Venkataraman B., and Rajan K.K, NSRP19 – **2012**, December 12-14, Radisson Blu Resort Temple Bay, Mamallapuram, Tamilnadu, India.

3. "Theoretical simulation of sodium aerosol mass concentration in the cover gas region", **Amit Kumar**, Subramanian V., Baskaran R., and Venkatraman B., IASTA-**2014,** Vol. 21, Issue 1&2, 147-151.

4. "Size Evolution of sodium combustion aerosol with various RH%", **Amit Kumar**, Subramanian V., Misra J., Baskaran R., and Venkatraman B., IAC-**2014**, Aug.31 – Sept. 5, 2014 Bexco, Busam, Korea.

5. "Effect of Gamma radiation on Sodium Aerosol Characteristics in cover gas region", **Amit Kumar**, Subramanian V., Krishnakumar S., Baskaran R., Chandramouli S. and Venkatraman B., International Conference on Radiological safety in workplace, Nuclear facilities and Environment (IARPIC-2016), Feb. 22-25, 2016, at Anupuram, Tamilnadu, India.

Amit

Amit Kumar

DEDICATED TO MY BELOVED PARENTS, BROTHER AND SISTER

ACKNOWLEDGEMENTS

I am immensely grateful to my Research Supervisor Dr. R. Baskaran, Head, Radiological Safety Division, for his teaching, invaluable guidance, encouragement and oriented me in right direction in completing this thesis. I thank Dr. V Subramanian, for helping me to solve the problems presented in this thesis. I thank him for his constant guidance, valuable advice, patience and active support.

I am thankful to my Doctoral Committee members Dr. B. Venkatraman, Dr. P. Mohankrishanan, Dr. R.S. Kesavamurthy, Dr. V. Ganesan, Dr. V Jayraman and Dr. D. Ponraju for their useful suggestions and interest in my research work.

I owe my sincere thanks to Dr. B. Vekatraman, Director, Health, Safety and Environment Group, for his keen interest in my work and his support.

I am grateful to Mr. S. Chandramouli and Mr. S. Krishanakumar rendering their help in conducting experiments and providing experimental facility of FRTG to conduct the experiments.

I acknowledge my scientific colleagues for carrying out conductometric titration measurements.

I place on record my thanks to my friends and well wishers for their support to make this day happen.

Finally I express my warm gratitude to my Father Mr. Ram Kishor and Mother Ms. Saraswati for showering their unbound love, care and affection throughout my life. I also owe my sincere thanks to my brother Shree Lalit Kumar and my sister Km. Soni Devi for their emotional support and take care of all responsibility of my family, which helped me to fulfill the task of completing thesis successfully.

CONTENTS

CHAPTER - I

INTRODUCTION

CHAPTER - II

EXPERIMENTAL FACILITIES AND AEROSOL DIAGNOSTIC EQUIPMENTS

CHAPTER - III

DEVELOPMENT AND VALIDATION OF SODIUM METAL AEROSOLS CHARACTERIZATION TECHNIQUE

CHAPTER - IV

DEVELOPMENT OF THEORETICAL MODEL AND VALIDATION

CHAPTER - V

SODIUM METAL AEROSOL CHARACTERISTICS IN COVER GAS REGION

CHAPTER - VI

GEOMETRICAL EFFECT ON SODIUM METAL AEROSOL CHARACTERISTICS IN COVER GAS REGION

CHAPTER VII

EFFECT OF GAMMA RADIATION ON AEROSOL CHARACTERISTICS

CHAPTER - VIII

CONCLUSION

APPENDICES

SYNOPSIS

1.0 Introduction

The Indian FBR program started with 40 MWt/13.2MWe Fast Breeder Test Reactor (FBTR) commissioned in 1985 at Kalpakkam [1]. FBTR is based on unique mixed Plutonium-Uranium Carbide fuel, which is first of its kind in the world. As a logical follow-up of FBTR a Prototype Fast Breeder Reactor (PFBR) is being constructed and after it's commissioning, a series of four more FBRs are proposed. The construction and commissioning of 500MWe Prototype Fast Breeder Reactor (PFBR) is in the final stage. In the fast reactors, the fast neutrons are utilized to sustain the chain reaction and also used to breed the Thorium. The core of the reactor is compact which results in a very high power density. For efficient removal of heat from the core, liquid sodium is used as coolant and the reactor is referred as Sodium cooled Fast Reactor (SFR). The thermal efficiency of SFR is more than the LWR and SFR is capable of producing more fuel than they consume. The SFR efficiently fission the long-lived radio-nuclides and thereby decreases the high level nuclear wastes. The SFR reactor is ideally suited for operation under a closed fuel cycle option. There are two basic designs for SFR namely: (i) Loop type SFR and (ii) Pool type SFR. The loop type SFR is similar to a conventional light water reactor in which individual component of the cooling system is outside the reactor vessel and interconnected by piping, while the reactor vessel contains only the core and associated equipment. Fast Breeder Test Reactor (FBTR) is a loop type SFR. In the pool type SFR, the reactor vessel contains not only the core, but also a number of other components such as, primary sodium pump, intermediate heat exchangers, decay heat exchanger etc. The Prototype Fast Breeder Reactor (PFBR) is a pool type SFR. The advantage of pool type SFR are, high thermal inertia of the primary system, sodium inventory kept inside the safety vessel, hydraulic cooling always maintained, favorable to natural convection, and favorable to radioprotection. The main advantages of using liquid sodium in fast reactors as coolant are: (i) compatibility with stainless steels, (ii) superior thermo-physical and thermo-hydraulic properties, (iii) excellent thermal and radiation stability, (iv) low fast neutron absorption and scattering cross section, (v) high thermal and electrical conductivity and (vi) low viscosity and high thermal capacity. However, sodium has a disadvantage due to its reaction with air/water, oxygen and halogens and component access under sodium. One of the major concerns of SFR safety is sodium aerosols produced due to various scenarios. The detailed scenario on the formation and consequences of sodium aerosols during accidental conditions as well as in the normal operation of the fast reactors, are described as follows:

- In the extremely unlikely event of Core Disruptive Accident (CDA), melting and vaporization of core inventory may produce one or several bubbles that expand into sodium pool and then to cover gas, imparting kinetic energy to the reactor vessel head. These bubbles carry radioactive materials mostly in the form of vapors, and leaks through the vessel head into the containment. These vapors condense to form aerosols. In addition to this, sodium leak in the Reactor Containment Building (RCB) leads to sodium burning, which produces dense sodium compound aerosols. Thus RCB is bottled-up with large amount of sodium, fuel and fission product aerosols [2]. Besides, there exists a possibility of release of these aerosols from the stack, duct and pores of the containment building to the environment due to pressure build up in the containment. The released aerosols will be carried away by the wind and the fallouts of particulates of the aerosols are expected in the surrounding area depending on the atmospheric conditions. Also, these aerosols deposit on the floor, walls and ceiling of the RCB.
- In the secondary loop, sodium leak can occur due to cracks developed in fluid carrying pipes and eventually, sodium may get in contact with atmosphere. The hot sodium burns

in air and give rise to large amount of aerosols in the Steam Generator Building (SGB). Sodium fires can be classified as pool, spray and Column fire [3]. The sodium aerosols pose serious problems such as chemical toxicity, corrosion of building materials and equipments due to the presence of peroxide and hydroxide. The sodium hydroxide aerosols have stringent inhalation health limit for human [Threshold Limit value (TLV) of 2 mg/ m^3].

- In SFR, the fuel is immersed in a sodium pool and the pool surface is covered with inert atmosphere using argon gas. The reactor vessel is closed by using a top shield above the argon gas region. The sandwiched region between the surface of hot sodium pool and the top shield (called as roof slab) of the reactor vessel is called as cover gas region [4]. Evaporation of sodium from the hot pool surface results in the formation of liquid metal aerosols in the cover gas region.

In the pool type SFR, the roof slab is designed to support rotatable plugs, control plug, in-vessel fuel handling machine, primary sodium pumps, IHX and decay heat removal system etc. There are two types of concepts adopted in the design of roof slab: viz. (i) Cold Roof Concept, and (ii) Warm Roof Concept. The ‘Cold Roof Concept' means, there is no heating element to the roof slab of the reactor. The top shield gets warmed only by natural convection and radiative heating by the sodium pool surface. FBTR is a cold roof concept type SFR. In cold roof concept design, the rotating motion of the top plug is restricted after the prolonged operation of the reactor, due to deposition of sodium metal aerosol and consequent oxidation in the top shield and annular gaps of rotating plugs. To avoid this 'Warm Roof Concept' is adapted. Here, top shield is heated with heating elements and it is maintained about more than 120^{o}C. Due to the temperature of top shield, the sodium metal aerosols melt and fall back in sodium pool. The warm roof concept is adopted in PFBR. In the normal operation of fast reactor, the difference in argon temperature between hot argon gas directly above the pool surface and cooler gas below the roof slab causes a natural convection between pool surface and roof slab. The sodium pool temperature is maintained at 550^{o}C and roof temperature is much lower around 120 -150^{o}C. The sodium vapors continuously evaporate from the sodium pool surface into the cover gas region. The vapor gets cooled in the cover gas region and at a particular point it becomes supersaturated which then begins to condense to become sodium metal aerosol [5]. The aerosol particles formed by this process are suspended by natural convection current until they get deposited on to the cooler surfaces within the cover gas space. Also suspended aerosols begin to grow, due to coagulation and when the size becomes sufficiently large they can no longer be suspended in the convection current. At this stage the aerosols get deposited on to the sodium pool by gravitational settling [6]. The sodium metal aerosols in the cover gas region absorb, emit, scatter and transmit the thermal radiation within the cover gas region. The thermal radiations are also absorbed, re-emitted and scattered by the side wall and roof top plug of the reactor vessel. So the net heat transfer to the roof and walls is very complex. Further sodium metal aerosol deposition on the roof surface and side wall affect the emissivity of roof surface and side wall, hence it has an influence of the net heat transfer. The presence of sodium metal aerosols may also affect the dynamics of the convective motion of the cover gas. The mass transfer occurs due to condensation of sodium aerosols on the bottom of roof plug and side walls resulting deposition of aerosols in the annular gaps of the roof plug by different mechanism, such as thermophoresis, diffusiophoresis and turbulent impaction, which hinders the rotational movement of rotating plug, fuel handling machine and control rods. Thus in order to predict the effect of thermal radiation passing through the aerosols and mass transfer due to condensation of aerosols, it is necessary to know the aerosol mass concentration and size distribution. Further, it is to be noted that in the reactor environment, gamma radiation presents in the cover gas region. It is well known that the gamma radiation field produces distribution of bi-polar ions in the environment. The aerosols suspended in the charged atmosphere, pick up ions at random and acquire distribution of charges and it is governed by Boltzmann distribution [7, 8]. The Brownian coagulation rate coefficients of sodium aerosol with and without the presence of gamma radiation field is nearly one order more in the presence of gamma field than without gamma field [9]. The sodium aerosol properties would get modified due to the possible enhanced coagulation of sodium aerosols upon interaction with gamma radiation.

2.0 Scope and objective of the study

In the context of safety studies of SFR, the physical and chemical characteristics of sodium aerosols are very important. In many countries, considerable efforts have been made towards a realistic assessment of the magnitude and nature of aerosols formation in the cover gas region and removal of aerosols. It is found in literature that the sodium aerosol size (d_{50}) and mass concentration are in the range of 2-26 µm and 1-50 g/m^3 respectively. The characteristics of sodium metal aerosols found to vary due to (i) change in sodium pool temperature, (ii) change in roof temperature, and (iii) temperature difference between the sodium pool and roof. The variation of sodium aerosol mass concentration in cover gas region has a definite pattern with the variation of roof and pool temperatures in all these studies. But in the case of sodium aerosol size distribution the general observation is that, there is no relation on the variation of aerosol size with the variation of pool and roof temperatures. It is further observed that, the sodium metal aerosol characteristics in cover gas region are strongly dependent on the geometrical dimension (D- diameter of the sodium pool surface, L- height of the argon cover gas and shape of roof top) of the cover gas. It is also expected that, inhomogeneity in aerosol density may exist in the cover gas region. No experimental study is found in literature to quantify the aerosol density gradient within cover gas space. The studies on the effect of gamma radiation and geometry of the vessel on sodium aerosol properties are also essential to understand the aerosol behavior in the cover gas region. Due to limited information available on the sodium aerosol characteristics in cover gas region, it is important to undertake detailed studies to characterize the sodium metal aerosols in the cover gas region by adopting suitable characterization procedures. The characteristics of sodium aerosols are studied (i) by changing sodium pool temperature with constant roof temperature, (ii) at various level in the cover gas region (near the pool and roof surface, and middle level of cover gas), (iii) for two different cover gas geometric dimension (diameter of the sodium pool surface, height of the argon cover gas and shape of roof top), and (iv) effect of gamma radiation on aerosol characteristics. Also, a theoretical model is developed to predict sodium metal aerosol characteristics in the cover gas region, and validated with the experimental results. The study would be useful for the realistic estimation of heat and mass transfer phenomena to the top shield of cover gas. Further, this study would help to understand the designing of cover gas purification system [10], useful for the designing of roof top and during handling of the fuel subassembly [11].

3.0 Structure of the thesis

The details of the research work carried out to meet the objectives will be submitted as a Ph.D. thesis and the structure of the thesis is given below:

Chapter 1 Introduction

In this chapter formation of sodium metal aerosols in cover-gas region and its consequences are described. This chapter deals with the scope and objectives of the research work. The basic description of aerosols, their properties and terms, which are used in this thesis and detailed literature survey on sodium metal aerosol characteristics related to SFR safety study are also described in this chapter.

Chapter 2 Experimental Facilities and Aerosol Diagnostic Equipments

The experimental work is carried out in Aerosol Test Facility (ATF) of Radiological Safety Division and SILVERINA loop facility of Fast Reactor Technology Group. In this chapter, detailed descriptions of experimental facilities ATF and SILVERINA loop are presented. The ATF includes various aerosol generation systems (Combustion cell, Thermal Plasma torch and Atomizer), on-line Data Acquisition System (DAS), auxiliary systems and various aerosol diagnostic equipments. The sodium combustion aerosols and sodium metal aerosols in cover gas region are generated by Combustion cell, whereas the non-radioactive fuel and fission product aerosol are generated by 25kW Thermal Plasma Torch and the standard aerosols (Polystyrene and Dioctyl Phthalate-DOP) are generated by Atomizer. The SILVERINA loop is an experimental facility for conducting various experiments related to PFBR and sodium technology. The description of Test Pot-1 and Test Pot-3 of SILVERINA loop, sampling procedures and safety aspects in sampling of sodium metal aerosol in cover gas region are described. This chapter also gives description of the aerosol diagnostic equipments used for characterization of aerosol generated in ATF and SILVERINA loop. The aerosol measurement techniques include a wide variety due to the large size spectrum of particles and cover various applications. There are two measurement approaches for characterization of aerosol viz., (i) passive sampling (Filter paper, Impactor, and Conductometer) and (ii) real time sampling (light scattering instruments like Mastersizer and Optical Particle Counter (OPC), Sequential Mobility Particle Seizer (SMPS), Electrical Low Pressure Impactor (ELPI) and Conductometer. The Mastersizer and Conductometer are also used as passive sampling.

Chapter 3 Developments of sodium metal aerosol characterization technique and validation

The sodium aerosols present in cover gas region are liquid metal aerosols (liquid phase). These aerosols are different than from sodium combustion aerosols. The sodium combustion aerosols are in the form of Na_2O, Na_2O_2, NaOH, Na_2CO_3 $NaHCO_3$ and combination of these aerosols. The determination of sodium aerosols characteristics in cover gas region requires special sampling procedure, in which sampling has to be carried out without exposing the aerosols to atmosphere (the sodium aerosols undergo chemical changes and properties would get modified when exposed to atmosphere) [12]. Hence, the measurement in open atmosphere could not be a true evaluation of sodium aerosol characteristics in the cover gas region. In order to characterize the sodium liquid metal aerosols, it is required to have in-situ sampling and suitable analysis technique. The development and validation of experimental methodology for characterization of sodium aerosol in cover gas region is described in this chapter. The development of methodology and validation involves, the sodium metal aerosol sampling by drawing them without exposing to atmosphere, trap them in paraffin oil medium and analyze the sample for sodium metal aerosol characteristics. The technique is initially tested in ATF and then validated for sampling the sodium metal aerosols in the cover gas region of SILVERINA loop. The Light scattering instrument (Mastersizer) and Conductometer techniques are used for measurement of sodium metal aerosols size distribution and mass concentration respectively. The sodium metal aerosols are in the size range of 5.68 – 12.20 µm with Mass Median Diameter (MMD) at 7.72 µm. The sodium metal aerosols mass concentration in the combustion cell is found to be around 0.173 g/m^3. The sodium metal aerosols mass concentration is also measured with conductometeric titration technique. The variation of sodium metal aerosol mass concentration in both techniques (conductivity and conductometeric titration) is within ±5.5%. The sodium aerosol sampling system is designed, fabricated and commissioned at SILVERINA loop. After taking the sample from cover gas region of SILVERINA loop, the samples are analyzed by Mastersizer and Conductometer for aerosol characteristics. The aerosol size distribution is found to vary from 1 to 12 µm with Mass Median Diameter (MMD) around 4.0 µm (σ_g = 1.5) and mass concentration is found to be ~ 9.50 g/m^3 and the values agree with the values found in the literature.

Chapter 4 Development of theoretical modeling and validation

This chapter describes the development of theoretical model to predict the steady state mass concentration of sodium metal aerosols and aerosol size in the cover gas region. The model is derived from standard aerosol mass and number concentration decay equations, taking into account of aerosol source term and various aerosol removal mechanisms. The input parameters of the model are initial radius of sodium aerosol, geometry of the vessel and temperatures of pool, roof and bulk cover gas. The source term for the model is taken from evaporation of sodium vapours from the pool surface and the vapours condensation in the cover gas region during transport due to convective motion set between hot sodium pool surface and cold roof top. The aerosol characteristics in cover gas region depends upon the evaporation rates, temperature gradient of sodium pool and roof, bulk cover gas temperature and geometry of the cover gas region. From these inputs, the model calculates concentrations iteratively until convergence is reached. The model is used to predict the steady state concentration and equilibrium size of the sodium aerosols in a confined environment. In this chapter, the details of theoretical model developed for predicting sodium metal aerosol mass concentration in cover gas region is presented. The details of validation exercise of this model for sodium combustion aerosols in predicting time evolution of aerosol size growth and concentration decay, with the experimental results obtained in ATF are also presented.

Chapter 5 Characterization of sodium metal aerosol in Test Pot -1 of SILVERINA loop

The sodium metal aerosols are continuously being generated in the cover gas region of SFR. The sodium metal aerosol characteristics in cover gas region are not homogeneous. The density gradient of sodium metal aerosol varies across the cover gas region. A study has been carried out by conducting the experiments in one of the Test Pot (TP-1) of SILVERINA sodium loop facility. This chapter describes the results and analysis of sodium metal aerosol characteristics measured in cover gas of TP-1 SILVERINA loop, measurement of temperature profile of cover gas region of TP-1, theoretical simulation of sodium aerosols mass concentration for the given pool (loop) condition and validation of the model with experimental results. The sodium metal aerosols are characterised at three levels (near the pool and roof and at middle level) of the cover gas by varying the pool temperature in the range 250^{o}C – 550^{o}C in step of 50^{o}C. The sodium metal aerosol size distribution in cover gas region is found to be mono-model. The Mass Median Diameter (MMD) of sodium metal aerosols is found to vary from 1.5 - 11.5 µm as a function of sodium pool temperature and found to increase linearly with increase of sodium pool temperature. The sodium metal aerosol mass concentration is found to vary from 0.026 - 35.6 g/m^{3} as a function of sodium pool temperature and it is found to follow 3rd order polynomial regression with increase of sodium pool temperature. The sodium metal aerosol mass concentration and MMD are found to be higher near the sodium pool compared to middle of the cover gas region and near the roof top. The temperature profile of the cover gas region is measured for various pool temperatures and found to have the ‘S’ pattern similar to the literature values. Theoretical simulation has been carried out to predict the sodium metal aerosol mass concentration with respect to pool temperature for the SILVERINA loop TP-1 geometry. The theoretical values of mass concentration of sodium metal aerosols are found to be in good agreement with experimental results.

Chapter 6 Effect of cover gas geometric dimension on sodium aerosol characteristics

The sodium metal aerosol characteristics in the cover gas region depend on geometry (L/D ratio, where L - height of cover gas region and D - diameter of sodium pool) of the vessel. Experiments have been carried out in another Test Pot (TP-3) of SILVERINA loop. The sodium aerosol characteristics obtained in TP-1 and TP-3 and the results from various experimental facilities are analysed to understand the geometrical effect of sodium aerosol characteristics, and presented in this chapter. The bulk cover gas temperature and sodium metal aerosol diameter are required as input parameters in addition to the geometric parameter of the vessel i.e. L/D ratio for the theoretical simulation of sodium metal aerosol mass concentration. It is to be noted that for some of the results of experimental facility found in literature do not have the bulk cover gas temperature. An empirical relation for bulk cover gas temperature is derived and validated with our experimental results and used for other geometries. Similarly, an empirical relation for sodium metal aerosol diameter is arrived based on our experimental results and available published works. The theoretical model is used for calculating the aerosol mass concentration for various geometries, by incorporating the empirical relation for particle diameter and bulk cover gas temperature. The simulated mass concentration of sodium metal aerosol in cover gas region of various studies showed good agreement with the experimental results. The sodium metal aerosol mass concentration and Mass Median Diameter (MMD) increases with increase of sodium pool temperature. However, the values strongly depend on the aspect ratio (L/D) of sodium cover gas geometry. It is also observed that MMD of sodium metal aerosols increase with increase of aspect ratio (L/D) while mass concentration increases with decrease of aspect ratio of the cover gas region.

Chapter 7 Effect of Gamma radiation on aerosol characteristics

In the reactor environment, the cover gas region is always associated with high intensity of gamma radiation field which produces distribution of bi-polar ions. Thus the aerosols in the in the cover gas, pick up ions at random and acquire distribution of charges and it is governed by Boltzmann distribution. The Brownian coagulation rate coefficients of sodium combustion aerosol with presence of gamma radiation field is nearly one order more than that of without gamma field [9]. Also, the aerosols acquire charges during the generation process. The average charge acquired by the aerosols would also depend on the number of ion-pair and aerosol concentrations. The sodium aerosol properties would get modified due to the possible enhanced coagulation of sodium aerosols upon interaction with gamma radiation, in resulting increase in aerosol sizes. This chapter describes the experimental studies carried out to determine (i) average number of charges acquired in the generation process (in three different generation route) by the aerosols, (ii) to determine the number of elementary charges increased (average number) if any, for the aerosols in the presence of gamma radiation field, then compare the results with the theoretical formula developed for the attachment of charges by Clement and Harrison and (iii) changes in characteristics of sodium metal aerosols in the cover gas region by exposing external gamma source. It is observed that, the aerosol charging differ significantly by generation mechanisms viz. (i) combustion route for sodium aerosols, (ii) atomization route for polystyrene latex particles and (iii) vaporization and condensation route by vaporizing non-radioactive fission product materials using plasma flame. In the case of polystyrene latex aerosols, the charge neutralization effect was seen when the aerosols are exposed to gamma radiation; whereas slight increase in the average charge acquired by the aerosols generated by other route say: combustion and vaporization & condensation. The results of the average charge obtained by theoretical and experimental values are nearly comparable. It is found that the mean charge acquired by the aerosols increases with increase of ion pair concentration for a given concentration of aerosols.

Sodium metal aerosol mass concentration and size distributions are determined in the presence of gamma radiation field in the cover gas region. It is observed that the value of Mass Median Diameter (MMD) of aerosol is found to be increased and mass concentration is found to be less in the presence of gamma field condition when compared that of without gamma source condition. The reason is attributed to the increase in size due to enhanced coagulation in the presence of gamma field. As the particle size is increased which resulted the gravitational settling, hence, the aerosol concentration after the steady state is less than that of without gamma source condition.

Chapter 8 Conclusion

This chapter gives the main conclusions of the thesis and highlights of major research findings of the thesis towards understanding the sodium aerosol characteristics in cover gas region relevant to the fast reactor safety. The following are the important results obtained from the thesis.

The characterization technique for sodium metal aerosols in cover gas region (without exposing the aerosol to atmosphere) is developed, validated and used for characterizing the sodium aerosols in cover gas.

Theoretical model is developed for predicting the sodium metal aerosol mass concentration and size growth with time. The experimental results obtained in ATF are used to validate the model values for size growth and concentration decay. The simulated values are in good agreement with the experimental values.

The sodium metal aerosols are characterized in the cover gas region of TP-1 of SILVERINA loop at three different levels for various pool temperatures. The sodium metal aerosol size

(MMD) and mass concentration increases with increase of sodium pool temperature for a given geometry. The MMD of sodium metal aerosol size is larger and mass concentration is more near the sodium pool compared to that of the middle level of cover gas region and near the roof for a given geometry. The temperature profile of the cover gas region is measured for various pool temperatures and found to have the ‘S’ pattern similar to the literature values. The theoretically predicted values of mass concentration of sodium metal aerosols are found to be in good agreement with experimental results.

The sodium metal aerosol characteristics are analyzed for geometric dimension effect (aspect ratio L/D). Experimental values obtained from our studies in TP-1 and TP -3 of SILVERINA loop and other available literature values are used for analyzing the geometrical effect on sodium metal aerosol characteristics in the cover gas region. Empirical relations for predicting the sodium metal aerosol size and bulk cover gas temperature are derived based on our experimental results and using available literature results and they are used in the modeling. The simulated mass concentration of sodium metal aerosol in cover gas region of various studies showed good agreement with the experimental results. The MMD of sodium metal aerosol increases and mass concentration of sodium aerosol decreases with the increase of aspect ratio (L/D) of cover gas region.

The charge acquired by aerosol in the generation process has a significant role. The mean charge acquired by the aerosols increases with increase of ion pair concentration for a given a concentration of aerosols. In the cover gas region, the MMD of sodium metal aerosol is found to be increased and mass concentration is found to be less in the presence of gamma field condition when compared to that obtained without gamma source condition. This is attributed to the enhanced coagulation of sodium metal aerosol followed by settling in the presence of gamma radiation.

The scope of the future work envisaged are (i) The sodium metal aerosol characterization in cover gas region with variation of roof temperature at fixed sodium pool temperature, (ii) the thermal radiation change due to presence of aerosol in cover gas region and deposition of sodium metal aerosol in top shield and penetrations. In the reactor environment, sodium metal aerosol and argon cover gas are radioactive and the aerosol characteristics may differ from the present experimental studies. It is planned to characterize the sodium aerosol in the cover region of FBTR.

References

1. G. Srinivasan, K. V. Suresh Kumar, B. Rajendran and P.V. Ramlingam, (2005), "The Fast Breeder Test Reactor - Design and operating experiences", Nuclear Engineering and Design, Vol. 236, 796-811.

2. Georges Berthoud, Albert W. Longes, Anthony L. Wright and Wolfgang P. Schutz, (1988), “Experiments on Liquid-Metal Fast Breeder Reactor Aerosol Source Terms after Severe Accidents”, Nuclear Technology, Vol. 81, 257- 277.

3. W. Cherdron and S. Jordan, (1982), “Physical and Chemical characterization of sodium fire aerosols”, Proceedings of the LMFBR Safety Topical Meeting, Lyon, France, July.

4. Y. L. Sinai, I. J. Ford, J. C. Barrett and C. F. Clement (1993), "Prediction of coupled heat and mass transfer in the fast reactor cover gas: the C-GAS code", Nuclear Engineering and Design, Vol. 140, 159-192.

5. C. F. Clement and M. Julian Dolias, (1987),"sodium aerosol formation in argon flow over hot sodium’ theoretical physics division", Harwell laboratory, Oxfordshire OX11 ORA. AERE R 12489.

6. I. J. Ford, (1993),"Sodium aerosol formation and removal mechanisms in the fast reactor cover gas space", J. of Aerosol Sci., Vol. 24, 237-253.

7. N.A. Fuchs, (1964),"The Mechanics of Aerosols", Pergamon, New York.

8. C.F. Clement and R.G. Harrison, (1991),“Charge distribution on aerosols”, Proceedings of 8th International Electrostatics Conference, Institute of Physics Conference Series, Oxford, Vol. 118, 275-280.

9. V. Subramanian, R. Baskaran and R. Indira, (2008), “Experimental study on enhanced Brownian Coagulation of Sodium Compound Aerosol in the presence of Gamma Field", J. of Aerosol Sci., Vol. 39, 814-818.

10. "Specialist meeting on fast reactor cover gas purification", IWGFR 61, Richland, Washingtan USA, Sept 24-26,1986.

11. D. N. Roberts, (1995), "Heat and Mass transfer studies in sodium – Argon filled enclosures", PhD thesis, South bank University, London.

12. V. Subramanian, P. Sahoo, N. Malathi, R. Anathanarayanan, R. Baskaran, and B. Saha (2009), "Studies on Chemical Speciation of Sodium aerosols produced in Sodium fire", Nuclear Technology, Vol. 165, 257-269.

LIST OF FIGURES

LIST OF TABLES

Table No. **Title of the table** **Page No.**

LIST OF ABBREVIATIONS

AAS	Atomic Absorption Spectroscopy
AMTL	Active Mass Transfer Loop
ATF	Aerosol Test Facility
CDA	Core Disruptive Accident
CMD	Count Median Diameter
CMAD	Count Median Aerodynamic Diameter
CO_2	Carbon dioxide
CPC	Condensation Particle Counter
DAS	Data Accusation System
DCP	Dry Chemical Powder
DHRS	Decay Heat Removal System
DM	Demineralised
DMA	Differential Mobility Analyzer
DOP	Dispersed Oil Particulate
ECD	Effective Cutoff Diameter
ECR	Expanded Cold Region
ELPI	Electrical Low Pressure Impactor
FBR	Fast Breeder Reactor
FRT	Fast Reactor Technology
FBTR	Fast Breeder Test Reactor
FRTG	Fast Reactor Technology Group
GSD	Geometric Standard Deviation
HV/HF	High Voltage/High Frequency
IGCAR	Indira Gandhi Centre for Atomic Research

IHX	Intermediate Heat Exchanger
LCM	Laser mist Concentration Meter
JCR	Joint Cold Region
LDMA	Long Differential Mobility Analyzer
LOF	Loss of Flow
LOHS	Loss Of Heat Sink
LWR	Light Water reactor
MMD	Mass Median Diameter
MMAD	Mass Median Aerodynamic Diameter
NaOH	Sodium Hydroxide
PC	Personal Computer
PCB	Printed Circuit Board
PFBR	Prototype Fast Breeder Reactor
PID	Proportional Integral Derivative
PLC	Programmable Logic Controller
PU	Polyurethane
PVC	Polyvinyl Chloride
QCM	Quartz Cristal Microbalance
RCB	Reactor Containment Building
RH	Relative Humidity
RSD	Radiological Safety Division
SCADA	Supervisory Control And Data Acquisition
SDS	Secondary Shutdown System
SFR	Sodium cooled Fast Reactor
SGB	Steam Generator Building

SMPS	Sequential Mobility Particle Seizer
SrO_2	Strontium Peroxide
SS	Stainless Steel
TLV	Threshold Limit Value
TOP	Transient Over Power
UDMA	Ultrafine Differential Mobility Analyzer

CHAPTER-I

INTRODUCTION

1.0 Fast Breeder Reactor

India has special interest in developing Fast Breeder Reactors (FBR), which forms the second stage of India’s nuclear program. The FBR uses mixed oxides or carbide of Uranium and Plutonium as a fuel and it not only uses Uranium efficiently (high burn-up) but also generates fissile material. The Plutonium for FBR is obtained from the first stage reactor operation (Thermal Reactor) and it serves as the main fissile element. U-238 kept as a blanket surrounding the fuel core will undergo nuclear transmutation to produce fresh Pu-239 as much as consumed during the operation. Besides, Th-232 is kept around the FBR core as a blanket also undergoes neutron capture reactions leading to the formation of U-233, which is the nuclear reactor fuel for the third stage of India’s Nuclear Power Programme.

1.1 India's Fast Breeder Reactors

Indian FBR program started with 40MWt/13.2MWe Fast Breeder Test Reactor (FBTR) commissioned in 1985 at Kalpakkam. FBTR is based on unique mixed Plutonium- Uranium Carbide fuel, which is first of its kind in the world. As a logical follow-up of FBTR a Prototype Fast Breeder Reactor (PFBR) is being constructed and after its commissioning, a series of two more FBRs are proposed. The construction and commissioning of 500MWe PFBR is in the final stage. In the fast reactors, the fast neutrons are utilized to sustain the chain reaction and also used to breed Thorium. The core of the reactor is compact which results in a very high power density. For efficient removal of heat from the core, liquid sodium is used as coolant and the reactor is referred as Sodium cooled Fast Reactor (SFR). The thermal efficiency of SFR is more than that of Light Water Reactor (LWR), and SFR is capable of producing more fuel than it consumes (by breeding). The SFR can also be efficiently used to fission the long-lived radio-nuclides and thereby decreases the high level nuclear wastes. The SFR reactor is ideally suited for operation under a closed fuel cycle option. There are two basic design concepts adopted for SFR namely: (i) Loop type SFR and (ii) Pool type SFR.

1.1.1 Loop type Sodium cooled Fast Reactor

The loop type SFR is similar to a conventional light water reactor in which individual component of the cooling system is outside the reactor vessel and interconnected by piping, while the reactor vessel contains only the core. The reactor vessel and associated equipment are housed inside a Reactor Containment Building (RCB). Fast Breeder Test Reactor (FBTR) is a loop type SFR[1.1]. The aim of the FBTR is to gain experience in fast reactor operation, large scale sodium handling and to serve as a test bed for the irradiation of reactor materials. FBTR has two primary and secondary loops and a common water circuit. The detailed description of all the systems of FBTR is given elsewhere [1.2].

1.1.2 Pool type Sodium cooled Fast Reactor

In the pool type SFR, the reactor vessel contains not only the core, but also a number of other components such as, primary sodium pump, intermediate heat exchangers, decay heat exchanger etc. and it is housed inside a RCB. The PFBR is a pool type SFR [1.3]. PFBR uses the mixed oxides of Pu and U as fuel. The advantages of pool type SFR are, high thermal inertia of the primary system, sodium inventory kept inside the main vessel, hydraulic cooling always maintained, favorable to natural convection, and favorable to radioprotection. It has two primary and two secondary sodium pumps, four steam generators, two intermediate heat exchangers per loop (there are two loops), two shutdown systems and two decay heat removal systems etc. The detailed description of all the systems of PFBR is given elsewhere [1.4]. The sodium is made to run in two loop, the primary loops takes away the heat generated in the core of the reactor and the secondary loop takes the heat from the primary loop and transfers the heat for the generation of steam.

1.2 Advantages and Disadvantages of sodium

The main advantages of using liquid sodium as coolant in fast reactors are: (i) compatibility with stainless steels, (ii) superior thermo-physical and thermo-hydraulic properties, (iii) excellent thermal and radiation stability, (iv) low fast neutron absorption and scattering cross section, (v) high thermal and electrical conductivity and (vi) low viscosity and high thermal capacity. However, sodium has disadvantages due to its reaction with air/water, oxygen and halogens and component access in liquid sodium. Hence, in all sodium systems, inert argon gas is maintained above the sodium pool surface to avoid sodium - air contact. One of the major concerns of SFR safety is sodium aerosols produced in various scenarios.

1.3 Aerosol sources and consequences of SFR

As liquid sodium runs through the primary loop and secondary loop, the hot sodium leaks through cracks developed in liquid sodium carrying pipes. When sodium comes out in the Steam Generator Building (SGB), it comes in contact with air, burns and forms dense sodium aerosols. Sodium also reacts violently when it comes in contact with water. In addition to the formation of sodic aerosols in the combustion process, evaporation of sodium from the hot pool surface inside the reactor vessel (cover gas region) results in the formation of liquid sodium metal aerosols in the cover gas region. The Fast Reactor Technology (FRT) has been evolved by addressing the problems associated with the generation of such aerosols. The detailed scenario on the formation and consequences of sodium aerosols during accidental conditions as well as in the normal operation of the SFR, are described as follows:

1.3.1 Core Disruptive Accident (CDA)

During normal operation of SFR, there will be a balance between the heat generated by the core and the heat removed by the heat exchanger [1.5]. If the heat removal is less than the heat generation, the excess heat will be accumulated in the core itself. The cause of this excess heat may be due to the following probable initiating events in the reactor: (i) Transient over power initiated by reactivity addition (TOP), (ii) Loss of coolant initiated by reduction in the flow of coolant liquid (LOF) and, (iii) Loss of coolant initiated by loss of heat sink (LOHS). The development of these initiating events should be detected, and by taking necessary steps immediately, the reactor should be brought to normal condition within a safe period of time. Any failure in detection and preventive measures, may lead to the following core disruptive events in the reactor core: (i) Core disassembly, (ii) Core meltdown and, (iii) both Core meltdown and Core disassembly. The after effects of core disruptive events are called CDA. In order to prevent the initiating events of CDA, the following two safety systems are provided in all nuclear reactors viz. (i) Shut Down System (SDS) and (ii) Decay Heat Removal System (DHRS). The above systems are normally designed to have the failure probability better than the mandatory requirements of 10^{-6}/ry for SDS and 10^{-7} /ry (ry-reactor year) for DHRS. Therefore, in case of initiating transient event occurring in the nuclear reactor, the CDA can be expected only in the event of failure of the above two safety systems. In other words CDA is viewed as the consequence of the initiation events followed by the failure of SDS and DHRS [1.6,1.7]. In the extremely unlikely event of CDA, melting and vaporization of core inventory may produce one or several bubbles that expand into sodium pool and then to cover gas, imparting kinetic energy to the reactor vessel head. These bubbles carry radioactive materials mostly in the form of vapors, and leaks through the vessel head into the containment. These vapors condense to form aerosols. In addition to this, sodium leak in the RCB leads to sodium burning, which produces dense sodium compound aerosols. Thus RCB is bottled-up with large amount of sodium, fuel and fission product aerosols [1.8]. Besides, there exists a possibility of release of these aerosols from the stack, duct and pores of the containment building to the environment due to pressure build up in the containment. The released aerosols will be carried away by the wind and the fallouts of particulates of the aerosols are expected in the surrounding area depending on the atmospheric conditions. Also, these aerosols deposit on the floor, walls and ceiling of the RCB and cause damage to the equipments. The amount and type of aerosols released from any nuclear reactor depends on the following two factors: (i) aerosol concentration inside the containment at various times, (ii) aerosol leakage rates from the containment stack, ducts and cracks [1.9]. Hence, it is important to study the behavior of these aerosols comprising fuel and fission products material along with sodium inside the containment [1.10].

1.3.2 Sodium leakage in SGB

In the secondary loop, sodium leak can occur due to cracks developed in fluid carrying pipes and eventually, sodium may get in contact with atmosphere. The hot sodium burns in air and give rise to large amount of aerosols in the SGB. Sodium fires can be classified as follows [1.11]: (i) pool fires: sodium rapidly flows down to form a pool in the lowest part of the space, (ii) spray fires: the leakage flow is dispersed into small droplets and burn along the trajectories, (iii) Column fire: This is due to the presence of leak jackets; sodium flows downward in the form of a column generating droplets. The sodium aerosols pose serious problems such as chemical toxicity, corrosion of building materials and equipments due to the presence of peroxide and hydroxide. The sodium hydroxide aerosols have stringent inhalation health limit for humans (Threshold Limit value (TLV) of 2 mg/m^3) [1.12]. The size distribution of sodium combustion aerosol formed at various RH% and chemical composition of these aerosols with progress of time are [1.13] important for the chemical hazard evaluation in the sodium fire consequences in SGB [1.14]. The generation and characterization of aerosols described in above two sections are not the scope of the present thesis.

1.3.3 Liquid sodium metal aerosol in cover gas region

In SFR, the fuel is immersed in a sodium pool and the pool surface is covered with inert atmosphere using argon. The reactor vessel is closed by using a top shield above the argon region. The sandwiched region between the surface of hot sodium pool and the top shield (called as roof slab) of the reactor vessel is known as cover gas region [1.15]. Evaporation of sodium from the hot pool surface results in the formation of liquid metal aerosols in the cover gas region. The characteristics of these aerosol are being studied in this thesis.

In SFR, the roof slab is designed to support rotatable plugs, control plug, in-vessel fuel handling machine, primary sodium pumps, IHX and decay heat removal system etc. There are two types of concepts adopted in the design of roof slab: viz. (i) Cold Roof Concept, and (ii) Warm Roof Concept. The ‘Cold Roof Concept' means, there is no heating element to the roof slab of the reactor. The top shield gets warmed only by natural convection and radiative heating by the sodium pool surface. FBTR is a cold roof concept type SFR. In cold roof concept design, the rotating motion of the top plug is restricted after the prolonged operation of the reactor, due to deposition of sodium metal aerosol and consequent oxidation in the top shield and annular gaps of rotating plugs. To avoid this 'Warm Roof Concept' is adapted. Here, top shield is heated and it is maintained about 120^{o}C. Due to the temperature of top shield, the sodium metal aerosols melt and fall back in sodium pool. The warm roof concept is adopted in PFBR. In the normal operation of fast reactor, the difference in argon temperature between hot argon gas directly above the pool surface and cooler gas below the roof slab causes a natural convection between pool surface and roof slab [1.16]. The sodium pool temperature is maintained at 550^{o}C and roof temperature is being maintained in the range of 120 -150^{o}C. The sodium vapors continuously evaporate from the sodium pool surface into the cover gas region. The vapor gets cooled in the cover gas region and at a particular point it becomes supersaturated which then begins to condense to become sodium metal aerosol [1.17]. The aerosol particles formed by this process are suspended by natural convection current until they get deposited on to the cooler surfaces within the cover gas space. Also suspended aerosols begin to grow, due to coagulation and when the size becomes sufficiently large, they can no longer be suspended in the convection current. At this stage the aerosols get deposited on to the sodium pool by gravitational settling [1.18]. The consequence of sodium metal aerosol in cover gas region of SFR is shown schematically in Fig. 1.1. The sodium metal aerosols in the cover gas region absorb, emit, scatter and transmit the thermal radiation within the cover gas region. The thermal radiations are also absorbed, re-emitted and scattered by the side wall and roof top plug of the reactor vessel so that net heat transfer to the roof and walls is very complex [1.19]. Further sodium metal aerosol deposition on the roof surface and side wall affect the emissivity of roof surface and side wall, hence it has an influence of the net heat transfer [1.19, 1.20].

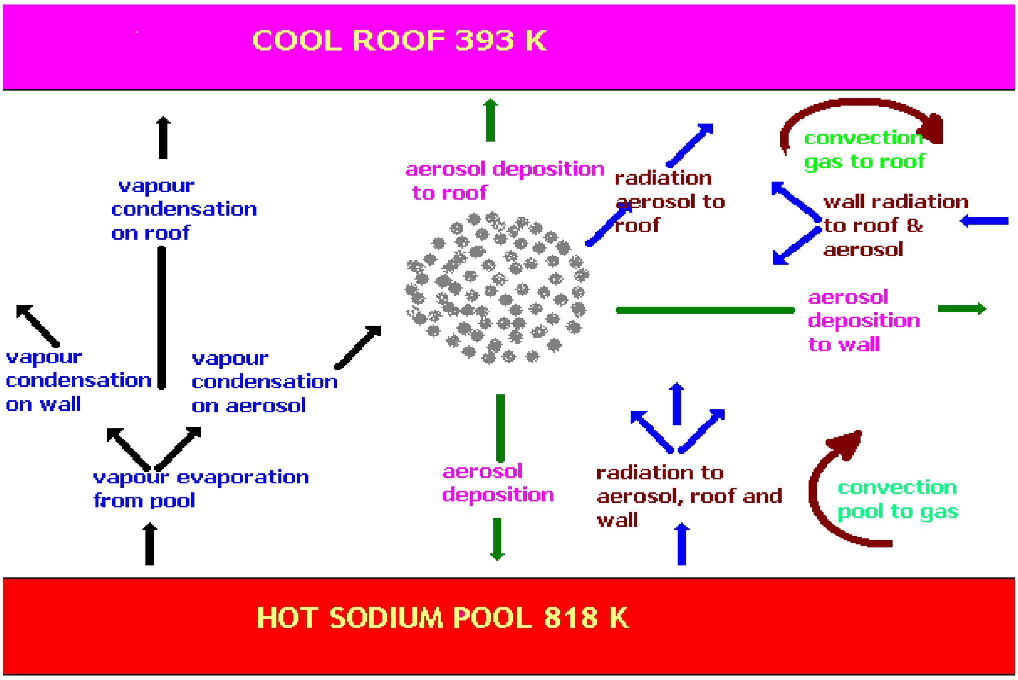

Fig.1.1 Sodium metal aerosol source and consequences in cover gas of SFR.

The presence of sodium metal aerosols may also affect the dynamics of the convective motion and temperature profile of the cover gas region. The mass transfer occurs due to condensation of sodium metal aerosols on the bottom of roof plug and side walls due to different mechanism, such as thermophoresis, diffusiophoresis and turbulent impaction [1.18]. The deposited aerosols hinder the rotational movement of rotating plug, fuel handling machine and control rods. Further, the release of volatile fission products is tightly bound to sodium evaporation and large part of the fission products is dissolved in the liquid sodium aerosol present in the cover gas region [1.21]. Thus, the presence of aerosols affect the thermal radiation passing through the aerosols and mass transfer due to condensation of aerosols. Hence it is important to study the characteristics of aerosols in the cover gas region of SFR towards better understanding of transfer of thermal radiation from hot pool surface to roof slab and the mass transfer process of aerosols towards cooler region. The work scope of present thesis is to study the characteristics of sodium metal aerosol present in the cover gas during normal operating condition with particular reference to FBTR plant. It is to be important to mention here that due to the presence of impurities like oxygen and moisture in argon gas and liquid sodium leading to formation of Na_2O and NaH aerosols, but it is very less (less than 5ppm) in nuclear grade argon gas and liquid sodium. Hence, the chemical boundary condition in sodium metal aerosols in cover gas region is not considered in the present work.

1.3.4 Gamma radiation effect on aerosol properties and process

In the extremely unlikely event of CDA, the RCB is bottled up with large amount of gamma radiation field in the order of kGy due to suspended radioactive aerosols [1.22, 1.23]. In normal operation of the SFR, cover gas region will be always subjected to intense radiation fields that result significant ionization of the gas. It is well known that the gamma radiation field produces distribution of bi-polar ions in the environment. The aerosols suspended in the charged atmosphere, pick up ions randomly and acquire distribution of charges governed by Boltzmann distribution [1.24, 1.25]. The coagulation and deposition rates of charged aerosol would be expected to differ from those of neutral aerosol. The sodium aerosol properties would get modified due to the possible enhanced coagulation of sodium aerosols upon interaction with gamma radiation. The Brownian coagulation rate coefficients of sodium aerosol is nearly one order more in the presence of gamma field than without gamma field [1.26]. In this context, one of the key studies is the behavior of sodium metal aerosols in cover gas region with presence of gamma radiation field.

To understand the aerosol process such as size growth, coagulation, chemical reaction, evaporation and condensation, removal, aerosol charging with radiation etc., it is important to be aware of aerosol terms and aerosol properties which are studied in this thesis. The basic description of aerosols, their properties and terms are described in Appendix A. In addition to the above basic terms, aerosols exhibit various phenomena such as Brownian motion, coagulation, settling, aerosol charging with radiation and the motion of aerosols under the external force field and these are also described in Appendix - A.

1.4 Literature review

One the important studies related to safety of SFR is characterization of physical and chemical properties of the sodium aerosols. An extensive literature surveys on aerosol studies is required in order to understand various aerosol issues of fast reactor safety. The major topics in aerosol safety study of SFR includes (i) aerosol characteristics in sodium fire, (ii) aerosol behavior in RCB after CDA, (iii) aerosol codes, (iv) aerosol leaks through cracks, capillary and ducts, (v) atmospheric dispersion of sodium aerosols (vi) sodium aerosol chemical speciation with various RH% (vii) sodium aerosol exposure limits, (viii) sodium aerosol cleaning, (ix) sodium metal aerosol behavior in cover gas region, (x) aerosol charging with and without radiation field and (xi) sodium aerosol measurement techniques. Among the various studies on sodium aerosols, the current research work deals with sodium metal aerosol characteristics in cover gas region, which also includes the effect of gamma radiation on sodium aerosols, as cover gas region in the reactor vessel is always under the gamma radiation field. Several studies have been conducted in various laboratories towards characterization of sodium metal aerosols in the cover gas region and its role in heat and mass transfer process to the roof top plug. Important results on sodium metal aerosol characteristics in cover gas region found in the literature are described in the following sections.

1.4.1. Sodium metal aerosol characteristics in cover gas

The research work carried out across international labs related to characterization of sodium metal aerosols for the fast reactor safety has been reviewed. The details of various aerosol experimental research facility and aerosol measurement techniques used for characterization of sodium metal aerosols are given in Table 1.1. It is observed from the Table 1.1 that, the sodium metal aerosol characteristics in cover gas region were studied for the variation of sodium pool temperature at constant roof temperature and for various roof temperatures at constant pool temperature. It is also observed that each of the facilities have different diameter of sodium pool and cover gas height. It is further noted that, there were several techniques used for the characterization of sodium aerosol viz: Andersen Impactor, laser light based techniques, sodium ionization detector, and SS mesh filter. Andersen multistage Impactor determines the mass-size distribution cumulatively over a period of time. By using stainless steel wire mesh filter (filtration technique), the size distribution is determined based on sieve size. It is observed from the experimental details that, the measurements were carried out by keeping the sampling unit/system in the atmospheric condition. Malvern 2600C (based on Franhofer diffraction) and Dantec particle dynamic analyzer were also found used for characterizing sodium aerosol in the cover gas region. In addition to the above detection systems, Laser mist concentration meter was also employed for sodium aerosol mass concentration measurements.

Table 1.1 Aerosol experimental research facility and aerosol measurement technique used for characterization of sodium metal aerosols in cover gas.

Lab Name	**Facility Description**	**Technique**	**Ref.**
South Bank University London	Cylindrical vessel (0.15m diameter & 0.35m height), Heated wall & cooled roof, (i) Constant roof temperature 150^{o}C, Varied Pool temperature: 250^{o}C – 550^{o}C, (ii) Constant pool temperature: 550^{o}C, Varied roof temperature: 150^{o}C – 250^{o}C.	Laser based instrument: (i) Malvern, (ii) Dantec	**[1.20]**
University of Manchester	Cylindrical vessel (0.80m diameter & 0.29m height), Constant pool temperature (550^{o}C), Varied roof temperature (120^{o}C – 400^{o}C)	Andersen Impactor	**[1.27]**
AMTL Harwell	Cylindrical vessel (1.0m diameter & 0.26m height), Constant pool temperature (550^{o}C), Varied roof temperature(180^{o}C – 380^{o}C)	SS wire mesh filter	**[1.28]**
South Bank University London	Heated Cylindrical vessel (0.60m diameter), variable aspect ratio (L/D=0.017 to 0.515), Constant pool temperature: 550oC, Varied roof temperature: 80^{o}C – 480^{o}C.	(i) Laser diffraction techniques (Malvern) (ii) Atomic absorption spectroscopy (AAS)	**[1.19]**
Japan	Cylindrical vessel (0.60m diameter)	SS wire mesh filter	**[1.29]**

	Varying pool temperature and difference between Pool to Roof temperature.		
NACOWA Germany	Cylindrical vessel (0.6m diameter & 1.1m height), Maximum Na temperature go up to 600^{o}C. Roof is cooled by air, pool temperature varied: 400^{o}C - 545^{o}C.	(i) Andersen Impactor (ii) Wet scrubbers using wash-bubbler	**[1.30] & 1.31]**
Tokyo, Japan	Cylindrical vessel (0.31m diameter & 1.4m height) Pool temperature varied: 200^{o}C - 520^{o}C, Varied roof temperature: 110^{o}C – 120^{o}C.	(i) SS wire mesh filter, (ii) Laser Mist Conc. Meter (LCM), (iii) collection plate	**[1.32 & 1.33]**
Japan	Cylindrical vessel (1.0m diameter & 0.5m height) and Theoretical studies	(i) Sodium ionization detector, (ii) metal fiber filter (iii) Andersen Impactor	**[1.34]**
Harwell, UK	Cylindrical vessel (2.0 m Diameter & 1.7m Height), Pool temperature 530^{o}C & roof temperature 400^{o}C,	Theoretical model & Experimental studies	**[1.17]**

1.4.2 Sodium metal aerosol mass concentration

The sodium metal aerosol mass concentration in cover gas region is dependent on the sodium pool temperature, roof temperature and dimension of the vessel. Fig. 1.2 shows the variation of sodium metal aerosol mass concentration Vs sodium pool temperature at a constant roof temperature found in various literature studies. It is observed from Fig.1.2 that, the sodium aerosol metal mass concentration increases with increase of sodium pool temperature for constant roof temperature (roof temperature is maintained at 120^{o}C for Himeno and Minges study and 150^{o}C for Glockimg study). The Glockling made similar type of study with Malvern and Dantec instruments, both are giving different results for same experimental conditions. But he concluded that results obtained by Malvern instrument were more reliable than that of Dantec instrument.

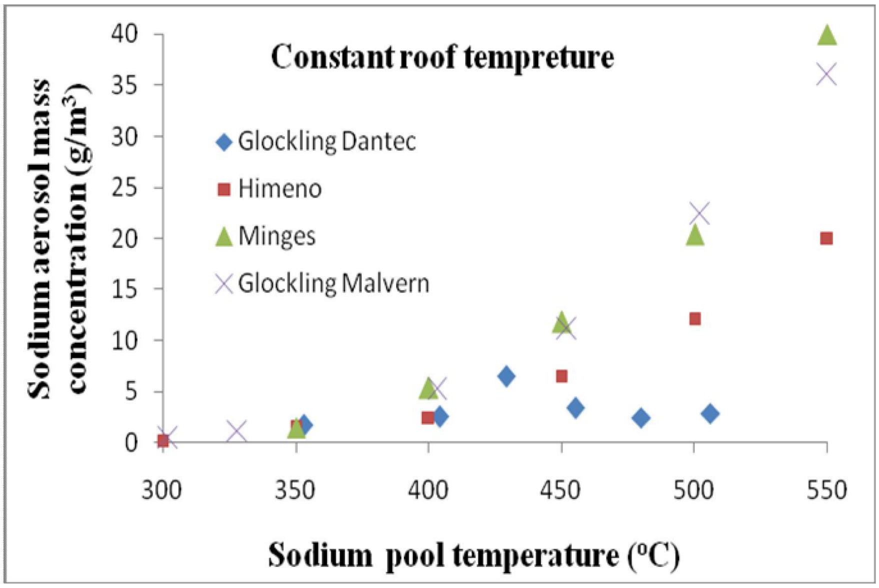

Fig. 1.2 Variation of sodium metal aerosol mass concentration Vs sodium pool temperature.

The variation of sodium metal aerosol mass concentration Vs roof temperature at a constant pool temperature is shown in Fig. 1.3. It is observed from Fig 1.3 that, the sodium metal aerosol mass concentration decreases with increasing of roof temperature at constant pool temperature (pool temperature is maintained at 520^{o}C - 550^{o}C for all studies). The variation of sodium metal aerosol mass concentration for difference in pool and roof temperature is shown in Fig. 1.4. It is observed from Fig 1.4 that, the sodium metal aerosol mass concentration increases with increase in difference between sodium pool and roof temperatures. Newson conducted experiment at pool temperature 550^{o}C while Frukawa performed experiment at pool temperatures 500, 530, 570 and 580^{o}C. Frukawa et al. conducted two types of experiments in cover gas environments which, they described as “Mist free” and “Thick mist”. For the “Thick mist” environment with a sodium pool temperature of 530°C and pool to roof temperature difference exceeding 130°C, the measured concentrations were found to vary from 10g/m^3 to 25g/m^3, with average value of 18g/m^3.

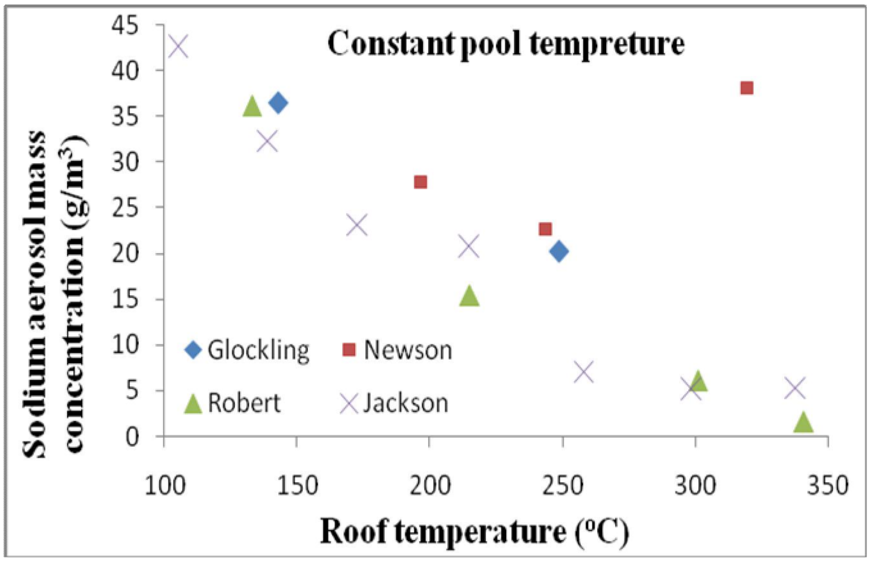

Fig. 1.3 Variation of sodium metal aerosol mass concentration Vs roof temperature.

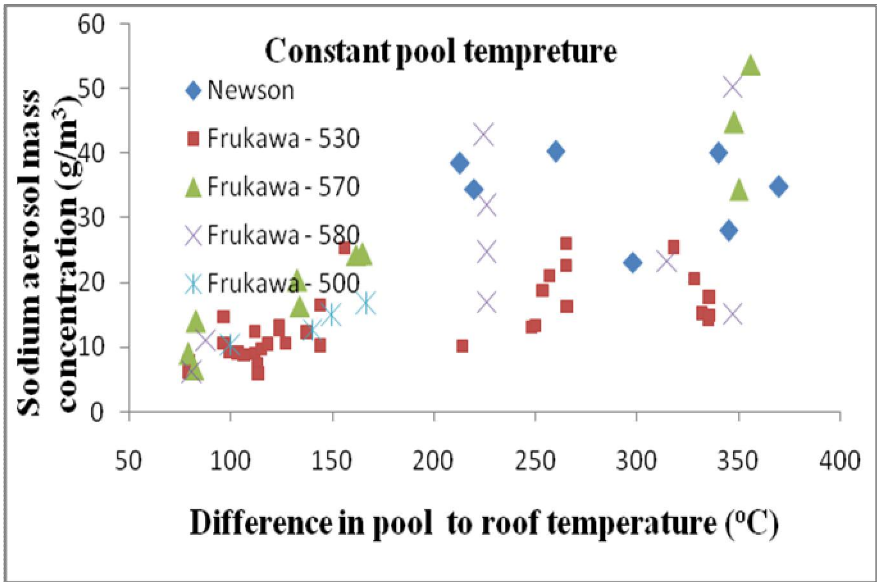

Fig. 1.4 Variation of sodium metal aerosol mass concentration with difference in pool and roof temperature.

The sodium metal aerosol mass concentration decreases rapidly for the difference of pool to roof temperature is less than 80°C. It became smaller than the saturated vapor concentration at the sodium pool surface if $dT = T_{Pool} - T_{Roof}$ was less than 50°C. A separate measurement showed that the mist formation could be neglected when the sodium pool temperature was less than 250°C. This condition was described as a "Mist free" environment and it was confirmed by visual observation through a viewing port.

1.4.3 Sodium metal aerosol size

The sodium metal aerosol size (MMD) in cover gas region is dependent upon the sodium pool temperature, roof temperature and dimension of the vessel. The variation of sodium metal aerosol size (MMD) with sodium pool temperature at a constant roof temperature is shown in Fig. 1.5. It is observed from Fig 1.5 that, the sodium metal aerosol MMD increases with increase of sodium pool temperature at constant roof temperature (roof temperature is maintained at 120°C for Himeno [1.32, 1.33] and Minges [1.30, 1.31] study and 150°C for Glocking [1.20] study). The variation of sodium metal aerosol MMD with sodium roof temperature at a constant pool temperature is shown in Fig. 1.6. It is observed from Fig 1.6 that, the MMD of sodium metal aerosol did not follow any pattern with increase of roof temperature at constant pool temperature (pool temperature is maintained at 520°C - 550°C for Jackson and Glockling studies). It is observed from the study by Robert et al., (1995) MMD of sodium metal aerosol increased with increase of roof temperature at constant roof temperature.

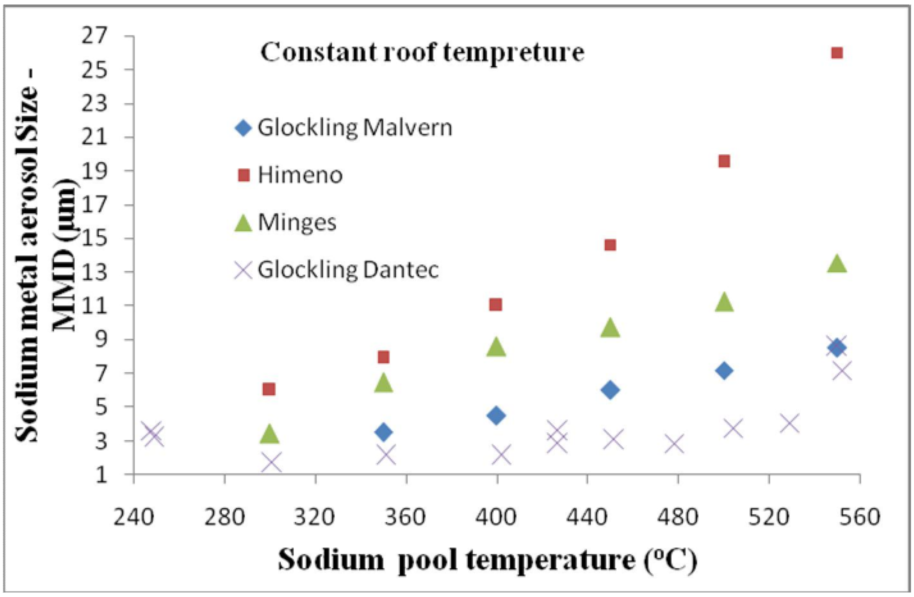

Fig. 1.5 Variation of sodium metal aerosol diameter Vs sodium pool temperature.

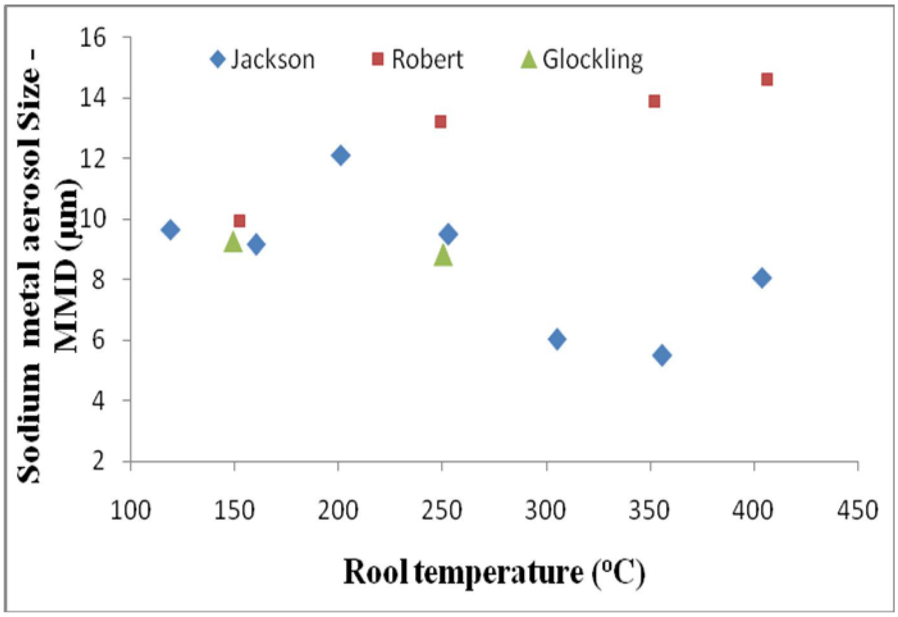

Fig. 1.6 Variation of sodium metal aerosol diameter Vs roof temperature.

1.4.4 Theoretical studies on sodium metal aerosol in cover gas region

Yamamoto et al. [1.34], Ford [1.18], and Sheth [1.16] made theoretical study on sodium metal aerosol characteristics in cover gas region. A model was developed by Yamamoto et al., to calculate mass distribution and number density of sodium metal aerosol with variation of roof temperature (300°C - 360°C) at constant pool temperature (530°C) [1.34]. The volumetric concentration of sodium metal aerosol increases with decrease of roof temperature and number density of sodium metal aerosol ranges from 10^3 - 10^4/cm^3 for all roof temperatures. The distribution of the particle size tends to shift to the larger particle size region as the temperature difference between sodium pool and roof top is increased. The measured particle size distribution appears nearly log- normal distribution. As the roof temperature decreases, the distribution curve tends to shift to the larger size region. The maximum deviation between theoretical and measured value is ±10%. The mean particle radius was found to be 2 - 10µm as the roof temperature varies between 300°C and 350°C. Ford (1993), developed a model to predict the cover gas aerosol dynamics and thermal hydraulics. Above 350°C the aerosol mass concentration increases with pool temperature.

The aerosol mass concentration is found to vary from 20g/m^3 at the highest pool temperature (520^{o}C) down to very low values of the order of 0.1g/m^3 at the lowest temperature (300^{o}C). The sodium aerosol number size distribution is found to be varying from 1-16µm at a pool temperature 520^{o}C. The maximum particle size which can be transported to the roof, by penetrating the roof boundary layer is 4µm. Sheth (1975), developed a model to predict sodium mass concentration in the cover gas region. It is found that the aerosol mass concentration and number concentration increases exponentially with increase of sodium pool temperature. The average particle size is found to increase with sodium pool temperature. The equilibrium aerosol mass and number concentration is a function of sodium metal aerosol initial size and pool boundary layer.

1.4.5 Charging effect on aerosol properties and processes

It is well known that, the gamma radiation field produces distribution of bi-polar ions in the environment. When aerosols are present in the sea of ion-pairs, aerosols pickup the ions randomly and become charged aerosols. Studies of gamma radiation effect on aerosol properties and processes were carried out by many countries and our earlier works. Several theoretical and experimental studies have been carried out to determine the number of charges acquired by an aerosols of given diameter and the coagulation of such charged aerosols. The experimental observation by Hautanen et al., (1995) showed that there is significant reduction in number concentration of soot particles when they are charged by corona discharge [1.35]. Clement et al., (1990) theoretically predicted that the radioactive aerosol charging would results in enhanced coagulation and it is emphasized that this prediction needs to be checked by the experiments [1.36]. But Park et al., (2005) in their modeling studies, bi-polar diffusion charging can significantly increase the coagulation rate of aerosols [1.37]. Bi-polar diffusion charging of non-radioactive aerosols by using Am-241 Alpha sources was compared with the soft X-ray source of 9.5 keV by Hye Moon Lee et.

al.,[1.38]. They reported that, a steady ion concentration rate was achieved by X-ray source and it is effective for the measurement of nano-particles. An experimental and theoretical study by Konstantaneous Barbenous showed that, increase of radioactivity concentration has minor deviation in the charge distribution of aerosols [1.39]. However, the product n and t (n -no. of ion pairs and t- resident time) would be a key factor for the particle charging to achieve Boltzmann equilibrium. Another important study on bi-polar charging on radioactive aerosols and comparison of their result with Clement & Harrison model was carried out by F. Gendarmes et. al.,[1.40]. In fact, the charging of radioactive aerosols is different from that of non-radioactive aerosols but their study, concludes that the charging varies with the intensity of ionization in the environment. Fuchs experimentally observed that, attractive forces between aerosols charged with unlike signs increase coagulation rates, overcoming other electrical repulsions [1.24]. Rosinski et al., have experimentally showed the increase in coagulation rate up to 2 times for the Cadmium aerosols of 0.2 µm radius when charged using photoelectric effects [1.41]. When the charged aerosols undergo Brownian coagulation, the coagulation enhancement factor is defined as $f = K'/K$ (where K' and K – coagulation kernels for the charged and uncharged particles respectively), [1.25, 1.35]. The experimental results at ATF showed that the Brownian coagulation enhancement of 5-8 times for the mono-dispersed sodium aerosols in a confined environment at the dose rate of the order of few mGy/h [1.26]. Powers and Burson [1.42], Clement and Harrison [1.36], and Williams and Loyalka [1.43] have proposed a model to estimate the effect of aerosol charging on the coagulation and deposition rates. Coagulation rates between aerosols of equal size were reduced from the uncharged aerosol case, whereas coagulation rates between aerosols of unequal size tends to be larger than the uncharged case. It is further reported that, by using general theory derived by Zebel [1.44] and by Williams and Loyalka [1.45], in order to get the coagulation enhancement factor of 5 times the modest charging required by the aerosol particle is about 8 charges for the particles of radius 0.5µm in a given ion concentration (radiation field of 4 mGy/h) [1.46]. Thus it is understandable that the electrical forces caused by the Coulomb interaction between the charged aerosol particles are responsible for the enhanced coagulation. In normal operation of the SFR, cover gas region is always subjected to intense radiation fields that result in significant ionization of gas. The sodium metal aerosol gets charged by picking of ions present in the cover gas region. No experimental or theoretical study was found in literature on radiation effect upon sodium metal aerosol in cover gas region.

1.4.6 Temperature profile of cover gas region

In the SFR, the temperature profile of cover gas region plays major role in governing the sodium metal aerosol characteristics and heat and mass transfer phenomena. In SFR, heat transfer from the sodium pool to the cooled roof occurs by natural convection and thermal radiation across the cover gas space filled with argon. The mass transfer across the cover gas space varies with sodium vapor pressure. The sodium metal aerosols characteristics also depend on the pool, roof and bulk cover gas temperatures. Sodium evaporation rate depends on sodium pool temperature and difference between pool and roof temperatures. Sodium vapor condensation depends on temperature gradient of pool to bulk cover gas. Aerosol deposition on the roof surface depends on roof temperature and convection source. And coagulation depends on bulk cover gas temperature. To quantify these phenomena, temperature profile of cover gas region and bulk cover gas temperature are essential parameters for calculation of sodium aerosol characteristics, aerosol deposition on top shield and heat and mass transfer analysis. The measurement of cover gas temperature profile and bulk cover gas temperature has been carried out simultaneously with sodium aerosol characteristics by Robert and it is detailed below:

The measurement of temperature in the cover gas region was carried out by Robert [1.19] in the vertical direction using 0.5mm diameter sheathed chromel-Alumel thermocouple. The thermocouple was contained within a 0.75mm diameter, 0.25mm wall thick, stainless steel support tube sealed at one end. The support tube was laid across the cover gas space and immersed below the free surface of sodium pool. The temperature within the cover gas space and pool and roof boundary layers were measured by traversing the thermocouple within the support tube against a scale graduated in mm from an initial position below the surface of sodium pool, across the cover gas space and to final position with the roof surface. The measured temperature profile was found to have the same characteristics given by Raithby and Holland (1974) [1.47] in 'Conduction layer Model'. Above the sodium pool there was a steep temperature gradient across the pool boundary layer to the cover bulk temperature. The bulk cover gas temperature then remain almost constant in the in the middle of the cover gas space. Another thermal boundary layer exists near the roof, which is known as roof boundary layer.

1.5 Scope and Objective of the study

In the context of the safety studies of SFR, the physical and chemical characteristics of sodium aerosols are very important. In many countries, considerable efforts have been made towards a realistic assessment of formation of sodium metal aerosols in the cover gas region and removal of these aerosols. The magnitude and nature of aerosols play a significant role in heat and mass transfer processes to the roof top plug. It is observed from literature that the sodium metal aerosol size (d_{50}) and mass concentration are in the range of 2-26µm and 1-50g/m^3 respectively. The characteristics of sodium metal aerosols found to vary due to (i) change in sodium pool temperature, (ii) change in roof temperature, and (iii) temperature difference between the sodium pool and roof. The variation of sodium aerosol mass concentration in cover gas region has a definite pattern with the variation of roof and pool temperatures in all these studies. But in the case of sodium metal aerosol size distribution the general observation is that, there is no relation on the variation of aerosol size with the variation of pool and roof temperatures. It is further observed that, the sodium metal aerosol characteristics in cover gas region are strongly dependent on the geometrical dimension (D-diameter of the sodium pool surface, L- height of the argon cover gas and shape of roof top) of the cover gas. It is also expected that, inhomogeneity in sodium metal aerosol mass concentration may exist in the cover gas region. No experimental or theoretical study is found in literature to quantify the sodium metal aerosol mass concentration gradient within cover gas space. Although, the study on gamma radiation effect of aerosol properties and processes available in literature but no experimental or theoretical study on effect of gamma radiation on sodium metal aerosol in cover gas region was found in literature. Hence, studies on the effect of gamma radiation and geometry of the vessel on sodium metal aerosol characteristics are also essential to understand the role of aerosol in heat and mass transfer in the cover gas region. Further, there were several techniques used for the characterization of sodium metal aerosol size and mass concentration viz: Andersen Impactor, laser light based techniques, sodium ionization detector, and SS mesh filter. However, the details of the sampling procedures are not described in these techniques. It is to be noted that, the sodium metal aerosols present in cover gas region are liquid metal aerosols (liquid phase). The determination of sodium metal aerosols characteristics in cover gas region requires special sampling procedure, in which sampling has to be carried out without exposing the aerosols to atmosphere (the sodium metal aerosols undergo chemical changes and properties would get modified when exposed to atmosphere) [1.14]. Hence, it is important to undertake suitable technique to characterize the sodium metal aerosols in the cover gas region. Development of theoretical models and their verification on specific experimental results remain necessary, particularly sodium aerosol mass concentration and sodium aerosol size distribution and thermal radiation in sodium aerosol filled areas [1.48]. To predict sodium metal aerosol characteristics in cover gas region by theoretical model without conducting experiment, the bulk cover gas temperature, roof and pool temperatures, geometry of the vessel and initial sodium metal aerosol size are important parameters. Hence, a comprehensive study has been undertaken towards characterization of sodium metal aerosol in cover gas region which includes (i) determination of sodium aerosol size distribution and mass concentration for various pool temperatures, (ii) Vertical profile of aerosol characteristics in the cover gas region, (iii) aerosol characteristics with respect to different cover gas geometry (Volume effect), (iv) gamma radiation effect on aerosol characteristics and (v) temperature profile of the cover gas region. Also, a theoretical model is developed to predict sodium metal aerosol characteristics in the cover gas region, and validated with our experimental results and available literature. The study would be useful for the realistic estimation of heat and mass transfer phenomena to the top shield of cover gas and annular gap present in the top shield. Because of mass transfer, sodium deposits may exit, especially in the cooler part of top shield [1.48]. Further, this study would help to understand the designing of cover gas purification system [1.49], useful for the designing of roof top and for handling of the fuel subassembly [1.19]. This study is also important for the evaluation of the source term, because the volatile fission product release is tightly bound to sodium evaporation and a large part of the fission product is dissolved in the liquid sodium aerosol present in the cover gas region [1.21].

1.6 Structure of the thesis

The outline of the thesis is described as follows. The thesis is divided in to eight chapters. Chapter II describes the details of experimental facilities viz. the Aerosol Test Facility and the SILVERINA loop facility and aerosol diagnosis techniques (both active and passive characterisation techniques). In chapter III, the detailed description of special characterisation technique developed for characterisation of sodium metal aerosol in ATF and validation of the technique in SILVERINA loop are explained. Chapter IV describes the development of theoretical model for predicting the sodium metal aerosols mass concentration and size growth with time. The experimental results obtained in ATF are used to validate the modeled values for size growth and concentration decay. Chapter V describes the characteristics of sodium metal aerosols in the cover gas region of TP-1 of SILVERINA loop sampled at three different levels for various pool temperatures. The sodium metal aerosol size (MMD) and mass concentration increases with increase of sodium pool temperature for a given geometry. The MMD of sodium metal aerosol is larger in size and mass concentration is more near the sodium pool compared to that of the middle level of cover gas region and near the roof for a given geometry. The temperature profile of the cover gas region is measured for various pool temperatures and found to have the ‘S’ pattern similar to that of literature values. Chapter VI describes the effect of various geometric dimensions (aspect ratio L/D, L- height of cover gas region and D - diameter of the sodium pool) on sodium metal aerosol characteristics. Experimental values obtained from our studies in TP-1 and TP -3 of SILVERINA loop and other available literature values are used for analyzing the geometrical effect on sodium metal aerosol characteristics in the cover gas region. Empirical relations for predicting the sodium metal aerosol size and bulk cover gas temperature are derived based on our experimental results and using available literature results and they are used in the modeling. The MMD of sodium metal aerosol increases and mass concentration of sodium aerosol decreases with the increase of aspect ratio (L/D) of cover gas region. The gamma radiation effect on the aerosol characteristics is described in chapter VII. In the cover gas region, the MMD of sodium metal aerosol is found to be increased and mass concentration is found to be less with presence of gamma field condition when compared to that obtained without gamma field condition. Finally, the conclusion and highlights of major research findings of the thesis towards understanding the sodium metal aerosol characteristics in cover gas region relevant to the

SFR safety are described in chapter VIII. The scope of the future work is also described in chapter VIII.

1.7 References

1.1 K.V. Suresh Kumar, A. Babu, B. Anandapadmanaban and G. Srinivasan, (2011), "Twenty five years of operating experience with the FBTR", Energy Procidia, Vol. 7, 323-332.

1.2 G. Srinivasan, K. V. Suresh Kumar, B. Rajendran and P.V. Ramlingam, (2005), "The Fast Breeder Test Reactor - Design and operating experiences", Nuclear Engineering and Design, Vol. 236, 796-811.

1.3 S. C. Chetal, V. Balasubramanian, P. Chelapandi, P. Mohanakrishanan, P. Puthiyavinayagam, C. P. Pillai, S. Raghupati, T. K. Shanmugham, and C. Sivathanu Pillai, (2006), "The design of PFBR", Nuclear Engineering and Design, Vol. 236, 852-860.

1.4 S. C. Chetal, P. Chelapandi, P. Puthiyavinayagam, S. Raghupati, V. balasubramanian, P. Selvaraj, P. Mohanakrishanan and Baldev Raj, (2010),"Current Status of Fast Reactors and Future Plans in India", Asian Nuclear Prospects, Energy Procedia, Vol. 7, 64 -73.

1.5 A. E. Waltar and A. B. Reynolds, (1981), "Fast Breeder Reactor", Pergamon Press.

1.6 G. S. Srinivasan, R. Harish and Om Pal Singh, (1999) “Core Disruptive Accident Analysis”, PFPR/ 01117/ DN/ 1012.

1.7 R. Baskaran, T. S .Selvakumaran and V. Subramanian, (2004) “Proposed aerosol studies in ATF”, RSD/RSAS/06/02-2004.

1.8 Georges Berthoud, Albert W. Longes, Anthony L. Wright and Wolfgang P. Schutz, (1988), “Experiments on Liquid-Metal Fast Breeder Reactor Aerosol Source Terms after Severe Accidents”, Nuclear Technology, Vol. 81, 257-277.

1.9 J. F. Van de vate, W.F. Van Leeuwen and H.C.D. Smit., (1982),“Aerosol leakage through containment walls”, Proceedings of LMFBR Safety Topical meeting, Lyon, France.

1.10 V. Subramanian, (2009)," Studies on characterization of sodium aerosols for the fast reactor safety", PhD/Confirm/62/PT/07/2003/7925, University of Madras, India.

1.11 W. Cherdron and S. Jordan, (1982), “Physical and Chemical characterization of sodium fire aerosols”, Proceedings of the LMFBR Safety Topical Meeting, Lyon, France.

1.12 “Safety and Health Topics: Sodium Hydroxide,” U.S. Department of Labor; available on the Internet at http:00www.osha.gov0dts0chemicalsampling0data0CH_267700.html.

1.13 V. Subramanian and R. Baskaran, (2007), “Initial size distribution sodium combustion aerosols”, Nuclear Technology, Vol.160, 308-313.

1.14 V. Subramanian, P. Sahoo, N. Malathi, R. Ananthanarayanan, R. Baskaran and B. Saha, (2009), “Studies on chemical speciation of sodium aerosols produced in sodium fire”, Nuclear Technology, Vol. 165, 257-269.

1.15 Y. L. Sinai., I. J. Ford., J. C. Barrett and C. F. Clement (1993), "Prediction of coupled heat and mass transfer in the fast reactor cover gas: the C-GAS code", Nuclear Engineering and Design, Vol. 140, 159-192.

1.16 A. Sheth (1975), "Parametric study of sodium aerosols in the cover gas-space of sodium-cooled reactors", Argonne National Laboratory, ANL-75-11.

1.17 C. F. Clement and M. Julian Dolias (1987), "Sodium aerosol formation in argon flow over hot sodium", Theoretical physics division, Harwell laboratory, Oxfordshire OX11 ORA. AERE R 12489.

1.18 I. J. Ford, (1993), "Sodium aerosol formation and removal mechanisms in the fast reactor cover gas space", J. of Aerosol Sci. Vol. 24, 237-253.

1.19 D. N. Roberts, (1995), "Heat and Mass transfer studies in sodium – Argon filled enclosures", PhD thesis, South bank University, London.

1.20 J. L. D. Glockling (1991), "Heat and Mass transfer in specific aerosol system. PhD thesis", Department of chemical engineering'. South bank University, London.

1.21 Technical committee meeting on, "Evaluation of radioactive materials and sodium fires in fast reactors", PNC O-ARAI Engineering Center, Japan, 11-14 November 1996.

1.22 R. Baskaran, V. Subramanian and R. Indira, (2007), "Aerosol Issues in Fast Reactor", IASTA-2007 NPL, Delhi, Nov.2007. IASTA Bulletin, Vol.18, 222 (2007).

1.23 P. V. N. Nair, J. P. Gupta, P. V. Joshi and B. K. Sapra, (1993), "A study of Aerosol size distribution in working areas of Nuclear Reactor", J. of Aerosol Sci., Vol. 24, 307-308.

1.24 N. A. Fuchs, (1964), "The Mechanics of Aerosols", Pergamon, New York.

1.25 C. F. Clement and R. G. Harrison, (1991), "Charge distribution on aerosols", Proceedings of 8th International Electrostatics Conference, Institute of Physics Conference Series, Oxford, Vol. 118, 275-280.

1.26 V. Subramanian, R. Baskaran and R. Indira, (2008),"Experimental study on enhanced Brownian Coagulation of Sodium Compound Aerosol in the presence of Gamma Field", J. of Aerosol Sci., Vol. 39, 814-818.

1.27 J. D. Jackson, J. F. Sanchis An Pei, and A. Alamar, (1993), "closing report of the MUSAC 3A project", Department of nuclear engineering, university of Manchester.

1.28 I. H. Newson, R. W. Dawoson, C. D. Wade, A. N. Moul and J. E. Finch, (1993), "Studies of caesium-134 transfer through argon and helium Cover gases above hot sodium pool in the Harwell active mass transfer loop (AMTL)", AEA Industrial technology, Report number AEA-In Tec-1220.

1.29 O. Frukawa, A. Furutani, N. Hattori and Iguchit, (1984),"Experimental study of heat and mass transfer through the cover gas in the Liquid Metal Fast Breeder Reactor

(LMFBR)", Proceeding of the third international conference on liquid metal engineering and technology, The British nuclear Society, Vol.1, 451-458. ISBN0-7277-0209-2.

1.30 J. Minges and W. Schutz, ‘Experiments on the enrichment of cesium in the cover gas aerosol of the European Fast Reactor (EFR)’. Nuclear Engineering and Design 147 (1993) 17-22.

1.31 J. Minges and W. Schutz, (1991), "Experiments to characterize the sodium aerosol system in the cover gas of the European Fast Reactor EFR", J. Aerosol Sci. Vol. 22, S761-S764.

1.32 Yoshiaki HIMENO and June TAKAHASHI, (1980),"Sodium Mist behavior in cover gas space of LMFBR", J. Nucl. Sci. and Tech. Vol. 17, 404-412.

1.33 Yoshiaki HIMENO and Yoshiaki YAMAGISHI, (1982), "Effect of barriers on sodium mist deposition on LMFBR components", J. Nucl. Sci. and Tech. Vol. 19 [10], 837-844.

1.34 H. YAMAMOTO, T. SAKAI and N. MURAKAMI, (1991), "Analytical study on mass concentration and particle size distribution of sodium mist in cover gas phase of LMFBR reactor vessel’, J. Aerosol Sci. Vol. 22, S713-S716.

1.35 J. Hautanen, T. Watanebe, Tsuchida, Y. Koizumi, F. Tochikubo, E. Kauppinen, K. Lehtinen and J. Jokiniemi, (1995), “Brownian Agglomeration of Bipolarly Charged Aerosol Particles”, J. of Aerosol Sci., Vol. 26, S21-S22.

1.36 C.F. Clement and R.G. Harrison, (1990), “Electric charge effects on aerosol behavior”, Workshop on Aerosol Behaviour and Thermal-Hydraulics in the Containment CEC/NEA, Fontenay-aux-Roses, France.

1.37 S. H. Park, K. W. Lee, M. Shimada and K. Okuyama, (2005), “Coagulation of bipolarly charged ultrafine aerosol particles”, J. of Aerosol Sci., Vol. 36, 830 -845.

1.38 Hye Moon Lee, Chan Soo Kim, Manabu Shimada & Kikuo Okuyama, (2005), "Bipolar diffusion charging for aerosol nanoparticle measurement using a soft X-ray Charger", J. of Aerosol Sci., Vol. 36, 813-829.

1.39 Konstantines Barbranis, (2009), "Bipolar diffusion charging: Experimental and Theoretical evaluation of the parameters affecting the charge distribution of nano-particles in the size range 10-100nm", M. S. Dissertation, University of Aegean, Greece.

1.40 F. Gensdarms, D. Boulaud, and A. Renoux, (2001), "Electrical charging of radioactive aerosols-comparison of the Clement-Harrison model with new experiments", J. of Aerosol Sci., Vol. 32, 1437-1458.

1.41 J. Rosinski, D. Werle and C. T. Naganoto, (1962), “Coagulation and scavenging of radioactive aerosols”, J. of colloidal Sci., Vol.17, 703-716.

1.42 D. Powers. and S. B. Burson, (1996), "A simplified model of aerosol removal by natural process in reactor containments", NUREG/CR-6189, SAND94-0407, Sandia National laboratories.

1.43 M. M. R Williams, and S. K. Loyalka, (1989), "Aerosol Science" Theory and Practice. Pergamon, Oxford.

1.44 G. Zebel, (1966), "Coagulation of aerosols", In: Davies C.N. (ed) Aerosol Science, Academic Press, London.

1.45 M. M. R. Williams and S. K. Loyalka, (1991), "Aerosol Science Theory and Practice", Pergamon, Oxford.

1.46 V. Subramanian, R. Baskaran and B. Venkatraman, (2011), "Studies on Sodium Aerosol characteristics in the presence of Gamma radiation field", 7th Asian Aerosol Conference, 17-21, August, 2011, Xi’an, China, 545-551.

1.47 G. D. Raithby and K. G. T. Hollands, (1974), "A general method of obtaining approximate solution to laminar and turbulent free convection problems", Advance in heat transfer, Vol.11, 266, Academic Press, New York, USA.

1.48 Baldev Raj, P. Chellapandi, P. R. Vasudeva Rao, (2014), "Sodium Fast Reactors with Closed Fuel Cycle", CRC press, Taylor and Francis Group, Boca Raton London NewYork.

1.49 "Specialist meeting on fast reactor cover gas purification", (1986) IWGFR 61, Richland, Washingtan USA, Sept 24-26.

CHAPTER -II

EXPERIMENTAL FACILITIES AND AEROSOL DIAGNOSTIC EQUIPMENTS

2.0 Introduction

The experimental work is carried out in Aerosol Test Facility (ATF) [2.1] in Radiological Safety Division (RSD) and SILVERINA loop [2.2] facility in Fast Reactor Technology Group (FRTG). The detailed descriptions of the experimental facilities, ATF and SILVERINA loop are presented in this chapter. The ATF is an experimental facility to study the nuclear aerosol characteristics, in particular sodium aerosol towards SFR safety. The SILVERINA loop is an experimental facility for conducting various experiments related to PFBR and sodium technology. This chapter also gives description of the aerosol diagnostic equipments used for characterization of aerosols generated in ATF and SILVERINA loop. The aerosol measurement techniques include a wide variety due to the large size spectrum of particles and cover various applications. There are two measurement approaches employed for characterization of aerosols in this study [2.3]. Filter paper, impaction, and conductivity techniques are used under passive sampling system, while, light scattering, electrical mobility, impaction coupled with charge measurements and conductivity techniques are used under real time sampling system. The light scattering and conductivity techniques are also used as passive sampling.

2.1 Aerosol Test Facility (ATF)

The ATF is in operation at RSD, IGCAR, Kalpakkam, since 2004. The Major component of ATF are (i) aerosol chamber, (ii) aerosol generators, (iii) auxiliary system like chilled water system, pneumatic control system, data acquisition system and Humidity controller and (v) aerosol measurement equipments. The detailed description of aerosol measurement equipments used for characterizing aerosol parameters is described in section 2.3.

2.1.1 Aerosol chamber

The schematic diagram of ATF is shown in Fig. 2.1. The aerosol chamber is in cylindrical shape having volume 1 m^3 (height = 60 cm and diameter = 150 cm) and it is made of SS-304L. The aerosol chamber weighs almost 1.0 Ton and the top plate weighs about 400 kg. The aerosol chamber is mounted on a suitable M.S bench and the top plate can be opened using 2.0 Ton gantry. The chamber is provided with eight numbers of 3″ ports, three numbers of 4″ ports and one number of 6″ port. A 25 kW Thermal Plasma torch is connected to a 4″ port 'C1'. Sodium combustion cell is connected in 4″ port 'C2' for the generation of sodium aerosols. Provision is made to flush the chamber with desired gas through a 3″ port 'B4'. A humidity controller system (to add and remove humidity contents in the aerosol chamber) is connected through 3″ ports 'B1 and B2'. A viewing window is made in 3″ port 'B7'. The aerosol diagnostic equipments such as Quartz Crystal Microbalance (QCM), Aerosol Dust Monitor, and Sequential Mobility Particle Sizer + Condensation Particle Counter (SMPS+C) are connected through a single 3″ port 'B3' (The port B3 is provided with 4 outlets of 8 mm inner diameter, for connecting various equipments). Low pressure impactor sampler and filter paper samplers are connected to an independent 3″ ports 'B8 and B5' respectively. The Mastersizer-S is integrated with aerosol chamber through an aerosol flow cell, which is connected to a 4″ port 'C3'. The aerosol flow cell is designed for the online measurement of aerosol characteristics using Mastersizer for the aerosols suspended in air [2.4]. The Electrical Low Pressure Impactor is connected to a 3″ port 'B7'.

2.1.2 Aerosol Generators

ATF is equipped with various types of aerosol generators to study aerosols generated through various routes related to SFR safety.

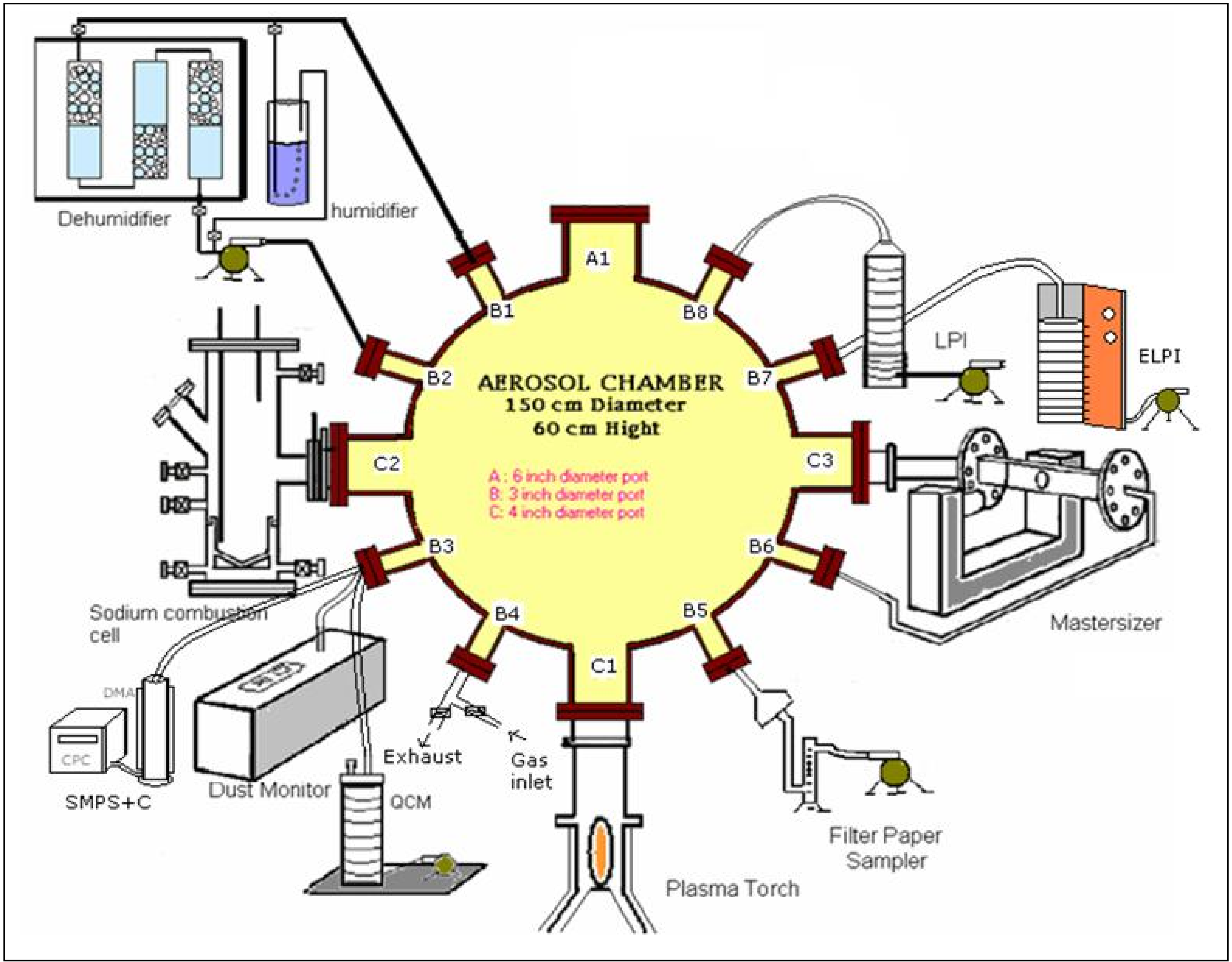

Fig.2.1 Schematic diagram of Aerosol Test Facility.

A combustion cell for generation of sodium aerosols and sodium metal aerosols, Plasma Torch for generation of fission product and fuel equivalent aerosols through vaporization and condensation route and atomizer aerosol generator for generation of Dispersed Oil Particulate (DOP) or polystyrene latex aerosols (test aerosols).

2.1.2.1 Sodium combustion cell

Sodium combustion cell is used for the generation of sodium combustion aerosols and sodium metal aerosols. The sodium combustion cell is designed and fabricated as a part of ATF. The cell is cylindrical in shape (height = 50cm, diameter = 20cm) having one viewing arm and a connecting port. The cell is connected with aerosol chamber through a pneumatically operated gate valve, so that cell can be isolated from the chamber. The cell is vacuum compatible and it is provided with two numbers of feed line and one bleed line. A Bunsen burner of capacity 150 g is kept inside the chamber and an external heater is used to energize the burner. In order to monitor the sodium heating process, the cell is provided with (i) two pressure sensors (one analog device and one digital device) to monitor the pressure inside the cell and (ii) two thermowells to monitor the temperature rise in the cell, located in a such way that, one is made to dip inside the sodium pool and another is just above the sodium pool. The signals from the digital pressure sensor and the thermocouples are fed to the data logger. The details of the temperature and pressure sensors and the data logging systems are described in section 2.1.5.

Generation of sodium combustion aerosol: About few grams of sodium is placed in a crucible and mounted on the heater. The sodium combustion cell is isolated, flushed and filled with argon gas, up to a pressure of 10-20kPa excess over atmosphere. The sodium is heated up to a required temperature (say 550^{o}C). The hot sodium is ignited by exposing it to air, after flushing out the argon. By combustion, sodium oxide aerosols are formed in the combustion cell. The gate valve is opened and aerosols are get filled into the aerosol chamber and the diagnostic ports immediately. The pressure inside the cell raises up to 70-80kPa excess over the atmosphere helps to fill the aerosol chamber and its diagnostic ports with sodium combustion aerosols. The cell is isolated again after one minute so that sodium aerosols are bottled-up inside the aerosol chamber.

Generation of sodium metal aerosol: About 5-10g of sodium is placed in a crucible and mounted on the heater. The sodium combustion cell is isolated, flushed and filled with argon gas, up to a pressure of 10-20kPa excess over atmosphere. The sodium is heated with the help of Bunsen burner. When the temperature of sodium reaches 98^{o}C, the solid sodium begins to melt down and the sodium evaporates from the free surface of liquid sodium. The evaporation of sodium from the sodium pool increases with increase of sodium pool temperature. Sodium vapor present in argon gas medium condenses and become sodium metal aerosol in the volume of combustion cell. These aerosols are liquid aerosols suspended in argon cover gas [2.5].

2.1.3 Plasma Aerosol generation system

Generation of aerosols by thermal plasma aerosol generation system has distinct advantages over the conventional technologies because of the high temperatures, combined with steep temperature gradient and quench rates [2.6]. Plasma aerosol generation system gives an intense and long aerosol source and it can be used to generate aerosols from metals, ceramics and composite materials through vaporization and condensation route. The plasma aerosol generation system consists of plasma torch, Main power supply and HV/HF power supply, Cooling water and Plasma/Sheath gas supply unit, and Programmable Logic Controller (PLC) automation unit.

2.1.3.1 Description of plasma aerosol generation system

A Thermal plasma torch (power 25 kW) has been designed and fabricated by Shree Raghavendra Technical Service Pvt. Ltd., Ahmadabad, India, as per our requirements. The plasma torch is operated in non-transferred arc mode, in atmospheric pressure. It has a rod type cathode, made of tungsten of 14 mm diameter with 1-2 % of thoria for better thermionic emission [2.7]. The anode is made of Zr - Cu alloy, in the form of divergent nozzle with a conical shape, having 17 mm inner diameter and 75 mm outer diameter. Both the anode and cathode are water cooled and immersed in an axial magnetic field provided by permanent magnet for the stabilization of the arc. The magnetic field is produced parallel to both anode and cathode axis. The overall dimension of the torch is 82 mm. Nitrogen is used as plasma generating gas and Nitrogen or Argon can be used as a sheath gas. The plasma torch power supply consists of three different circuits namely, (i) High Voltage and High frequency generator (3kV-3MHz), (ii) Three phase rectifiers and (iii) 12V DC supply for operation of relays. Sustainability of the arc flow depends on the plasma gas flow rate and the electric power to the torch for the fixed electrodes design. The arc is initiated between the cathode and anode. The arc route at the anode side was rotated by magnetic field by permanent magnet. The plasma gas flow rate and the electric power to the torch are carefully metered to sustain the flow of arc. The open circuit voltage is observed to be varied depending on 3 phase input line voltage from 470 V to 490 V. Arc is formed between cathode and anode using 3 kV/3 MHz pulse for 400 mS duration. A typical arc is stabilized at a power of 20 kW with 15lpm gas flow rate for both plasma generating gas and sheath gas.

Programmable logic controller (PLC) is used for automation of the processes/parameters of the plasma torch operation. It is provided with a digital display to monitor the status of the system, Control panel sends temperatures and flow rates data to PLC continuously using wireless data transmission. Main screen will display the arc current, voltage and system status. When PLC is started, it should show “SYSTEM HEALTHY” for safe operation of the system, attaining the sustained arc, some of the parameters are set as given in Table 2.1.

Table 2.1 Interlocks and the corresponding set points.

Interlock	Inference	Set value
WT FLOW	Water is not flowing in Plasma Torch	7lpm
WT TEMP	Inlet water Temperature is high	30^0C
CHECK GAS FLOW	Gas is not flowing in Plasma Torch	10-25lpm
STACK TEMP. HIGH	Thyristor heat sink temperature is high	40^0C
OVR CUR	Arc current value is crossed to set value	95 - 300A
OVR VOLT	Arc volts value crossed to set value	30 - 600V

2.1.3.2 Testing of Plasma aerosol generation system

About 5g of Strontium peroxide (SrO_2) powder was palletized. The pellet was rigidly fixed in to the wire feeder tube and kept in front of the plasma flame. Nitrogen is used as both plasma generating gas and the sheath gas. Input power is adjusted for a stable plasma jet. The torch was operated for two minutes. The pellet was melted and vaporized. The vapor is condensed and become aerosols by homogeneous nucleation or by heterogeneous nucleation on air molecules in the plenum chamber. The pneumatic valve separating the plenum chamber and aerosol chamber was closed after two minutes operation of plasma torch, such that aerosols are bottled-up in the chamber. The generated aerosols are analyzed using particle analyzer [2.8]. The number size distribution of SrO_2 aerosols is presented in Fig. 2.2. It shows that the Count Median Aerodynamic Diameter (CMAD) is 137nm with standard deviation σ_g =1.57. It is understood that, the torch is capable of producing particles from nano-meter to micrometer range of aerosols by vaporization and condensation route. Thus the torch is suitable for production of aerosols.

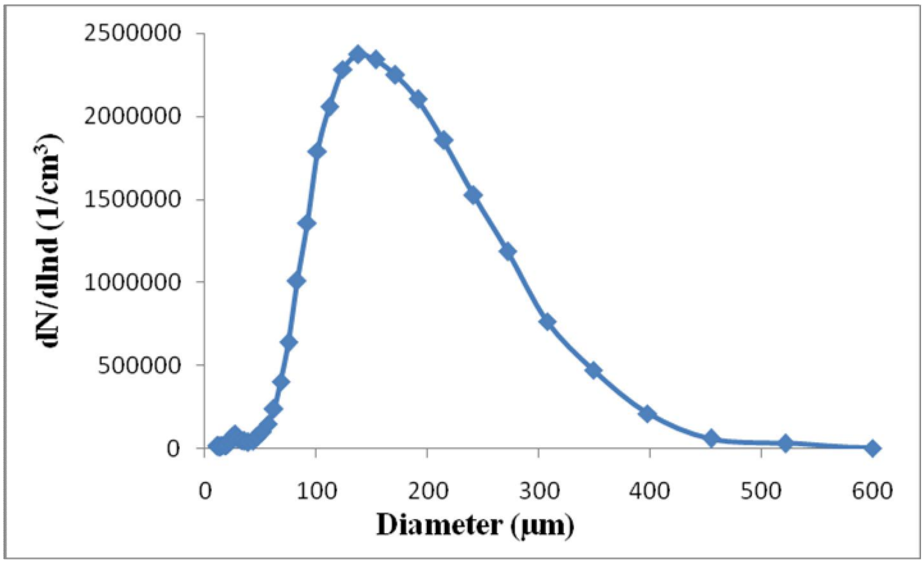

Fig.2.2 Number - size distribution of strontium peroxide aerosols.

2.1.4 Atomizer aerosol generator

The ATF has an aerosol generator (Model: 7.811, M/s Grimm aerosol generator, GmbH, Germany) for the production of test aerosols with defined reproducible features by atomization [2.9]. The atomizer gives wide range of aerosol concentration by changing the atomization pressure by varying the pump speed. The instrument is suitable for the generation of monodispersed and polydispersed aerosols like Polystyrene latex particle and DOP aerosols. The photograph of atomizer is shown in Fig. 2.3. Atomization is carried out in de-ionized water to which few drops of DOP or polystyrene latex particles are added. After the atomization, the aerosols are made to pass through a condenser (cooling the transport line on a thermostat filled with chilled water) followed by line heater (heating the transport line by using heating coil wounded over the line) and finally transported to the aerosol chamber. The ratio of aerosol solution and dispersant is maintained about 1.6:100, which is proved to give good number concentration of aerosols generated by atomization processes. Thus the aerosols are pumped into the chamber and they are made to suspend in a chamber where number - size distribution measurements are carried out [2.10]. The Number - size distribution of polystyrene latex particle of 1.3 µm generated with atomizer is shown in Fig.2.4. It is observed from figure that, the aerosol generated from atomizer have good concentration with CMD - 1.25 µm (σ_g=1.2), with the variation of 4% from test particle size.

Fig. 2.3 Photograph of atomizer

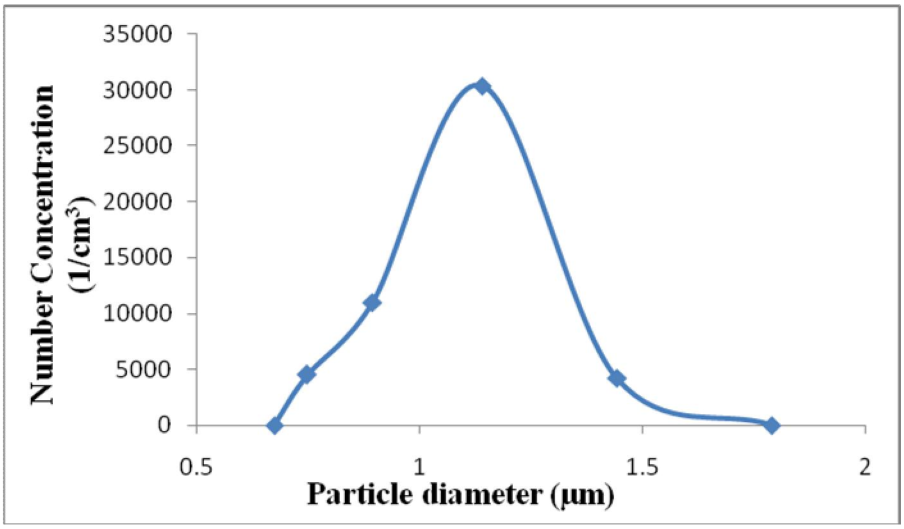

Fig. 2.4 Number - Size distribution of polystyrene latex particle.

2.1.5 Auxiliary systems

The ATF requires chilled water-cooling system, Gas flow system (Argon, Nitrogen, Air), pneumatic control systems, Humidity controller system, Exhaust system and gantry. The description and the function of these systems are described below.

2.1.5.1 Chilled water-cooling system

The Plasma torch body and plenum chamber portions are subjected to extreme conditions of temperature or heat flux. For sustaining the integrity of the system against thermal, electrical, mechanical stress, cooling water system is provided. The chilled water-cooling system consists of a 400-liter capacity water cooler (Make: M/s Bluestar, Chennai, India), a water pump (one hp), Polyvinyl chloride (PVC) water pipe lines, polyurethane (PU) pipe lines, valves and headers. A closed loop of water line is connected from the cooler unit to the torch body and the plenum chamber through the water pump and control panel. The hot water comes back from the torch to the cooler unit and gets cooled (18°C). The flow through the torch and plenum chamber is controlled with the help of return valve attached with flow meters. Temperature controller mounted on the panel displays the torch inlet and outlet water temperatures. Panel sends temperatures and flow rates data to PLC continuously using wireless data transmission.

2.1.5.2 Gas flow system

The choice of the plasma gas is generally based on the energy it can carry, reactivity and cost. Nitrogen gas is selected here as it is diatomic (more internal energy) and low cost. The plasma flame is generated by striking an arc with nitrogen as plasma generating gas. The plasma column is stabilized by gas flow stabilization method. The nitrogen is also flowing as an external cold layer of gas surrounding the arc column and forms as a sheath. A gas line made of PU tube is connected from the nitrogen cylinder to the torch body through control panel. Gas flow rates are controlled by flow control valve connected in the panel.

2.1.5.3 Pneumatic system, Exhaust system and Material handling system

A compressor (Model: KND-SPTC 9, M/s. Whitestar, Coimbatore, India) is used for the supply of compressed air to the pneumatic control valves. The gaseous outlet from sodium combustion cell, aerosol chamber, and aerosol diagnostic equipments is connected to an exhaust pipe, which has a vent outside the room. In order to clean the aerosol chamber, the top plate of aerosol chamber is removed by a 2.0 Ton gantry installed in ATF.

2.1.5.4 Humidity controller

The RH% is adjusted by using a humidifier (bubbling through water column or passing through silica gel column). Dehumidification of the chamber below 40% is achieved by blowing hot air inside the chamber while discharging the chamber air through exhaust. Thus RH% can be adjusted from 20% to 90% inside the chamber. The RH% is continuously monitored on-line by using Humidity monitor (capacitance type) (Make: Rotronics, INC, USA – HC2 series) inserted into the chamber.

2.1.6 On line data acquisition system

The schematic diagrams of various sensor locations and Data Acquisition System (DAS) are shown in the Fig. 2.5(a) and Fig. 2.5(b) respectively. The ATF is provided with sensors, (i) for the measurement of temperature (4 Nos., 3- K type and 1- S type), (ii) pressure (2 Nos.) and (iii) relative humidity (RH - 1No.). During the experiments, a control panel for receiving signal forms the sensors and wall mounted Personal Computer (PC) system for display the various parameters are also installed in ATF. The sodium combustion cell is equipped with two K - type of thermocouples and one pressure transducer to monitor the temperature of the sodium pool, atmosphere above the sodium pool, and the pressure inside the combustion cell respectively. The aerosol chamber is equipped with one K -type of thermocouple, one humidity meter and one pressure transducer to monitor the temperature, relative humidity and pressure inside the chamber respectively. One S- type thermocouple is connected in the plenum chamber of plasma torch to monitor the temperature of the atmosphere of plenum chamber. The PL100 system handles data through multi-channel I/O modules. The input module 8AIIS is used for the signals from sensors. A computer is used for the transmission of commands through an Ethernet cable. A window based software Supervisory Control And Data Acquisition (SCADA) is used for the storage, on-line display and retrieval of the data.

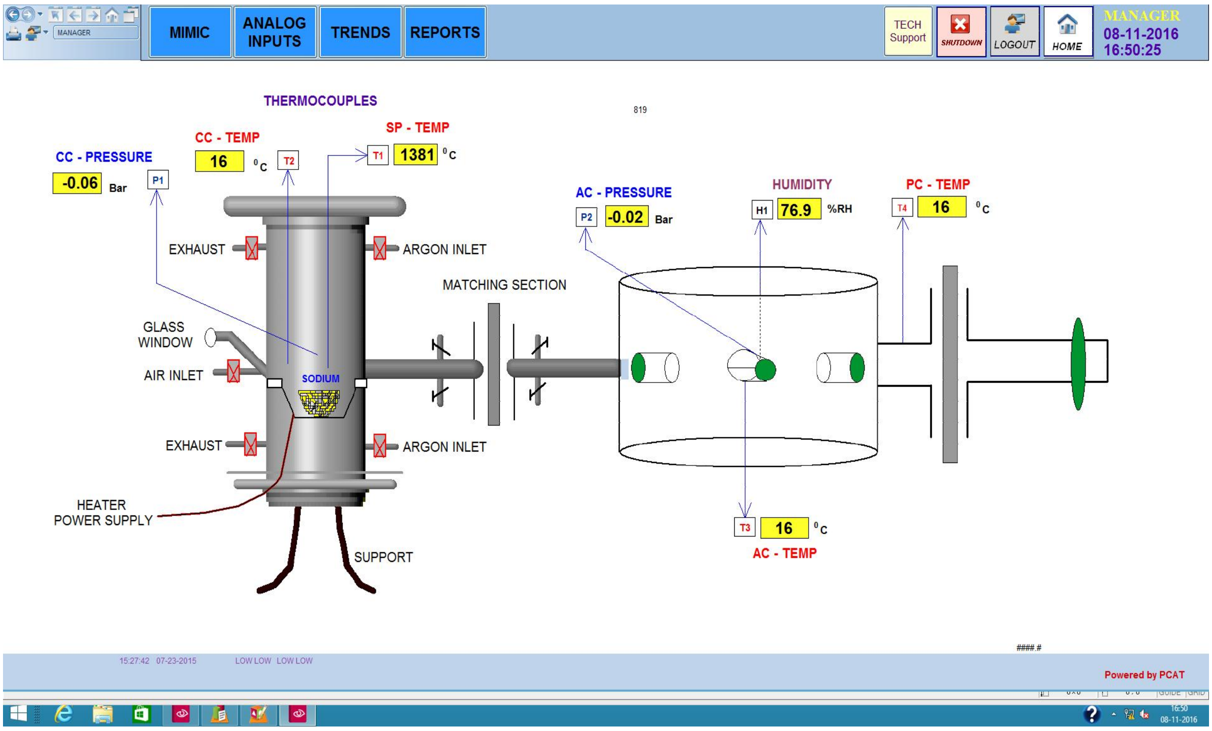

Fig. 2.5 (a) Schematic diagram showing various monitoring locations.

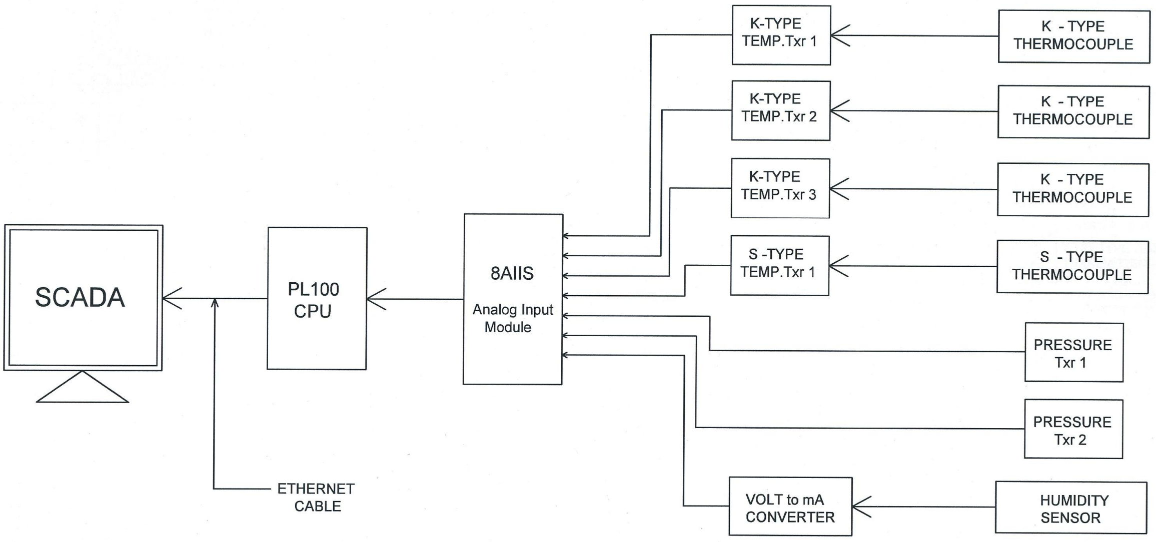

Fig. 2.5 (b) Schematic diagram of data acquisition system.

2.2 SILVERINA sodium Loop facility

The SILVERINA loop is housed in Fast Reactor Technology Group (FRTG), Indira Gandhi Center for Atomic Research (IGCAR), Kalpakkam. SILVERINA sodium loop was constructed and commissioned at Engineering Hall-I in IGCAR for conducting various experiments related to PFBR and general Sodium Technology. The objective of the

SILVERINA loop facility is to carry out the following experiments Viz. (i) sodium aerosol deposition in narrow annular gaps, (ii) calibration of sodium level probes, (iii) Radar type level probe testing and, (iv) sodium metal aerosol characterization in cover gas region. The flow sheet of SILVERINA loop is shown in Fig.2.6. The SILVERINA loop has dynamic sodium loop having (i) three cylindrical test pot namely Test Pot-1(TP-1), Test Pot-2 (TP-2) and Test Pot-3(TP-3), (ii) associated system viz. AC conductive type electromagnetic pump, cold trap, plugging indicator, sodium sampler, heater vessel, (iii) one storage tank (capacity - 1300kg), (iv) interconnecting pipe lines, bellows sealed valves, flow meters and , (v) cover gas circuits with diaphragm valves and vapor traps.

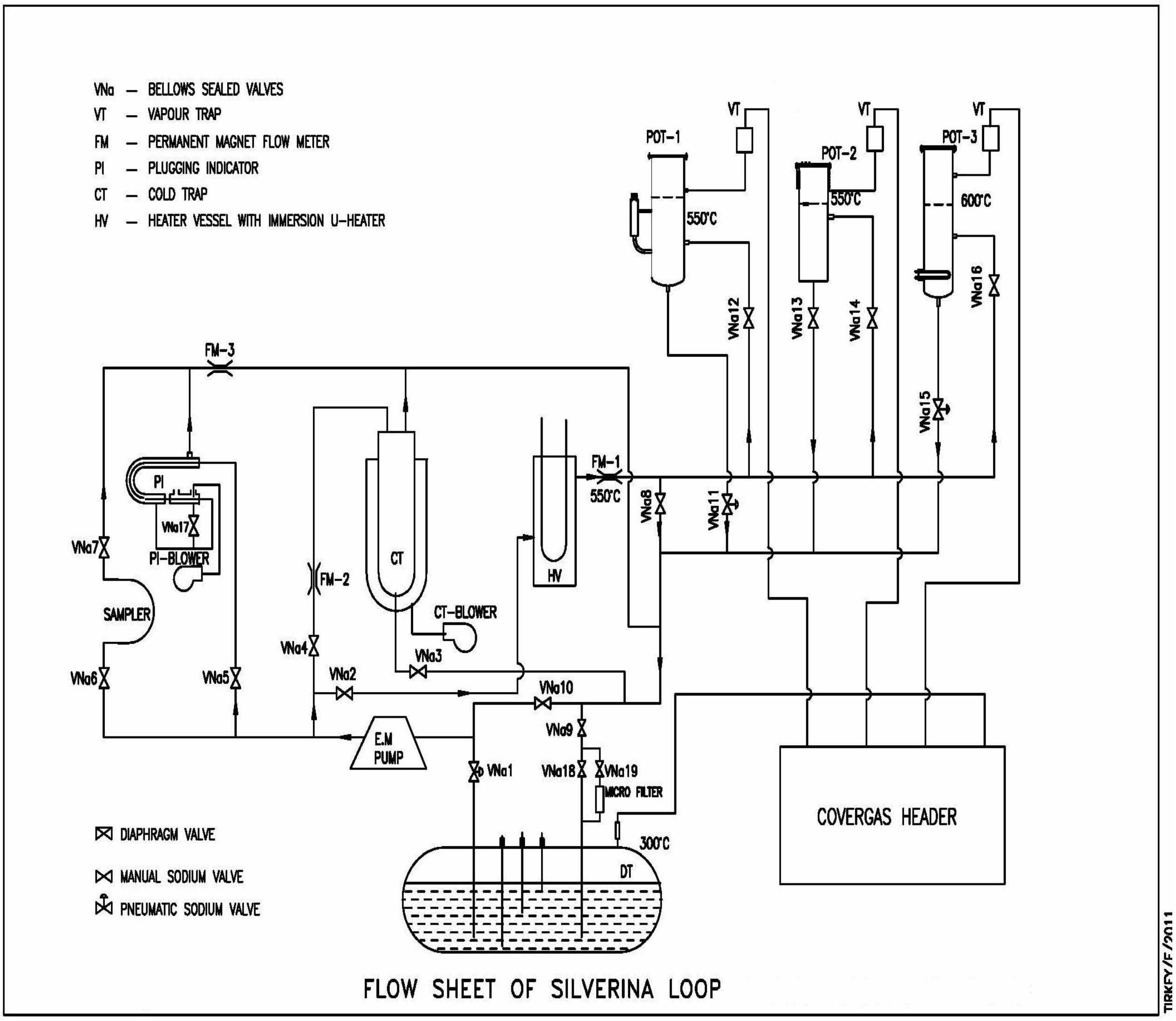

Fig. 2.6 Flow sheets of SILVERINA loop.

Sodium is filled in all the Test Pots from a storage tank. The internal diameter and length of storage tank are 1m and 2.03m respectively. The storage tank made of AISI304 and total volume is 1.79m^3. The design temperature of the sodium in dump tank is 540°C. All the three test pot are connected to a common pump loop, which is connected to storage tank. The detailed engineering description of SILVERINA loop is available in STD/99124/SR/3004/R-C [2.11].

2.2.1 Test Pot (TP-1) of SILVEINA loop

Test Pot -1 is the largest vessel in the SILVERINA loop. The TP-1 vessel is made with AISI304 and it has torishperical dish end. Sodium heating is provided by four number of Expanded Cold Region (ECR) and two number of Joint Cold Region (JCR) heaters fixed on the surface of vessel to keep the sodium in liquid state. In this two ECR and two JCR heaters will be in service and two ECR will be spares. The sodium aerosol characterization experiments are carried out in TP-1. The schematic diagramme of the TP-1 is shown in Fig.2.7. Some of the important design specifications are presented in Annexure-I of this Chapter. The top flange of TP-1 is provided with three nozzles for sodium level indications (low, middle and high level) and a spare nozzle (D1). The internal diameter of spare nozzle is 60.3mm. The sodium metal aerosol sampling is installed in the spare nozzle. The sodium level is maintained in the low level such that cover gas height is 820mm. The detail description of sodium metal aerosol sampling system is explained in the next chapter.

2.2.2 Test Pot (TP-3) of SILVEINA loop

The TP-3 vessel is made with AISI316 and it has torishperical dish end. TP-3 has two numbers of immersion U type heaters. Sodium heating is provided by four number of ECR heaters fixed on the surface of vessel to keep the sodium in liquid state. In this two heaters will be in service and two will be spares. The height and internal diameter of the TP-3 vessel are 1600 mm and 400 mm respectively and the height of the cover gas region is 750 mm.

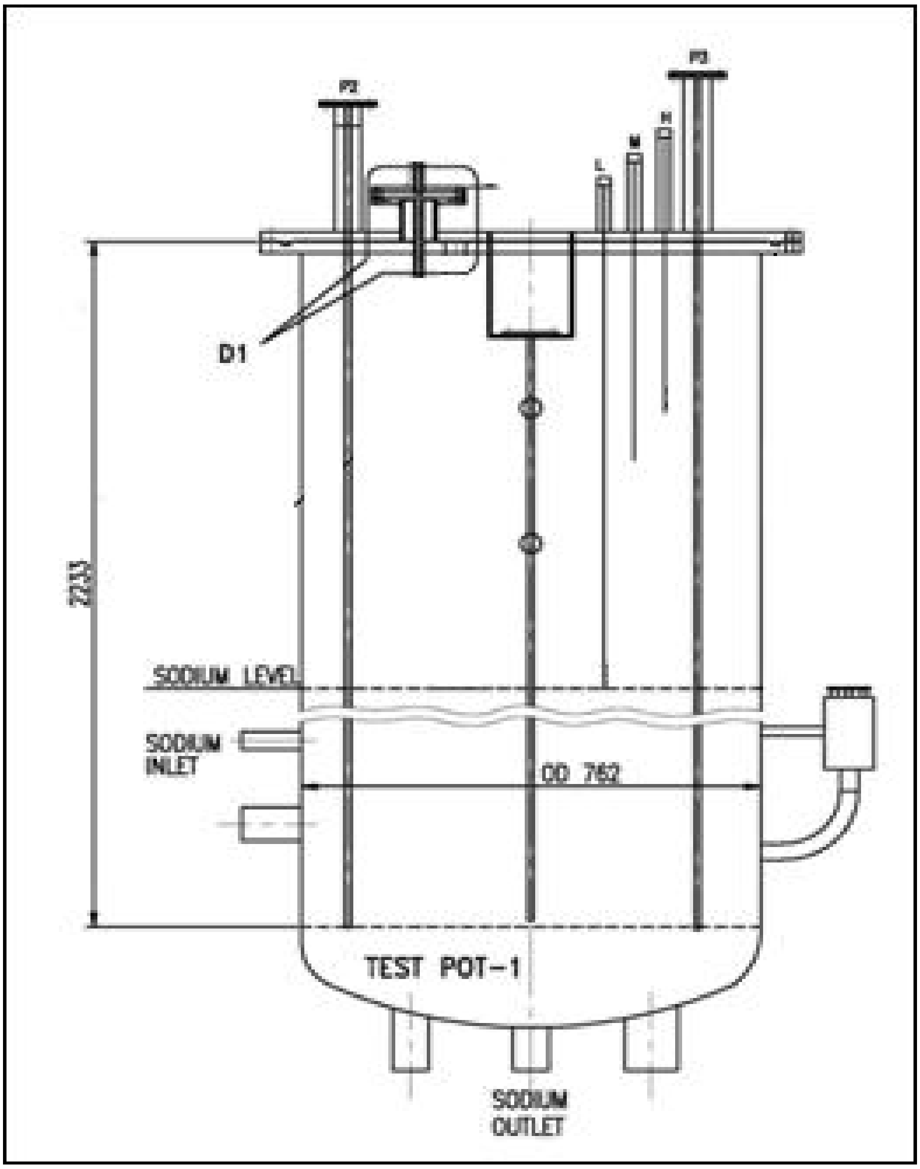

Fig.2.7 Schematic diagram of TP-1 vessel.

The schematic diagramme of the TP-3 is shown in Fig.2.8. The total volume and quantity of sodium holdup in TP-3 are 0.208 $m^3$and 0.11 m^3 respectively. The top flange of TP-3 is provided with three nozzles for sodium level indication (low, middle and high levels) and a spare nozzle. The spare nozzle is used for aerosol measurement. Some of the important design features of TP-3 are presented in Annexure-II of this chapter. To study the geometrical effect on sodium aerosol characteristics in the cover gas region, the experiments are also carried out in TP-3.

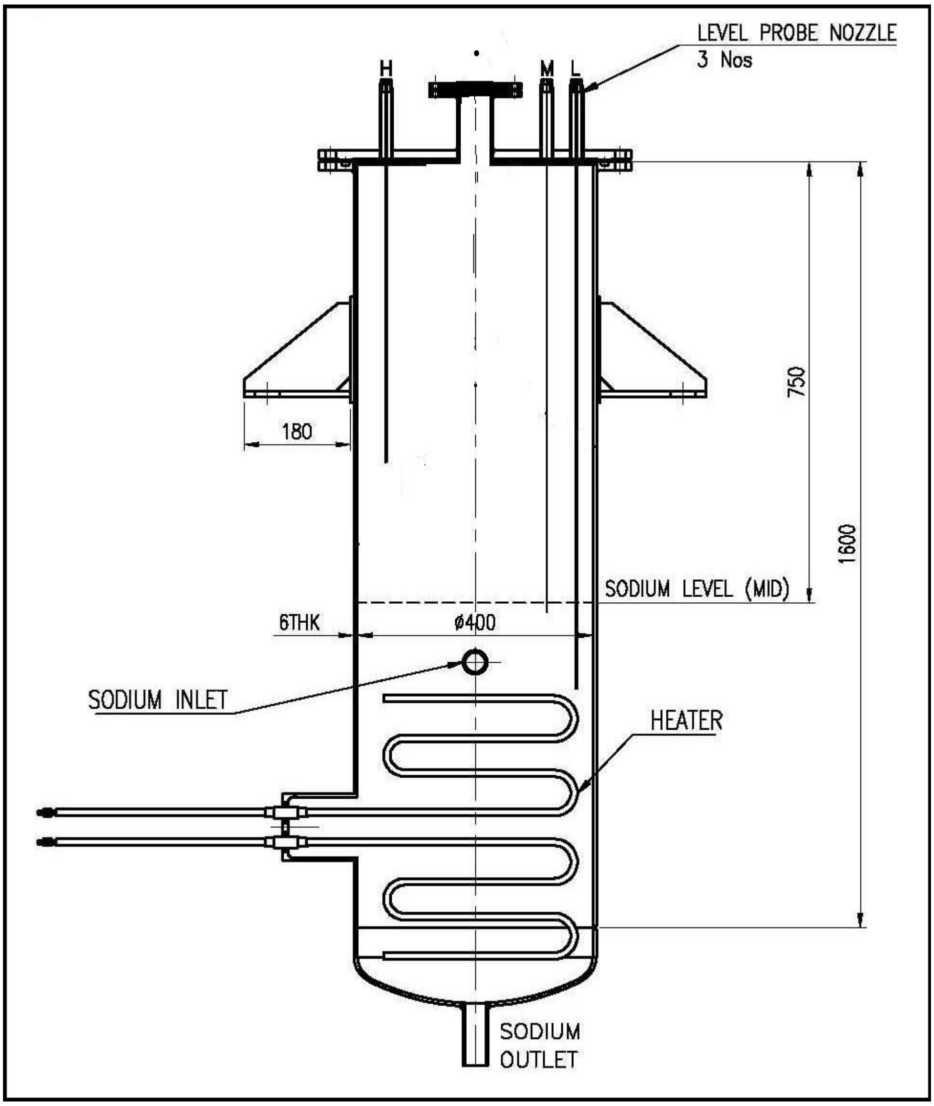

Fig.2.8 Schematic diagram of TP-3 vessel.

2.3 Aerosol Diagnostic Techniques

The aerosol measurement methods adopted in ATF and for sodium metal aerosol samples collected from TP-1 and TP-3 of SILVERINA loop are described in this section. The details of sodium metal aerosol sampling and characterization techniques developed is described in next chapter. There are two measurement approaches for characterization of aerosol viz., (i) passive sampling and (ii) real time sampling. The techniques that are used in the passive sampling include filtration, impaction, sedimentation and electrostatic collection. In these techniques samples are collected on a substrate and analyzed. The techniques adopted for real time sampling are light scattering, electrical mobility and impaction of particles on quartz crystals. In order to study wide range of particle sizes and their properties pertaining to SFR safety, both passive and real time sampling techniques are employed in ATF. Table 2.2 summarizes the details of aerosol measurement equipments used for characterization of sodium metal aerosol characteristics and other aerosols at ATF.

2.3.1 Passive sampling

Passive sampling is to sample the particles on a collection surface and then analyze the collected particles in the laboratory. Particle collection is usually achieved by deposition of the particles onto a filter/substrate. Impaction, sedimentation, electrostatic collection, thermal precipitation and diffusion are the major techniques used for the deposition of particles onto a collection surface. The major constrain of passive sampling is the time delay between sampling and the subsequent analysis. The instruments used at ATF for passive sampling are described below.

2.3.1.1 Filter paper sampler

The most common technique used for collection of aerosols from the air is filter paper sampling. This technique is used to determine the aerosol mass concentration by gravimetric analysis. A schematic diagram of filter paper sampler is shown in Fig. 2.9. Aerosol laden air is drawn through a sampling probe into the filter holder containing a suitable filtering medium. Here, a known volume of air or gas is made to pass through a filter, that passes the air or gas to flow, but retains all or a fraction of particles suspended in the flow. The flowing air first goes into flow measurement device such as a rotameter and after that into a pump, a rotary vane pump in this case. The filter paper used here is made of glass fibre with 25mm/47mm diameter. The filter is weighed before and after sampling. This technique requires isokinetic sampling, accurate weighing of filter paper, accurate measurement of sampling flow rate and sampling time.

Table 2.2 Aerosol diagnostic equipments and their operation principle.

Mode of sampling	**Sl. No.**	**Equipment**	**Principle**	**Make and Model**	**Aerosol Parameter**	**Size range (µm)**
Passive sampling	1	Filter paper sampler	Gravimetric	In house	Mass concentration	---
	2	Conductometer	conductivity of Ions	M/s Metrohm, Switzerland Model: 856	Conductivity	---
Real time sampling	3	Aerosol Dust Monitor	Light scattering	M/s Grimm, Germany Model: (1.108 and 1.109)	Count-size distribution and number concentration	0.3 - 20 (1.108) 0.2 - 32 (1.109)
	4	Mastersizer-S	Light scattering	M/s Malvern, UK Model: Mastersizer-S	Volume-size distribution / Mass-size distribution for known density	0.5 - 900 in dry and 0.05 - 900 in wet suspension
	5	SMPS+C+E	Electrical mobility	M/s Grimm, Germany Model: 5.403	Count-size distribution and particle collection	0.005 - 0.35
	6	ELPI	Impaction & Electrical	M/s Dekati Ltd., Finland Model: 97 2E	count-size and charge-size distribution	0.03 - 10

The filtration medium in the holder is held in a passive seal to constrain the air drawn by the sampling pump to pass through the filter. The seal is provided using O-ring or gasket of material that does not damage the filter paper. Typical filters used for aerosol sampling consist of glass, cellulose or plastic fibers, porous membrane or poly carbonate pore materials. An analytical balance with an accuracy of 0.1 mg (Model No.GR 200, M/s AND Corporation, Japan) was used for the gravimetric analysis. Aerosol sampling was carried out for 1 minute with a flow rate of 5lpm/10lpm. The cumulative experimental errors associated with measurement in time, flow rate and mass is nearly ±7-10%. A photograph of the filter paper sampler used in current research work is shown in Fig 2.10. The advantage of this method is that the sample can be used for further analysis. The mass concentration is obtained as $M_{col} = M_{conc} .f . t$, where M_{col} = mass collected in the filter paper in mg, M_{conc} = mass concentration in $mg.m^{-3}$, Flow volume $(f*t) = 0.01\ m^3$. (1 minute sampling for 10lpm flow rate).

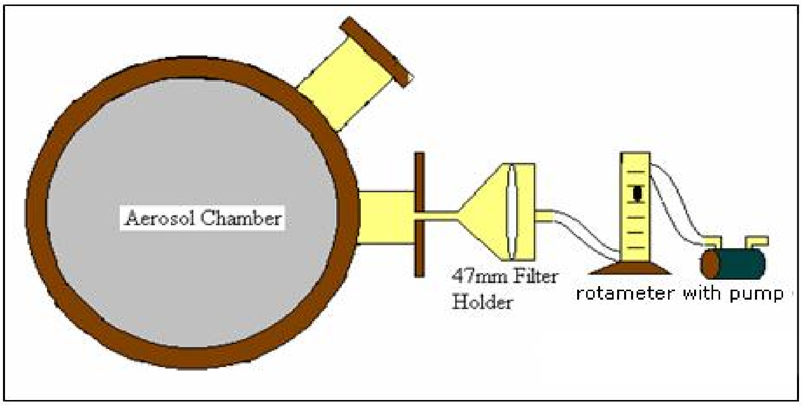

Fig 2.9 Schematic of filter paper sampler

Fig 2.10 A photograph of filter paper sampler

2.3.1.2 Conductometer

The measurement of sodium aerosol mass concentration is carried out by using Conductometer (M/s Metrohm, 856 conductivity module, Switzerland) [2.12]. The photograph of the instrument is shown in Fig.2.11.

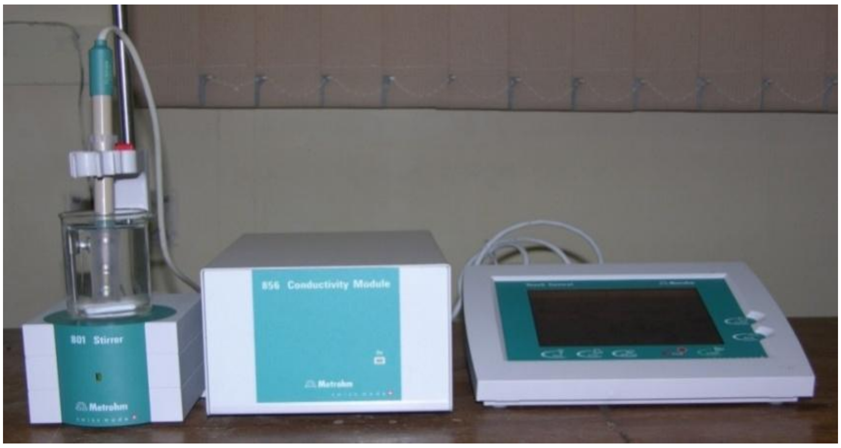

Fig.2.11 Photograph of Metrohm Coductometer.

The principle by which instruments measure conductivity is simple - two plates are placed in the sample, a potential is applied across the plates (normally a sine wave voltage), and the current is measured. Conductivity (G), the inverse of resistivity (R) is determined from the voltage and current values according to Ohm's law. The mass of sodium aerosols is measured by transferring them into a water medium (to become NaOH) and measuring the change in conductivity of the NaOH solution by using Metrohm Conductometer. Sodium aerosol mass concentration in solution is estimated by using a pre-established calibration graph between conductivity vs concentration of NaOH [2.13]. The calibration graph between sodium aerosol mass concentrations (mg/l) vs. conductivity (µS/cm) is shown in Fig.2.12 and it is found to follow a linear fit. Using this graph the trapped sodium mass concentration in the solution is determined. The conductivity of DM water is around 1 µS/cm. The conductivity of NaOH is determined after subtracting the background conductivity of DM water (1µS/cm). Once we know the conductivity of the solution then, by using the calibration graph the quantity of sodium aerosol concentration tapped in liquid medium is estimated.

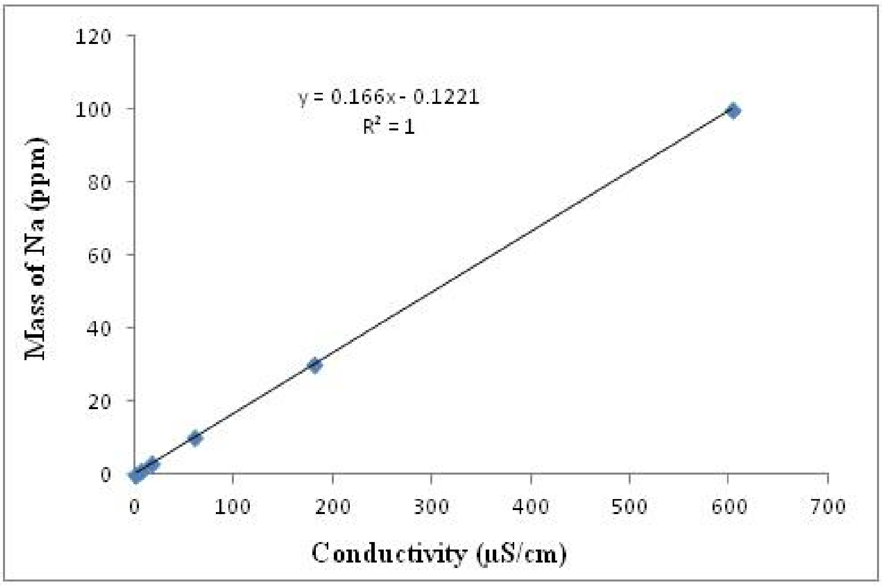

Fig. 2.12 Sodium mass concentration Vs conductivity.

After knowing the sodium mass concentration in solution, by adopting suitable corrections for the volume of the sample (flow rate and sampling time), the sodium aerosols mass concentration is calculated as.

Sodium mass concentration (mg/l) = (M (mg/l)*V (l))/ (f (lpm)*t (m))

where “f” is sampling flow rate in lpm, “t” is sampling time in minutes, “M” is the mass concentration of sodium in solution in ppm or mg/l and "V" total volume of liquid used for collection of sodium aerosol in liter.

2.3.2 Real time sampling

The on-line sampling is carried out by using dynamic measuring devices. The techniques that are used in the real time sampling are light scattering, electrical mobility, impaction of particles on quartz crystals and impaction coupled with charge measurements. It is important to mention here that all the real time instruments are periodically tested for its performance and accuracy of measurements by using standard polystyrene latex particles.

2.3.2.1 Optical measurement technique

Light scattering and extinction by small particles suspended in gases are used to obtain information on the concentration and size distribution of the particles. The instrument based on these principle are of two kinds viz. (i) light scattering and extinction by single particles and (ii) light scattering and extinction by an assembly of particles. Devices working in this technique, with necessary electronics and automation are employed for real-time measurement. Both scattering and absorption characteristics of a particle are described with a complex refractive index $m = n - in'$ where the real part 'n' describes scattered light characteristics and the imaginary part 'n'' describes that of absorption. Also, in the case of scattering, the scattered angle is inversely proportional to the size of the particle. By measuring the forward angle of scattering and intensity of the scattering light, both size distribution and mass concentration can be determined. The ATF is equipped with two optical instruments viz (i) Aerosol Dust Monitor (single particle counter) and (ii) Mastersizer – S (ensemble particles counter).

Aerosol dust monitors (Models 1.108 and 1.109 of M/s GRIMM Aerosol technik, GmbH, Germany) [2.14]: The schematic diagram of Aerosol dust monitor is shown in Fig. 2.13. It has a sample drawing unit through a volume controlled pump at a rate of 1.2lpm. The scattered signal by a particle is collected on a mirror and transferred to a recipient diode. The signal from the diode, after reinforcement, is analyzed by a multi channel analyzer. The scattered angle and intensity of the scattered light are the measure of particle size and number of particles respectively in that size range. The monitor gives the spectrum from 0.3 - 20µm in 15 channels in terms of number of particles/liter in the case of model number 1.108 and in the case of model number 1.109, the monitor gives the spectrum from 0.22 - 32 µm in 31 channels in terms of number of particles/liter. The aerosol dust monitor is otherwise called as an Aerosol Spectrometers. The instrument has data acquisition system and windows based software for control and operation of the instrument and also for the analysis of particle spectrum. The aerosol dust monitor is connected with aerosol chamber in one of the port through a 1:100 dilutor (Model No.:1.159 for 1.2lpm, M/s Grimm Aerosoltechnik, Germany).

The dilutor is used here to take care of both excess concentration of aerosol and excess pressure of 4kPa above ambient atmosphere.

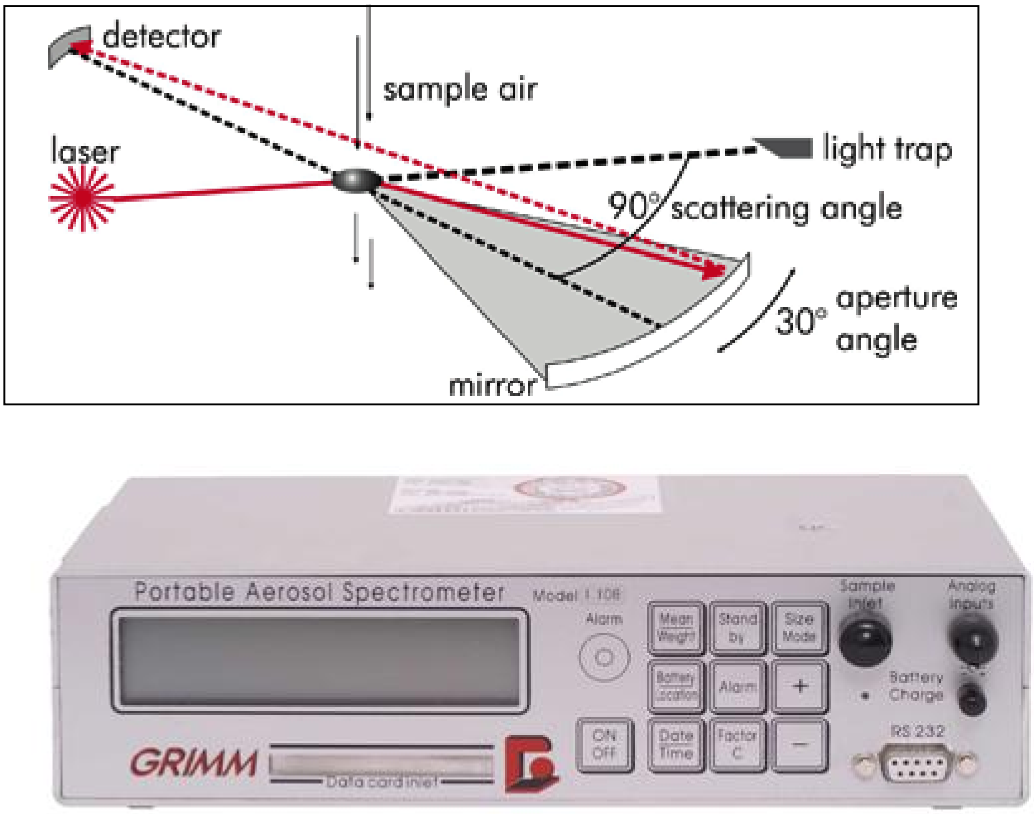

Fig. 2.13 Schematic representation and photograph of single particle counter.

Mastersizer-S (M/s Malvern Instruments Ltd., UK) [2.15]: The Mastersizer uses the principle of ensemble diffraction technique. A photograph of Mastersizer instruments is shown in Fig. 2.14 and a schematic representation of ensemble diffraction of the instrument is shown in Fig. 2.15. A laser beam is expanded and then collimated into a beam of several mm diameter (2 mW He-Ne laser, 633 nm, with 18 mm beam diameter), which passes through the particle cloud. Particles in the beam scatter light in all directions. A receiving lens is used to focus both the transmitted beam and forward scattered beam onto a detector located at the focal plane of the lens. The transmitted light is focused to a point on the optical axis while the diffracted light form a series of concentric rings (Fraunhofer diffraction pattern). As the receiving lens performs a Fourier transform on the scattered light, light scattered at a given angle ‘θ’ by a particle located anywhere in the illuminated sample volume will be focused at a same radial position in the detector array. The Mastersizer has 48 detectors arranged in a conical form and the sampling time for all 48 detectors together is about 10μs. The computer readout time of the data is approximately 2ms. The results will be displayed within a second. The instrument is provided with a liquid flow cell and an aerosol flow cell and these units are useful for the measurement of particle size distribution in liquid and air medium respectively.

Fig.2.14 Photograph of Mastersizer instrument

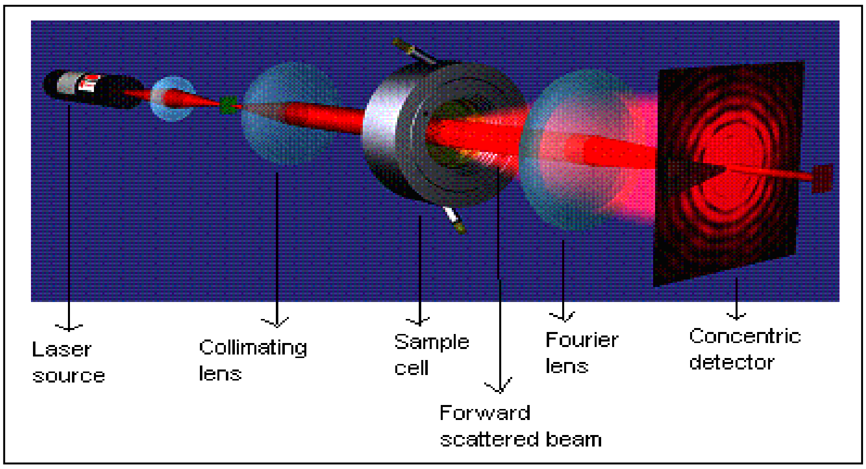

Fig. 2.15 Schematic representation of ensemble diffraction.

In liquid flow cell, the sampling liquid (dispersant) with suspended aerosols is made to circulate across the laser beam. Particles in the beam scatter light in all directions. By measuring the scattered light intensity spectrum at an angle ‘θ’ and obscuration of the laser beam by the aerosol and comparing this to a background measurement taken under identical conditions with no aerosol present, gives the particle size distribution. The Mastersizer measures the volume-size distribution of particles in the laden volume of liquid medium from 0.05 – 900 μm. To measure the particle size distribution suspended in air medium, the Mastersizer is integrated with aerosol chamber using aerosol flow cell. Aerosol flow cell is a hallow stainless steel pipe with rectangular cross section of 14.3 mm width (standered length for optical path specified by Mastersizer) and 103mm breath and it has a length of 730mm. Suitable opening are made in the side plates of the flow cell and laser window are connected. The aerosols are drawn through the aerosol flow cell whose optical window is aligned with the laser path of Mastersizer (within ± 0.1 deg.). A constant air flow (~ 0.5lpm) through aerosol flow cell from the aerosol chamber is maintained by a pump to avoid turbulence and giving laminar flow of the aerosol in flow cell. Performance test of the aerosol flow cell was carried out with polystyrene latex particles of diameter 2.799 μm and methylene blue aerosols [2.4]. The Mastersizer measures the volume-size distribution of particles in the laden volume of air from 0.5 – 900 μm.

2.3.2.2 Sequential Mobility Particle Sizer + Counter + Electrostatic precipitator [2.8]

The Sequential mobility particle Sizer **(**SMPS) is a real time aerosol monitoring instrument for size spectrum and number concentration of the nanoparticle aerosols. The system is a combination of Differential Mobility Analyzer (DMA), Condensation Particle Counter (CPC) and 32-bit software program (M/s Grimm Aerosol technik, Germany). The SMPS operates by charging particles and separating them based on their mobility passing between electrodes. Separated particles are then counted to count size distribution. The Electrostatic Precipitator is a device, which would collect particle on a substrate when it is attached at the exit of the DMA instead of CPC. The schematic diagram of the system SMPS+C is shown in Fig. 2.16. The photograph of the SMPS used in ATF is shown in Fig.2.17.

Differential mobility analyzer (DMA): The system used in our measurement is Universal DMA, where long-range classifier or medium range classifier can be mounted on a single bottom base depending upon our requirement. The experiments are conducted with LDMA and it can measure particles from 10-1083nm with a particle concentration up to 10^{10} particles per liter. The particles are made to pass through a selected impactor nozzle and properly neutralized with Alpha particles (Am-241 source), then flows into the DMA for electrostatic classification. The DMA contains two concentric cylinders. The inner cylinder is maintained at controlled negative potential and outer cylinder is grounded. The sample air (1.5lpm) and sheath air (3lpm) are introduced into the annular space of the cylinders. The classification occurs based on electrical mobility. The negative field causes the positively charged particles attracted through the sheath air to the inner cylinder while negatively charged particles are flown towards outer cylinder. As the potential in the cylinder varies, only the particles with matched mobility could enter into the collection nozzle and they are flown into the CPC (refer DMA diagram).

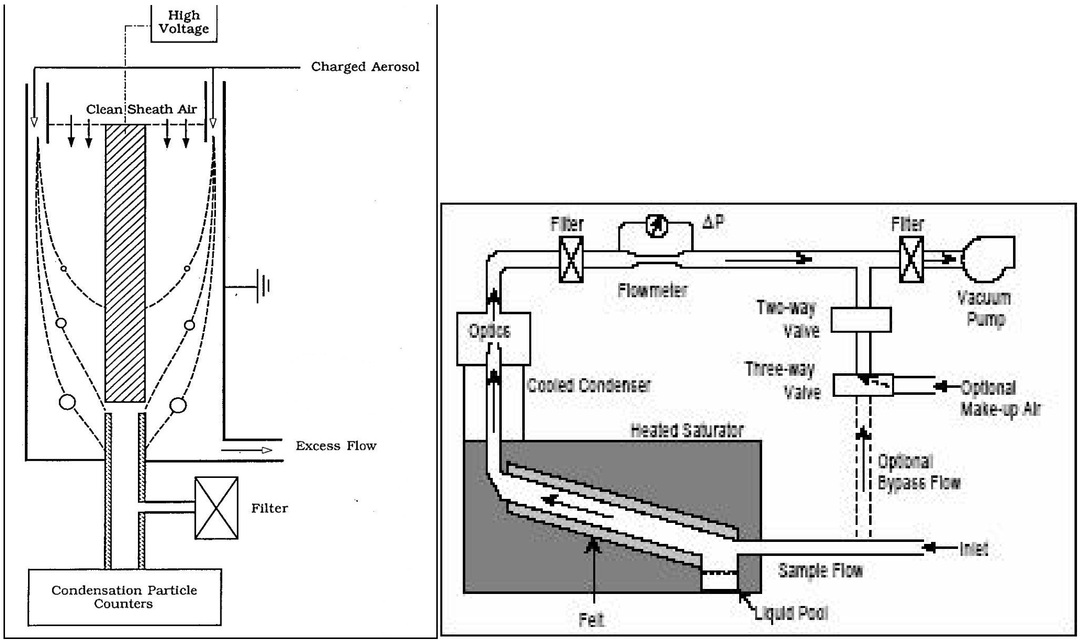

DMA CPC

Fig. 2.16 Schematic representation of the SMPS+C.

Condensation particle counter (CPC): The system operates with a flow rate of 1.5lpm, up to particle concentration of 10^7 particles per liter. The sample flow is made to pass through a saturator where it crosses a heated (35°C) N-butyl alcohol. Particles and vapor then flow into the cooling condenser (10°C), where supersaturated vapor condenses on the particles. In this process, all the particle size is increased. The increased size particles are counted by a laser particle counter.

Fig. 2.17 Photograph of the Sequential Mobility Particle Sizer

The SMPS operates with a 32-bit Grimm software program. The program is used for the operation and control of the instrument and used for data scanning. Further it is used to calculate particle size distribution, surface area distribution, volume distribution and mass distribution. The SMPS is integrated with aerosol chamber through a 3″ port and used for the measurement of particle size distribution of inactive fission product aerosols generated using plasma torch.

2.3.2.3 Electrical Low Pressure Impactor (Model 97 2E, M/s Dekati Ltd., Finland)[2.16]

The schematic diagram of Electrical Low Pressure Impactor (ELPI) is shown in Fig. 2.18. ELPI consists of 13 stage cascade impactor with cut sizes between 30nm and 10µm. Particle inertia is an important property that is utilized for the collection of particles in this technique.

The principle and operation of a typical impactor is discussed elsewhere [2.17]. In ELPI, each stage of impactor is electrically connected with electrometer. The impactor stages are electrically insulated and the current signal from each impactor stage is measured with sensitive electrometers. Aerosols are charged with the help of corona charger and then made to pass through the impactor. The uppermost impactor stage acts as a pre-cut but has no electrical detection. The particle number concentration in each size class (impactor stage) can be calculated from the measured current signals obtained from the deposited aerosols. The ELPI operates at a flow rate of 10lpm and integrated with aerosol chamber through 25mm sampling head. The instrument is provided with dilutor 1:100 and provision is available to sample the aerosols with and without connecting dilutor. The ELPI measures count-size distribution when the instrument is operated with charger ON condition where the particles are charged by corona charger before entering into the classifier.

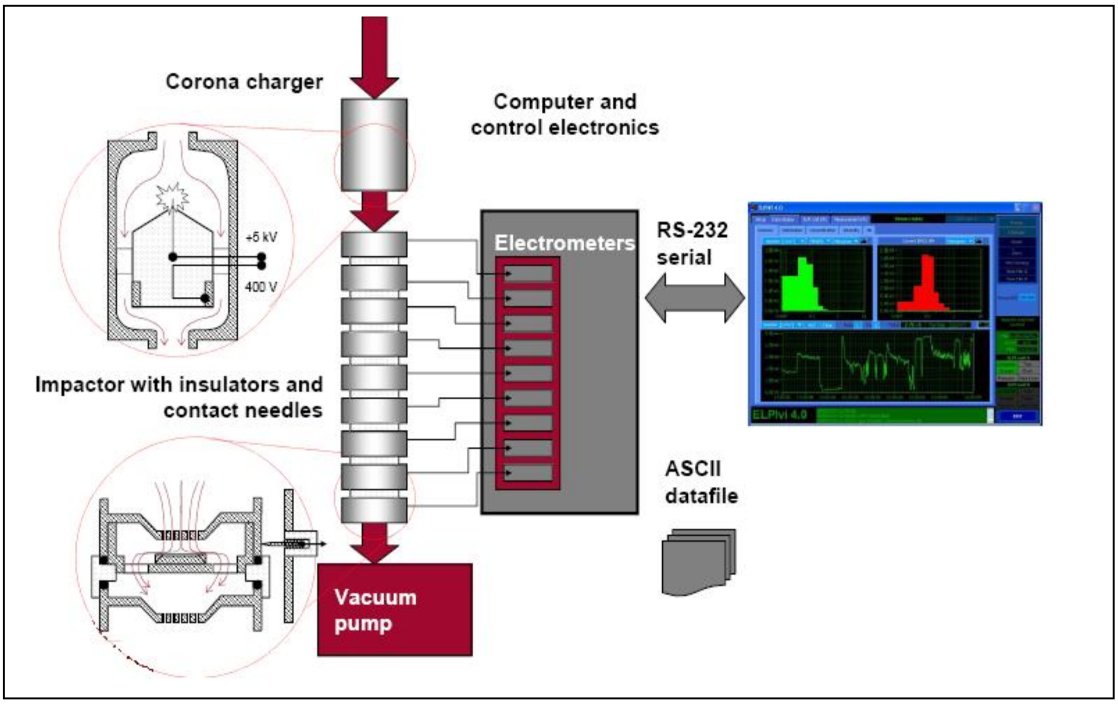

Fig. 2.18 Schematic diagramme of Electrical Low Pressure Impactor

The instrument measures the charge-size distribution of aerosols when the instrument is operated with charger OFF condition i.e. the charges associated with particles before entering into the sampler will be measured as charge-size distribution. There exists an in-built software for the measurement of charge-size distribution. The macros calculate both count-size distribution and charge-size distribution, for which the equipment must be operated with equal sampling time of charger ‘ON’ and charger ‘OFF’ condition. The salient feature of ELPI such as (i) charging efficiency function, (ii) measurement of uncertainty in the charge measurement and (iii) measurement of number-size distribution for bi-polarly charged aerosols in particular to positively charged aerosols are briefed explained elsewhere [2.17].

2.4 Summary

In this chapter, the various engineering aspects of ATF, aerosol generation systems, and various subsystems are described. The description of TP-1 and TP-3 of SILVERINA loop facility are also described in this chapter. The detailed description of aerosol diagnostic equipments used for characterizing sodium metal aerosols sampled from SILEVRINA loop and in current research work is found to be versatile and fulfill the requirements.

ANNEXURE-I

DATA SHEET OF TEST POT-1

DESIGN PRESSURE (INTERNAL) : 1.0 kg/cm^2

(EXTERNAL) 1.0 kg/cm^2

DESIGN TEMPERATURE : 550 °C

DESIGN BASIS : ASME SEC.VIII DIV-I

SIZE : ID – 750 mm, THICKNESS – 6 mm

HEIGHT - 2210 mm

VOLUME OF POT : 1.04 m^3

SODIUM HOLD-UP : 0.512 m^3

MATERIAL : AISI 304

DISHED END : TORI SPHERICAL AT BOTTOM

TOP CLOSURE : FLAT PLATE FLANGE

WEIGHT (EXCLUDING SODIUM) : 400 kg

TESTS:

DYE PENETRANT CHECK : ON ALL NEW WELD JOINTS

(ROOT & FINAL PASS)

RADIOGRAPHY : 100% ON NEW BUTT WELD JOINTS

PNEUMATIC TEST : 2.0 kg/cm^2 FOR 30 MINUTES

LEAK TEST : SOAP BUBBLE TEST

HELIUM LEAK TEST : LEAK RATE < 10^{-8} std cc/sec

ANNEXURE-II

DATA SHEET OF TEST POT-3

DESIGN PRESSURE (INTERNAL)	:	2.0 kg/cm^2
(EXTERNAL)		FULL VACUUM
DESIGN TEMPERATURE	:	600 °C
DESIGN BASIS	:	ASME SEC.VIII DIV-I
SIZE	:	ID – 400 mm, THICKNESS – 6 mm
		HEIGHT - 1600 mm
VOLUME OF POT	:	0.208 m^3
SODIUM HOLD-UP	:	0.11 m^3
MATERIAL	:	AISI 316
BOTTOM CLOSURE	:	TORI SPHERICAL DISHED END
TOP CLOSURE	:	FLAT PLATE FLANGE
WEIGHT (EXCLUDING SODIUM)	:	150 kg
TESTS:		
DYE PENETRANT CHECK	:	ON ALL NEW WELD JOINTS
(ROOT & FINAL PASS)		
RADIOGRAPHY	:	100% ON NEW BUTT WELD JOINTS
PNEUMATIC TEST	:	5.0 kg/cm^2 (g)
LEAK TEST	:	SOAP BUBBLE TEST
HELIUM LEAK TEST	:	LEAK RATE < 10^{-8} std cc/sec

2.5 References

2.1 R. Baskaran, T. S. Selvakumaran, and V. Subramanian, (2004), “Aerosol Test Facility for Fast Reactor Safety Studies”, Indian Journal of Pure and Applied Physics, Vol. 42, 873-878.

2.2 S. Chandramouli, S. Sakthivel, P. Vijayamohana Rao, K. Gurumoorthy, K. K Rajan, P. Kalyanasundaram, and G. Vaidyanathan, (2006), "Commissioning and Operation of SILVERINA sodium loop", OPENUPP-2006, Nov. 13-15, BARC, Mumbai. Proceedings of National Conference on Operating experiences of Nuclear reactors and power plants 203-209.

2.3 K. Willeke and P.A. Baron, (1993), "Aerosol Measurement: Principles, Techniques, and Applications", Van Nostrand Reinhold, New York.

2.4 R. Baskaran, V. Subramanian and T. S. Selvakumaran, (2006), “Real time measurement of aerosol size distribution using MASTERSIZER”, Indian Journal of Pure and Applied Physics, Vol. 43, 576 - 580.

2.5 C. F. Clement and M. Julian Dolias, (1987), "Sodium aerosol formation in argon flow over hot sodium", Theoretical Physics Division, Harwell laboratory, Oxfordshire OX11 ORA. AERE R 12489.

2.6 E. Pfender and R. M. Young, (1986), "Generation of ultrafine particles in thermal plasmas", 2nd International conference on Aerosol formation and reactivity, Berlin.

2.7 R. M. Young and E. Pfender, (1985) “Generation and Behaviour of Fine Particles in Thermal Plasmas-A Review”, Plasma Chemistry and Plasma Processing, Vol. 5, 1 - 37.

2.8 GRIMM Aerosol Technik Manual 5.400, 5.500 and 5.5461, SMPS+C+E, Dorfstrabe 9, 83404, Ainring, Germany. – www.GRIMM-aerosol.com.

2.9 GRIMM Aerosol Technik, Particle Generator Manual, Model - 7.811, Germany - www.GRIMM-aerosol.com.

2.10 Amit Kumar, V. Subramanian, R. Baskaran, J. misra and P. Chellapandi, (2010), “A study on Aerosol Charging in Generation Mechanism”, IASTA-2010, 24-26, March, 2010, Bose Institute, Darjeeling, INDIA.

2.11 S. Chandramouli, G. Vijayakumar, V. A. Sureshkumar, K. K. Rajan, G. Elumalai, and M. Rajan, :Silverina A Multipurpose Sodium Loop Safety Report", STD/99124/SR/3004/R-C.

2.12 Manual of Metrohm, 856 conductivity module, Switzerland - www.metrohm.com

2.13 http://myweb.wit.edu/sandinic/Research/conductivity%20v%20concentration.pdf, May 2013.

2.14 GRIMM Aerosol Technik Manual, OPC (1.108 and 1.109), Grimm Germany. – www.GRIMM-aerosol.com.

2.15 Set of Operating Manuals, MASTERSIZER-S, M/s Malvern Instruments Ltd., Spring Lane South, Malvern, Worecestershire, WR14 1XZ, UK.

2.16 ELPI user Manuals Ver.4.02, (2007), Dekati Ltd., Finland.

2.17 Marko Marjamaki, Jorma Keskinen, Da-Ren Chen and David Y. H. Pui, (2010), "Performance evaluation of the Electrical Low Pressure Impactor (ELPI)", J. Aerosol Sci., Vol. 31, No. 2, 249-261.

CHAPTER - III

DEVELOPMENT AND VALIDATION OF SODIUM METAL AEROSOLS CHARACTERIZATION TECHNIQUE

3.0 Introduction

In the normal operating condition of SFR, evaporation of sodium vapor from the hot sodium pool surface and subsequent condensation of vapors results in the formation of sodium metal aerosol within cover gas space [3.1]. Sodium metal aerosols suspended in cover gas are in liquid phase. The determination of sodium metal aerosols characteristics from a cover gas region requires special sampling procedure, in which sampling is to be carried out without exposing the metal aerosols to atmosphere (the sodium aerosols undergo chemical changes and properties would get modified when exposed to atmosphere) [3.2]. It is to be noted from the literature that, there were several techniques used for the characterization of sodium metal aerosol characteristics in cover gas region (size distribution and mass concentration) viz: Andersen Impactor, laser light based techniques, sodium ionization detector, and SS mesh filter. But, it is important to adopt suitable method by drawing aerosols from the cover gas region and trap them in a suitable medium without exposing them to the atmosphere, to determine the characteristics of the sodium metal aerosols. Jackson et al., 1993, Minges, J. & Schutz, W. 1991 & 1993, and Yamamoto, H. et al., 1991 in their studies, used Andersen multistage impactor [3.3, 3.4, 3.5,& 3.6]. Andersen multistage Impactor determines the mass-size distribution cumulatively over a period of time. By using stainless steel wire mesh filter (filtration technique), Newson et. al., 1993, Yamamoto et. al., 1991, Yoshiaki & Takahashi 1980, Yoshiaki & Yamagishi, 1982 and Frukawa et al., 1984, determined the size distribution based on sieve size of stainless steel wire mesh filter [3.7, 3.6, 3.8, 3.9 & 3.10]. In the above methods, it is observed from the experimental details that, the measurements were carried out by keeping the sampling unit/system in the atmospheric condition. Glockling et al., 1991 used

Malvern 2600C (based on Franhofer diffraction) and Dantec particle dynamic analyzer for characterizing sodium metal aerosol in the cover gas region, but the results obtained in both techniques were found different for the same experimental condition [3.11]. In addition to the above detection system, Laser mist concentration meter was also employed for sodium metal aerosol mass concentration measurements by Yoshiaki and Takahashi 1980, Yoshiaki and Yamagishi, 1982 [3.8 & 3.9]. In the above three investigations, the methodologies adopted in their measurements were not dealt in details. Roberts, et al., 1995 used a technique to collect the sodium aerosol and measured mass concentration by using atomic absorption spectroscopy and size distribution by using laser scattering technique [3.12]. However, the detailed sampling and analysis procedures are not described in this technique. It is to be noted that, the sodium metal aerosols present in cover gas region are liquid metal aerosols (liquid phase). If the sampling is carried out in atmospheric condition, the sodium aerosols undergo reaction with atmospheric constituents (oxygen, moisture and CO_2) to form various compounds like oxide, hydroxide and carbonate resulting changes in both physical and chemical characteristics [3.13]. Hence, the measurement in open atmosphere could not be a true evaluation of sodium metal aerosol characteristics in the cover gas region. In order to characterize the sodium metal aerosols, it is required to have in-situ sampling and suitable analysis technique. In this chapter, the development of experimental methodology for characterization of sodium metal aerosol in cover gas region and validation of methodology in a sodium loop SILVERINA facility at Fast Reactor Technology Group (FRTG), IGCAR are described [3.14].

3.1 Experimental methodology

The methodology for characterization of sodium metal aerosols is developed in ATF [3.15, 3.16]. The methodology involves: (i) sodium metal aerosol generation in combustion cell, (ii) sodium metal aerosols are drawn from the combustion cell are allowed to get trapped in liquid paraffin oil medium without exposing them to atmosphere, (iii) determination of mass concentration by using conductivity measurement technique and (iv) determination of size distribution carried out using Malvern Mastersizer.

3.1.1 Sampling technique

The details of sodium metal aerosol generation in combustion cell are described in Chapter - II. Methodology for the determination of size distribution and mass concentration of sodium metal aerosol has been evolved and it is successfully carried out in ATF. A schematic diagram of sodium aerosol sampling system adopted in ATF is shown in Fig.3.1. The sampling system consists of combustion cell and sampling line, wire heater and temperature controller, gas washing bottles, flow meter and gate valve. The dimension of gas washing bottle are 25cm length and 8cm diameter. About 5-10g of sodium is taken in a crucible and heated in the sodium combustion cell under argon environment.

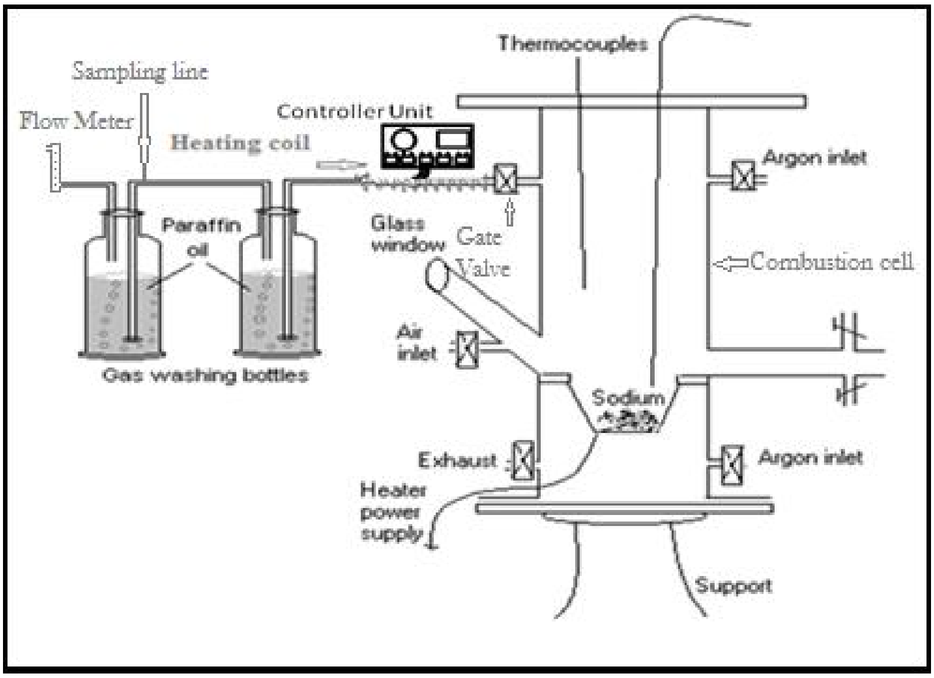

Fig.3.1 A schematic diagram of sodium metal aerosols sampling system.

The pressure of argon gas inside the combustion cell is kept1.0 kg/cm^2 above atmosphere and monitored by pressure sensor through DAS system. The temperature of the argon gas (above sodium pool) and sodium pool is monitored through thermocouples and recorded continuously throughout experiment with DAS system. The temperature is raised up to 500°C and maintained, which results in formation of sodium vapors above the pool surface subsequently these vapor condense to become sodium metal aerosols. The gate valve is opened after temperature reached to 500°C, the sodium metal aerosols along with argon cover gas is made to bubble through a gas washing bottle filled with liquid paraffin oil (250ml) kept at room temperature. The aerosols sampling flow rate and sampling time is kept at 2lpm and 10minutes respectively. Condensation of sodium metal aerosol and solidification of aerosol particle would occur as the aerosol passes through the paraffin oil while argon escapes out. The photograph of sampling gas washing bottle filled with paraffin oil and the trapped sodium metal aerosol are shown in Fig.3.2. The second bottle is used to trap the sodium metal aerosols escaped if any, from the first bottle. To prevent sodium metal aerosols condensation and solidification within the sampling tube the wall temperature of the sampling tube is maintained more than 110^{o}C by externally wound wire heaters. Temperature of sampling tube is monitored by thermocouple and the current in heating coil is controlled by using Proportional Integral Derivative (PID) temperature controller.

Fig. 3.2 Gas washing bottle filled with paraffin trapped sodium metal aerosol.

3.1.2 Characterization of sodium metal aerosols

The measurement of sodium metal aerosols size distribution is carried out by using Mastersizer (M/s Malvern Instruments, UK). The liquid paraffin from the bottles was analyzed in the Mastersizer to determine the size distribution of trapped sodium aerosols. The volume size distribution of sodium aerosol is given in Fig. 3.3. It is observed from the Fig. 3.3 that, the aerosol size range is found from 5.68 – 12.20 µm with Mass Median Diameter (MMD) at 7.72 µm. The performance evaluation of Mastersizer is carried out by analyzing standard latex particles dispersed in water medium having size of same range of aerosol particles prior to the experiments.

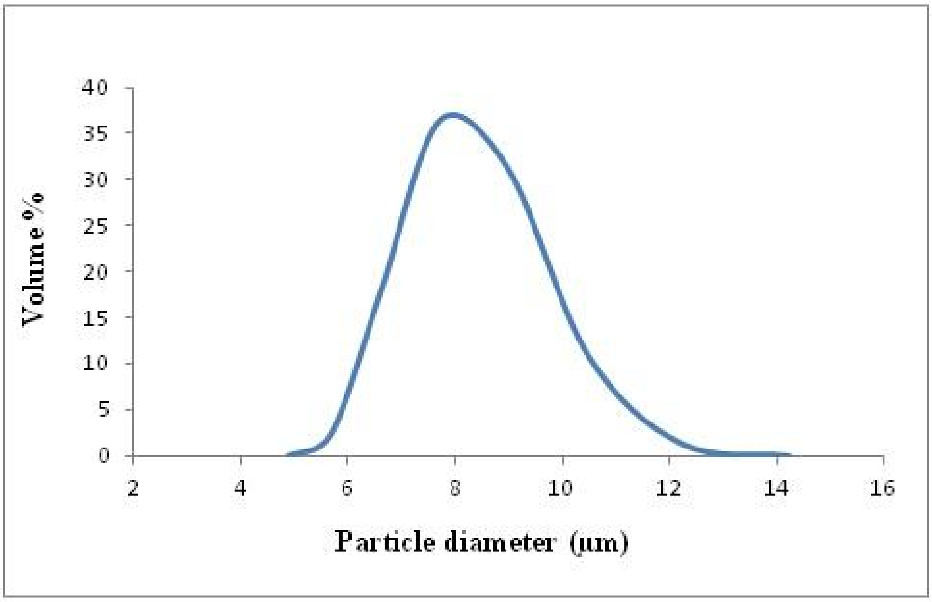

Fig. 3.3 Volume – size distribution of sodium metal aerosol.

The mass of sodium metal aerosols trapped in the liquid paraffin oil is determined by transferring sodium metal aerosol into a water medium (to become NaOH) and then the conductivity of the NaOH solution is measured. The conductivity measurement of NaOH solution is carried out by using Conductometer (M/s Metrohm, 856 conductivity module, Switzerland). 200ml of liquid paraffin (trapped with sodium metal aerosols) is mixed with same amount of DM water (1:1 ratio) in a separating funnel and vigorously shaked for several hours to transfer the sodium metal aerosols into the water medium (to become

NaOH). Out of 200ml solution, 100 ml solution is taken for the conductivity measurement. The conductivity of the 100ml solution is found to be 125µS/cm. The photographs of the separating funnel and Conductometer titration unit are shown in Fig.3.4. Using the calibration graph the quantity of sodium aerosol trapped in the paraffin is estimated (See Section 2.3.1.2 of Chapter-II) and it is found to be 1.719 mg [3.17]. After knowing the sodium mass, by adopting suitable corrections for the volume of the sample, the sodium metal aerosols mass concentration in combustion cell is calculated and it is found to be 0.173g/m^3. It is observed that, in few trial experiments, the conductivity of the paraffin oil filled in the second bottle hardly show 2-5µS/cm, for which the estimated sodium aerosol mass concentration is negligible. Hence, it is taken that for the sample concentration of 1g/m^3, the first bottle is sufficient to trap all aerosols. However if the sample concentration exceeds more than 1g/m^3, the concentration estimated from the second bottle will be added-up to estimate the actual concentration of the sample.

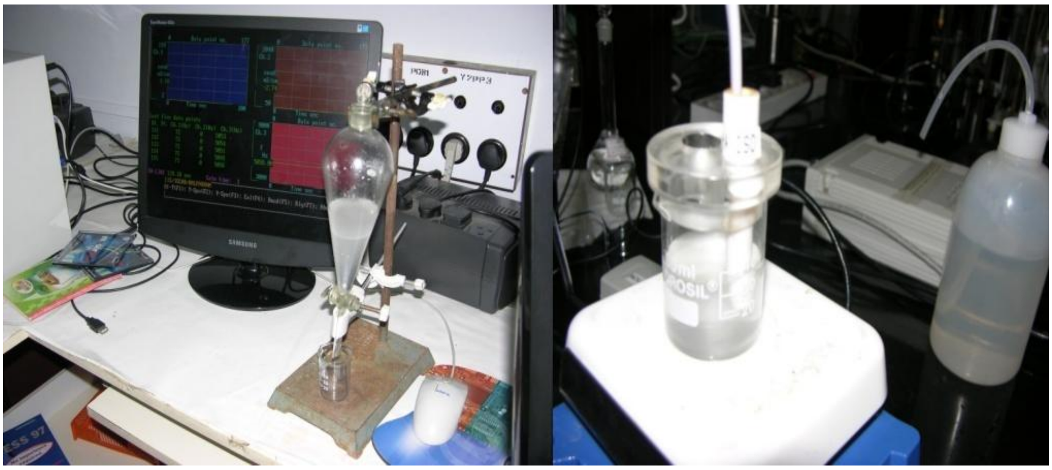

Fig. 3.4 Orbital shaker and Conductometer titration unit.

The result obtained from the conductivity measurement is cross checked with conductometric titration method [3.18]. The same solution was analyzed and the sodium metal aerosols mass concentration in combustion cell is estimated to be 0.18 g/m^3. It is observed that, the error associated with measurement of mass concentration between these two methods is estimated to be ±5.5% [3.17].

3.2 Validation of sodium metal aerosol characterization technique

After developing methodology for characterization of sodium metal aerosols in ATF, the experiments are conducted in SILVERINA Loop for validating the methodology. The sodium aerosol characterization experiments are carried out in TP-1 of SILVERINA loop. The details of SILVERINA sodium loop and TP-1 are described in Chapter -II. The main design features of SILVERINA Loop are as follows: (i) the loop consists of a sodium tank in which liquid sodium could be maintained at various temperatures from 200 - 550°C and it simulates the reactor pool condition, (ii) the region above the sodium pool is filled with cover gas (argon) and the cover gas height equals to that of FBTR in IGCAR. Experiments have been carried out in SILVERINA loop by designing, fabricating and installing of sodium metal aerosol sampling system. The integrated view of sodium metal aerosol sampling system with TP-1 is shown in Fig.3.5. The aerosol sampling system consists of aerosol sampling tube, aerosol sampling bottle, aerosol flow controlling device, tube heaters and controllers and filter paper assembly.

3.2.1 Aerosol sampling tube

The aerosol sampling tube is made of SS316 with internal diameter of 10mm and 1.5mm wall thickness. Sampling tube is inserted into Test Pot through an experimental channel. The sampling tube is divided into the two parts. One part of the sampling tube goes inside the Test Pot and other part is on the outside and both the parts are connected with the flange. Before starting the experiment the sampling tube which goes inside the test pot up to middle level of cover gas region is attached with the flange and inserted into TP-1. The outer side sampling tube is fabricated in two segments, namely segment - 1 and segment - 2. Sampling tube which connects with the flange and sampling bottle – 1 forms segment – 1 and sampling tube which connects sampling bottle 1 & 2 forms segment – 2. Sampling bottle – 1 and sampling bottle – 2 are filled with paraffin oil and they are connected to the sampling tube to collect the sodium metal aerosols suspended in the cover gas region. A Nupro valve is provided in the sampling line to isolate sampling bottles so as to remove them after sampling. Sampling bottle – 2 is provided to collect the residual aerosols if any, which flow out of sampling bottle – 1. In order to avoid solidification of sodium aerosols on the sampling tube, tube heaters with heater controller is provided to maintain the tube temperature at 110^{o}C up to the segment - 1. There is no heating arrangement in segment-2. It is expected that the aerosol size distribution and its median diameter is of the order 1- 20µm (literature review). Hence the sampling tube inner diameter is selected as 10mm, such that to avoid wall deposition by impaction (according the Davis criteria) for a flow rate of 2lpm. The maximum particle diameter that can be collected without bias due to particle settling is 20µm [3.19].

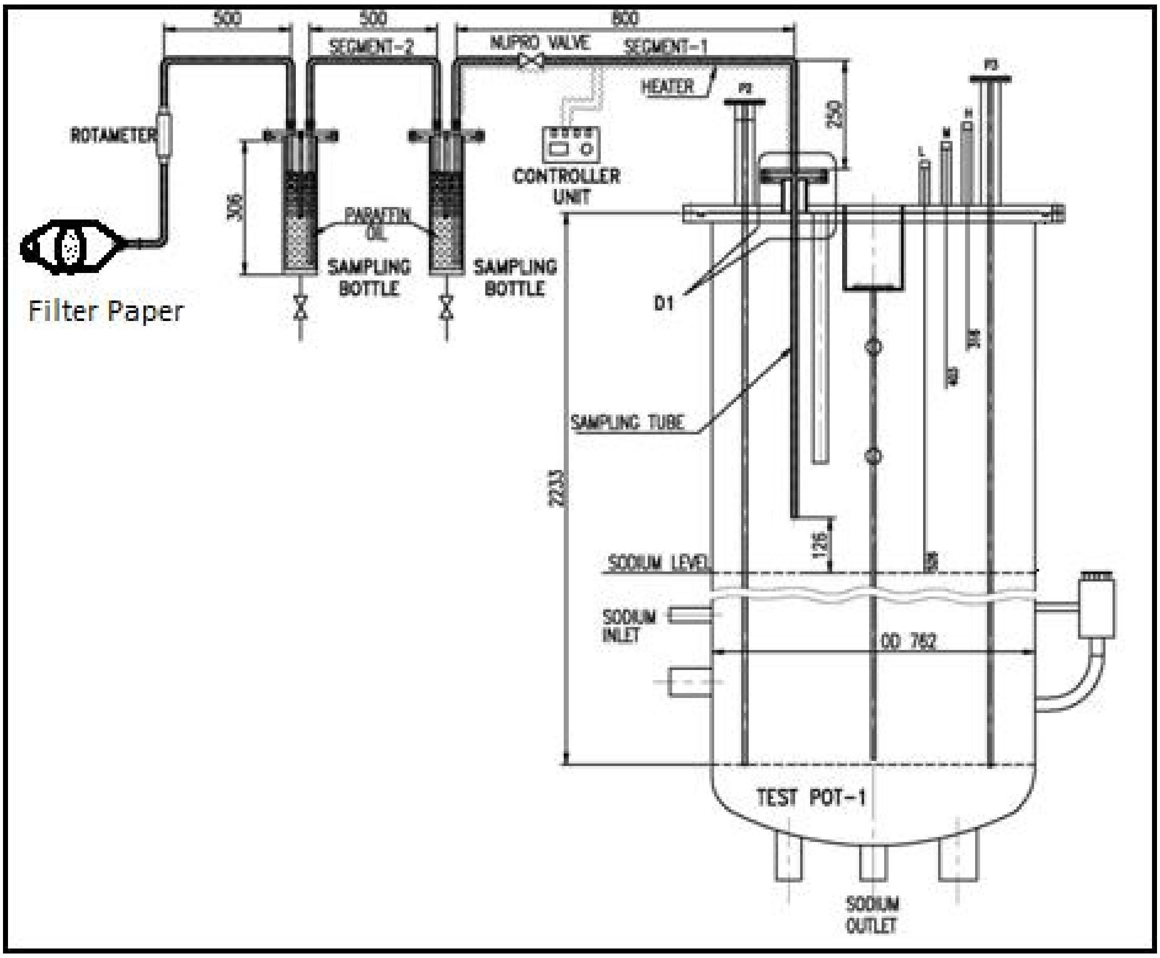

Fig.3.5 Integrated view of aerosol sampling system installed in TP-1.

3.2.2 Aerosol sampling bottle

The schematic diagram of the sampling bottle is shown in Fig.3.6. The capacity of the sampling bottle is 1.2 liter and made of perspex (height and diameter of the bottle are 306mm and 80mm respectively). The bottle is closed on top side by perspex flange arrangement.

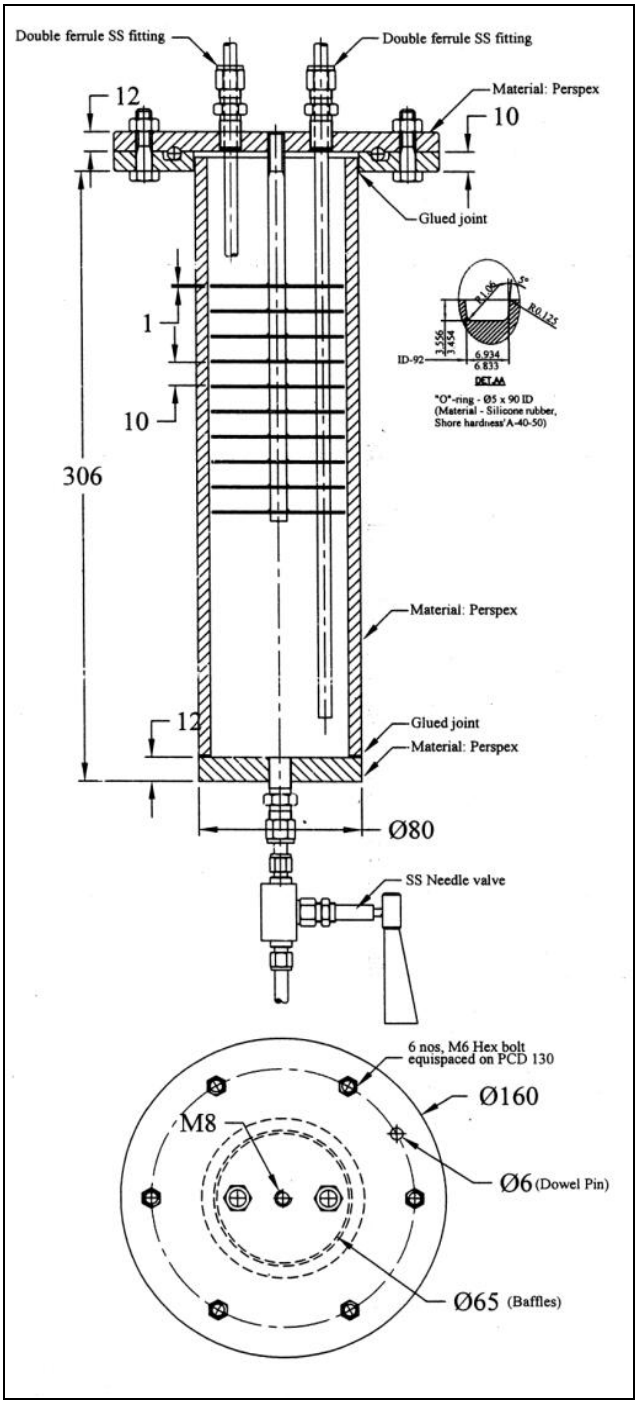

Fig.3.6 Schematic of the sampling bottle

The flange is provided with two opening for the insertion of inlet and outlet tubes. The inlet tube which is connected to segment – 1 of sampling tube is inserted into the bottle up to the bottom. The outlet tube is fitted above the liquid paraffin level. The tubes are fitted with flange by a pair of SS fittings and ferrules. The bottom side of the bottle is fitted with needle valve, using SS fittings with ferrule arrangement, for draining the liquid. A series of off-set baffles are placed inside the bottle to increase the residence time of the cover gas coming out of the bottle by forming bubbles. The baffle plates are made of stainless steel. The plates are drilled with holes on one side and they are fitted inside the bottle such that the holes are off-center to one another. After isolating the bottles from the system the sampling bottles will be taken for analyzing the samples.

The sampling bottle is filled with 0.6 liter of paraffin oil and maintained at ambient temperature. The aerosol sample laden cover gas is made to pass through the bottle, thus condensation of sodium aerosol and solidification of aerosol particle would occur as the cover gas enters into the paraffin oil. The residence time of the cover gas is increased due to baffle arrangement, which ensures that all sodium aerosols get trapped from the cover gas before it goes out of the bottle. Besides, the cover gas coming out the sampling bottle – 1 is made to pass through sampling bottle – 2 so as to remove aerosols escaped, if any, from the 1st bottle.

3.2.3 Aerosol flow control

The cover gas is drawn from the cover gas space of TP-1 at a low flow rate by using a rotameter, due to positive pressure of cover gas region. The flow rate is metered in such a way that (i) it takes into account of positive pressure of the cover gas inside the TP-1 and (ii) sufficient flow up to the second bottle is obtained. The rotameter are specified for a maximum flow rate of 10lpm.

3.2.4 Tube heaters and controller

To prevent sodium metal aerosol condensation and aerosol solidification within the tube during experimental measurements, the wall temperature along the sampling tube is to be maintained at the cover gas temperature. This is done by means of externally wound heaters. The heating coil is wounded on the sampling tube along with insulation. The temperature along the sampling tube is monitored by 2 thermocouples. The current through the heating coil is controlled by using PID controller. In order to have a redundancy in heating, a spare heater is also provided. The tube heater controller set-up consists of a panel board, in which one PID controller, temperature display units, 3 pole rotary switch for double heaters, allied PCBs etc are mounted.

3.2.5 Filter paper assembly

The filter paper holder is made of SS304. A glass fiber filter of 25 mm was used to prevent aerosols escaped, if any, after the 2nd bottle. The aerosol retention efficiency of filter paper used in this study for 0.3µm particles is 99.93%.

3.3 Sodium metal aerosol sampling procedure

Before start of the experiment, adequate quantity of paraffin oil is filled in sampling bottles 1 and 2. The sampling tube which goes middle level of the cover gas region is inserted in TP-1. The pressure hold up testing of TP-1 and sampling line is carried out by pressurizing TP -1 up to 0.5kg/cm^2. The cover gas pressure is maintaned at 0.2 kg/cm^2 after leak check. The functioning of surface heaters of the sampling tube and temperature controlling device is checked. Then, preheating of sodium in the loop along and TP-1 is started. Nupro valve in the sampling tube segment – 1 is kept closed during loop heating and venting. Sodium is heated up to 200°C and the molten sodium is filled in TP-1 up to middle level after purification. Dip stick type level probe in TP-1 is used to check the level rise during sodium heating and venting. The segment-1 sampling tube heater is switched ON and temperature of the sampling line is maintained more than 110°C. The flow rate is adjusted using rotameter, after opening the gate valve of segment-1 in the sampling tube. After collecting the aerosol samples, the sampling bottles are isolated and the surface heaters of sampling tube are switched off. Sampling bottles are disconnected from the system and taken for analysis. The open end of the sampling tube is closed with PVC cap after cleaning the line. After analysis, the sampling bottles are also cleaned, fresh paraffin oil is filled and connected back. The sampling line is tested using argon gas and communication to cover gas region is ensured to rule out the plugging of aerosol in the sampling line before start of every experiment.

3.4 Safety on sodium metal aerosol sampling

The safety aspects followed during characterization of sodium metal aerosol experiment in cover gas region are (i) after installation of the sodium metal aerosol sampling setup, pressure hold up test is conducted to ensure leak tightness of aerosol sampling tube, (ii) the experiment is carried out only after ensuring no leak in the system, (iii) the sampling bottles are removed only after isolating from the sampling line and the surface heaters of the line are switched off, (iv) the sampling tube was disconnected from sampling bottle after ensuring sampling line are cooled, (v) sodium metal aerosol sticking in the sampling line are cleaned and the line was closed using PVC cap to prevent atmospheric air ingress, (vi) the availability of alcohol, white cloth, helmet with face shield, gloves, goggles, DCP loose powder with shovel, etc are to be ensured during sampling line disconnection, (vii) TP-1 cover gas pressure of 0.2kg/cm^2 is maintained always, (viii) sampling bottle inlet and outlet pipes covered using cork to avoid air ingress during transportation.

3.5 Sodium metal aerosol characterization in SILVERINA loop

The photograph of the sodium metal aerosol sampling system in SILVERINA loop is shown in Fig.3.7. The sampling tube is inserted at the middle level of cover gas region (415mm from the top). Sodium cover gas height and pressure were kept as 820mm and 0.35 kg/cm^2

respectively. The sodium pool temperature was maintained at 500°C. Argon gas is made to bubble through liquid paraffin oil at a flow rate of 2lpm for 15 minutes. After sampling, the paraffin oil is analyzed using Mastersizer and the aerosol size distribution is found to vary from 2 to 12 µm with MMD around 4.0 µm ($\sigma_g = 1.5$) (Fig.3.8). The mass of trapped sodium aerosol in the bottle was estimated and then the mass concentration of sodium aerosol in cover gas region of SILVERINA loop is determined to be 9.50 g/m^3 [3.20].

Fig. 3.7 Photograph of the sampling system arrangement in TP-1.

In the cover gas region, sodium metal aerosol are liquid state and they are generated from hot sodium pool surface of various temperatures (200-550^{o}C) and they are suspended in cover gas space above the pool surface where temperature of the gas is found to be in the range of 90-400^{o}C. The sodium metal aerosol trapped in liquid paraffin oil are in room temperature. The expected change in aerosol material density due to change in temperature is within 3%. Hence, the MMD measured would have variation of about 3%. However, the present study is focused on determination of size distribution and mass concentration of sodium metal aerosol suspended in the cover gas region after reaching steady state condition for a given pool temperature. The mass collected in the second bottle was negligible (< 1% of the first bottle).

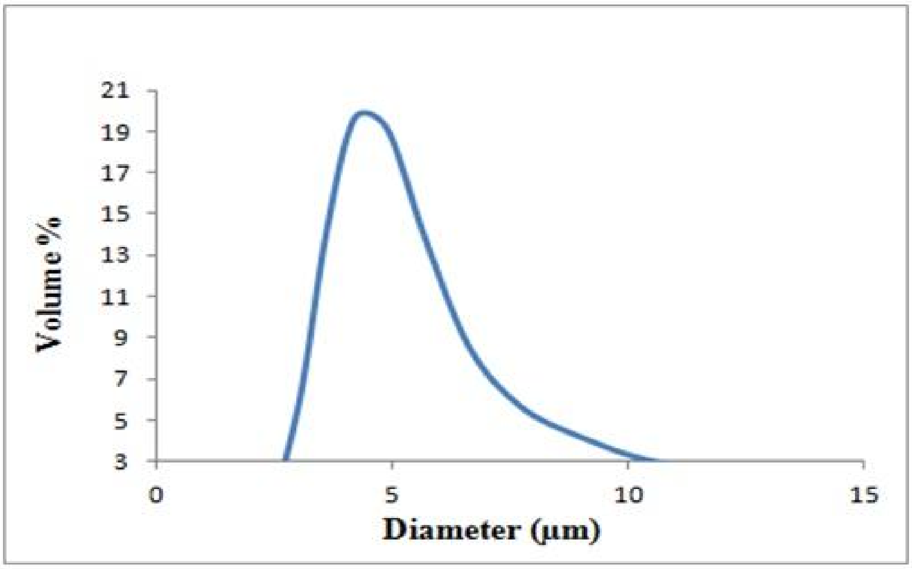

Fig. 3.8 Sodium metal aerosol size distribution in SILVERINA Loop

It is observed from Fig. 3.8 that, the size distribution is mono model. It was observed that the measured concentrations and particle size distributions were found to be in accordance with results in the literature. The sampling time and flow rate are kept such that the mass of sodium aerosol in the bottle is optimum for measurement of size distribution and mass concentration. Test runs showed that up to a trapped sodium aerosol mass of 50mg in the bottle, the coagulation of aerosols in the sampling bottle was not noticed before analyzing with Mastersizer (within 20 minute). The size measurements was also carried out of a single sample immediately after the sampling and followed by after 12hrs, 24hrs, and 48hrs. We have not noticed change in size.

3.6 Summary

The experimental procedure and sampling/analysis techniques adopted for the measurement of sodium metal aerosols were standardized at ATF and experiments were conducted in SILVERINA loop facility. The result obtained using this technique was evaluated by conventional chemical analysis, and it is proved to have good agreement. This technique will be used further for characterization of sodium metal aerosols in cover gas region of SILVERINA sodium loop facility at Fast Reactor Technology Group (FRTG). It was observed that the measured concentrations and particle size distributions were found to be in accordance with results in the literature. The design of sampling system in SILVERINA Loop is found very useful for next phase of experiments.

3.7 References

3.1 I. J. Ford, (1993), "Sodium aerosol formation and removal mechanisms in the fast reactor cover gas space", J. of Aerosol Sci., Vol. 24, 237-253.

3.2 V. Subramanian, P. Sahoo, N. Malathi, R. Anathanarayanan, R. Baskaran, and B. Saha, (2009), "Studies on Chemical Speciation of Sodium aerosols produced in Sodium fire", Nuclear Technology, Vol. 165, 257-269.

3.3 J. D. Jackson, J. F. Sanchis An Pei, and A. Alamar, (1993), "closing report of the MUSAC 3A project", Department of nuclear engineering, university of Manchester.

3.4 J. Minges and W. Schutz, ‘Experiments on the enrichment of cesium in the cover gas aerosol of the European Fast Reactor (EFR)’. Nuclear Engineering and Design 147 (1993) 17-22.

3.5 J. Minges and W. Schutz, (1991), "Experiments to characterize the sodium aerosol system in the cover gas of the European Fast Reactor EFR", J. Aerosol Sci. Vol. 22, S761-S764.

3.6 H. YAMAMOTO, T. SAKAI and N. MURAKAMI, (1991), "Analytical study on mass concentration and particle size distribution of sodium mist in cover gas phase of LMFBR reactor vessel’, J. Aerosol Sci. Vol. 22, S713-S716.

3.7 I. H. Newson, R. W. Dawoson, C. D. Wade, A. N. Moul and J. E. Finch, (1993), "Studies of caesium-134 transfer through argon and helium Cover gases above hot sodium pool in the Hawell active mass transfer loop (AMTL)", AEA Industrial technology, Report number AEA-In Tec-1220.

3.8 Yoshiaki HIMENO and June TAKAHASHI, (1980),"Sodium Mist behavior in cover gas space of LMFBR", J. Nucl. Sci. and Tech. Vol. 17, 404-412.

3.9 Yoshiaki HIMENO and Yoshiaki YAMAGISHI, (1982), "Effect of barriers on sodium mist deposition on LMFBR components", J. Nucl. Sci. and Tech. Vol. 19 [10], 837-844.

3.10 O. Frukawa, A. Furutani, N. Hattori and Iguchit, (1984),"Experimental study of heat and mass transfer through the cover gas in the Liquid Metal Fast Breeder Reactor (LMFBR)", Proceeding of the third international conference on liquid metal engineering and technology, The British nuclear Society, Vol.1, 451-458. ISBN0-7277-0209-2.

3.11 J. L. D. Glockling, (1991), "Heat and Mass transfer in specific aerosol system", PhD thesis, Department of chemical engineering. South bank University, London.

3.12 D. N. Roberts, (1995), "Heat and Mass transfer studies in sodium – Argon filled enclosures", PhD thesis, South bank University, London.

3.13 R. Anantha Narayanan, V. Subramanian, P. Sahoo, J. Misra, Amit Kumar, R. Baskaran, B. Venkatraman, and N. Murali, (2015), "Experimental Investigations on Carbonation of Sodium Aerosol Generated from Sodium Fire in the Context of Fast Reactor Safety", Annals of Nuclear Energy, Vol., 80, 188–194.

3.14 Amit Kumar, V. Subramanian, R. Baskaran, S. Krishnakumar, S. Chandramouli, B. Venkatraman, (2014), "Development and Validation of a Methodology for Characterization of Sodium Aerosols in Cover Gas Region", Aerosol and Air Quality Research, Vol. 14, 1534 –1541.

3.15 R. Baskaran, T. S. Selvakumaran, and V. Subramanian, (2004), "Aerosol Test Facility for Fast Reactor Safety Studies", Indian J. Pure Appl. Phys., Vol., 42, 873-878.

3.16 J. Misra, V. Subramanian, Amit Kumar, R. Baskaran, and B. Venkatraman, (2012), "Investigation of Aerosol Mass and Number Deposition Velocity in a Closed Chamber", Aerosol and Air Quality Research, Vol., 13, 680–688.

3.17 Amit Kumar, V. Subramanian, J. Misra, R. Baskaran, and B. Venkataraman, (2012), "Standardization of sodium aerosols characterisation techniqes", IASTA-2012, Navi Mumbai, IASTA Bulletin, Vol. 1&2, 441- 445.

3.18 P. Sahoo, N. Malathi, K. Praveen, R. Ananthanarayanan, A. D. Arun, N. Murali, and P. Swaminathan. (2010), "High performance conductivity monitoring instrument with pulsating sensor", Rev. Sci. Instrum., Vol., 81, 065109.

3.19 William C. Hinds, (1982), "Aerosol Technology", John Wiley & Sons.

3.20 R. Baskaran Amit Kumar, V. Subramanian, S. Krishnakumar S. Chandramouli, B. K. Nashine B.Venkataraman and K. K. Rajan, (2012), “Characterization of Sodium Aerosol (Metal Vapor) from cover gas region of Sodium Cooled Fast Reactor”, NSRP19 – 2012, December 12-14, Radisson Blu Resort Temple Bay, Mamallapuram, Tamilnadu, India.

CHAPTER - IV

DEVELOPMENT OF THEORETICAL MODEL AND VALIDATION

4.0 Introduction

For the design of roof structures of SFR, one needs to know heat and mass transfer rate to the roof from the hot sodium pool in order to asses cooling requirements, thermal stress within the structure and the possible influence of sodium metal aerosol deposition on the annular gap of roof top [4.1]. In this context, development of theoretical models and their verification on specific experimental results remain necessary, to know the aerosol mass concentration and size distribution in order to predict effectively the heat and mass transfer phenomena and sodium metal aerosol deposition in cooler part of roof structure [4.2]. Towards this, we have formulated a theoretical model for the estimation of steady state sodium metal aerosol mass concentration based on the rate equations of mass and number concentrations. The model is derived from standard aerosol mass and number concentration decay equations, taking into account of aerosol source term and various aerosol removal mechanisms. The sodium metal aerosol characteristics in cover gas region depends upon the evaporation rate, temperature difference between sodium pool and roof slab, bulk cover gas temperature and geometry of the cover gas region. The input parameters of the model are initial radius of sodium aerosol, geometry of the vessel and temperatures of pool, roof and bulk cover gas. The source term for the model is taken from evaporation of sodium vapours from the pool surface and the vapours condensation in the cover gas region during transport due to convective motion set between hot sodium pool surface and cold roof top. From these inputs, the model calculates concentrations iteratively until convergence is reached. The model is used to predict the steady state concentration and equilibrium size of the sodium aerosols in a confined environment. In this chapter, a brief description of the model formulation and the results on comparison between theoretically simulated sodium metal aerosol mass concentration and experimental values for various pool temperatures are presented. The model is validated using the inputs from the experimental work of Minges [4.3 and 4.4] and Glockling [4.5]. The details of validation exercise of this model for sodium combustion aerosols in predicting time evolution of aerosol size growth and concentration decay, with the experimental results obtained at ATF are also presented [4.6].

4.1 Theoretical formulation

A schematic diagram of cover gas region along with sodium pool and roof top are shown in Fig.1.

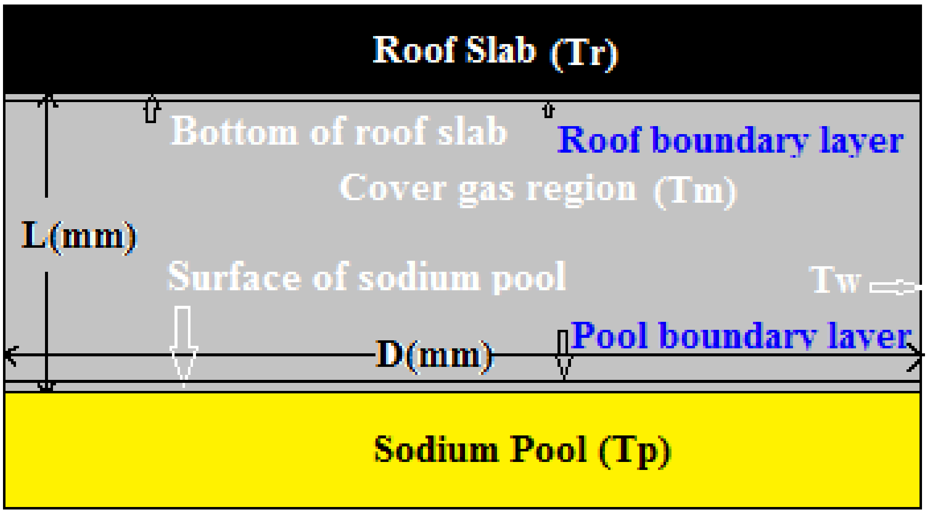

Fig. 4.1 Schematic diagram of cover gas region along with sodium pool and roof.

Fig 1 describes diameter of sodium pool (D) and height of cover gas region (L) having boundary on the bottom side with sodium pool, on top side with roof slab and at the side with wall of the reactor vessel. The temperatures of the corresponding regions are described as T_p, T_r, T_m and T_w as sodium pool temperature, bottom of roof slab temperature, bulk cover gas temperature and wall temperature respectively. In the cover gas region, there is pool boundary layer near the sodium pool and roof boundary layer near the roof slab exit due to temperature gradient near the sodium pool and roof slab respectively. The thickness of the boundary layers varies with temperature of the pool, roof and dimension of the cover gas region [4.7]. The temperature gradient exits only in pool boundary layer and roof boundary layer, the temperature profile remain almost constant in the middle level of cover gas. Hence, the thermophoretic force exits only in boundary layers. Evaporation of sodium vapors from the pool surface and subsequent condensation above the pool boundary layer results in the formation of aerosols. The aerosol undergoes convection motion due to difference in the temperature of the pool and roof boundary layers.

In the cover gas space, aerosol particles are formed by a single source term (evaporation and condensation) and removed continuously by several mechanisms (gravitational, wall plating, and ventilation). Since, all the removal mechanisms are dependent on particle size, a theoretical model is developed to predict the sodium metal aerosol mass and number concentration in cover gas region by including the effect of continuous source term and various removal mechanisms [4.8]. Taking initial size of the aerosols as an input from the experimental results, the steady state mass concentration is evolved by solving rate equation of mass concentration and number concentration numerically. In this model, the inputs parameters are (i) temperature of sodium pool surface, bottom surface of roof top and bulk cover gas, (ii) geometry of the vessel (diameter of the pool surface and height of the cover gas region) and (iii) initial radius of aerosol. The rate equations for mass concentration and number concentration of the aerosols are given below:

$$\frac{dC}{dt} = -\lambda C + \delta C + S_e \tag{4.1}$$

$$\frac{dN}{dt} = -\lambda N - K N^2 + S_n \tag{4.2}$$

$$C = \frac{4}{3}\pi r^3 \rho N \tag{4.3}$$

Where C – Mass concentration (g/cm^3)

N – Number concentration (1/cm^3)

K – Coagulation rate (1/s)

ρ – Particle density (g/cm^3)

r – Radius of particle (cm)

t – Time (s)

δ – Convective source rate (1/s)

S_e – Evaporative source term (g/cm^3$*$s)

S_n - Source term for number concentration (no. of particles/cm^3$*$s)

The correlation λ, δ and K are given below:

$$\lambda = \lambda 1 + \lambda 2 + \lambda 3 \qquad (4.4)$$

Where $\lambda 1$ - Decay rate due to gravitational (1/s)

$\lambda 2$ - Decay rate due to wall plating (1/s)

$\lambda 3$ - Decay rate due to ventilation (1/s)

$$\lambda 1 = \frac{2*r^2*\rho*g}{9*H*\eta}\varphi \qquad (4.4a)$$

$$\lambda 2 = \frac{k*T_m*A_W}{6*\pi*\eta*r*\Delta*V}\varphi \qquad (4.4b)$$

$$\lambda 3 = \frac{Q}{V} \qquad (4.4c)$$

$$\delta = 0.63\,\frac{\rho_c*D_{em}}{r*H*\rho}\left(\frac{g*\Delta T*L^3*\rho_c}{T_m*\eta*D_{em}}\right)^{0.25}\left(\frac{P_p*M}{R_g*T_p*\rho_c*P_p*M}\right) \qquad (4.5)$$

$$K = \frac{4*k*T_m}{3*\eta}\varphi \qquad (4.6)$$

Where g – Gravitational constant (cm^2/s)

L – Height of cover gas region (cm)

η- Viscosities of argon cover gas (g/cm$*$s)

φ- Cunningham correction factor

k – Boltzmann’s constant (cm^{2}∗g/Kal∗s)

T_m – Bulk Cover gas temperature (^{o}C)

A_w –Area of walls (cm^{2})

Δ – Wall platting parameter

V – Volume of cover gas region (cm^{3})

Q – Ventilation Rate (cm^{3}/s)

ρ_c – Density of cover gas (g/ cm^{3})

D_{em} – Diffusion coefficient of sodium vapour (cm^{2}/s)

ΔT – temperature difference between sodium pool surface to roof surface (^{o}C)

P_p – Partial Pressure of sodium vapor (g∗cm/s^{2})

M – Sodium molecular weight

R_g – Gas Constant (g∗cm^{4}/ Kal∗mol∗s^{2})

T_p – Sodium pool temperature (^{o}C)

Due to evaporation of sodium vapors from the sodium pool, the concentration of sodium vapors is more near the pool boundary than bulk cover gas region. The flux of sodium vapors across the sodium pool is written as:

$$j = -D_{em}\frac{dC_e}{dx} \qquad (4.7)$$

Where Ce – Sodium vapour concentration (g/cm^{3}) and

x- Thickness of pool boundary layer (cm)

$$D_{em} = 0.424\left(\frac{T_p}{642.83}\right)^{1.823} \qquad (4.8)$$

$$C_e = \left(\frac{P_p * M}{R_g * T_p}\right) \qquad (4.9)$$

The source term due to evaporation (S_e) is defined as: Se= J∗A_p/V, where, A_p – Surface area of sodium pool (cm^2)

$$S_e = 0.424 \left(\frac{T_p}{642.83}\right)^{1.823} \left(\frac{P_p * M}{R_g * T_p}\right)\left(\frac{A_p}{Q * V}\right) \quad (4.10)$$

The aerosol that is generated when the sodium vapor condenses in the cover gas region is called initial particle and the size measured at this moment is known as initial size. As the time progresses, the particle size grows and reaches equilibrium size, simultaneously the concentration of the aerosols in the cover gas region increases and reaches steady state value. By taking into account of particle radius and density, source term due to number concentration is defined as

$$S_n = \frac{3 * S_e}{4\pi r^3 \rho} \quad (4.11)$$

To begin with the concentrations C and N are set to zero. The evaporation rate (equation 4.10) S_e and the number source term S_n (equation 4.11), are calculated by taking geometry of the region into account, with initial particle radius fed from the experimental results available in literature. In the next time step, for the initial particle radius, the convection source rate δ (equation 4.5), the coagulation kernel rate K (equation 4.6), the particle decay rate constant λ (equation 4.4) are calculated. Then for these conditions the mass concentration C and the number concentration N are calculated. In the next time step from the calculated value of C and N, the new particle radius is calculated. The particle radius in this step is different from the initial radius. Subsequently all parameters are calculated until the convergence of mass concentration value is reached. At this time, the mass and number concentrations reach equilibrium value, while the particle radius also reaches steady state value. Hence, the measured mass concentration and the theoretically calculated mass concentrations are steady state values.

There are some approximations taken in the calculations of cover gas aerosol mass concentration. The aerosol particles are always spherical and the collision efficiency is unity.

There is no hindrance in the cover gas space. The aerosol concentration is uniform in the cover gas region. The evaporation rate is constant for the fixed pool and roof temperatures with respect to time. The sodium vapor concentration is zero outside the pool boundary layer. The aerosol size is large when compared with mean free path of cover gas. The mean free path of argon cover gas is varied from 0.09 – 0.14 µm when pool temperature varied from 250°C -550°C at fixed cover gas pressure (1.38 kg/cm^2). The Knudsen number (for the aerosol size) ($Kn=2\lambda/d$) is less than 1 for all pool temperatures. Hence it is considered that, gravitational removal is dominated in the cover gas region and thermophoresis makes only smaller contribution. Hence thermophoretic force is neglected in our modeling. The model does not include the formation of aerosols from the molecular radius of sodium in vapor state followed by nucleation.

4.2 Validation of theoretical model with available literature

The model is validated with the results of Glockling and Minges studies. The experimental parameters for the Glockling and Minges studies are presented in Table 1. In both studies, the sodium metal aerosol mass concentration was measured by varying sodium pool temperature while keeping roof top temperature at a constant value.

Table 4.1 Experimental parameters of Glockling and Minges studies

Sl. No.	Experimental parameters	Glockling [4.5]	Minges [4.3 & 4.4]
1	Diameter of the pool (cm)	15	60
2	Height of cover gas region (cm)	35	33
3	Sodium pool temperature (^{o}C)	300 -550	350 - 550
4	Roof temperature (^{o}C)	150	120
5	Aerosol Diameter (MMD) (µm)	3 - 13	4 - 9

As stated in section 4.1, the bulk cover gas temperature is also one of the input parameter apart from other inputs given in Table 4.1. The bulk cover gas temperature is taken as average value of sodium pool and roof temperatures. The sodium metal aerosol mass concentration is simulated with theoretical model and compared with experimental results for Glockling and Minges studies. Fig. 4.2 and Fig.4.3 show the experimental and simulated sodium metal aerosol mass concentration for various pool temperatures for Glockling study (roof temperature 150°C) and Minges study (roof temperature 120°C) respectively.

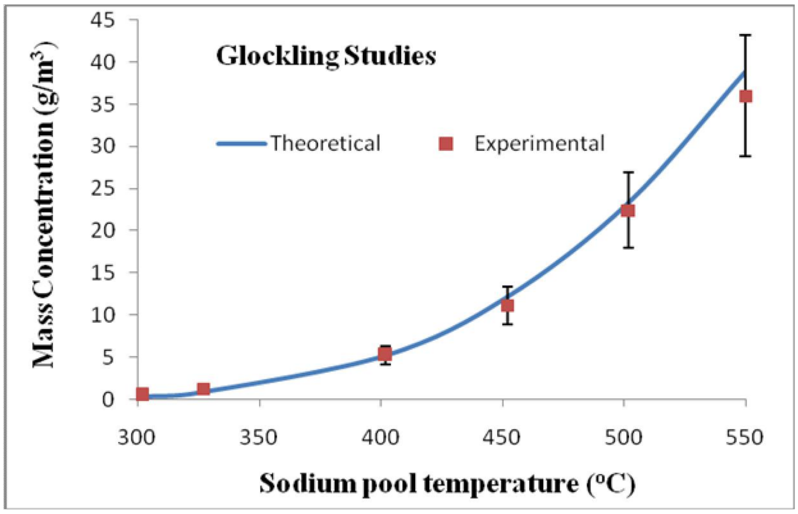

Fig. 4.2 Experimental and simulated sodium metal aerosol mass concentration for Glockling study.

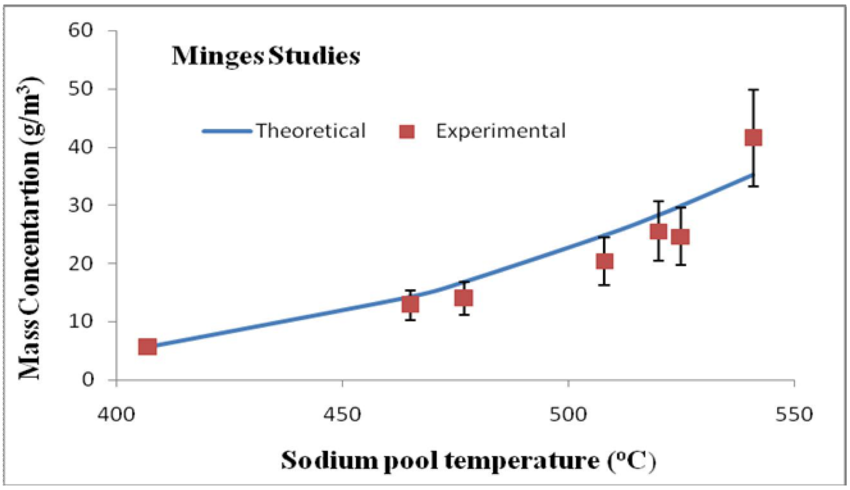

Fig. 4.3 Experimental and simulated sodium metal aerosol mass concentration for Minges study

It is observed from Fig.4.2 and 4.3, that the sodium metal aerosol mass concentration (steady state value) increases exponentially with increase of sodium pool temperature and the theoretical simulation is found to have good agreement with the experimental values for the entire range of pool temperatures. It is to also to be noted here that our predicted value differ by maximum value of ±20% [4.9]. The study reveals that the sodium metal aerosol mass concentration also depends upon the geometry of cover gas region. The modeling is found useful in predicting the steady state sodium metal aerosol mass concentration for a given geometry and pool temperature for similar experimental conditions. In continuation of this work, the characterization of sodium metal aerosols in the cover gas region are carried out at sodium loop facility in SILVERINA Loop, FRTG, IGCAR and the results are presented in chapter V and VI.

4.3 Validation exercise for sodium combustion aerosol

Although the model is developed to predict sodium metal aerosol characteristics in cover gas region. But the same model is also validated with sodium combustion aerosol with some modification. The sodium combustion aerosols are formed by combustion process. When these aerosols are suspended in a confined volume, they are removed continuously from the suspended space by several mechanisms i.e. mass concentration is reduced by gravitational settling, wall plating, and ventilation if there. The model is modified for sodium combustion aerosol present in the confined environment by taking source term and convection term set as zero in equation 4.1 and 4.2. The model predicts the decay of suspended mass concentration and size growth of sodium combustion aerosols in closed chamber with progress of time. In this simulation, the inputs parameters are (i) initial sodium combustion aerosol mass concentration (at $t=0$, $C=C_o$), (ii) geometry of the vessel (diameter and height of the vessel) and (iii) initial radius of sodium combustion aerosol. The initial particle size taken from the empirical relation derived from the previous experimental results conducted in ATF, [4.10] in which Cooper's relation for initial particle size of sodium combustion aerosol is modified by taking a empirical constant as 0.97 and dry particle radius (r_0) =0.45 measured in ATF at RH% of 20. The modified initial radius at various RH% is given as

$$r\ (initial\ radius) = r_0 * 0.97 / (1 - RH)^{1/3} \qquad (4.12)$$

The above empirical relation is valid for 20 - 90 RH%. The modified rate equations for mass concentration, number concentration and inter-relating equation of mass and number concentration of the aerosols are given below:

$$\frac{dc}{dt} = -\lambda c \qquad (4.13)$$

$$\frac{dN}{dt} = -\lambda N - KN^2 \qquad (4.14)$$

$$c = \frac{4}{3}\pi r^3 \rho N \qquad (4.15)$$

By taking initial sodium combustion aerosol radius from the modified Cooper relation, the parameters λ (equation 4.4), and K (equation 4.6) are calculated. Using these values, above equations are solved for next time step and the process continued till the convergence of size and concentration is reached.

4.3.1 Mass concentration simulation

The simulation is carried out for our earlier experimental results obtained in ATF [4.11]. The initial sodium combustion aerosol mass concentration in aerosol chamber is 1.9 g/m^3 i.e. C_o = 1.9 g/m^3 and r_o= 1.08µm (from equation 4.12) for the relative humidity condition of 50%. The simulated mass concentration decay and experimental results are compared and shown in Fig.4.4. It is observed from Fig.4.4 that, the experimental and simulated mass concentration decay with progress of time has good agreement. In the first 90 minute duration, the maximum variation between predicted and experimental value differ by ±10% and there after predicted value is less than 30 - 50% of measured value. The difference is due to hygroscopic nature and chemical conversion of sodium combustion aerosol with progress of time cause change in material density of aerosol [4.12 and 4.13].

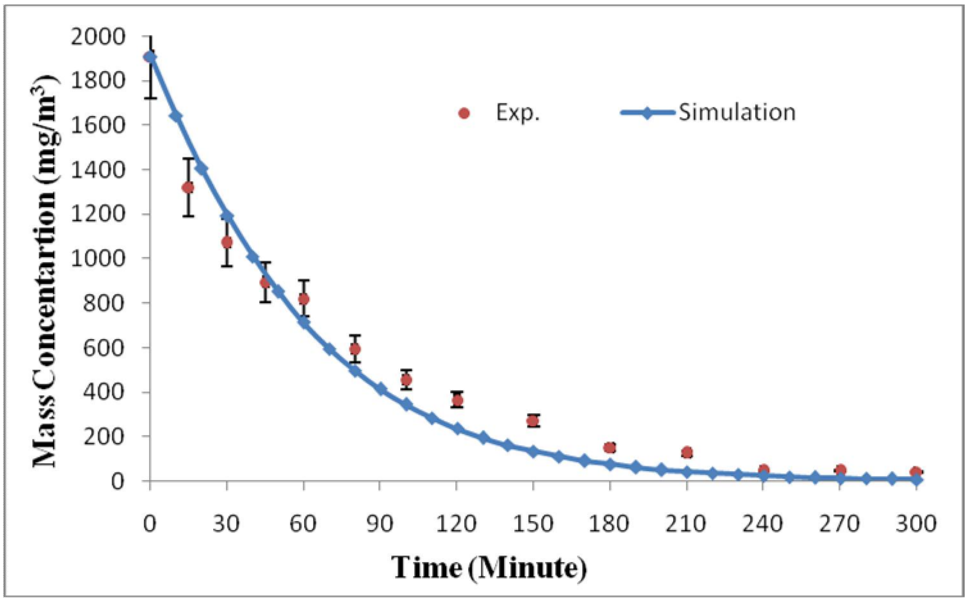

Fig. 4.4 Sodium combustion aerosol concentration decay with progress of time.

4.3.2 Size evolution simulation

The evolution of sodium combustion aerosol size growth with progress of time is carried out in ATF. The real time measurement of sodium combustion aerosol size is carried out by using Mastersizer. Sodium combustion aerosol are generated with desired mass concentration and the aerosol size distribution and corresponding MMD is measured continuously with progress of time (every minute) for about 1 hour. The desired initial mass concentration is obtained by optimizing the parameters viz. quantity of sodium, combustion time, rate of injection of air etc. The aerosol chamber is maintained with ambient atmospheric conditions viz. temperature (25-30°C), 50% RH and CO_2 content (390ppm), before injection of aerosols. The measured initial sodium combustion aerosol mass concentration is found to be $3 g/m^3$. The initial volume - size distribution of sodium combustion aerosol is shown in Fig.4.5. It is observed from Fig.4.5, that the initial size distribution is mono model with MMD - 1.1µm. The experimentally measured particle size (MMD) with progress of time is shown in Fig.4.6. It is observed from Fig. 4.6, the MMD of sodium aerosol enlarges from 1.1 to 1.56µm in 20 minutes and thereafter, the size is approaching to equilibrium values around 1.**7**µm in about 60 minutes.

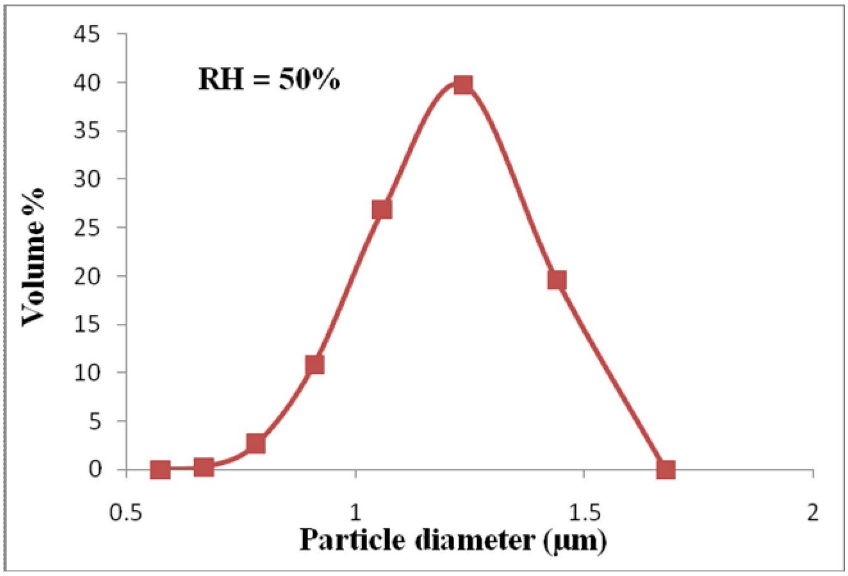

Fig. 4.5 Initial volume – size distribution of sodium combustion aerosol.

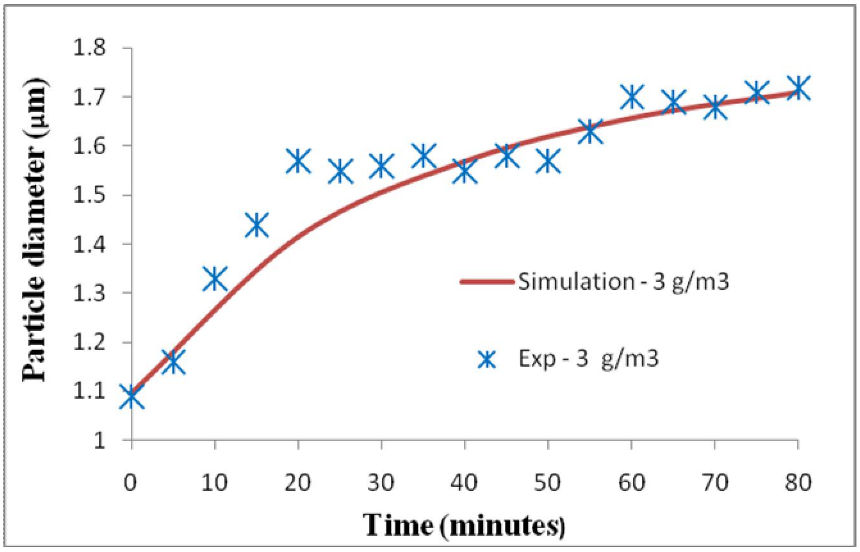

Fig.4.6 Growth of particle size with time.

The theoretically simulated particle size growth with progress of time is included in Fig.4.6. In the case of theoretical simulation, the particle size enlarges progressively from 1.1µm and in 20 minutes it increases around 1.4µm then slowly increases to the equilibrium value of 1.7µm at about 80 minutes. It is evidenced in Fig 4.6, the difference in the particle size at 20 minutes is about 12% and it would be due to hygroscopic growth [4.12]. The rate of growth in both theoretical simulation and experimental observation is nearly same after 40 minutes. But within 30 minutes, the particle size enlarges upon absorption of moisture. If we compare the rate of enlargement in size after the initial period of time say 20 minutes, both theoretical growth and experimental growth are almost same but only with the difference of particle radius at 20 minutes (say starting diameter). It is to be noted here, the chemical composition of sodium combustion aerosols changes with progress of time, which could influence the change in size of the aerosols.

4.4 Summary

A theoretical model is developed to predict the sodium metal aerosol mass concentration in cover gas region and it is validated with available experimental results of Glockling and Minges. The predicated sodium metal aerosol mass concentration is in good agreement with experimental values. The same model is also modified to predict the sodium combustion aerosol mass concentration decay and size growth with progress of time in a closed vessel. The theoretical simulation for decay of aerosol mass concentration and size growth for sodium combustion is in good agreement with experimental results. The theoretical model is found to be useful for further study.

4.5 References

4.1 Y. L Sinai., I. J. Ford., J. C. Barrett and C. F. Clement (1993), "Prediction of coupled heat and mass transfer in the fast reactor cover gas: the C-GAS code", Nuclear Engineering and Design, Vol. 140, 159-192.

4.2 Baldev Raj, P. Chellapandi, P. R. Vasudeva Rao, (2014), "Sodium Fast Reactors with Closed Fuel Cycle", CRC press, Taylor and Francis Group, Boca Raton London NewYork.

4.3 J. Minges and W. Schutz, ‘Experiments on the enrichment of cesium in the cover gas aerosol of the European Fast Reactor (EFR)’. Nuclear Engineering and Design 147 (1993) 17-22.

4.4 J. Minges and W. Schutz, (1991), "Experiments to characterize the sodium aerosol system in the cover gas of the European Fast Reactor EFR", J. Aerosol Sci. Vol. 22, S761-S764.

4.5 J. L. D. Glockling, (1991), "Heat and Mass transfer in specific aerosol system", PhD thesis, Department of chemical engineering, South bank University, London.

4.6 Amit Kumar, V. Subramanian R. Baskaran, and B. Venkatraman, (2015), “Size Evolution of sodium combustion aerosol with various RH%”, Aerosol and Air Quality Research, Vol.15, 2270-2276.

4.7 OHIRA Hiroaki, (2002), "Numerical simulation of aerosol behavior in turbulent natural convection", Journal of Nuclear Science and Technology, Vol. 39, No. 7, 743-751.

4.8 A. Sheth, (1975), "Parametric study of sodium aerosols in the cover gas-space of sodium-cooled reactors", Argonne National Laboratory, ANL-75-11.

4.9 Amit Kumar, V. Subramanian, R. Baskaran, and B. Venkatraman, (2014), “Theoretical simulation of sodium aerosol mass concentration in the cover gas region”, IASTA-2014, November 11-13, 2014, BHU, India, Vol. 21, Issue 1&2, P147-151.

4.10 Amit Kumar, V. Subramanian, J. Misra R. Baskaran, and B. Venkatraman, (2014), “Size Evolution of sodium combustion aerosol with various RH%”, IAC-2014, Aug.31 – Sept. 5, 2014 Bexco, Busam, Korea.

4.11 R. Baskaran, V. Subramanian, B. Venkatraman, and P. Chellapandi, (2011), "Sodium aerosol studies for fast reactor safety", Energy Procidia, Vol. 7, 660-665.

4.12 C. F. Clement, (1988), "Water condensation on hygroscopic aerosols", J. of Aerosol Sci., Vol.19, No.7, 875-877.

4.13 R. Anantha Narayanan, V. Subramanian P. Sahoo, J. Misra, Amit Kumar, R. Baskaran B. Venkatraman N. Murali (2015), "Experimental investigations on carbonation of sodium aerosol generated from sodium fire in the context of fast reactor safety", Annals of Nuclear Energy, Vol. 80, 188–194.

CHAPTER - V

SODIUM METAL AEROSOL CHARACTERISTICS IN COVER GAS REGION

5.0 Introduction

In cover gas region of SFR, it is at most important to know the sodium metal aerosol mass concentration and size distribution in order to predict effectively the heat and mass transfer phenomena, which will get changed due to interaction of thermal radiation with aerosols and mass transfer due to condensation of aerosols [5.1]. In order to account for the role of sodium metal aerosols, it is important to know the sodium metal aerosol properties, which would get modified due to temperature difference between the sodium pool surface and bottom of the roof top plug.

It was observed from the literature, the size distribution of aerosols ranges from 1-20µm and mass concentration ranges from 1-50g/m^3 [5.2, 5.3, 5.4, 5.5, and 5.6]. It is further noted from the literature, the sodium aerosol mass concentration increases with increase in difference between roof and pool temperatures whereas, there is no definite correlation of aerosol size distribution with the variation of pool and roof temperatures. The sodium metal aerosol characteristics also differ across in the cover gas region. There is no work found in literature to quantify the mass concentration gradient of sodium metal aerosols in the cover gas space. Taking into consideration of the above aspects a study has been conducted in SILVERINA loop of Fast Reactor Technology Group (FRTG), IGCAR to characterize the sodium metal aerosols in cover gas region. The characterization of sodium metal aerosols includes experimental determination of aerosol characteristics and theoretical simulation to predict the aerosol mass concentration in the cover gas region. The theoretical simulation is carried out with the purpose that, it can be useful for other similar type of geometry and to understand the role of sodium metal aerosol in cover gas region of the reactor. In this chapter, temperature profiling measuring system for the cover gas region of SILVERINA loop, experimentation, results and analysis of sodium metal aerosol characteristics, theoretical simulation of sodium metal aerosol mass concentration for the given pool temperature and geometry and validation of the model with experimental results are presented [5.7].

5.1 Materials and Methods

The sodium metal aerosol characterization experiments are carried out in TP-1 of SILVERINA loop [5.8]. The detail description of TP-1 is given in (Chapter - II). The integrated view of aerosol sampling system with TP-1 is given in chapter - III (see figure 3.5). A suitable technique for characterization of sodium aerosol in cover gas region has been developed in ATF and validated in SILVERINA loop [4.9]. The details of sodium metal aerosol sampling system, sampling and characterization procedures, safety aspects in sampling are described in chapter - III. The sodium metal aerosol sampling tube which goes inside cover gas space of TP-1 has been fabricated of three different lengths (near the roof - 215mm, middle level of cover gas region - 415mm and near the sodium pool - 715mm) to enable the sampling at three different levels in the cover gas region. Aerosol sampling is carried out in TP-1 at various sodium pool temperatures varying from 250 - 550°C in steps of 50°C. Experiments are repeated at the above temperatures by varying the sampling height (i.e. distance between sampling tube bottom and sodium pool surface inside cover gas region).

5.1.1 Temperature measurement system

The pool, roof and cover gas temperatures are important parameters for the theoretical simulation of sodium metal aerosol mass concentration in cover gas region of SILVERINA loop. A temperature measurement system has been fabricated, installed in top flange of SILVERINA loop TP-1 (spare nozzle) and measurements were carried out. A photograph and schematic diagram of the temperature measurement system are shown in Fig.5.1. The system consists of matched top flange for the aerosol port, a vertical cylindrical shaft welded below the top flange and six grooves to insert 6 thermocouples which are terminated at six different heights. Temperature was measured by using chromel - aluminium K-type thermocouples at the six locations in the cover gas region.

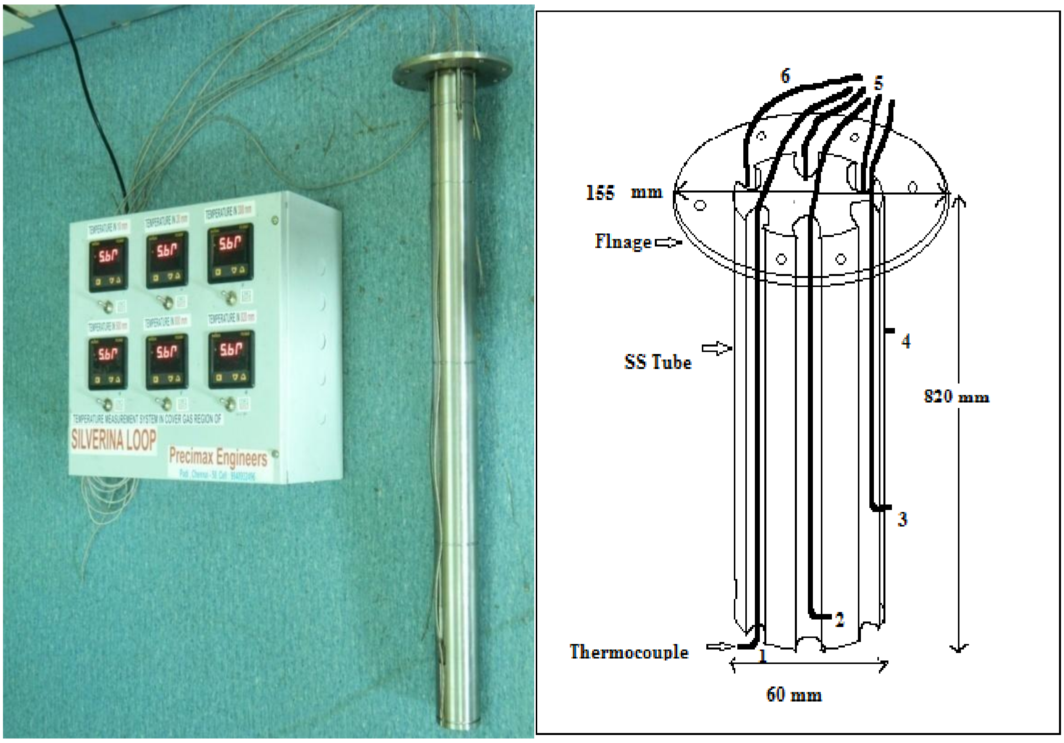

Fig.5.1 A photograph and schematic diagram of the temperature measurement system.

The material used for the fabrication of cylindrical soft and flange is SS316. The diameter and length of the cylindrical shaft is 60mm and 820mm respectively. Proper O-ring arrangements were made to prevent leakage of cover gas through thermocouple holes. The temperature measurement locations from the top of flange are (i) the pool surface (820mm), (ii) near to the pool (790 mm), (iii) two locations on the middle of the cover gas region with 300mm difference in height (400mm and 100mm), (iv) near to the roof surface (20mm) and (v) roof surface (0mm). Accordingly, the thermocouples were terminated at 82 mm, 790mm, 400mm, 100mm, 20mm, and 0mm from bottom surface of the top flange. Each thermocouple is connected with 3½ - digit digital indicator.

5.1.2 Aerosol sampling and analysis

The TP-1 is filled with sodium up to a middle level before starting the experiment. The argon is filled above the sodium surface at pressure 34kPa above the atmosphere. The temperature of the sodium is elevated by heater and monitored continuously by using thermocouples and DAS. Aerosols are drawn from the cover gas region and allowed to get trapped in liquid paraffin oil medium without exposing them to atmosphere. There is no ventilation path other than sampling line. After isolating the bottles from the system the sampling bottles were taken for analyzing the samples. The size distribution and MMD of sodium metal aerosols is determined by using Mastersizer (M/s Malvern Instruments, UK). The measurement of sodium metal aerosol mass concentration is carried out by conductivity method (M/s Metrohm, 856 conductivity module, Switzerland). The cover gas (argon gas) is made to bubble through liquid paraffin oil at a flow rate of 2lpm. The sampling time is varied from 20 minute to 2 minute according to sodium pool temperature. Since the sodium metal aerosol mass concentration increases with increase of sodium pool temperature and in order to avoid coagulation of aerosol trapped in the paraffin oil, the sampling time was kept for 20 minutes for the pool temperature 250°C and progressively reduced to 2 minutes when pool temperature is 550°C. The maximum volume of sample would be 40 litres, when the sodium pool temperature is 250°C and the minimum volume of sample is 4 litres, when sodium pool temperature is 550°C. The total volume of cover gas is 500 litres at 34kPa pressure inside the cover gas region. The maximum pressure drop in the cover gas region is from 34kPa to 25kPa during 40 liter sampling. Test runs showed that, up to 50mg of trapped sodium aerosol mass in the bottle, the coagulation of aerosols was not noticed for next 24 hrs after sampling. It is observed that, total sampled aerosol mass is found to get trapped in the first bottle itself for the sampling temperature up to 350°C, while, for the temperature of 400-550°C, there exists trapping of aerosols mass in the second bottle up to a maximum of 10% of the first bottle. The filter paper is analyzed for retention of sodium aerosol by chemically. There is no trapping of aerosol is observed in filter paper in all the runs.

5.1.3 Sodium metal aerosol sampling procedure and safety

The sodium metal aerosol sampling and safety are described in chapter-III. The experiment is repeated for the same sampling height after raising sodium pool temperature by another 50°C. The experiments are continued for temperature of sodium pool up to 550°C. After completing one set of reading up to 550°C for sampling height 415mm (middle level of cover gas), experiments are repeated for other sampling heights 715mm and 215mm (near the sodium pool and near the roof). The sampling line tested using argon gas and communicated to cover gas region is ensured to rule out the plugging of sodium metal aerosol in the sampling line before starting every sampling. The change of sampling tube is carried out only after draining the sodium from TP-1. The SILVERINA loop is in dumped condition and argon purging continued when sampling tube is replaced. The pressure hold up test of loop at 0.5kg/cm^2 for four hours carried out after each replacement of sampling tube.

5.2 Results and Discussion

5.2.1 Temperature profile of cover gas region

The temperature profile of cover gas region in SILVERINA loop was measured by varying sodium pool temperature from 250 - 550°C. The temperature profiles of the cover gas region with cover gas height for various pool temperatures are shown in Fig. 5.2. It is observed that, temperature profile is found to follow a similar pattern as found in the literature [5.10]. The temperature started decreasing from the pool surface (820-790 mm) - region C, then has uniform temperature region (790-20 mm) for about 770 mm height - region B, and decreases towards roof temperature (20-0 mm) - region A. The temperature of the roof top found to vary from 90 to 150°C for the sodium pool temperatures from 250 to 550°C respectively. The decrease of temperature in the region A varies according to the temperature difference between bulk cover gas temperature and bottom surface of the roof top.

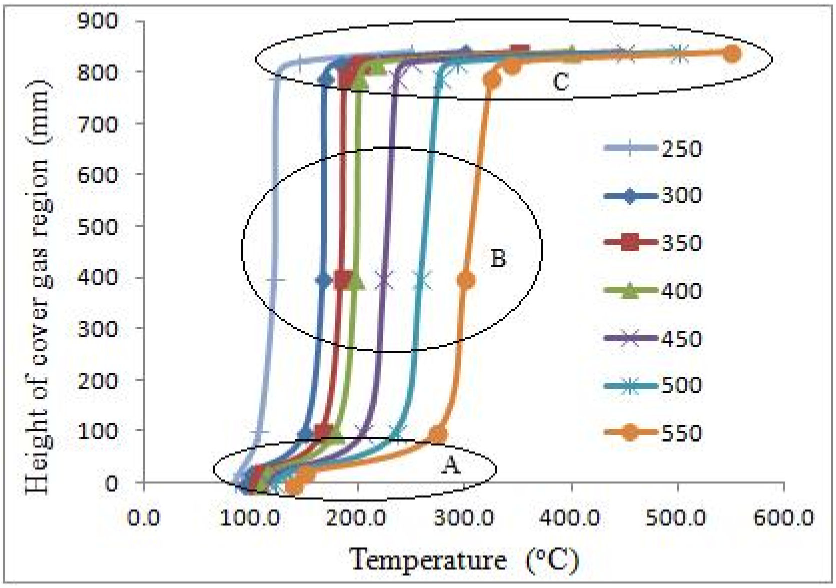

Fig.5.2 Temperature profile of cover gas region with various pool temperatures.

5.2.2 Aerosol size distribution

The liquid paraffin oil sampled after each measurement is analyzed and mass-size distribution and MMD were determined. The size distribution and MMD were obtained for all the three sampling heights (near the sodium pool, middle level of cover gas region and near the roof) and for all the pool temperatures. A typical steady state size distribution at middle region of cover gas for 400°C pool temperature is shown in Fig.5.3. It is observed from Fig.5.3, that particles are found in the range of 1 to 16 µm with MMD around 7.0 µm ($\sigma_g = 1.5$). The MMDs obtained for three different sampling levels for various pool temperatures are shown in Fig.5.4. It is observed from Fig.5.4, that, MMD found to increase linearly with increase of sodium pool temperature. It is also noted from the figure, for all the pool temperatures, the value of MMD is found to be higher near the pool surface (715 mm) when compared with that of near the roof (215 mm) and middle level of cover gas region (415 mm).

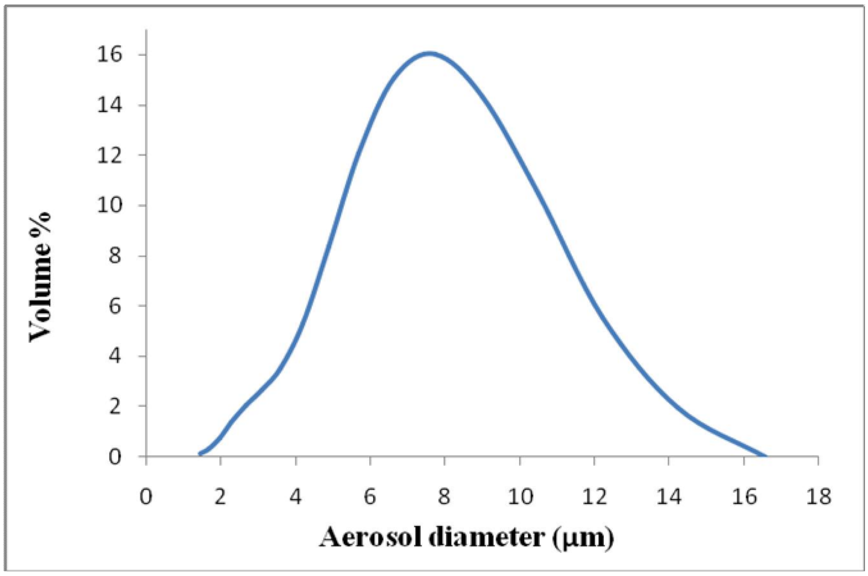

Fig.5.3 Volume – size distribution of sodium metal aerosol at the middle level of cover gas region for 400°C pool temperature.

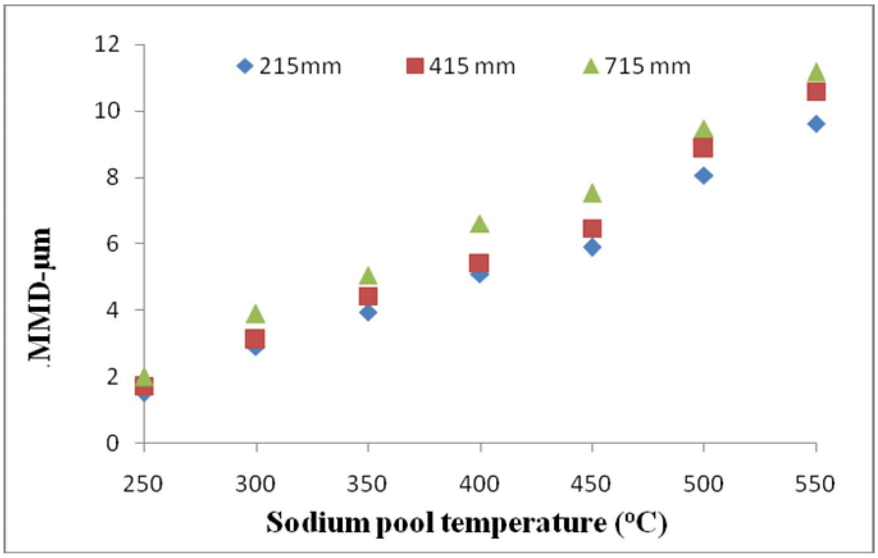

Fig.5.4 MMD of sodium metal aerosol for various pool temperatures.

5.2.3 Aerosol mass concentration

The mass of trapped sodium metal aerosols in the bottles for all the samples was determined by conductivity method and found to vary from 0.026 – 35.6g/m^3. The variation of sodium metal aerosol mass concentration for various pool temperatures at three different levels is shown in Fig.5.5. It is observed that, the mass concentration increases with increase of sodium pool temperature and found to fit in 3rd order polynomial regression. It is also observed from the figure, for all the pool temperatures, the sodium metal aerosol mass concentration is higher near the pool than that of near the roof and middle level of cover gas region.

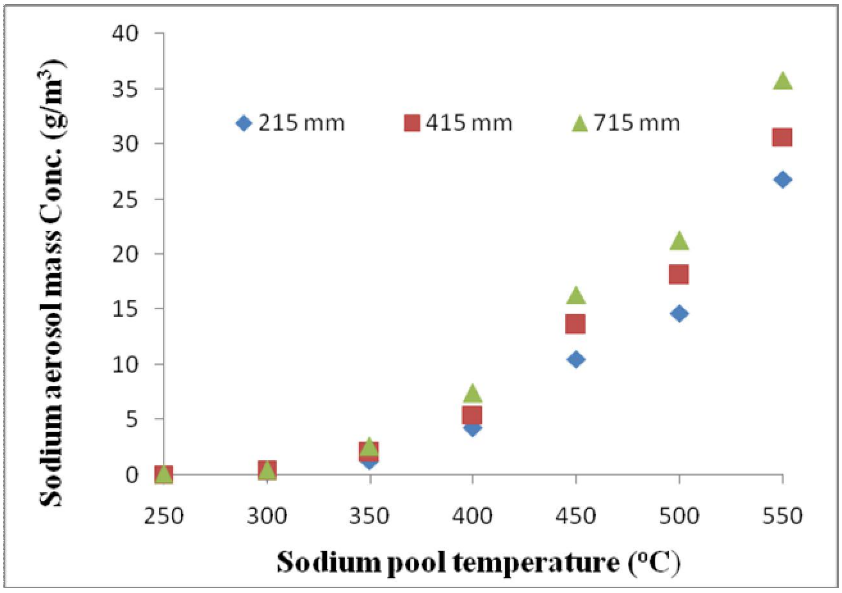

Fig.5.5 Sodium metal aerosol mass concentration for various pool temperatures

5.2.4 Theoretical simulation

Fig.5.6 shows the MMD of sodium aerosols measured in the middle region of cover gas for various pool temperatures along with fitted equation (linear regression). This fitted equation is used as an input for calculating mass concentration of the sodium aerosols for various pool temperatures in the cover gas region. Since, the sodium aerosols are continuously generated in the pool when rising the pool temperature, to calculate the mass concentration of aerosols for a particular temperature, the initial particle size is taken for the temperature below that of particular temperature by using the fitted equation. For example, if we want to calculate the mass concentration at pool temperature of 300^{o}C, the initial radius is taken from fitted equation at 290^{o}C. It is observed that, the mass concentrations predicted for pool temperature of 250^{o}C and 300^{o}C did not show significant difference when the initial particle size is taken for the temperature difference of more than 10^{o}C, but it shows significant variation (>15%) in the range of 400°C and above. (It is to be noted that aerosol mass concentration is very less in 250°C and 300°C, when compared with 400°C and above).

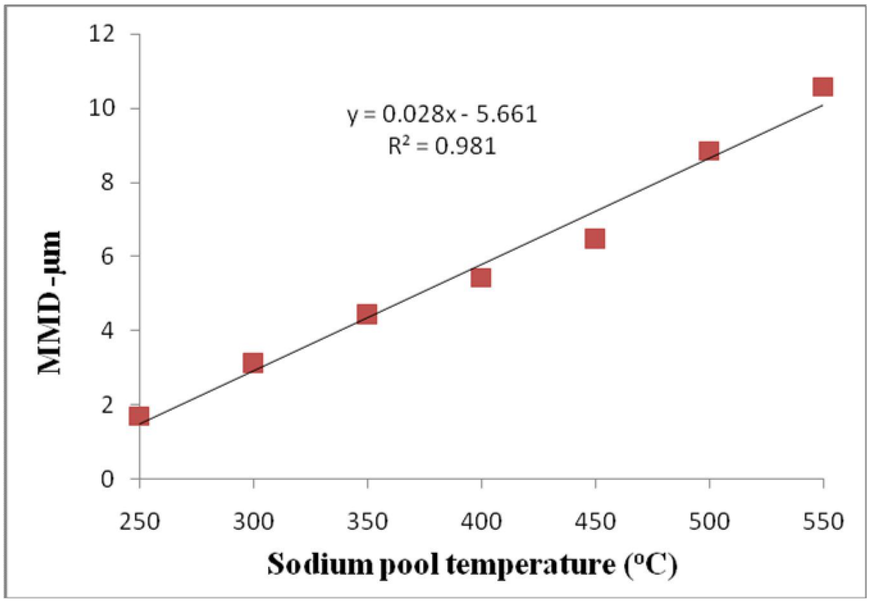

Fig.5.6 Experimental variation of MMD of sodium metal aerosol for various pool temperatures at the middle level of cover gas region

Fig.5.7 shows the simulated and experimentally measured mass concentration for various pool temperatures at the middle level of the cover gas region. It is noted from the figure that, mass concentration predicted by the simulation is found to be underestimated by 10-15% with experimental value for the temperatures between 250°C and 450°C. Afterwards the trend begins to change and at 550°C the mass concentration is overestimated by 15%. The variation of 10-15% in the lower temperature region (250-450°C) is attributed to the spatial variation of concentration in the actual scenario, whereas, it is assumed to be uniform in the theoretical estimation. As the evaporation rate increases with increase of sodium pool temperature, the sodium metal aerosol mass concentration as well as MMD found increased. Due to higher concentration, the larger sized particles undergo cloud settling resulting the difference in the measured concentration by about -15% from the predicted value for 550°C; whereas, the simulation deals with individual particle settling.

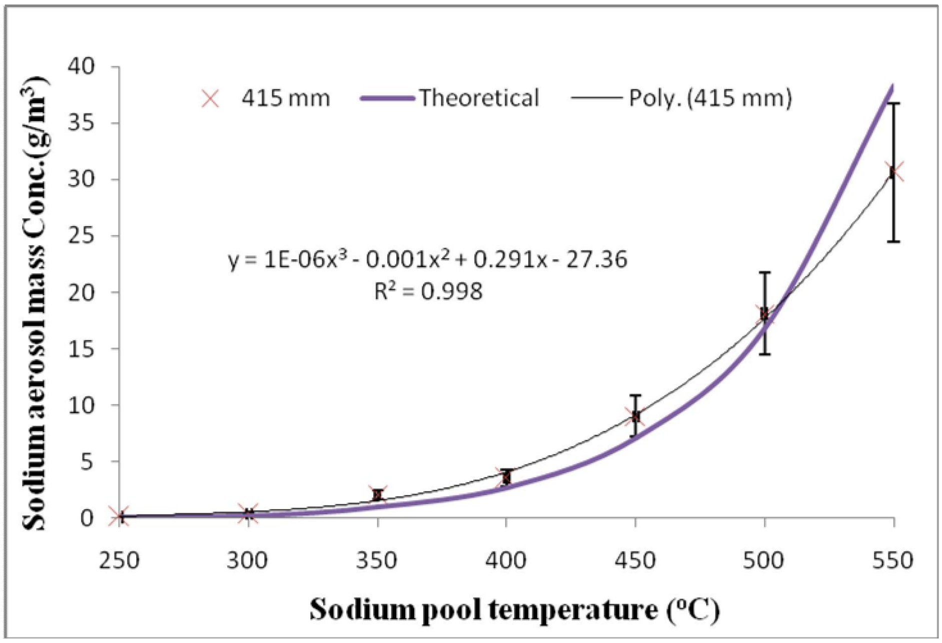

Fig.5.7 Theoretical and experimental comparison of sodium metal aerosol mass concentration.

It is to be noted here that, similar trend is observed between the predicted mass concentrations and measured concentrations for other two levels (lower and upper cover gas regions). It is also to be noted that, the experimental error associated due to flow rate, sampling time and analysis is 7-10%.

5.2.5 The role of aerosols in the cover gas region

A brief description on the role of aerosols in the cover gas region in heat and mass transfer process is given below: The scope of the thesis is not focused on this subject.

The thermal radiation from the pool surface is scattered by the presence of aerosols in the cover gas region and it reduces the heat flux reaching the bottom of the roof top. The modified Stephan’s law for heat transfer between two surfaces is given below, including absorption and scattering of thermal radiation by aerosols [5.10].

$$\varphi^{'} = \sigma * A_p * (T_p^4 - T_r^4)/(1/\varepsilon_p + 1/\varepsilon_r - 1 + \tau) \qquad (5.1)$$

Where σ Stefan-Boltzmann constant

ε_p Emissivity of sodium pool surface

ε_r Emissivity of roof bottom surface

T_r Roof bottom surface temperature

T_p Sodium pool temperature

A_p Area of the sodium pool surface

Optical thickness $\tau = \kappa * L$

where κ is extinction coefficient of sodium metal aerosol = $C*K_c$,

where K_c is the mass extinction coefficient and to be determined experimentally by conducting experiments for the absorption of black body radiation for a various known concentration C, L is height of cover gas region.

It is further observed that, particle size plays important role in the forward scattering (Mie Scattering) of thermal radiation. The thermal radiation transfer is unique feature to a particular geometry [5.10]. The heat transfer to roof top decreases with increase of sodium metal aerosol mass concentration due to scattering of thermal radiation by the aerosols. The mass transfer occurs mainly due to condensation of sodium aerosols reaching the bottom surface of roof top. At higher roof temperature, the mass transfer rate decreases and mass deposited on the roof bottom surface also begin to decrease. It is noted that, the sodium metal aerosols begin to condense in the bulk gas region before reaching the roof surface.

5.3 Summary

It is observed from our experiments, the sodium metal aerosol size distribution is found to be mono-model. Both, MMD and mass concentration of sodium metal aerosols increases with increase of sodium pool temperature. The sodium aerosol mass concentration and MMD are found to be larger near the sodium pool compared to middle of the cover gas region and near the roof top. The simulated and experimental measured mass concentration of sodium metal aerosol in cover gas region is found to have good agreement. The modeling is found useful in predicting the sodium metal aerosol mass concentration for a given geometry and sodium pool temperature.

5.4 Reference

5.1 O. Frukawa, A. Furutani, N. Hattori and Iguchit, (1984),"Experimental study of heat and mass transfer through the cover gas in the Liquid Metal Fast Breeder Reactor (LMFBR)", Proceeding of the third international conference on liquid metal engineering and technology, The British nuclear Society, Vol.1, 451-458. ISBN0-7277-0209-2.

5.2 J. Minges and W. Schutz, ‘Experiments on the enrichment of cesium in the cover gas aerosol of the European Fast Reactor (EFR)’. Nuclear Engineering and Design 147 (1993) 17-22.

5.3 J. Minges and W. Schutz, (1991), "Experiments to characterize the sodium aerosol system in the cover gas of the European Fast Reactor EFR", J. Aerosol Sci. Vol. 22, S761-S764.

5.4 J. L. D. Glockling, (1991), "Heat and Mass transfer in specific aerosol system", PhD thesis, Department of chemical engineering. South bank University, London.

5.5 Yoshiaki HIMENO and June TAKAHASHI, (1980),"Sodium Mist behavior in cover gas space of LMFBR", J. Nucl. Sci. and Tech. Vol. 17, 404-412.

5.6 Yoshiaki HIMENO and Yoshiaki YAMAGISHI, (1982), "Effect of barriers on sodium mist deposition on LMFBR components", J. Nucl. Sci. and Tech. Vol. 19 [10], 837-844.

5.7 Amit Kumar, V. Subramanian, R. Baskaran, S. Krishnakumar, S. Chandramouli, B. Venkatraman, (2015), "Characterisation of Sodium Aerosol in Cover Gas Region of SILVERINA Loop", Aerosol and Air Qual. Res., Vol., 15, 1813 –1822.

5.8 S. Chandramouli, S. Sakthivel, P. Vijayamohana Rao, K. Gurumoorthy, K. K. Rajan, P. Kalyanasundaram and G. Vaidyanathan, (2006), "Commissioning and Operation of

SILVERINA sodium loop," OPENUPP-2006, Nov. 13-15, BARC, Mumbai. Proceedings of National Conference on Operating experiences of Nuclear reactors and power plants 203-209.

5.9 Amit Kumar, V. Subramanian, R. Baskaran, S. Krishnakumar, S. Chandramouli, B. Venkatraman, (2014), "Development and Validation of a Methodology for Characterization of Sodium Aerosols in Cover Gas Region", Aerosol and Air Quality Research, Vol. 14, 1534 –1541.

5.10 D. N. Roberts, (1995), "Heat and Mass transfer studies in sodium – Argon filled enclosures", PhD thesis, South bank University, London.

CHAPTER - VI

GEOMETRICAL EFFECT ON SODIUM METAL AEROSOL CHARACTERISTICS IN COVER GAS REGION

6.0 Introduction

The sodium metal aerosol characteristics in the cover gas region of SFR is important for determining the heat and mass transfer phenomena from the hot sodium pool surface to the roof slab of the reactor vessel. It is inferred from the literature that, the dimension of cover gas region influences the aerosol characteristics. It is observed from the studies by Minges and Schutz, 1991 & 1993, and Yamamoto *et al.,* 1991, Newson *et al.*, 1993, Himeno and Takahashi, 1980 and 1982 Frukawa *et al.*, 1984, Glockling *et al.* 1991, and Roberts *et al.*, 1995, the sodium metal aerosol characteristics (size distribution and mass concentration) are different for different geometries [6.1, 6.2, 6.3, 6.4, 6.5, 6.6, 6.7, 6.8 and 6.9]. The variation of sodium metal aerosol characteristics in the cover gas region for different geometries and for various pool temperatures at constant roof temperatures is shown in table 6.1. It is observed that measurements were carried out for pool temperature of 250 - 550^{o}C and with almost constant roof temperature 85 -150^{o}C. The MMD of sodium metal aerosols found to be in the range from 1.5 - 26µm i.e. for lower temperature it is 1.5µm and for higher temperature it is 26 µm, in particular, the value at 550^{o}C found to increase with increase of L/D value. Further, the mass concentration found in the range from 0.2 - 40g/m^{3} i.e. the value at 550^{o}C found to decrease when L/D value increased. It is noted from the table 6.1 that, the sodium metal aerosol characteristics depend on geometry of the vessel (L/D ratio, where L - height of cover gas region and D - diameter of sodium pool). In order to ascertain the dimensional dependence of sodium metal aerosol characteristics in cover gas region, experiments have been carried out in another Test Pot (TP-3) of SILVERINA loop. The aspect ratio (L/D) of TP-3 is 1.875, which is higher than that of TP-1 (1.075) i.e. diameter of sodium pool TP-3 is smaller than TP-1. The detailed description of TP-3 vessel is given in chapter -II. It is determined in the earlier chapter, the sodium metal aerosol characteristics also depends on the pool, roof and bulk cover gas temperatures i.e. sodium metal aerosol characteristics in the cover gas region is the function of (i) sodium evaporation rate which depends on sodium pool temperature and difference between pool & roof temperature, (ii) sodium vapor condensation in the cover gas region which depends on bulk cover gas temperature, (iii) aerosol deposition on the roof surface, side walls and annular space due to temperature difference between bulk cover gas region and with respective area and (iv) convection source and coagulation which depend on bulk cover gas temperature.

Table 6.1 Variation of sodium metal aerosol characteristics in the cover gas region for different geometries.

	L/D	**Pool Temp. (°C)**	**Roof Temp. (°C)**	**Range of MMD (μm)**	**Range of Mass Conc. (g/m^3)**
Minges [6.1, 6.2]	0.55	350 -550	120	3.5 - 8.5	1.5 - 40.0
TP-1 [6.11]	1.076	250 - 550	85 - 140	1.5 - 11.5	0.6 - 30.6
Glockling [6.8]	2.333	300 -550	150	3.3 - 13.5	0.5 - 36.5
Yoshiaki [6.5, 6.6]	4.516	300 - 550	120	6.0 -26.0	0.2 - 20.0

To quantify these phenomena, temperature profile of cover gas region and bulk cover gas temperature are essential parameters for (i) the determination/estimation of sodium metal aerosol characteristics, (ii) aerosol deposition on to the cooler surfaces and (iii) heat and mass transfer analysis. To predict the temperature of cover gas region, an empirical relation is derived from our experimental results of TP-1 and TP-3. This empirical relation is used for predicting the bulk cover gas temperature for other studies. Similarly an empirical relation derived to predict the sodium metal aerosol diameter (MMD) based on our experimental results of TP-1 and TP-3 of SILVERINA loop and with available published work by Minges et al., Glockling et al., and Yoshiaki et al. It is to be noted that these experiments were carried out by varying sodium pool temperature for a fixed roof temperature as similar to our experiments i.e. similar to our experimental condition. Using these empirical relations (for sodium metal aerosol diameter and bulk cover gas temperature) as input and coupling with aspect ratio, our earlier model is redefined and applied for predicting sodium metal aerosol mass concentration for the given pool temperature and aspect ratio. In this chapter, the details of the experimental results obtained from TP-3 of SILVERINA loop, the empirical relations for bulk cover gas temperature and the sodium metal aerosol diameter are described. The validation of theoretical simulation on sodium metal aerosol mass concentration with the experimental results of TP-1, TP-3 and the experimental results published by Minges et al., Glockling et al., and Yoshiaki et al., are also presented.

6.1 Materials and Methods

A schematic diagram of sodium metal aerosol sampling system and cover gas temperature profile measuring system installed in TP-3 of SILVERINA loop is shown in Fig.6.1. TP-3 is a similar vessel like TP-1, the sodium level is maintained with cover gas height of 750mm, the sodium temperatures is maintained from 200-550°C and the region above the sodium pool is filled with argon gas. In the present experimental set-up, the portion of the sampling tube which goes inside TP-3 has been fabricated with a length of 385 mm to enable the sampling at the middle level of cover gas region. The aerosol sampling tube is made of SS316 with internal diameter of 10mm (1.5mm wall thickness). The maximum particle diameter that can be collected is 20µm, without having bias due to wall deposition by impaction for a flow rate of 2lpm [6.10]. Before starting the experiment the sampling tube is attached with the flange and inserted into TP-3. The pressure holdup test for sampling tube and gate valve has been carried out by pressurizing TP-3 up to 0.5kg/cm^2 above atmosphere. The functioning of surface heaters, temperature controller and thermocouples (fitted in the sampling line) has been checked by heating the heater up to 150^{o}C.

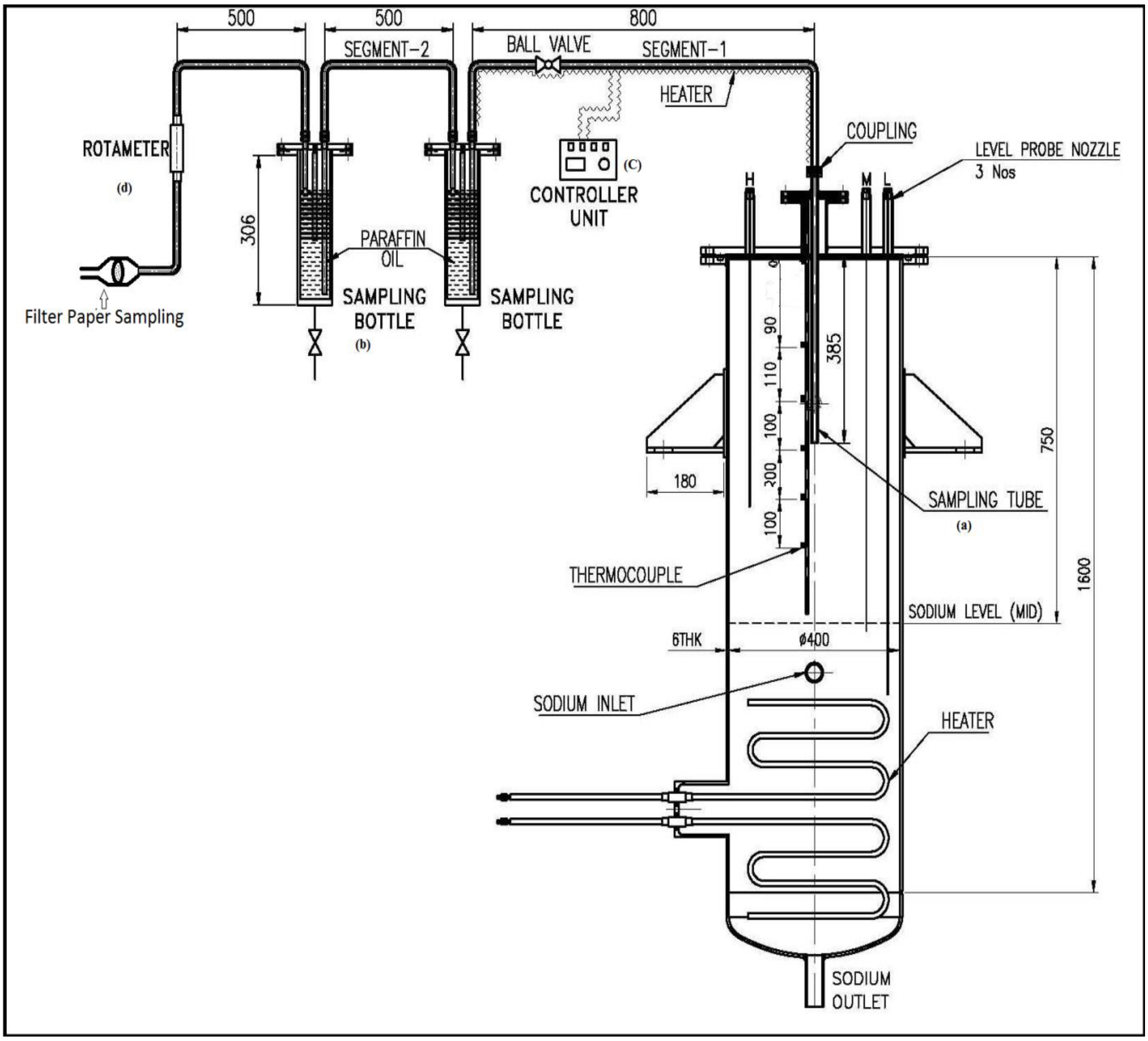

Fig. 6.1 A schematic diagram of sodium metal aerosol sampling system and cover gas temperature profile measuring system installed in TP-3 of SILVERINA loop.

6.1.1 Sodium metal aerosol sampling system

Aerosols are drawn from the cover gas region and allowed to get trapped in liquid paraffin oil medium without exposing them to atmosphere. The cover gas (argon) is made to bubble through liquid paraffin oil at a flow rate of 2lpm. The sodium pool temperature was varied from 250 - 550°C in step of 50°C. In order to avoid coagulation of sodium metal aerosol trapped in the paraffin oil, the sampling time was kept for 10 minutes for the pool temperature 250°C and progressively reduced to 2 minutes when pool temperature is 550°C.

After isolating the bottles from the system the sampling bottles were taken for analyzing the samples. The size distribution of sodium aerosols is determined by using Mastersizer (M/s Malvern Instruments, UK). The measurement of sodium aerosol mass concentration is carried out by conductivity method (M/s Metrohm, 856 conductivity module, Switzerland).

6.1.2 Cover gas temperature profile measuring system

A photograph of the sampling system along with cover gas temperature measurement system is shown in Fig.6.2.

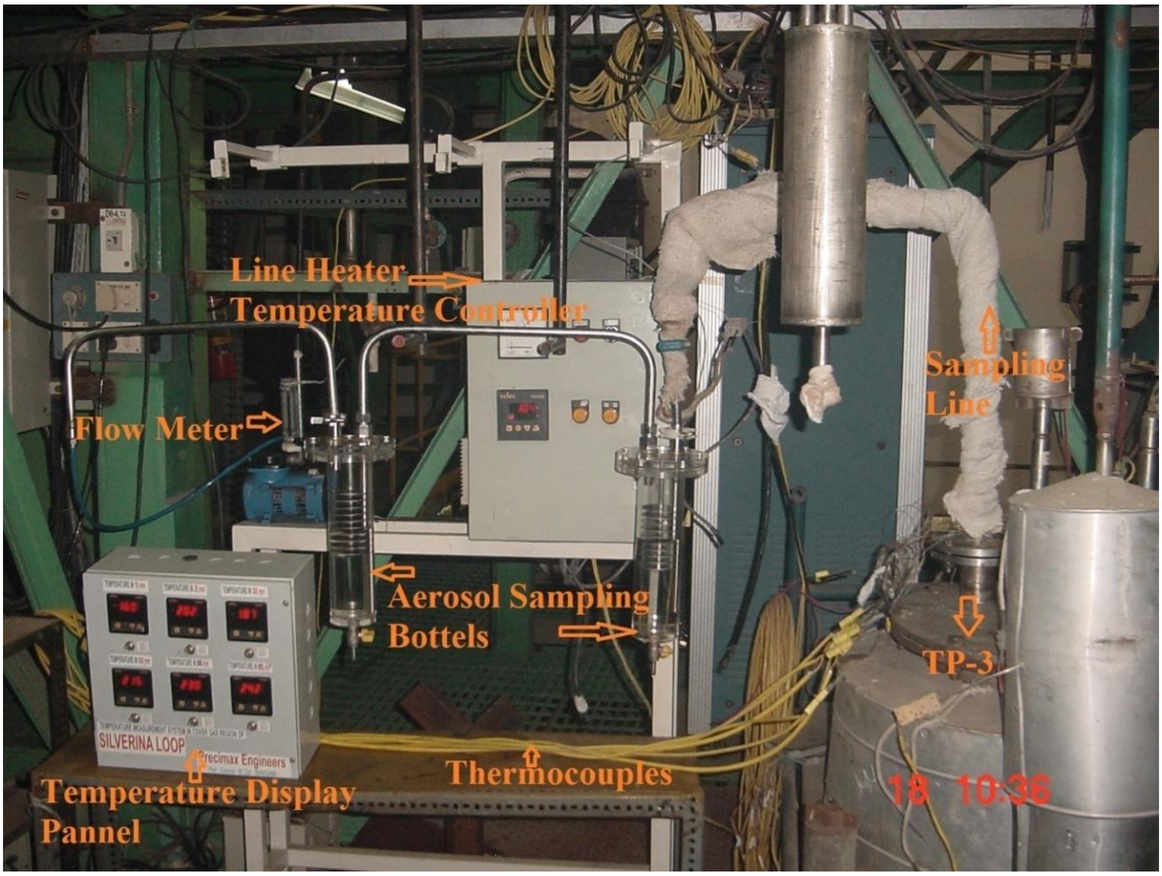

Fig.6.2 A photograph of the sodium metal aerosol sampling system along with temperature measurement system of TP-3.

A similar type of temperature measurement system as described in Amit et. al., 2015 for TP-1 [6.11], has been fabricated with matched top flange for the aerosol port, a vertical cylindrical shaft welded below the top flange and six grooves to insert 6 thermocouples which are terminated at six different heights. Temperature was measured by using chromel-aluminium

K-type thermocouples at the six locations in the cover gas region. The temperature measurement locations from the top of flange are (i) roof surface (0 mm), (ii) one location near to the roof surface (90 mm), (iii) three locations on the middle of the cover gas region (200 mm, 300 mm and 500 mm), (iv) one location near to the sodium pool surface (600 mm). Sodium pool temperature is measured separately. Accordingly, the thermocouples were terminated at 600 mm, 500 mm, 300mm, 200 mm, 90 mm, and 0 mm from bottom surface of the top flange. Each thermocouple is connected with 3½ - digit digital indicator.

6.2 Results and Discussion

6.2.1 Temperature profile of cover gas region of TP-3

The temperature profile in TP-3 of cover gas region is measured by varying sodium pool temperatures from 250 - 550°C. The temperature profiles of the cover gas region with cover gas depth for various pool temperatures are shown in Fig. 6.3. It is observed that, temperature profile is found to follow a similar pattern as found in the literature [6.9] and the results obtained in TP-1 [6.11].

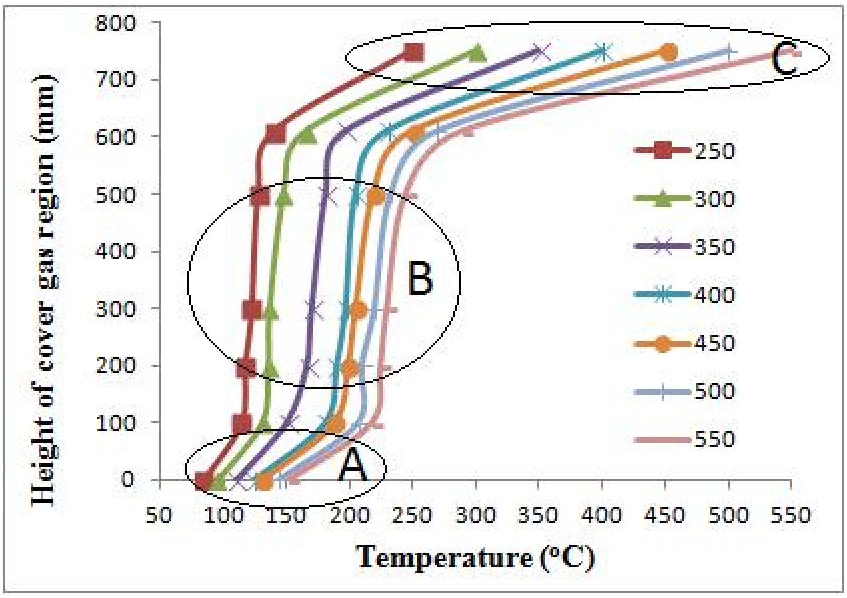

Fig.6.3 Variation of temperature in cover gas region with cover gas height for various pool temperatures for TP-3.

The temperature started decreasing from the pool surface (750-600mm) - region C, then has almost uniform temperature region (600-90 mm) for about 500mm height - region B, and decreases towards roof temperature (90-0mm) - region A. The temperature of the roof top found to vary from 90 to 160°C for the sodium pool temperatures from 250 to 550°C respectively.

***Determination of bulk cover gas temperature*:** The bulk cover gas temperature is an important parameter for theoretical prediction of aerosol mass concentration in cover gas region. There are two ways found in the literature to predict bulk cover gas temperature viz. the first one is by taking average temperature between pool and roof ($(T_p+T_r)/2$) and the second one is shown by the formula ($T_r+0.6*(T_p-T_r)$) [6.12]. Where T_p and T_r are the sodium pool, and roof temperatures respectively. The bulk cover gas temperature of TP-1 and TP-3 are calculated using above relations and given in table 6.2 and 6.3 respectively. It is observed from table 6.2 and 6.3 that, the variation in estimated bulk cover gas temperature is found to have deviation of 15 - 50% from the measured value for the pool temperatures 250 - 550^{O}C.

Table 6.2 Comparisons of predicted and experimentally measured bulk cover gas temperature (T_m) for various pool temperatures of TP-1.

Tp (^{o}C)	**Tr (^{o}C)**	**Tm (^{o}C) Exp.**	**$T_m = (T_p+T_r)/2$**	**Deviation (%)**	**$T_m = T_r+0.6*(T_p-T_r)$**	**Deviation (%)**
250	85	120	167.5	40	184	53
300	95	160	197.5	23	218	36
350	105	180	227.5	26	252	40
400	110	200	255	28	284	42
450	120	230	285	24	318	38
500	130	270	315	17	352	30
550	140	330	345	5	386	17

Table 6.3 Comparisons of predicted and experimentally bulk measured cover gas temperature (T_m) for various pool temperatures of TP-3.

Tp (^oC)	**Tr (^oC)**	**T_m (^oC) Exp.**	**T_m = (T_p+T_r)/2**	**Deviation (%)**	**Tm = T_r+0.6*(T_p-T_r)**	**Deviation (%)**
250	85	120	102.5	40	184	53
300	95	140	117.5	41	218	55
350	110	170	140	35	254	49
400	125	190	157.5	38	290	52
450	130	210	170	38	322	53
500	145	230	187.5	40	358	55
550	160	260	210	37	394	51

In the present work to arrive bulk cover gas temperature, an empirical relation is derived by taking into account of cross sectional area of cover gas region and temperatures of sodium pool, roof and wall surface and it is given as:

$$T_m = (T_p * A_p + T_r * A_r + T_w * A_w)/(A_p + A_r + A_w) \qquad (6.1)$$

where Tm and T_w are the bulk cover gas and wall surface temperatures respectively, A_p, A_r and A_w are the area of sodium pool, roof and wall surface respectively. The above empirical relation for bulk cover gas temperature is validated with the experimentally measured temperature from 250-550^{O}C of cover gas region of TP-1 and TP-3 and it is given in Table 6.4. It is noted from table 6.4 that, the predicted cover gas temperature is slightly higher compared to the experimentally measured cover gas temperature for TP-1 and TP-3. The variation in the experimental and estimated bulk cover gas temperature is well within 10%. Since, the bulk cover gas temperature is not available in the published work by others, this empirical relation (equation-6.1) is used for predicating the bulk cover gas temperature for the geometry of other works for theoretical modeling.

Table 6.4 Comparisons of predicted and experimentally measured cover gas temperature (T_m) for various pool temperatures of TP-1 and TP-3.

T_p (°C)	TP-1			TP-3		
	T_w (°C)	T_m (°C) Estimated	Deviation (%)	T_w (°C)	T_m (°C) Estimated	Deviation (%)
250	120	135	13	120	130	8
300	160	172	7	140	152	8
350	180	195	8	170	182	7
400	200	217	9	190	205	8
450	230	247	6	210	226	8
500	270	284	5	230	249	8
550	330	335	2	260	279	7

6.2.2 Aerosol Characteristics in TP-3

The MMD obtained for middle level of cover gas region for various pool temperatures of TP-3 is shown in Fig.6.4 and it is found to vary from 2.1 to 16μm. It is observed from Fig.6.4, that, MMD found to increase linearly with increase of sodium pool temperature. Fig 6.4 also includes linear fitted equation for MMD with temperature. The variation of sodium metal aerosol mass concentration for various pool temperatures (theoretically and experimentally) is shown in Fig.6.5 for TP-3. The mass concentration of the sodium metal aerosols is found to vary from 0.04 – 21.98g/m^3. It is observed that, the mass concentration increases with increase of sodium pool temperature and found to fit polynomial regression. The simulated and measured sodium aerosol mass concentration has good agreement and the variation between measured and predicted value are within ±20%. In the cover gas region, there exists convection current due to thermal gradient between hot pool surface and bottom of the roof slab. The aerosols, formed due to evaporation of vapor for a particular temperature of the sodium pool surface, are carried by the convection current, undergo coagulation and reaches steady state value. Further, the cover gas region is being maintained at a positive pressure of 0.5 kg/cm^2 before starting of every sampling.

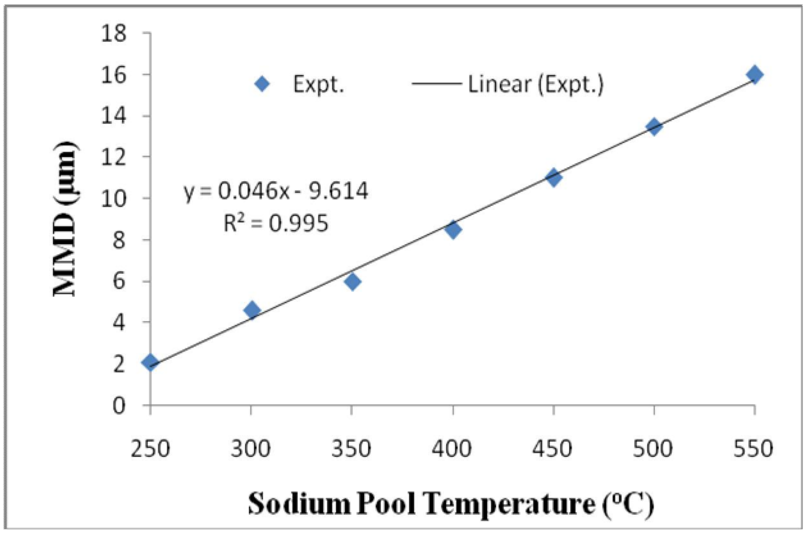

Fig.6.4 MMD of sodium metal aerosol in the middle region of the cover gas of TP-3 for various pool temperatures.

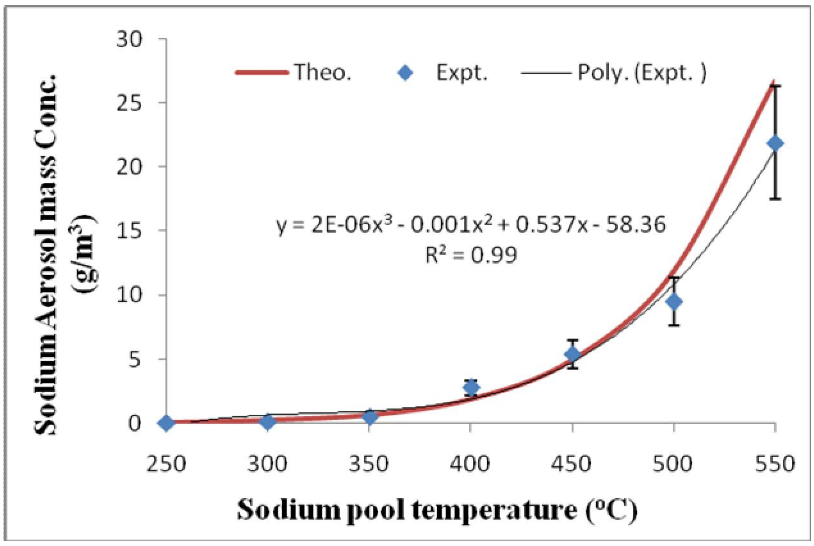

Fig.6.5 Sodium metal aerosol mass concentration (Theo. and Expt.) in the middle region of cover gas of TP-3 for various pool temperatures.

The positive pressure ensures the uniform distribution of aerosols through-out the region and sampling flow rate of 2lpm without any pump. Besides, aerosol deposition does occur on colder roof slab when the particles enter into the upper boundary layer. We have noticed in our experiment in TP-1 and TP-3, for a given difference in temperature between sodium pool surface and roof slab, the steady state condition is reached in about 20-30 minutes. The measured values of concentration and diameter are after this period. Hence, hydrodynamic condition in cover gas region viz., convection current, aerosol deposition and sampling flow rate are taken care once steady state values are reached i.e. the repeat measurement showed that the variation of sodium metal aerosol characteristics are within ±5%.

6.2.3 Determination of sodium metal aerosol size in cover gas region

A theoretical simulation for the sodium metal aerosol mass concentration in the cover gas region is formulated in our earlier work (Amit et. al., 2015) [6.11 & 6.13] using mass and number concentration decay equation by including the effect of continuous source term and various removal mechanisms (Sheth et al., 1975) [6.14]. A first order differential equation is formulated to predict the equilibrium mass and number concentrations of the sodium aerosols in cover gas region. In this model, the input parameters are (i) temperature of sodium pool surface, roof and bulk cover gas, (ii) geometry of the vessel (diameter of the pool surface and height of the cover gas region) for a given cover gas region and (iii) initial radius of aerosol. In our earlier work, the initial radius is taken from the linearly fitted equation derived from the actual measurement in that cover gas region. This approach requires sampling of sodium aerosol from the cover gas region.

To improve theoretical modeling for predicting the sodium metal aerosol characteristics in cover gas region for different geometry, an empirical relation has been derived to predict the initial particle size of aerosols and used as input for the theoretical simulation. The empirical relation includes variation of L/D ratio and sodium pool temperatures. The empirical relation is validated with the experimental results obtained from our works in TP-1 and TP-3 and Minges et al., Glockling et al., and Yoshiaki et al., [6.1, 6.2, 6.5, 6.6 and 6.8]. The empirical relation for aerosol radius is given below:

$$R = \left(\frac{Ro}{2}\right) * \left(0.5046 * \frac{L}{D} + 1.0634\right) * \left(\frac{Tp}{\mathrm{Tpi}}\right)^{2.5} \qquad (6.2)$$

where R(µm) - radius of aerosol for T_p, Ro - 1.0µm (radius of aerosol for T_{pi}), L - height of cover gas region (mm), D - diameter of the sodium pool (mm), T_p - sodium pool temperature (^oC), T_{pi} - temperature at which measurable aerosol mass concentration is observed which is 250^{o}C.

It is observed in our study (in TP-1 and TP-3), sodium metal aerosol mass concentration is measurable at sodium pool temperature of 250^{o}C. The average aerosol diameter (MMD) measured around 2.0µm. Hence, the initial radius Ro is taken as 1.0µm. By using this empirical relation, the initial sodium aerosol radius is estimated for any similar geometry of the cover gas region and for all pool temperatures (250°C - 550°C). The estimated and experimentally measured sodium metal aerosol diameter (MMD) for various pool temperatures of TP-1, TP-3, Minges et al., Glockling et al., and Yoshiaki et al., are given in Table 6.5. It is noted from Table 6.5 that, the deviation of estimated and experimentally measured sodium aerosol size (MMD) is within ±20% for all cases. The variation of MMD versus sodium pool temperature for various L/D ratios for both experimentally determined values and empirically fitted equation is shown in Fig.6.6. It is observed from Fig.6.6 that, for a given pool temperature the value of MMD is found to increase with increase in L/D ratio. Moreover, the MMD is found to increase with increase of pool temperature for a given geometry (L/D) of the cover gas region and found to follow super-linear pattern with increase of L/D value, i.e. for smaller diameter vessel. The large MMD value and super-linearity can be the result of enhanced coagulation of the aerosols during convection motions in the smaller cover gas region. It is also observed from Fig.6.6, for L/D ratio of 0.55, the MMD follows linear pattern. The condition of super-linearity is observed for L/D values of 2.33 and 4.516. Hence, empirical relation is formulated with exponent 2.5 to accommodate the increment of size with increase of pool temperature for different geometry starting from 0.55 to 4.516. The empirical relation is found useful in predicting all the conditions satisfactorily.

Table 6.5 Comparison of predicted and measured sodium metal aerosol MMD for various pool temperatures of TP-1, TP-3, Minges et al., Glockling et al., and Yoshiaki et al.

Sodium pool temperature (^{o}C)		**250**	**300**	**350**	**400**	**450**	**500**	**550**
Minges (L/D-0.55)	Exp. MMD (μm)			3.5	4.5	6	7.2	8.5
	Theo. MMD (μm)			3.11	4.34	5.83	7.58	9.63
	Variation (%)			11.14	3.55	2.83	5.27	13.29
TP-1 (L/D-1.076)	Exp. MMD (μm)	1.5	2.89	4.33	5.44	6.47	8.86	11.5
	Theo. MMD (μm)	1.61	2.53	3.73	5.2	6.98	9.09	11.53
	Variation (%)	7.33	12.45	13.85	4.41	7.88	2.59	0.26
TP-3 (L/D-1.875)	Exp. MMD (μm)	2.11	3.95	5.62	7.59	10.81	12.85	15.79
	Theo. MMD (μm)	2.01	3.17	4.66	6.51	8.75	11.37	14.43
	Variation (%)	4.73	19.74	17.08	14.22	19.08	11.51	8.61
Glockling (L/D-2.333)	Exp. MMD (μm)		3.43	6.45	8.58	9.72	11.24	13.55
	Theo. MMD (μm)		3.53	5.19	7.25	9.73	12.67	16.07
	Variation (%)		2.91	19.53	15.5	0.1	12.72	18.59
Yoshiaki (L/D-4.516)	Exp. MMD (μm)		6	7.9	11	14.6	19.5	26
	Theo. MMD (μm)		5.27	7.75	10.82	14.53	18.91	23.99
	Variation (%)		12.16	1.89	1.63	0.47	3.02	7.73

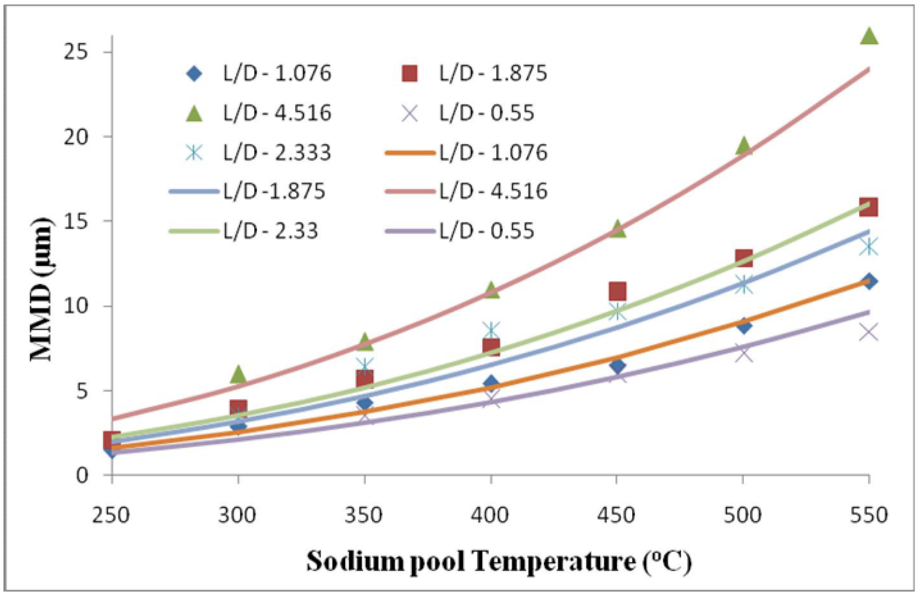

Fig.6.6 Variation of MMD (Expt. and Theo.) with sodium pool temperature for various L/D ratio.

6.2.4 Theoretical simulation of sodium metal aerosol mass concentration for different geometries

The initial radius of sodium metal aerosol is calculated using equation - 6.2 for a given sodium pool temperature. Using initial radius, roof & wall temperatures and geometry of cover gas region (diameter of the sodium pool and height of cover gas region), the sodium metal aerosol mass concentration in the cover gas region is estimated by the theoretical model. The theoretical simulation for mass concentration is carried out for our work in TP-1, TP-3 and for the available literature works (Minges et al., Glockling et al., 1991, Yoshiaki et al.). The calculated values are presented in Table 6.6. It is observed from Table 6.6 that sodium aerosol mass concentration increases with increase of L/D ratio of cover gas region ($0.55 \leq L/D \leq 4.52$) for a given pool and roof temperatures. It is noted from the Table 6.6 that, the maximum variation of theoretically simulated sodium metal aerosol mass concentration and experimentally measured aerosol mass concentration is found to vary within ±30% [6.15]. The theoretical modeling is found useful to predict the sodium metal aerosol mass concentration with respect to pool temperature for a given geometry of the vessel. This study helps to predict the sodium aerosol mass concentration for any similar geometry.

Table 6.6 Comparison of theoretically predicted and experimentally measured sodium aerosol mass concentration for of TP-1, TP-3, Minges et al., Glockling et al., and Yoshiaki et al.

Pool temperature (^oC)		**250**	**300**	**350**	**400**	**450**	**500**	**550**
Minges (L/D-0.55)	Exp. C (g/m^3)			1.52	5.39	11.86	20.39	40
	Sim. C (g/m^3)			1.31	3.73	8.72	18.02	33.39
	Var. (%)			13.81	30.79	26.47	11.62	16.52
TP-1 (L/D-1.076)	Exp. C (g/m^3)	0.06	0.33	1.85	4.95	12.02	18.12	30.62
	Sim. C (g/m^3)	0.06	0.33	1.31	3.75	9.59	17.89	34.11
	Var (%)	0	0	29.18	24.24	20.21	1.26	11.39
TP-3 (L/D-1.875)	Exp. C (g/m^3)	0.04	0.17	0.69	2.01	5.12	11.97	21.98
	Sim. C (g/m^3)	0.05	0.21	0.89	2.61	6.45	14.46	28.67
	Var.(%)	25	23.52	28.98	29.85	25.97	20.80	30.43
Glockling (L/D-2.333)	Exp. C (g/m^3)		0.47	1.24	5.22	11.12	22.41	36.13
	Sim. C (g/m^3)		0.34	1.39	3.83	8.92	18.33	33.87
	Var. (%)		27.65	12.09	26.62	19.78	18.20	6.25
Yoshiaki (L/D-4.516)	Exp. C (g/m^3)		0.21	1.39	2.45	6.51	12.14	20
	Sim. C (g/m^3)		0.26	0.98	2.52	5.79	11.51	20.89
	Var. (%)		23.80	29.49	2.85	11.05	5.18	4.45

6.3 Summary

A new set of experiments are carried out in TP-3 of SILVERINA loop and compared with the results of TP-1 (our earlier study) and with published literature works to understand the geometrical effect on sodium aerosol characteristics. The bulk cover gas temperature and sodium aerosol diameter are used as an input parameter for theoretical simulation of sodium aerosol mass concentration. An empirical relation for bulk cover gas temperature is derived and validated with our experimental results and used for other geometry. Similarly, an empirical relation for sodium aerosol diameter is derived based on our experimental results and from available published works. The theoretical model developed earlier is used for predicting the sodium aerosol mass concentration in which, the particle radius and bulk cover gas temperatures are replaced with present empirical relation for calculating particle radius and bulk cover gas temperature taking in to account of aspect ratio (L//D) and area of the cover gas region respectively. The simulated mass concentration of sodium metal aerosols in cover gas region of various geometries showed good agreement with the experimental results. The sodium aerosol mass concentration and MMD increases with increase of sodium pool temperature. However, the values strongly depend on the aspect ratio (L/D) of cover gas geometry. It is also observed that MMD of sodium aerosols increases with increase of aspect ratio (L/D) while mass concentration increases with decrease of aspect ratio of the cover gas region. The modeling is found useful in predicting the sodium aerosol mass concentration for any similar type of geometry and pool temperature.

6.4 References

6.1 J. Minges and W. Schutz, ‘Experiments on the enrichment of cesium in the cover gas aerosol of the European Fast Reactor (EFR)’. Nuclear Engineering and Design 147 (1993) 17-22.

6.2 J. Minges and W. Schutz, (1991), "Experiments to characterize the sodium aerosol system in the cover gas of the European Fast Reactor EFR", J. Aerosol Sci. Vol. 22, S761-S764.

6.3 H. Yamamoto, T. Sakai, and N. Murakami, (1991), "Analytical study on mass concentration and particle size distribution of sodium mist in cover gas phase of LMFBR reactor vessel", J. of Aerosol Sci. Vol. 22, S713-S716.

6.4 I. H. Newson, R. W. Dawoson, C. D. Wade, A. N. Moul and J. E. Finch, (1993), "Studies of caesium-134 transfer through argon and helium Cover gases above hot sodium pool in the Hawell active mass transfer loop (AMTL)", AEA Industrial technology, Report number AEA-In Tec-1220.

6.5 Yoshiaki HIMENO and June TAKAHASHI, (1980),"Sodium Mist behavior in cover gas space of LMFBR", J. Nucl. Sci. and Tech. Vol. 17, 404-412.

6.6 Yoshiaki HIMENO and Yoshiaki YAMAGISHI, (1982), "Effect of barriers on sodium mist deposition on LMFBR components", J. Nucl. Sci. and Tech. Vol. 19 [10], 837-844.

6.7 O. Frukawa, A. Furutani, N. Hattori and Iguchit, (1984),"Experimental study of heat and mass transfer through the cover gas in the Liquid Metal Fast Breeder Reactor (LMFBR)", Proceeding of the third international conference on liquid metal engineering and technology, The British nuclear Society, Vol.1, 451-458. ISBN0-7277-0209-2.

6.8 J. L. D. Glockling, (1991), "Heat and Mass transfer in specific aerosol system", PhD thesis, Department of chemical engineering. South bank University, London.

6.9 D. N. Roberts, (1995), "Heat and Mass transfer studies in sodium – Argon filled enclosures", PhD thesis, South bank University, London.

6.10 William C. Hinds, (1982), "Aerosol technology", John Wiley & Sons.

6.11 Amit Kumar, V. Subramanian, R. Baskaran, S. Krishnakumar, S. Chandramouli, B. Venkatraman, (2015), "Characterisation of Sodium Aerosol in Cover Gas Region of SILVERINA Loop", Aerosol and Air Qual. Res., Vol., 15, 1813 –1822.

6.12 V. Ramakrishnan, C. Meikandamurthy, K. K. Rajan and M. Rajan, (1997), " Heat transfer studies in roof slab model", IGC/EDG/STD/99116/EX3024/R-A.

6.13 Amit Kumar, V. Subramanian, R. Baskaran, B. Venkatraman, (2015), "Size Evolution of Sodium Combustion Aerosol with Various RH%", Aerosol and Air Qual. Res., Vol., 15, 2270 –2276.

6.14 A. Sheth, (1975), "Parametric study of sodium aerosols in the cover gas-space of sodium-cooled reactors", Argonne National Laboratory, ANL-75-11.

6.15 Amit Kumar, V. Subramanian, S. Krishnakumar, R. Baskaran, S. Chandramouli, B. Venkatraman, (2016), "Studies on Geometrical Effect on Sodium Aerosol Characteristics in Cover Gas Region", Aerosol and Air Qual. Res., Vol., 16, 1832–1840.

CHAPTER - VII

EFFECT OF GAMMA RADIATION ON AEROSOL CHARACTERISTICS

7.0 Introduction

It is well known that gamma radiation field produces distribution of bi-polar ions in the environment. The aerosols suspended in the charged atmosphere, pick up ions at randomly and acquire distribution of charges governed by Boltzmann distribution [7.1 and 7.2]. In normal operation of the SFR, cover gas region is always being subjected to intense radiation field that results in significant ionization of the gas. The sodium metal aerosol suspended in these ionized gas medium get charged by picking up ions. The sodium metal aerosol properties would get modified due to the possible enhanced coagulation between charged aerosols which could result in enhanced settling. Thus, gamma radiation field affects the aerosol characteristics (mass concentration, size distribution, coagulation and deposition) and affect the heat transfer through cover gas region, visibility of cover gas region and mass deposition on the cooler parts. The studies on gamma radiation effect on aerosol properties are carried out and presented in this chapter.

Several theoretical and experimental studies have been carried out to determine the number of charges acquired by the aerosols of given diameter and the coagulation of such a charged aerosols. The experimental observation of Hautanen et al., showed that there is significant reduction in number concentration of soot particles when they are charged by corona discharge [7.3]. Clement et al., theoretically predicted that the radioactive aerosol charging would results in enhanced coagulation and it is emphasized that this prediction needs to be checked by the experiments [7.4]. But Park et al., in their modeling studies, bi-polar diffusion charging can significantly increase the coagulation rate of aerosols [7.5]. Bi-polar diffusion charging of non-radioactive aerosols by using Am-241 Alpha sources was compared with the soft X-ray source of 9.5 keV by Hye Moon Lee et. al., [7.6]. They reported that, a steady ion concentration rate was achieved by X-ray source and it is effective for the measurement of nano-particles. An experimental and theoretical study by Konstantaneous Barbenous showed that, increase of radioactivity concentration has minor deviation in the charge distribution of aerosols [7.7]. However, the product n and t (n -no. of ion pairs and t- resident time) would be a key factor for the particle charging to achieve Boltzmann equilibrium. Another important study on bi-polar charging on radioactive aerosols and comparison of their result with Clement & Harrison model was carried out by F. Gendarmes et. al., [7.8]. In fact, the charging of radioactive aerosols is different from that of non-radioactive aerosols but their study, concluded that the charging varies with the intensity of ionization in the environment. Fuchs experimentally observed that, attractive forces between aerosols charged with unlike signs increase coagulation rates, overcoming other electrical repulsions [7.1]. Rosinski et al., have experimentally showed the increase in coagulation rate up to 2 times for the Cadmium aerosols of 0.2 µm radius when charged using photoelectric effects [7.9]. The coagulation enhancement factor for the charged aerosol is defined as $f = K'/K$ (where K' and K – coagulation kernels for the charged and uncharged particles respectively), [7.2 and 7.3]. The experimental results in ATF showed that the Brownian coagulation enhancement of 5-8 times for the mono-dispersed sodium combustion aerosols in a confined environment at the dose rate of the order of few mGy/h [7.10]. Powers and Burson [7.11], Clement and Harrison [7.4], and Williams and Loyalka [7.12] have proposed a model to estimate the effect of aerosol charging on the coagulation and deposition rates. It is further reported that, by using general theory derived by Zebel [7.13] and by Williams and Loyalka [7.12], in order to get the coagulation enhancement factor of 5 times the modest charging required by the aerosol particle is about 8 charges for the particles of radius 0.5µm in a given ion concentration (radiation field of 4 mGy/h) [7.14]. Thus it is understandable that the electrical forces caused by the Coulomb interaction between the charged aerosol particles are responsible for the enhanced coagulation. Due to intense radiation field in the cover gas region, significant ionization of argon gas occurs. The sodium metal aerosol gets charged by picking up ions present in the cover gas region. No experimental or theoretical study was found in literature on radiation effect on sodium metal aerosols in cover gas region. The average charge acquired by the aerosols would also depend on the number of ion-pair and aerosol concentrations. Hence, sodium metal aerosol characteristics under the charged environment has been determined for various pool temperatures and reported in this chapter.

Understanding the mechanism of aerosol charging during generation of aerosols is important in aerosol science, particularly to understand the aerosol process like particle deposition, electrical migration, sampling & transport and coagulation etc. Hence our experimental study includes determination of charging of aerosols in three generation process viz. (i) combustion route (generating sodium compound aerosols), (ii) vaporization and condensation route (SrO_2 aerosols) and (iii) atomization route (polystyrene latex and DOP aerosols) and by comparing the average charge acquired by a particular sized aerosols generated in all the three process. Since the formation of sodium metal aerosols in cover gas region follows the evaporation – condensation route, determination of aerosol characteristics in this generation process and with applied radiation field is essential for this study. The formation of ions in gas medium and aerosol charging of non - radioactive aerosol are explained in annexure - B.

By keeping all these aspects, the experimental studies are carried out to determine (i) average number of charges acquired by the polydispersed aerosols in the generation process (in three different generation route) and with applied gamma radiation field, (ii) the number of elementary charges increased (average number) for a given sized aerosols in the presence of gamma radiation field and (iii) changes in characteristics of sodium metal aerosols in the cover gas region by exposing external gamma source. Since, the number of charges acquired by the aerosols cannot be determined for sodium metal aerosols in cover gas region due to restriction in the measuring environment, the first two objectives are carried out in ambient atmosphere using ELPI and third one is carried out by exposing the cover gas region by using external source and aerosol characteristics are determined after ion - pair concentration reaches equilibrium. All these results are presented in this chapter.

7.1 Studies on average charge acquired by the aerosols in generation process and with gamma radiation field

Aerosols are generated in three different generation process viz. evaporation and condensation (SrO_2 aerosols), combustion (sodium combustion aerosols), and atomization process (polystyrene latex aerosols) to study the charge acquired in the generation process and with applied gamma radiation field. The detailed description is given in following section.

7.1.1 Generation of non-radioactive fission product aerosols

SrO_2 aerosols are generated using the 25kW thermal plasma torch [7.15]. A known weight of SrO_2 powder (procured from M/s ACROS Organics, USA) is palletized. Typical weight of the pellets was 5 ± 0.2 g. The pellets were rigidly fixed in to the wire feeder tube and kept in front of the plasma flame. The pellet melts and the molten vapors after leaving the flame zone condense to produce aerosols, i.e. at a particular point the vapor pressure exceeds the saturated vapor pressure of the condensed phase and nucleation of the condensed phase occurs. At the same time the vapors are flown into the aerosol chamber (distance between plasma flame and the chamber is 50cm) along with the sheath gas (Nitrogen) (flow rate ~ 20lpm) used in the plasma torch. The vapor is diluted and re-condenses to produce aerosols in the chamber by homogeneous nucleation or by heterogeneous nucleation on air molecules [7.16]. The gate valve on the plasma torch side of the aerosol chamber is closed after plasma torch is switched off.

7.1.2 Generation of Sodium combustion aerosols

The sodium combustion cell is isolated, flushed and filled with argon gas, up to a pressure of 10-20 kPa excess over atmosphere. About 5-10 g of sodium is placed in a crucible and mounted on a heater. The sodium is heated upto a required temperature (say 550°C, the temperature of the primary sodium in the fast reactor). The hot sodium is ignited by exposing it to air, after flushing out the argon. By combustion, sodium oxide aerosols are formed in the combustion cell. The aerosol chamber and the diagnostic ports are get filled with aerosols as soon as the gate valve is opened. The pressure inside the cell rises up to 70-80 kPa excess over the atmosphere (before opening the gate valve) helps to fill the aerosol chamber and its diagnostic ports with sodium aerosols. The cell is isolated after two minutes so that sodium aerosols are bottled-up inside the aerosol chamber [7.17].

7.1.3 Generation of Polystyrene latex aerosols by atomization

DOP poly-dispersed and mono-dispersed Polystyrene latex particles (d=1.3µm obtained from M/s Polyscience Inc., USA) are generated by using aerosol generator (Model No:7.811, M/s Grimm aerosol generator, GmbH, Germany). Atomization is carried out in de-ionized water to which few drops of DOP or polystyrene latex particles are added. After the atomization, the aerosols are made to pass through a condenser (cooling the transport line on a thermostat filled with cooled water) followed by line heater (heating the transport line by using heating coil wounded over the line) and finally transported to the aerosol chamber. The interference of moisture condensing on aerosols and consequent perturbation on charge measurements were eliminated by cooling and heating techniques. The ratio of aerosol solution and dispersant is maintained about 1.6:100, which is proved to give good number concentration of aerosols generated by atomization processes. Thus the aerosols are pumped into the chamber and they are made to suspend in a chamber where charge measurements are carried out [7.18].

7.1.4 Aerosol charge measurement

For the real time measurement of aerosol number size distribution and charge size distribution, Electrical Low Pressure Impactor (ELPI) (Marko Marjamaki et.al., 2000) is used.

7.1.5 Aerosol sampling

To begin with, aerosol chamber is kept in the ambient atmospheric condition i.e. atmospheric pressure ~101kPa and ~65% RH. During the experiments the aerosol chamber is bottled-up with aerosols. By running ELPI with corona charger 'OFF' and 'charger 'ON' condition for a constant time say 100s or 60s (for polydispersed aerosol the sampling time was 100s where as monodispersed aerosols it was 60s), the charges associated with generation process of aerosols along with number-size distribution are measured. The results are derived by repeating the measurement for the next 100s and taking average value [Since the average charge acquired by aerosols significantly differs, due to change in number concentration of aerosols, when the measurements are continued further]. By using charge-size distribution, number-size distribution, the flow rate of the instrument, total charge measured and by taking the elementary charge value, the average number of charges associated with the aerosols is determined. The experiments are repeated by exposing the aerosol chamber volume panoramically with gamma radiation source, Cs-137, of 0.5TBq. The ^{137}Cs decays into ^{137}Ba***** through beta decay, $_{55}Cs^{137} \rightarrow {}_{56}Ba^{137*} + {}_{-1}e^{0} + \bar{\gamma}$ (514 keV), which in-turn decays through gamma decay, $_{56}Ba^{137*} \rightarrow {}_{56}Ba^{137} + \gamma$ (662 keV). The source is mounted on top of the chamber on the centre axial line and it was fixed at a position such that it gives desired dose rate inside the chamber. The dose rate inside the chamber was measured using Teletector (Model 6112, M/s Automation Uno Mentechnik, Germany).

7.1.6 Poly-dispersed Aerosols

The charge-size distribution (average number of charges in particular size ranges) of background aerosols (in the chamber) without and with gamma field (4.0mGy/h) and its number-size distribution measured simultaneously by using ELPI, are given in Fig. 7.1(a) and Fig.7.1(b) respectively. As expected, it is observed that number of elementary charges acquired in all sized aerosols is found to be more in the presence of gamma radiation field. The mean number of charges <j> (for the whole distribution), without and with gamma field is found be -1.4 and +2 units respectively (as described by equation - B.2 of appendix - B). This is calculated by drawing frequency distribution with number of particles in each cut-off size versus total number of charges in fC (femto Coulomb) measured in that size range and then finding arithmetic mean value. Typical calculation of arithmetic mean charge for the charge distribution of background aerosols (without gamma radiation) is given in Table 7.1. The charge-size distribution and number-size distributions for poly-dispersed SrO_2 aerosols are given in Fig.7.1(c), and Fig. 7.1(d) respectively. Similarly, the results of the DOP aerosols, generated via atomization route are shown in Fig. 7.1(e) and Fig. 7.1(f) respectively. It is observed from the figures [Figs. 7.1(c) and 7.1(d)], there is a significant reduction of average number of charges when the particle concentration above 10^6 particles.cm^{-3} ($0.32\mu m \leq ECD \leq 3.21\mu m$, where ECD-Effective cut-off diameter). The mean charge over the distribution of aerosols with and without gamma radiation field is found to be +0.5 and -0.15 units respectively (calculated as shown in Table 7.1). In the case of DOP aerosols ($N_{max}= 10^5 cm^{-3}$) generated via atomization route has significant reduction of charges in the presence of gamma radiation i.e. charge neutralization is taking place. The average number of charges in each size range during generation process is more than that of with gamma radiation field ($n=10^7 cm^{-3}$).

Table 7.1 Mean charge $\bar{j}$ associated with background aerosols without gamma field.

Stokes diameter (d_p) µm	**No of particles /cm^3 (N_j)**	**No. of particle collected by sampling**	**Charge measured (Columb)**	**No. of ions**	**Average number charges (j)**	**Frequency number j x N_j**
[1]	[2]	[3]	[4]	[5]	[6]	[7]
0.021	1320	220064	2.30E-14	143921	0.65	858
0.043	1200	200107	9.38E-14	586314	2.93	3516
0.082	2251	375257	-1.03E-13	645443	-1.72	-3871.72
0.137	6447	1074625	-3.79E-13	2374921	-2.21	-14247.9
0.214	4007	667944	-3.59E-13	2244295	-3.36	-13463.5
0.329	1268	211385	1.07E-13	674318	3.19	4044.92
0.516	87	14636	5.94E-15	37175	2.54	220.98
0.817	449	74846	-3.20E-14	200588	-2.68	-1203.32
1.299	26	4455	3.17E-15	19870	4.46	115.96
2.042	9	1621	5.94E-16	3712	2.29	20.61
3.208	2	380	7.97E-17	498	1.31	2.62
6.388	1	242	2.53E-16	1587	6.54	6.54
ΣN_j	17067				ΣjxN_j	-23987.09
			Mean charge <j> = ΣjxN_j / ΣN_j =			**-1.4**

1. Column [1], [2] and [4] are obtained by ELPI measurement.
2. Stokes diameter is obtained by taking geometric mid-point for the successive stages and density.
3. Flow rate of the instrument is 10 lpm and duration of the sampling is 60s.
4. Column [3] is calculated as (N_j x 10 x 1000) / (60), the number of particles per second.
5. Column [5] is obtained by dividing column 4 by 1.6 x 10^{-19} the elementary charge value.
6. Column [6] is obtained by dividing column 5 by column 3.
7. Column [7] is obtained by multiplying column 6 and column 2.

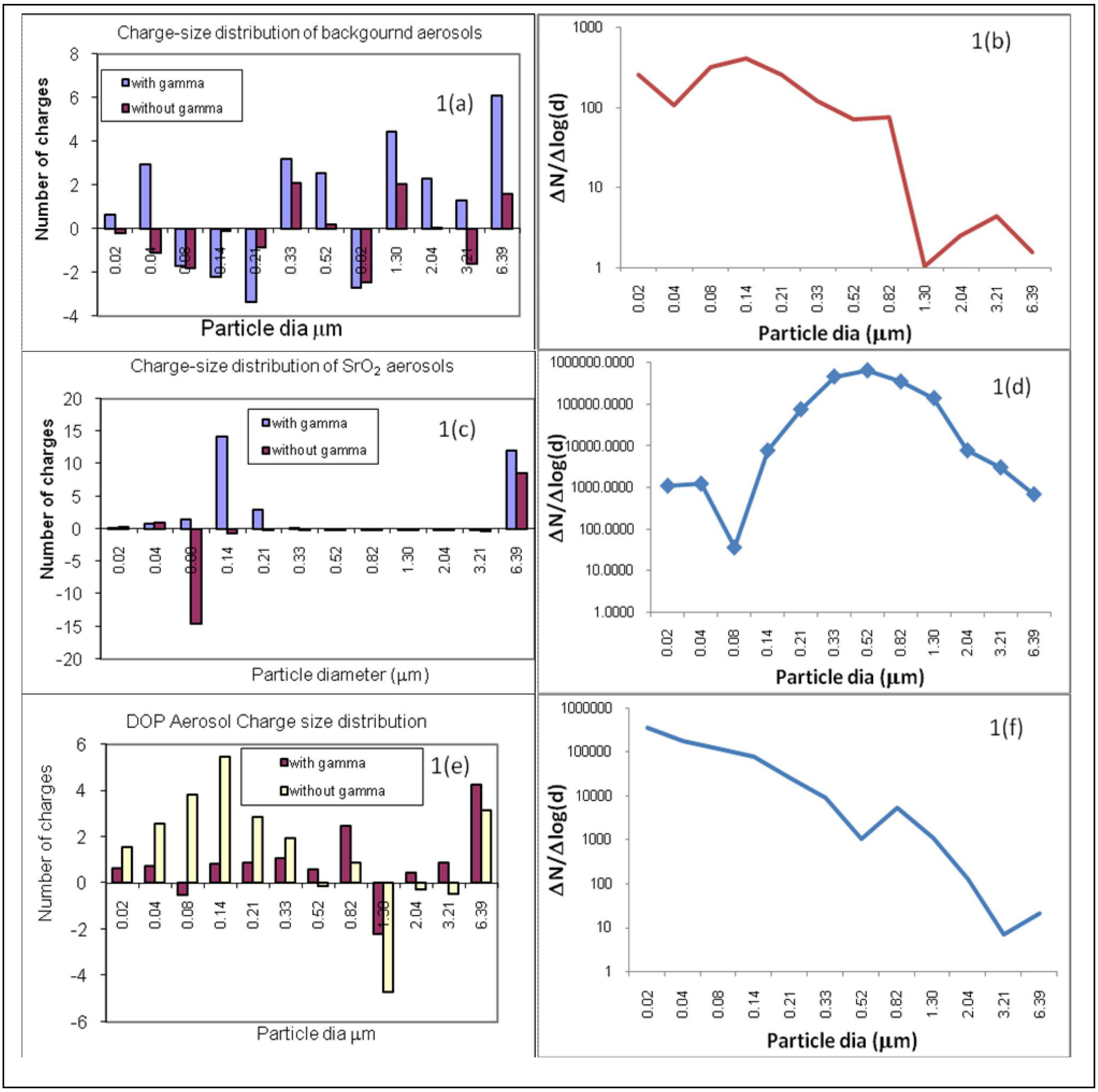

Fig.7.1 Charge-size distribution and their number concentrations of background aerosols, polydispersed SrO_2 and DOP aerosols.

The mean number of charges for whole distribution of DOP aerosols with and without gamma field is found to be +0.5 and +2.5 respectively (calculated as shown in Table 7.1). The variation in the magnitude of charge seen in the charge-size distribution is due to (i) the aerosols are polydispersed and having multiple modes, hence the larger sized particle could have wider charge distribution while the smaller sized particle could have singly or doubly charged [7.19] and (ii) the normalized data (charge/particle) is presented in the graph. Accordingly the average charge decreases when the number of particles in those size ranges increases.

7.1.7 Mono-dispersed aerosols

The measurement of mean charge for the whole distribution gives the weighted average distribution because; it has influence on number of aerosols in that particular size range. But, in order to investigate the phenomena of aerosol charging by the excess ion-pairs generated due to gamma radiation; we have conducted experiment by generating mono-dispersed aerosols. The measured average charge acquired by the aerosols in the generation process is compared with the additional charge acquired, if any, by the same aerosols, by applying gamma radiation field panoramically (40.0mGy/h). For this we have generated (i) sodium combustion aerosols which has mono-dispersed size with MMD of 1.0 µm, (ii) polystyrene latex aerosols of size 1.3 µm and (iii) SrO_2 aerosols of diameter 1.29 µm selected from the poly-dispersed aerosols generated by plasma synthesis and determined the charge acquired by theses aerosols during generation process and with applied gamma field. The reason for selecting the size is that, initial size distribution of sodium combustion aerosols at 50%RH is 1.0µm [7.20] hence, polystyrene latex particles of 1.3µm is used for atomization technique, while in the case of SrO_2 aerosols, vaporization and condensation route produce poly-dispersed aerosols, of which, particles corresponding to 1.29µm (ECD) is chosen for this study. Table 7.2 gives, the charge acquired 'abs <j>' by the mono-dispersed Polystyrene-latex aerosols of size 1.3µm (diameter), mono-dispersed sodium combustion aerosols of 1.0µm (diameter) and 1.29µm (diameter) sized SrO_2 aerosols with and without the presence of gamma radiation field.

In the case of combustion route, the particles are formed generally as a solid by condensation of sodium fumes. The condensation produces little or no charge on the aerosols but these aerosols acquire charges by Brownian collision with omnipresent air ions and attain Boltzmann equilibrium. In vaporization and condensation route, particle charging is significant as evaporation produce significant number of high mobility ions. Hence, charge-associated with these aerosols also attain Boltzmann equilibrium. In the atomization process of polystyrene latex particles, it is observed that average-number of charges associated with these aerosols are maximum. Since polystyrene is a dielectric liquid associated with surface charges, during the atomization the charged surface gets disrupted hence the aerosols acquire charges by spray electrification. Thus the average number of charge acquired by the polystyrene latex particles is found to be more than other two aerosols.

Table 7.2 Average number of charge 'abs <j>' acquired by the aerosols in three generation mechanism with and without the presence of gamma radiation field (40.0 mGy/h).

Generation method	**Aerosol material**	**Number concentration**	**Particles diameter**	**Average number of charges abs<j>**	
				Without gamma field	**ion conc. 1.4x10^8 ion-pair/cm^3/min**
Combustion	Sodium aerosol	10^6 cm^{-3}	1.0 µm	1.8	3.4
Vaporisation and condensation	SrO_2	10^6 cm^{-3}	1.29 µm	0.4	3.02
Atomisation	Polystyrene latex particules	10^5 cm^{-3}	1 .3 µm	4.53	5.1

It is observed from Table 7.2 that, magnitude of charge determined with additional ion-pair concentration in all the three process is found to be higher than that of without additional ion-pair situation. Aerosols are injected into the sea of ion-pairs. The aerosols begin to get charged, then, as time progresses the aerosol charging would be a steady state charging and attain Boltzmann equilibrium. As the time further progresses, aerosols with higher number of charges begin to appear, caused by multiple charging of the particles and the spread become wider. Thus, the magnitude of average charge gets increased in the presence of given additional ion-pairs due to gamma radiation.

7.2 Effect of Gamma radiation on sodium metal aerosols in cover gas

The cover gas space is always associated with high gamma radiation field resulting large amount of bi-polar ions. When the sodium metal aerosols are immersed in the sea of bi-polar ions, aerosols acquire charges (steady state charging) and there is an increased force of Columb attraction in addition to thermal coagulation, resulting increase in size [7.10]. The experiments conducted in TP-3 of SILVERINA loop and sodium aerosol characteristics are studied with and without applying gamma radiation field. A schematic diagram of sodium aerosol sampling system in TP-3 and gamma source is shown in Fig.7.2. Co-60 source (Activity - 4.5mCi) encapsulated in steel capsule, kept in plastic container is used. The ^{60}Co decays into ^{60}Ni through beta and gamma decay, ${}_{27}\mathrm{Co}^{60*} \rightarrow {}_{56}\mathrm{Ni}^{137} + {}_{-1}\mathrm{e}^{0}$ (0.31MeV) + $\bar{\gamma}$ (1.17MeV), and ${}_{27}\mathrm{Co}^{60*} \rightarrow {}_{56}\mathrm{Ni}^{137} + {}_{-1}\mathrm{e}^{0}$ (1.48MeV) + $\bar{\gamma}$ (1.33MeV). The source is kept at 1 m distance from the middle of cover gas region of TP-3 (volume is 0.1m^{3}), to get panoramic exposure in the cover gas region. The exposure rate at the centre of the cover gas region at about 1.0m distance (taking SS wall thickness of the TP-3 into account) is calculated to be 5.0 mR/hr. Assuming the entire volume is uniformly irradiated for the exposure period of 10minutes, the absorbed dose in the cover gas region would be 0.83 mRads which corresponds to the production of 2.8 x 10^{08} ion-pairs/s. (1R produces 2.08 x10^{15} ionpairs/m^3). The absorbed dose was measured by using Condenser – R meter (M/s Victoreen, UK) on the front and rear side of the TP-3 in order to verify the dose estimation.

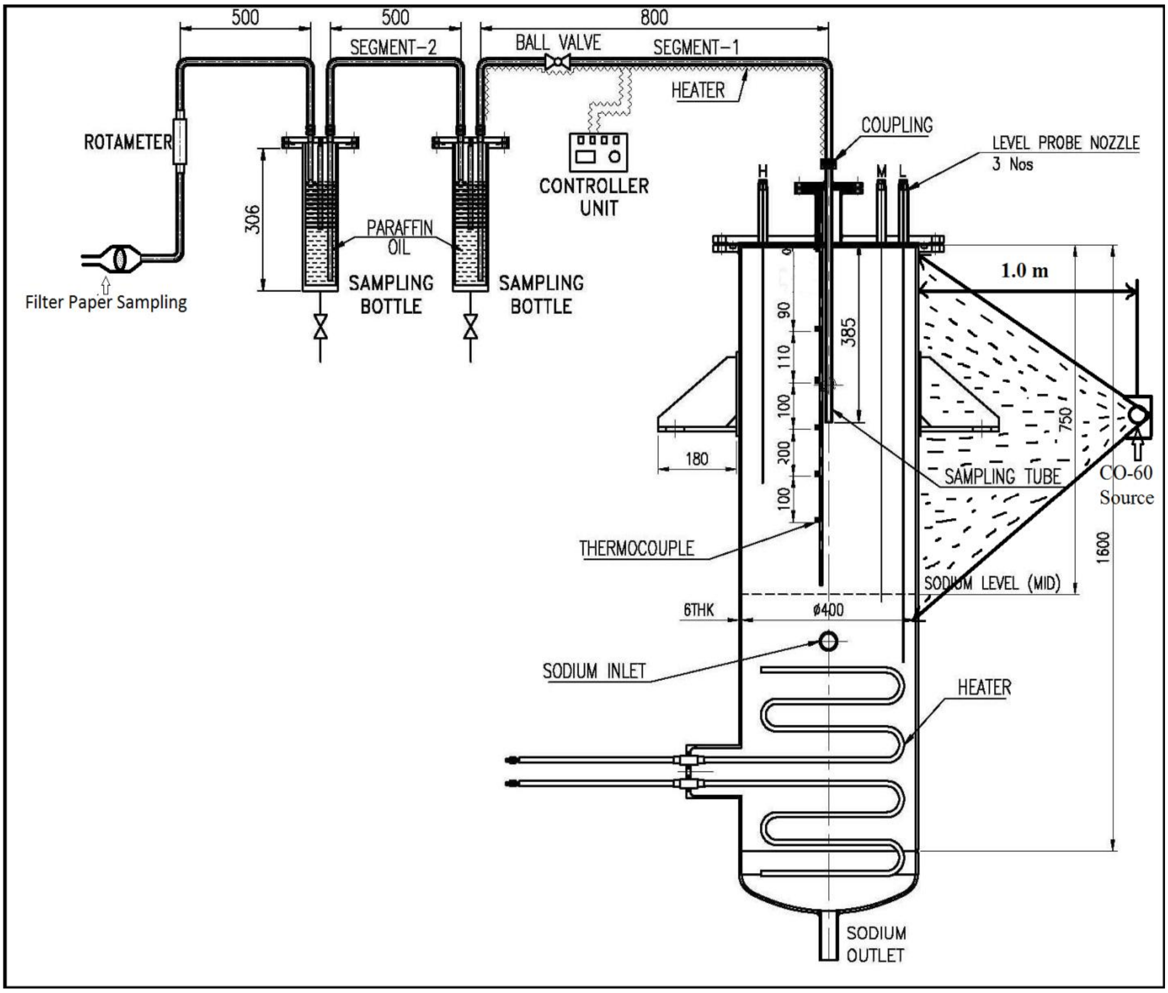

Fig. 7.2 A schematic diagram of sodium metal aerosol sampling system in TP-3 of SILVERINA loop along with Co-60 source.

It is observed from Table 7.3, that sodium metal aerosol mass median diameter (MMD) is found to be increased in the presence of gamma field condition when compared with without gamma field condition. It is inferred that, particles acquire steady state charges (Boltzmann equilibrium) and net charges $Ni = \Sigma(n_i d_i)$ [where n_i number of charges on particle of diameter d_i and N_i is the net charges on particle of diameter d_i] acquired by the particles of given size increases by 2 or 3 numbers (with either sign) and the resulting total net charges of the particle distribution [$\Sigma\ N_i d_i + N_j d_j + N_k d_k$ …where i, j, and k are particles of different diameters] enhances the Brownian coagulation of aerosols [7.10 & 7.21]. The MMD is found to be increased due to enhanced coagulation. As the particle size is increased which resulted the gravitational settling, hence, the aerosol concentration after the steady state is less than that of without source condition.

Table 7.3 Sodium metal aerosol characteristics in cover gas region with and without gamma source.

Temp. (^{o}C)	**Without γ Source**		**With γ Source**	
	MMD(μm)	**Concentration (g/m^3)**	**MMD(μm)**	**Concentration(g/m^3)**
450	10.9	5.4	11.3	3.7
500	11.1	7.5	12.5	5.92
550	15.5	21.9	16.7	17.6

7.3 Summary

The effect of gamma radiation field on sodium metal aerosol characteristics is studied. Since the aerosols are generated by evaporation and condensation process in the cover gas region of SFR, the charging of aerosols could occur in generation process. Hence, the experiments are carried out by generating aerosols in evaporation and condensation route and number of charge acquired in the generation process is determined and compared with charges acquired in other generation process like combustion and atomization. It is observed that, charge acquired in the generation process has a significant role. In the case of polystyrene latex aerosols (generated via atomization), the charge neutralization effect was seen when the aerosols are exposed to gamma radiation; whereas slight increase in the average charge acquired by the aerosols generated by other route say: combustion and vaporization & condensation was found.

The sodium metal aerosol mass concentration and size distributions are determined in the presence of gamma radiation field in the cover gas region. It is observed that the value of MMD of sodium metal aerosols is found to be higher and mass concentration is found to be less in the presence of gamma field condition when compared that of without gamma field condition. The reason is attributed to the increase in size due to enhanced Brownian coagulation in the presence of gamma field. As the particle size is increased which resulted the gravitational settling, hence, the aerosol concentration after the steady state is less than that of without gamma source condition.

7.4 References

7.1 N. A. Fuchs, (1964), "The Mechanics of Aerosols", Pergamon, New York.

7.2 C. F. Clement and R. G. Harrison, (1991), “Charge distribution on aerosols”, Proceedings of 8th International Electrostatics Conference, Institute of Physics Conference Series, Oxford, Vol. 118, 275-280.

7.3 J. Hautanen, T. Watanebe, Tsuchida, Y. Koizumi, F. Tochikubo, E. Kauppinen, K. Lehtinen and J. Jokiniemi, (1995), “Brownian Agglomeration of Bipolarly Charged Aerosol Particles”, J. of Aerosol Sci., Vol. 26, S21-S22.

7.4 C.F. Clement and R.G. Harrison, (1990), “Electric charge effects on aerosol behavior”, Workshop on Aerosol Behaviour and Thermal-Hydraulics in the Containment CEC/NEA, Fontenay-aux-Roses, France.

7.5 S. H. Park, K. W. Lee, M. Shimada and K. Okuyama, (2005), “Coagulation of bipolarly charged ultrafine aerosol particles”, J. of Aerosol Sci., Vol. 36, 830 -845.

7.6 Hye Moon Lee, Chan Soo Kim, Manabu Shimada & Kikuo Okuyama, (2005), "Bipolar diffusion charging for aerosol nanoparticle measurement using a soft X-ray Charger", J. of Aerosol Sci., Vol. 36, 813-829.

7.7 Konstantines Barbranis, (2009), "Bipolar diffusion charging: Experimental and Theoretical evaluation of the parameters affecting the charge distribution of nano-particles in the size range 10-100nm", M. S. Dissertation, University of Aegean, Greece.

7.8 F. Gensdarms, D. Boulaud, and A. Renoux, (2001), "Electrical charging of radioactive aerosols-comparison of the Clement-Harrison model with new experiments", J. of Aerosol Sci., Vol. 32, 1437-1458.

7.9 J. Rosinski, D. Werle and C.T. Naganoto, “Coagulation and scavenging of radioactive aerosols”, Journal of colloidal science, Vol.17, p.703 (1962).

7.10 V. Subramanian, R. Baskaran and R. Indira, (2008),“Experimental study on enhanced Brownian Coagulation of Sodium Compound Aerosol in the presence of Gamma Field”, J. of Aerosol Sci., Vol. 39, 814-818.

7.11 D. Powers. and S. B. Burson, (1996), "A simplified model of aerosol removal by natural process in reactor containments", NUREG/CR-6189, SAND94-0407, Sandia National laboratories.

7.12 M. M. R Williams, and S. K. Loyalka, (1989), "Aerosol Science" Theory and Practice. Pergamon, Oxford.

7.13 G. Zebel, (1966), "Coagulation of aerosols", In: Davies C.N. (ed) Aerosol Science, Academic Press, London.

7.14 V. Subramanian, R. Baskaran and B. Venkatraman, (2011), "Studies on Sodium Aerosol characteristics in the presence of Gamma radiation field", 7th Asian Aerosol Conference, 17-21, August, 2011, Xi’an, China, 545-551.

7.15 V. Subramanian, R. Baskaran, and H. Krishnan, (2009), "Thermal Plasma synthesis of Iron oxide aerosols”, Aerosol and Air Quality Research, Vol., 9, 172-186.

7.16 R. M. Young and E. Pfender, (1985), "Generation and Behaviour of Fine Particles in Thermal Plasmas-A Review", Plasma Chemistry and Plasma Processing, Vol., 5, 1-37.

7.17 V. Subramanian, P. Sahoo, N. Malathi, R. Anathanarayanan, R. Baskaran, and B. Saha, (2009), "Studies on Chemical Speciation of Sodium aerosols produced in Sodium fire", Nuclear Technology, Vol., 165, 257-269.

7.18 Amit Kumar, V. Subramanian R. Baskaran J. Misra and P. Chellapandi, (2010), "A study on Aerosol Charging in Generation Mechanism", IASTA-2010 March-2010, Bose Institute, Darjeeling, IASTA Bulletin, 19, 1&2, 277-279.

7.19 C. F. Clement and R. G. Harrison, (1992), "Charging of radioactive aerosols", J. of Aerosol Sci., Vo., 23, 481-504.

7.20 V. Subramanian and R. Baskaran, (2007), "Initial size distribution of sodium combustion aerosol", Nuclear Technology, Vol., 160, 308-313.

7.21 V. Subramanian, Amit Kumar, R. Baskaran, J. Misra, and B. Venkatraman, (2012), "An experimental study on the charging of non-radioactive aerosols with and without the presence of gamma radiation", J. of Aerosol Sci., Vol., 52, 98–108.

CHAPTER - VIII

CONCLUSION

8.0 Introduction

In the normal operating condition of SFR, the temperature difference between the sodium pool and the bulk gas temperature leads to considerable evaporation of sodium from the pool surface and subsequent condensation results in the formation of sodium metal aerosols within the cover gas region either by heterogeneous nucleation or self-nucleation (homogeneous nucleation). There is significant heat and mass transfer from the hot sodium pool surface to argon cover gas space and to the roof slab. When sodium metal aerosols have sufficient concentration, would modify the total heat transfer to the cooled roof structure by absorption and scattering of thermal radiation. Further, the mass transfer occurs due to condensation of sodium metal aerosols on the cooler surfaces like annular gaps, roof top, control plug, rotating plugs, fuel handling machine control and diverse safety rods resulting deposition of aerosols, which hinders the rotational movement of rotating plug, operation of fuel handling machine and affect normal performance of control and diverse safety rods mechanism. The aerosol mass concentration influences the operation of cover gas purification system and changes its efficiency (flow through cold trap circuit). Also, the aerosols with sufficient concentration reduce the visibility of cover gas region (fuel handling and core inspection).

8.1 Research significance

It is observed from the literature that, theoretical and experimental study on characterization of sodium metal aerosol in cover gas region has been carried out by many researchers. There were several techniques used for the characterization of sodium metal aerosol size and mass concentration viz: Andersen Impactor, laser light based techniques, sodium ionization detector, and SS mesh filter. It is further observed that, the sodium metal aerosol characteristics in cover gas region are dependent on sodium pool temperature and difference between pool and roof temperatures. The sodium metal aerosol characteristics also strongly dependent on the geometric dimension (diameter of the sodium pool surface, height of the argon cover gas and shape of roof top) of the cover gas system. The sodium metal aerosol size (MMD) ranges from 1-20µm and the mass concentration ranges from 1-50g/m^3. In general the sodium metal aerosol size distribution and mass concentration (i) increases with the increase of sodium pool temperature at constant roof temperature and (ii) increases with the increase of difference between pool to roof temperatures. It may be concluded that, the variation of sodium metal aerosol mass concentration in cover gas region has a definite pattern with the variation of roof and pool temperatures in all the studies. But in the case of sodium aerosol size distribution the general observation is that, there is no consistency with the variation of aerosol size with the variation of pool and roof temperature. It is also observed from earlier work that boundary layers exits just above the sodium pool surface and below the roof slab in the cover gas region. In the boundary layer, a steep temperature gradient exits and the temperature between boundary layers remain almost constant (bulk gas temperature). The bulk cover gas temperature and gradient of temperature at pool and roof boundary layers depends on pool and roof temperature.

It is noted that, the sampling of sodium metal aerosol characteristics is carried out in open atmosphere by all researchers but it is essential to consider that the sodium metal aerosols in cover gas region are liquid droplet suspended in argon gas. The sampling of these liquid metal aerosols required special sampling technique for characterization without exposing to the atmosphere. Further, the sodium metal aerosol characteristics are spatially varying within the cover gas space i.e. with respect to height. It is well known that that, the gamma radiation affect the aerosol process such as coagulation and deposition rates, aerosol removal etc. Since cover gas region is associated with intense gamma radiation field, the sodium metal aerosol characteristics needs to be studied under gamma radiation field.

The design of roof slab of SFR is a very complex task requiring development of theoretical model, validation and support by experimental research on thermal loading, temperature distribution and resultant stress, mass deposition and cooling system for roof slab. However, before designing the roof cooling system, it is very important to understand the physical process of heat and mass transfer through the cover gas space to the roof slab with the consideration of sodium metal aerosol characteristics presence in cover gas region. Hence, a theoretical modeling and validation with experimental results are required to predict the aerosol characteristics for given pool temperature and geometry. Experimental and theoretical modeling study has been carried out to address all the above issues. The main conclusions of the research work and highlights of major research findings of the study towards understanding the sodium metal aerosol characteristics in cover gas region are presented in this chapter.

8.2 Summary of the study

The sodium metal aerosol characteristics in cover gas region is determined for sodium pool temperature ranges from 250^{o}C - 550^{o}C taking into account of spatial variation within the cover gas space. The effects of geometric dimension and gamma radiation on sodium metal aerosol characteristics are also studied. The theoretical model developed to predict sodium metal aerosol characteristics in cover gas region and validated with experimental results. The important results obtained from the study are summarized as follows:

- The characterization technique for sodium metal aerosols in cover gas region without exposing the aerosol to atmosphere is developed, validated and used for characterizing the sodium metal aerosols in cover gas.
- Theoretical model is developed for predicting the sodium metal aerosol characteristics in cover gas region and validated with experimental results available in literature. The

theoretically predicted values of sodium metal aerosols mass concentration are found to be in good agreement with experimental results.

- The model is applied to experimental results obtained in ATF to validate for the size growth and suspended concentration decay of sodium combustion aerosols in a confined environment. The simulated values are in good agreement with the experimental values.
- The sodium metal aerosols are characterized in the cover gas region of TP-1 of SILVERINA loop at three different levels for various pool temperatures ranging from 250°C - 550°C in step of 50°C. The sodium metal aerosol size (MMD) and mass concentration increases with increase of sodium pool temperature for a given geometry. The MMD of sodium metal aerosol size is larger and mass concentration is more near the sodium pool compared to that of the middle level of cover gas region and near the roof for a given geometry. The theoretically simulated sodium aerosol mass concentration has good agreement with experimental results of TP-1.
- The temperature profile of the cover gas region is measured for various pool temperatures and found to have the ‘S’ pattern similar to the literature values i.e. it has pool and roof boundary layer having sharp gradient in temperature and a sandwiched region having almost constant temperature between boundary layers. Empirical relation for predicting the bulk cover gas temperature is derived based on our experimental results and used in modeling.
- Empirical relation for predicting the sodium metal aerosol size is derived based on our experimental results and with available literature results and used for modeling. The simulated sodium metal aerosol characteristics in cover gas region of various studies showed good agreement with the experimental results.
- The sodium metal aerosol characteristics are analyzed for geometric dimension effect (aspect ratio L/D) of cover gas region. Experimental values obtained from our studies

(different geometric dimension of TP-1 and TP -3) of SILVERINA loop and from the other available literature values are used for analyzing the geometrical effect on sodium metal aerosol characteristics in the cover gas region. The MMD of sodium metal aerosol increases and mass concentration of sodium aerosol decreases with the increase of aspect ratio (L/D) of cover gas region.

- The effect of gamma radiation on sodium metal aerosol properties in cover gas region is studied. The study includes an aerosol charge measurement in generation process and with gamma radiation field. It is found that the number of charges acquired by the mono-dispersed aerosols in the presence of gamma radiation filed is found to be more than that obtained without gamma radiation condition i.e. during generation process. In the cover gas region, the MMD of sodium metal aerosol is found to be higher and mass concentration is found to be less in the presence of gamma field when compared to that of without gamma field condition. This is attributed to the enhanced coagulation of charged sodium metal aerosols followed by settling in the presence of gamma radiation.

Research deliverable: The study is found to be useful for prediction of sodium metal aerosol characteristics in cover gas region for aspect ratio $0.55 \leq L/D \leq 4.52$ *and for the sodium pool temperature* $250^{o}C \leq Tp \leq 550\,^{o}C$.

8.3 Future scope

The scope of the future work envisaged is

- The sodium metal aerosol characterization in cover gas region for various roof temperature for a fixed sodium pool temperature.
- The study of model applicability for sodium aerosol characteristics in cover gas of reactor geometry L/D < 0.55.
- In the reactor environment, sodium metal aerosols and argon cover gas are radioactive and the aerosol characteristics may differ from the present experimental studies.

Hence the theoretical formulation is also required to be incorporated with charging effect of aerosols in the presence of gamma radiation field.

- In continuation of the above, it is planned to characterize the sodium aerosols in the cover region of FBTR.
- The effect of aerosol characteristics in thermal radiation change and deposition of sodium metal aerosols in roof slab and its penetrations.
- The influence of convection velocity in carrying various sized aerosols in cover gas region and the iodine vapors scavenging in sodium metal aerosols in cover gas region

.

APPENDIX -A

AEROSOL BASICS

To understand the aerosol process such as size growth, coagulation, chemical reaction, evaporation and condensation, removal, aerosol charging with radiation etc., it is important to be aware of aerosol terms and their properties. The basic description of aerosols, their properties and terms are [A.1, A.2, and A.3] described in the fallowing section.

A.1 Aerosol basic definition

Aerosols are microscopic particles, solid or liquid or both, that float in gas; their size range varies from 0.001 – 100μm. Aerosols are two-phase systems comprising both the particles and gas in which they are suspended. Depending on the two phase system they exhibit wide phenomena such as dust, fume, smoke, mist, fog, haze, smog.

A.1.1 Aerosol size

In reality, the shapes of the liquid particles are spherical and solid particles are complex in nature. In practice the complex spherical particles are always measured corresponding to a specific physical property. The particle size are characterized either by measuring the size such as aerodynamic diameter, optical equivalent diameter, electrical mobility equivalent diameter. An equivalent diameter is the diameter of the sphere that has the same value of particular physical property as that of the irregular particle. Fig.A.1 shows an irregular particle and its equivalent sphere. Stokes diameter is the diameter of the sphere that has the same density and gravitational settling velocity as the particle being measured. Stokes diameter standardizes the particles of various shapes to sphere having the same aerodynamic property and settling velocity. Aerodynamic diameter is the diameter of the unit density sphere that has the same gravitational settling velocity as the irregular shaped particle being measured. Aerodynamic diameter standardizes not only for shape but also for density.

Aerosols having a wide range of sizes are known as poly-dispersed aerosols and aerosols having same size are known as mono-dispersed.

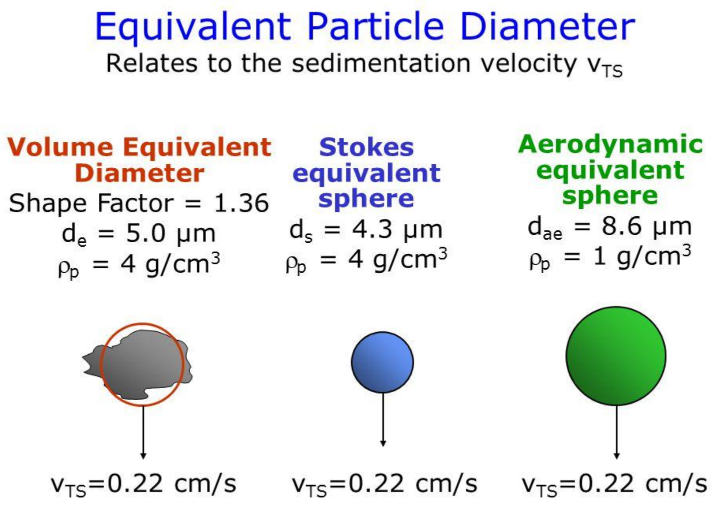

Fig A.1 An irregular particle and its equivalent sphere.

A.1.2 Aerosol concentration

The aerosol concentration is expressed in terms of two parameters viz. the mass concentration and number concentration. The mass of the aerosol particulate matter in a unit volume is called mass concentration and it is expressed in g/m^3, mg/m^3, µg/m^3, ng/m^3. The number of the aerosols in a unit volume is called number concentration and it is expressed in number/cm^3 or number/m^3.

A.1.3 Aerosol size distribution

Most aerosols being poly-dispersed in nature have a wide size range and thus it becomes necessary to accurately characterize their size distribution by statistical means. They exhibit skewed shape while describing with normal distribution function. The particle size distribution often has standard deviations that are large in comparison with the mean size. Such distributions are usually described mathematically as lognormal distribution. It has been found that the log normal distribution describes the skewed (asymmetrical) aerosol distribution properly. The lognormal distribution is actually a normal distribution of logarithms of particle size log(d_p). The frequency distribution for a Gaussian shape lognormal distribution is given as

$$f(d_p)dd_p = \frac{1}{\sigma_g\sqrt{2\pi}}\exp\left[-\frac{(\ln d_p - \ln \bar{d}_g)^2}{2\sigma_g^{\,2}}\right]dd_p \qquad \text{(A.1)}$$

ln(d_p), $\bar{d}_g$ and σ_g are particle diameter, Geometric mean and Geometric Standard Deviation (GSD) respectively. The frequency distribution of log normal distribution is shown in Fig.A.2.

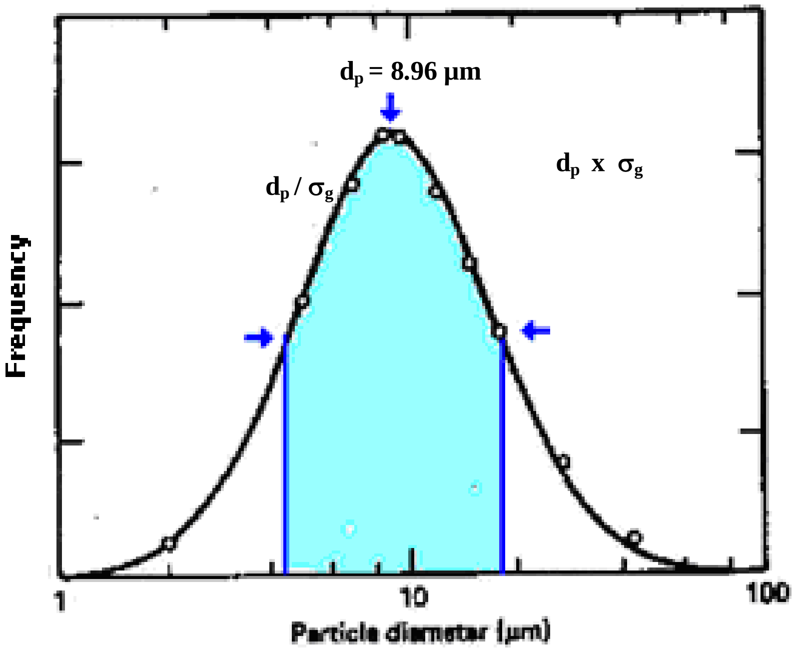

Fig. A.2 Frequency distribution of log normal distribution.

The measure of central tendency is the median d_{50}, which equals the geometric mean for a lognormal distribution and the measure of spread is the geometric standard deviation labeled 'σ_g'. The median is the 50th percentile particle size. The common medians in use are mass median, number median, area median, volume median etc. The geometric standard deviation is the ratio of the 50th percentile size to the 16th percentile size or the ratio of the 84th percentile size to the 50th percentile size. The weighted distributions of any lognormal distribution will be lognormal and have same geometric standard deviation. Fig. A.3 shows the distribution of count and mass plotted on the same logarithmic diameter scale. The mass size distribution has the same shape as the count size distribution but it is displaced along the size axis by a count amount equal to MMD/CMD, where MMD and CMD are Mass and Count Median Diameters respectively. CMD is the **p**article size for which half of the total numbers of particles are larger and half smaller. Same is true for CMAD where the diameter considered is aerodynamic diameter. Particle diameter for which half the mass is contributed by particles that are larger than MMD and half by particles smaller than the MMD. The MMD/CMD can be calculated by knowing only GSD.

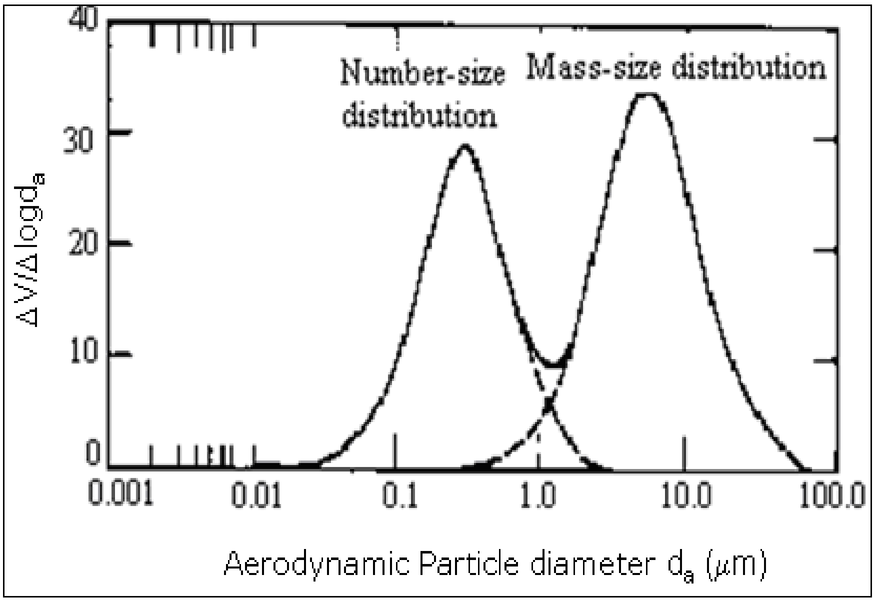

Fig. A.3 Count and Mass size distribution.

A.1.3.1 Hatch- Chaote equation

In a lognormal distribution, if one distribution is known completely, the other median diameter can be found out using the log normal conversion equations given by Hatch and Chaote. Accordingly the mass-size and count-size distribution are related as Hatch-Chaote equation. Thus, any type of average diameter can be calculated from this equation for a log normal distribution.

$\text{MMD} = \text{CMD} \exp (3 \ln^2\sigma_g)$ (A.2)

A.1.3.2 Probits

Probit indicates how many standard deviations from the mean that a given percentile value represented, for a truly normal distribution or Probit plots give the linear displacement from midpoint (50%) in units of standard deviation.

The Probit can be calculated as

$\text{Probit} = 4.9 * \{(\text{cum}\%/100)^{0.14} - (1-\text{cum}\%/100)^{0.14}\}$ (A.3)

1.4.3.3 Log-Probability graph

When the particle diameter scale is logarithmic, the graph is called log -probability graph. In the plots where cumulative percentage has been plotted against Effective Cutoff Diameter (ECD), the percent near the median i.e 50% gives the value of MMAD and CMAD as the case may be. The log- probability graph is shown in Fig. A.4. For log-normal distribution, geometric standard deviation (GSD), σ_g is the ratio of size associated with cumulative count of 84% and the median (50% cumulative count) size or between 50% cumulative size and 15.9% cumulative size.

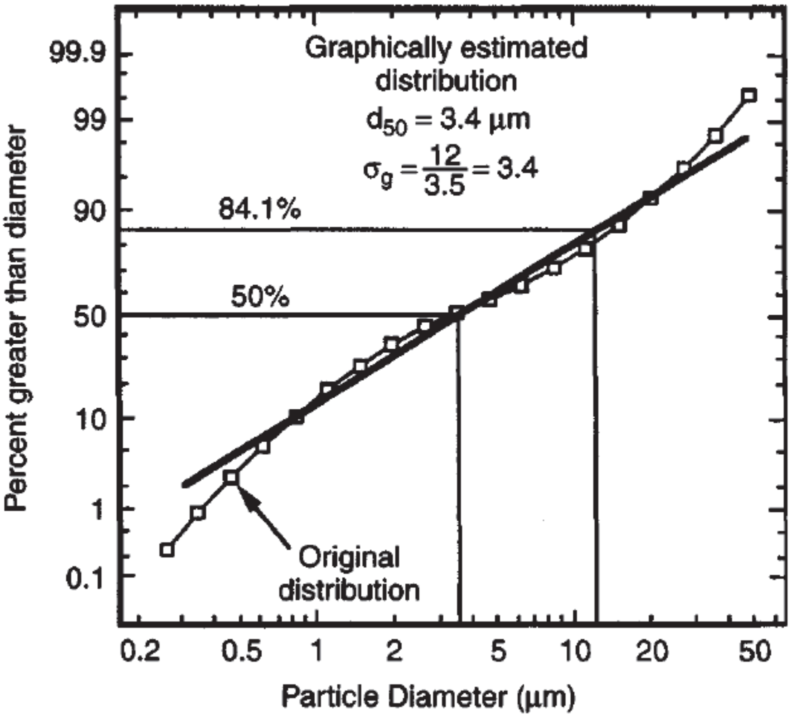

Fig. A.4 Log-probability graph.

In addition to above basic terms, aerosols exhibit various phenomena such as Brownian motion, coagulation, settling, aerosol charging with radiation and the motion of aerosols under the external force field. Next section describes the important terms which are involved in aerosol motion related to this thesis.

A.2 Reynolds number

The important type of particle motion is steady, straight-line motion. The uniform motion is the result of two forces, a constant external force such as gravity and the resistance of the gas to a particle motion (drag force). To understand the aerodynamic properties of aerosol, Reynolds number (dimensionless number) is used to describe the motion of the fluid as turbulent or steady. The motion of the particle in flow field is characterized by Particle's Reynolds Number and it is described as

$$\mathrm{Re} = \frac{\rho_g V_r d_p}{\eta} \tag{A.4}$$

Where V_r is the relative velocity of the gas to the particle, η the dynamic gas viscosity, ρ_g the gas density and d_p the characteristic dimension of the particle (diameter). The particle's Reynolds number has got four regions.

***Stokes region*:** $\mathrm{Re} < 1$. Fluid flow around the particle is laminar. The frictional force on the particle is predominant and the inertial force is negligible.

***Transient region*:** $1 < \mathrm{Re} < 5$. Turbulence starts to occur. Both the inertial force and the frictional force are important to the particle's behavior.

***Turbulent region*:** $5 < \mathrm{Re} < 1000$. Fluid flow around the particle is turbulent. The drag coefficient of the particle increases as Reynolds number increases.

***Newton's region*:** Re > 1000. Fluid flow around the particle is highly turbulent and the drag coefficient is nearly constant.

The relationship between the drag coefficient and the particle Reynolds number over a wide range of Reynolds numbers is shown in Fig. A.5. The aerosol motion occurs at Stokes region, because of the low velocities and small particle sizes involved. When we consider the particle motion in the Stokes region, the resistance force has two components, the normal component $F_n = \pi\eta v d_p$ and the frictional component $F_t = 2\pi\eta v d_p$, where η is the viscosity of gas, v is velocity of the particle relative to the fluid and d_P is the diameter of the particle.

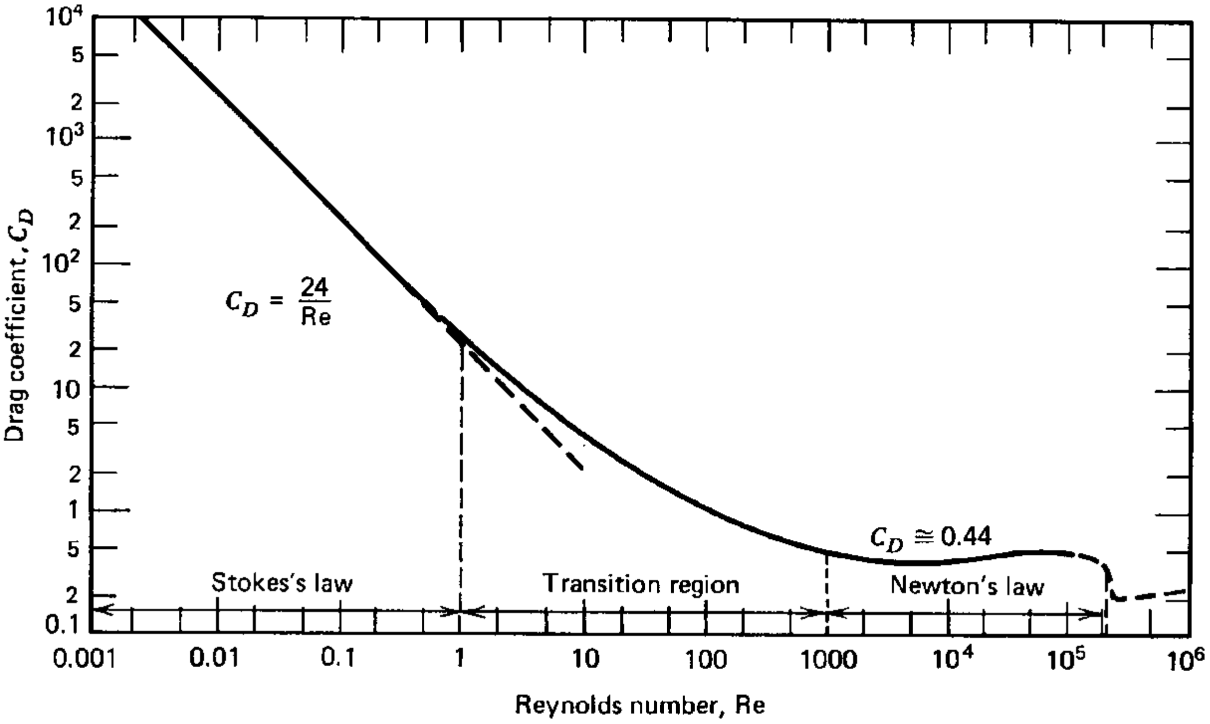

Fig. A.5 Drag coefficient as a function of particles Reynolds number

The total resisting force on the spherical particle is

$$F_D = F_t + F_n = 3\pi\eta v d_p \text{ (Stoke's Law)} \qquad (A.5)$$

The resultant force (F_R) on the particle is

$$F_R = mg - F_D \tag{A.6}$$

Where m is the mass of the particle and g is the acceleration due to gravity.

At equilibrium, $F_R = 0 = mg - F_D$ or $mg = F_D$

When the aerosol particle dimension is much smaller than the mean free path of the gas molecule, the particle experience less frictional force and the particle settles faster than predicted by the Stoke's Law. This error becomes significant for particles less than 1μm in diameter. A correction factor "Cunningham Slip Correction Factor C_c", is introduced in the Stoke's drag force by

$$F_D = \frac{3\pi\eta V d_p}{C_c} \tag{A.7}$$

Where $C_c = 1 + (2.52\lambda / d_p)$, C_c is always greater than one.

It is convenient to describe more complex shapes of a solid particle by a single diameter with an additional flow resistance or drag represented by a factor. This dynamic shape factor 'χ', is the ratio of actual resistance force of complex shape particle to the resistance force of a sphere has the same volume and velocity.

$$\chi = \frac{F_D}{3\pi\eta V d_e} \tag{A.8}$$

Where d_e – equivalent volume diameter.

Hence for the non-spherical particle the drag force

$$F_D = \frac{3\pi\eta V d_e \chi}{C_c} \tag{A.9}$$

A.3 Terminal settling velocity

The gravitational field exerts a force pulling the aerosol down. When the aerosol begins to move, the gas surrounding the particle exerts an opposing drag force. When the drag force equals the gravitational force, the particle reaches a velocity called the terminal settling velocity V_{TS} i.e,.

At equilibrium $0 = mg - F_D$ or $F_D = F_G = mg$ (A.10)

$$\frac{3\pi\eta V d_p}{C_c} = \frac{\pi}{6} d_p^3 \rho_p g \qquad \text{(A.11)}$$

Where ρ_p is the particle density.

$$V_{TS} = \frac{\rho_p d_p^2 C_c g}{18\eta} \qquad \text{(A.12)}$$

Where $V = V_{TS}$

Terminal settling velocity is an indicator of the particle settling property. Fig. A.6 explains the free falling particle attaining terminal settling velocity.

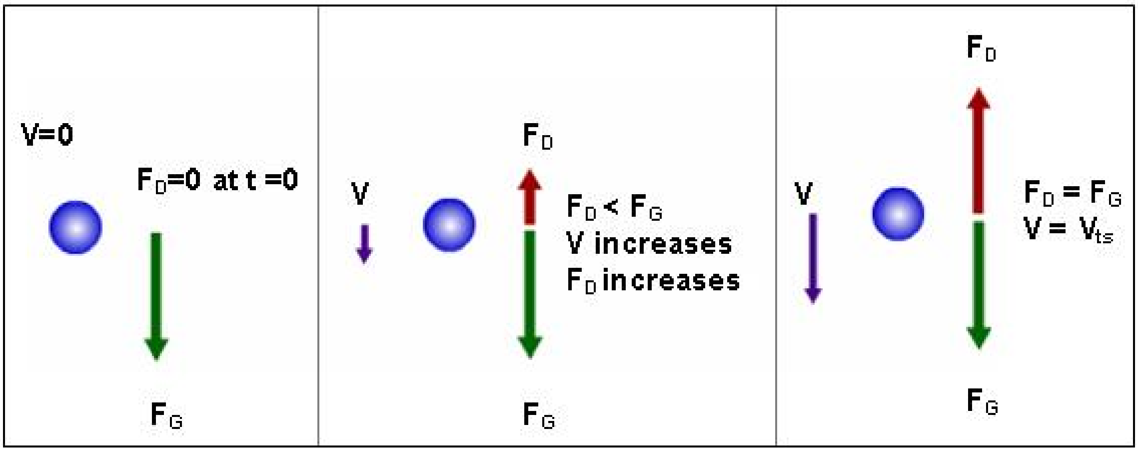

Fig. A.6 Schematic representation of terminal settling velocity

A.4 Deposition velocity

Deposition velocity is the effective velocity with which particles migrate to a surface and is analogous to the settling velocity. Deposition velocity is defined as the ratio of flux to the concentration.

$$V_{dep}(cm.s^{-1}) = \frac{\text{Number flux (cm}^{-2}\text{.s}^{-1}\text{)}}{\text{Number Concentration } (cm^{-3})} \qquad \text{(A.13)}$$

A.5 Relaxation time (τ)

It is the time for a particle to reach 1/e of its final velocity from an initial velocity or from the rest when subjected to an external force

$$\tau = \frac{\rho_p d_p^2 C_c}{18\eta} \qquad \text{(A.14)}$$

It is an indicator of particles ability to adjust to changes in flow velocity.

$$V_{grav} = \tau g \qquad \text{(A.15)}$$

A.6 Brownian motion

Brownian motion is the irregular wiggling motion of an aerosol particle in still air that is caused by random variations in the incessant bombardment of gas molecules against the particle. The net displacement of particles during its wandering motion over a period of time (longer than relaxation time) depends on the statistical combination of many such small scale motions. Hence the root mean square displacement $\overline{X}$ along any axis during time t is.

$$\bar{X} = \sqrt{2Dt} \qquad \text{(A.16)}$$

This equation relates Brownian displacement to Diffusion Coefficient 'D' and it is given by

$$D = kTB \tag{A.17}$$

where k is Boltzmann's constant, T is temperature and B is particle mobility.

A.7 Coagulation

Coagulation of aerosols is a process whereby aerosol particles collide with one another due to a relative motion between them and adhere to form larger particles. When the relative motion between particles is due to Brownian motion the process is called Thermal coagulation. When the relative motion arises from the external forces such as gravity or electrical forces, the process is called Kinematic coagulation. The Brownian coagulation coefficient is given as

$$K = 4\pi d_p D \tag{A.18}$$

where K is coagulation coefficient, D is diffusion coefficient and d_p is aerosol diameter.

A.8 References

A.1 William C. Hinds, (1982), "Aerosol Technology", John Wiley & Sons.

A.2 K. Willeke and P.A. Baron, (1993), "Aerosol Measurement: Principles, Techniques, and Applications", Van Nostrand Reinhold, New York.

A.3 N.A. Fuchs, (1964), "The Mechanics of Aerosols", Pergamon, New York.

APPENDIX - B

IONS PRODUCTION AND AEROSOL CHAREGING

B.1 Ions production

Interaction between energetic radioactive particles and molecules in the air results in the formation of ions. The interaction may be direct collision or by electrical interactions. The direct collision results in ionization which produces showers of ions where as gamma radiation interacts mainly in the form of photoelectric effect, Compton scattering and pair production. The principle positive ion formed in the atmosphere is the hydronium ion $H^+(H_2O)_n$ where n is between one to ten. The negative ions are formed by the attachment of low energy electron to an oxygen molecule (O_2^-). Then they attach to produce hydrate $O_2^-(H_2O)_n$. There also exists formation of secondary chemical species ions like $NO^+(H_2O)_n$ or $NO^-(H_2O)_n$. Increasing levels of hydration increase the mass of an ion which correspondingly reduces its mobility. It is also understood that ion mass and its mobility has the influence in charging of aerosols The background ion concentration is expected to be between 500 and 700 cm^{-3}, while with gamma source it is calculated to be 10^8 cm^{-3} (in our experimental condition). The mobility of the positive and negative ion are considered to be 1.14 $cm^2.V^{-1}.s^{-1}$ and 1.25 $cm^2.V^{-1}.s^{-1}$ respectively.

B.2 Charging of aerosol

The charges acquired by the aerosol in the presence of gamma radiation are due to the interaction ions and aerosols, by exposing the aerosols with a given concentration of bi-polar ions. At this juncture, the aerosol charging is considered to be a steady state charging. A collision between the aerosol and a small ion will cause the aerosol's charge to increase or decrease by one charge unit depending upon the polarity of the charge carried by the ion. When steady state condition is reached, formation of one kind of charge condition is achieved either by gaining or loosing of charge from less charged aerosol or excess charged aerosols respectively. Hence, at this condition; the ion properties are taken to be or tend to be unity. It is well known that the charged aerosols, in particular, the bipolar charging of mono dispersed aerosols are described for the given ion concentration by Modified Boltzmann distribution described by Clement & Harrison (1991) [B.1] and it is given as

$$\frac{N_j}{N_0} = \left[\frac{n_+\mu_+}{n_-\mu_-}\right]^j \frac{8\pi\varepsilon_0 akT}{je^2} \sinh\left[\frac{je^2}{8\pi\varepsilon_0 akT}\right] \exp\left[\frac{-j^2e^2}{8\pi\varepsilon_0 akT}\right] \tag{B.1}$$

The corresponding mean charges <j> for the particles is

$$\langle j \rangle = \sum_{j=-\infty}^{j=+\infty} jN_j \Bigg/ \sum_{j=-\infty}^{j=+\infty} N_j = \sum_{j=-\infty}^{j=+\infty} jN_j \Big/ Z \tag{B.2}$$

where j is average number of charges

N_j is aerosol number concentration having j charge

N_o is total number concentration of aerosol

μ_+ is mobility of positive ions

μ_- is mobility of negative ions

n_+ is positive ions concentration

n_- is negative ions concentration

ε_0 is permittivity of free space

a is aerosol radius

k is Boltzmann constant

T is temperature

e is elementary charge value

<j> is mean charge over a distribution

Z is total number of aerosol

It has been considered the use of an attachment coefficient ‘β’ to characterize the acquisition of charges by the mono dispersed aerosols in the presence of electrical force. Many formulations have been studied to derive ‘β’ which was compiled by Harrison (1992). Of which, (i) The theory used by Fuchs (1964) uses steady state charging of aerosols, which is used for the aerosols of sizes of the order of mean free paths of ions; (ii) The theory used by Gunn is quite simple for micron-sized aerosols and based on diffusion and ionic motilities. C.F. Clement and R.G. Harrison (1991) and R.G. Harrison and C.F. Clement (1992), in their study derived a single expression, which is widely used with approximation for the average aerosol charge. In the equation (B.1), it is taken into account that (i) for large radii the sinh function is small and may be neglected and (ii) the remaining pre factor, which depends on the ion asymmetry tend to unity as the ion properties become identical, which is the first approximation made. It is derived from the equation (B.1), in which, both the numerator and denominator are simplified leading to the simpler expression and finally the expression for the mean particle charge <j> is given by

$$< j >= \ln\left[\frac{n_{+}\mu_{+}}{n_{-}\mu_{-}}\right]\frac{4\pi\varepsilon_{0}akT}{e^{2}} \qquad \text{(B.3)}$$

This expression (Equation B.3) is same as that of coefficient of attachment derived and given by J. Bricard and J Pradel (1966) in Aerosol Science, edited by C.N. Davies (1966). They expressed that median charge $\bar{p}$ is a function of the ratio of q and N viz. (i). When q/N^2 is greater than 10^{-5}, the median charge $\bar{p} = {}^{1}/_{\epsilon}\, ln\frac{D^{'}}{D^{''}}$ where $\epsilon = {}^{e^2}/_{kTR}$; e- elementary charge, k- Boltzmann's constant, T-absolute temperature, R-the particle radius, D′-diffusion coefficient of positive ion & D″-diffusion coefficient of negative ion and (ii) When q/N^2 is less than 10^{-7}, which corresponds to a week intensity of ionization where $\bar{p}$ can be neglected; and it follows that: $\frac{n^{'}}{n^{''}} = \frac{D^{''}}{D^{'}} = 1.25\ and\ \frac{N_p^{'}}{N_p^{''}} = 1$; n', D' & $N_p^{'}$ are the number concentration of negative ions, their diffusion coefficient and Number of particles with p magnitude of negative charges and n", D" & $N_p^{''}$ are the number concentration of positive ions, their diffusion coefficient and Number of particles with p magnitude of positive charges.

Thus in an environment of a sea of bi-polar ions in which, aerosols are injected would establish the charge on aerosol particle (described generally by means of diffusion and ionic motilities) and it can be described in two ways viz. (i) to assume average/mean charge for a particle, which is representative of the entire aerosols and (ii) aerosol carry a distribution of charges. In all practical cases, it is possible to derive aerosol concentration-based criteria (developed by Harrison) to establish mean charge after charging has reached its final steady value (the positive and negative ion attachments rates are equal), and the ion concentration are steady,

$$\bar{j} = \frac{1}{2\varphi + (N/\ddot{n})} \ln\left(\frac{\mu_+}{\mu_-}\right) \qquad \text{(B.4)}$$

Analysis of the charging equations has shown that there are two distinct aerosols charging situations viz (i) In the case of recombination limit (the ion concentration is such that, ion recombination begins to dominate) and (ii) In the attachment limit, when the number concentration of aerosols determines the ion concentrations, the mean aerosol charge developed is small. Accordingly, The average charge in the recombination limit is given as

$$\bar{j} = \frac{1}{2\varphi + \left(N\sqrt{\left(\alpha/q\right)}\right)} \ln\left(\frac{\mu_+}{\mu_-}\right) \qquad \text{when } N \ll \sqrt{(\alpha q)/\beta} \qquad \text{(B.5)}$$

The average charge in the attachment limit is given as

$$\bar{j} = \frac{1}{2\varphi + (\beta N^2/q)} \ln\left(\frac{\mu_+}{\mu_-}\right) \qquad \text{when } N \gg \sqrt{(\alpha q)/\beta} \qquad \text{(B.6)}$$

Hence the aerosol acquire large charges when (i) there must be some asymmetry in the ion properties and (ii) there is a significant difference in aerosol concentration with ion concentration ($N << n$).

B.3 References

B.1 C. F. Clement and R. G. Harrison (1991), "Charge distribution on aerosols", In: O'Neill B. C. Proceedings of 8th International Electrostatics Conference, Oxford, Institute of Physics Conference Series 118, 275-280.

Journal of Aerosol Science 52 (2012) 98–108

Contents lists available at SciVerse ScienceDirect

Journal of Aerosol Science

journal homepage: www.elsevier.com/locate/jaerosci

An experimental study on the charging of non-radioactive aerosols with and without the presence of gamma radiation

V. Subramanian, Amit Kumar, R. Baskaran*, J. Misra, B. Venkatraman

Radiological Safety Division, Indira Gandhi Centre for Atomic Research, Kalpakkam 603102, India

ARTICLE INFO

Article history:
Received 2 September 2011
Received in revised form
14 May 2012
Accepted 14 May 2012
Available online 1 June 2012

Keywords:
Aerosol charging
Gamma radiation
Aerosols generation
Core disruptive accident

ABSTRACT

Electrical charging of non-radioactive aerosols was studied. The mean charge acquired by the poly-dispersed and mono-dispersed aerosols is determined for the two cases, viz. with and without the presence of additional ion pairs generated by gamma radiation. The results are separated accordingly by determining average charge acquired by the aerosols in three generation route (atomization, combustion and vaporization & condensation) and compared with the charge acquired in the presence of gamma radiation field. Using theoretical formulation developed by Clement and Harrison, the mean charge acquired by the aerosols (mono-dispersed) for a given concentration of both aerosols and ion pairs were calculated and compared with that of experimental results. The study is extended to determine the mean charge obtained for the distribution of DOP aerosols (poly-dispersed), by varying number concentration of aerosols and number concentration of ionpairs. It is found that the mean charge acquired by the aerosols increases with increase of ion pair concentration for a given concentration of aerosols.

1. Introduction

One of the important studies in the safety analysis of sodium cooled fast reactor, is the characteristics and the behavior of aerosols suspended in the Reactor Containment Building (RCB), in particular during Core Disruptive Accident (CDA)[1] condition (Abbey & Silberberg, 1979). The time evolution of the quantity of suspended mass concentration of aerosols and their leak rate from RCB determine the environmental source term (Indira et al., 2006). The environmental source term is the quantity of radioactive materials released, that would be carried away in the down wind direction and get deposited over the ground, resulting ground contamination as well as the health hazards to the public living at the site boundary (Baskaran et al., 2007). Hence, in order to undertake the aerosol studies, an Aerosol Test Facility (ATF) has been constructed

---

* Corresponding author. Tel.: +91 44 27480062; fax: +91 44 27480235.
E-mail address: rb@igcar.gov.in (R. Baskaran).

[1] During the normal operation of the sodium cooled fast reactor, there will be a balance between the heat generated in the core and the heat removed by the coolant. When the heat balance is lost due to initiating events such as, loss of coolant, loss of coolant flow, transient over power, and subsequent failure in the removal of such heat, may lead to the following core disruptive events in the reactor core viz., (i) Core disassembly, (ii) Core meltdown, and (iii) Both Core meltdown and Core disassembly. The after effects of core disruptive events are called Core Disruptive Accident (CDA). But to prevent the initiating events, there are two safety system provided in the reactors: (a) the shutdown system and (b) the decay heat removal system. Thus in case of the occurrence of initiating events, a CDA can be expected only with the failure of safety systems. In the unlikely event of CDA in sodium cooled fast reactor, the sodium slug may impact the reactor top plug. This provides a pathway for the escape of radioactive material (fission products and fuel material) and sodium into the RCB volume. Fuel and fission product vapors will condense and form aerosols. In addition, sodium burning will give rise to various compounds of sodium aerosols.

0021-8502/$ - see front matter © 2012 Elsevier Ltd. All rights reserved.
http://dx.doi.org/10.1016/j.jaerosci.2012.05.004

Nomenclature

N	number concentration of aerosols/cm^3
n	number concentration of ionpairs/cm^3 (n_+ and n_- are positive and negative ions) $\bar{n}$–$(n_+ + n_-)/2$
a	particle radius (cm)
d	particle diameter (cm)
j	magnitude of charge (number) (j_1—number of charges for a particle with radius a_1)
$\bar{J}$	average number of charges based on theoretical estimation
$\langle j \rangle$	mean change over a distribution
e	elementary charge value
ε_0	permittivity of free space
ε_r	relative permittivity
k	Boltzman constant
T	temperature (K)
μ	mobility of ions (μ_+ and μ_- mobilities of positive and negative ions)
Z	total number of particles $Z = \sum_{p=1 \text{ to } 12}^{p+1} N_p$ where p–collection stages 1–12.
φ	$e^2/8\pi\varepsilon_0 akT$
α	ion recombination coefficient 1.6×10^{-6} cm^3/s
β	ion attachment coefficient 1.4×10^{-6} cm^3/s
q	ion pair production rate (ionpairs/cm^3/s)

in our division and various characteristics of aerosols and their behavior have been studied. The study includes physical and chemical characteristics of sodium aerosols, behavior of aerosols in the presence of gamma radiation field and the behavior of mixed aerosols in a confined environment.

In this context, one of the key studies is the behavior of sodium aerosols under the gamma radiation field. It is noted that in the event of CDA, the entire RCB volume is occupied by the bi-polar ions that are generated due to the prevailing gamma radiation. When the sodium and other fission product aerosols are made to suspend in the volume of RCB, i.e. in the sea of bi-polar ions, the aerosols acquire charges. When these aerosols undergo coagulation with the acquired charges, the Brownian coagulation is found to be enhanced. Experimental results at ATF showed that the coagulation enhancement of 5–8 times for the mono-dispersed sodium aerosols in a confined environment at the dose rate of the order of few mGy/h (Subramanian et al., 2008). It is further reported that, by using general theory derived by Zebel (1966) and by Williams and Loyalka (1991),[2] in order to get the coagulation enhancement factor of 5 times the modest charging required by the aerosol particle is about 8 charges for the particles of radius 0.5 μm in a given ion concentration (radiation field of 4 mGy/h) (Subramanian et al., 2011). Thus it is understandable that the electrical forces caused by the Coulomb interaction between the charged aerosol particles are responsible for the enhanced coagulation. Hence it is customary to get the number of elementary charges acquired by the aerosols in the presence of given concentration of bi-polar ions. Thus the study has been extended to determine the charge-size distribution of aerosols for a given concentration of bi-polar ions and aerosols number concentration.

Before getting into the measurement of charges on the aerosols, it is imperative to consider the charges acquired by the aerosols during generation process besides during the presence of gamma radiation. Understanding the mechanism of aerosol charging during generation of aerosols is important in aerosol science, particularly to understand the aerosol process like particle deposition, electrical migration, sampling & transport and coagulation, etc. Hence our experimental study includes determination of charging of aerosols in three generation process viz. (i) combustion route (generating sodium compound aerosols), (ii) vaporization and condensation route (SrO_2 aerosols) and (iii) atomization route (polystyrene latex and DOP aerosols) and by comparing the average charge acquired by a particular sized aerosols generated in all the three process.

Interaction between energetic radioactive particles and molecules in the air results in the formation of ions. The interaction may be direct collision or by electrical interactions. The direct collision results in ionization which produces showers of ions whereas gamma radiation interacts mainly in the form of photoelectric effect, Compton scattering and pair production. The principle positive ion formed in the atmosphere is the hydronium ion $H^+(H_2O)_n$ where n is between one and ten. The negative ions are formed by the attachment of low energy electron to an oxygen molecule (O_2^-). Then they attach to produce hydrate $O_2^-(H_2O)_n$. There also exists formation of secondary chemical species ions like $NO^+(H_2O)_n$ or $NO^-(H_2O)_n$. Increasing levels of hydration increase the mass of an ion which correspondingly reduces its mobility. It is also understood that ion mass and its mobility has the influence in charging of aerosols. The background ion concentration is expected to be between 500 and 700 cm^{-3}, while with gamma source it is calculated to be 10^6–10^8 cm^{-3} (in our experimental condition). The mobilities of the positive and negative ions are considered to be 1.14 cm^2 V^{-1} s^{-1} and 1.25 cm^2 V^{-1} s^{-1} respectively. Then, charges acquired by the aerosol in the presence of gamma radiation are due to the interaction of ions and aerosols, by exposing the aerosols with a given concentration of bi-polar ions. At this juncture, the aerosol charging is considered to be a steady state charging (Clement & Harrison, 1992). A collision between the aerosol and a small ion will cause the aerosol's charge to increase or decrease by one charge unit depending upon the polarity of

---

[2] The coagulation enhancement factor $f = K'/K$ where $K'$and K are coagulation kernels for the charged and uncharged particles respectively. The coagulation enhancement factor particles in the presence of bi-polar ions concentration is calculated by using formula: The coagulation enhancement factor $f(Y) = Y/\exp(Y) - 1$where $Y = j_1 e j_2 e / 4\pi\varepsilon_0 kT(a_1 + a_2)$.

the charge carried by the ion. When steady state condition is reached, formation of one kind of charge condition is achieved either by gaining or loosing of charge from less charged aerosols or excess charged aerosols respectively. Hence, at this condition; the ion asymmetry tends to be or taken as unity which follows ions have the same concentration and mobility, which is the first approximation used in this paper, the charge acquired by the aerosols under steady state charging condition is determined (Harrison, 1992).

It is well known that the charged aerosols, in particular, the bi-polar charging of mono-dispersed aerosols are described for the given ion concentration by Modified Boltzmann distribution described by Clement & Harrison (1991a) and it is given as

$$\frac{N_j}{N_0}=\left[\frac{n_+\mu_+}{n_-\mu_-}\right]^j\frac{8\pi\varepsilon_0akT}{je^2}\sinh\left[\frac{je^2}{8\pi\varepsilon_0akT}\right]\exp\left[\frac{-j^2e^2}{8\pi\varepsilon_0akT}\right] \tag{1}$$

The corresponding mean charges $\langle j\rangle$ for the particles is

$$\langle j\rangle=\sum_{j=-\infty}^{j=+\infty}jN_j\Big/\sum_{j=-\infty}^{j=+\infty}N_j=\sum_{j=-\infty}^{j=+\infty}jN_j/Z \tag{2}$$

Brownian agglomeration of charged soot particles was studies by Hautanen et al. (1995) and reported a reduction of aerosol concentration by coagulation (not quantified). But Park et al. (2005), in their modeling studies, bi-polar diffusion charging can significantly increase the coagulation rate of aerosols. Bi-polar diffusion charging of non-radioactive aerosols by using Am-241 Alpha sources was compared with that of soft X-ray source of 9.5 keV by Lee et al. (2005). They reported that, a steady ion concentration rate was achieved by X-ray source and it is effective for the measurement of nano-particles. An experimental and theoretical study by Konstantaneous Barbranis (2009) showed that, increase of radio-activity concentration has minor deviation in the charge distribution of aerosols. However, the product n and t (n—no. of ion pairs and t—resident time) would be a key factor for the particle charging to achieve Boltzmann equilibrium. Another important study on bi-polar charging on radioactive aerosols and comparison of their result with Clement & Harrison (1991a) model was carried out by Gensdarms et al. (2001). In fact, the electrical charging of radioactive aerosols is different from that of non-radioactive aerosols but their study, concludes that the electrical charging varies with the intensity of ionization in the environment.

By keeping all these aspects and to answer the questions on the number of elementary charges acquired by the aerosols, experiments are planned to determine (i) the charge size distribution of aerosols, (ii) average number of charges acquired in the generation process (in three different generation route) by the aerosols and (iii) to determine the number of elementary charges increased (average number) if any, for the aerosols in the presence of gamma radiation field, then compare the results with the theoretical formula (Harrison, 1992; Clement & Harrison, 1992) developed for the attachment of charges by the aerosols. These results are presented in this paper.

2. Aerosol charging on non-radioactive aerosols

It has been considered the use of an attachment coefficient 'β' to characterize the acquisition of charges by the mono-dispersed aerosols in the presence of electrical force. Many formulations have been studied to derive 'β' which was compiled by Harrison (1992). Of which, (i) the theory used by Fuchs (1964) uses steady state charging of aerosols, which is used for the aerosols of sizes of the order of mean free paths of ions; (ii) the theory used by Gunn is quite simple for micron-sized aerosols and based on diffusion and ionic mobilities. Clement & Harrison (1991a) and Harrison & Clement (1992), in their study derived a single expression, which is widely used with approximation for the average aerosol particle charge. It is derived from Eq. (1), in which, both the numerator and denominator are simplified[3] leading to the simpler expression and finally the expression for the mean particle charge $\bar{j}$ is given by

$$\bar{j}=\ln\left[\frac{n_+\mu_+}{n_-\mu_-}\right]\frac{4\pi\varepsilon_0akT}{e^2} \tag{3}$$

This expression (Eq. (3)) is same as that of coefficient of attachment derived and given by Bricard & Pradel (1966) in Aerosol Science, edited by Davies (1966). They expressed that mean charge $\overline{p}$ is a function of the ratio of n and N viz.: (i) When n/N^2 is greater than 10^{-5}, the mean charge $\overline{p}=1/\epsilon\ ln\,D^+/D^-$ where $\epsilon=e^2/kTR$; e the elementary charge, k the Boltzman's constant, T the temperature in Kelvin, R the particle radius, D^+ the diffusion coefficient of positive ion and D^- the diffusion coefficient of negative ion; and (ii) When n/N^2 is less than 10^{-7}, which corresponds to a week intensity of ionization where $\overline{p}$ can be neglected, and it follows that: $n^-/n^+=D^-/D^+=1.25$ and $N_p^+/N_p^-=1$; n^-, D^- and N_p^- are the number concentration of negative ions, their diffusion coefficient and number of particles with p magnitude of negative charges and n^+, D^+ and N_p^+ are the number concentration of positive ions, their diffusion coefficient and number of particles with p magnitude of positive charges respectively.

---

[3] In Eq. (1), it is taken into account that (i) for large radii the sinh function is small and may be neglected and (ii) the remaining pre factor, which depends on the ion asymmetry tend to unity as the ion properties (concentration and mobility) become identical, which is the first approximation made.

Thus in an environment of a sea of bi-polar ions in which, aerosols are injected would establish the charge on aerosol particle (described generally by means of diffusion and ionic mobilities) and it can be described in two ways viz. (i) to assume average/mean charge for a particle, which is representative of the entire aerosols and (ii) aerosol carry a distribution of charges. In all practical cases, it is possible to derive aerosol concentration-based criteria (developed by Harrison) to establish mean charge after charging has reached its final steady value (the positive and negative ion attachments rates are equal), and the ion concentration are steady,

$$\bar{j} = \frac{1}{2\varphi + (N/\bar{n})} \ln\left(\frac{\mu_+}{\mu_-}\right) \tag{4}$$

Analysis of the charging equations has shown that there are two distinct aerosols charging situations (Clement & Harrison, 1991b) viz., (i) in the case of recombination limit (the ion concentration is such that, ion recombination begins to dominate) the aerosol may develop a large charge. Accordingly, the average charge in the recombination limit is given as

$$\bar{j} = \frac{1}{2\varphi + (N\sqrt{(\alpha/q)})} \ln\left(\frac{\mu_+}{\mu_-}\right) \quad \text{when } N \ll \sqrt{(\alpha q)/\beta} \tag{5}$$

and (ii) in the attachment limit, when the number concentration of aerosols determines the ion concentrations, the mean aerosol charge developed is small. Accordingly, the average charge in the attachment limit is given as

$$\bar{j} = \frac{1}{2\varphi + (\beta N^2/q)} \ln\left(\frac{\mu_+}{\mu_-}\right) \quad \text{when } N \gg \sqrt{(\alpha q)/\beta} \tag{6}$$

Hence the aerosol acquire large charges when (i) there must be some asymmetry in the ion properties and (ii) there is a significant difference in aerosol concentration with ion concentration ($N \ll n$). The experimental verification of the later condition is attempted in this paper and the results are presented.

3. Experimental

3.1. Aerosol test facility (ATF)

The major components of ATF (Baskaran et al., 2004)) are: (i) Aerosol chamber, (ii) Aerosol generators viz. sodium combustion cell for the generation of sodium aerosols and plasma torch for the generation of SrO_2 aerosols, (iii) Aerosol diagnostic equipments, and (iv) Auxiliary systems like vacuum system, chilled water system, pneumatic control system, data acquisition system and humidity controller. The aerosol chamber is in cylindrical shape having volume 1 m^3 (height=60 cm and diameter=150 cm) and it is made of SS-304 L. The chamber is provided with eight numbers of 3″ ports, three numbers of 4″ ports and one number of 6″ port. A vacuum pumping system is connected to 6″ port. Sodium combustion cell for the generation of sodium aerosols and a 25 kW thermal plasma torch are connected into two 3″ ports. The schematic diagram of ATF is shown in Fig. 1.

3.2. Aerosol diagnostics

For the real time measurement of aerosol particle size distribution, a single particle counter, “Aerosol Dust Monitor” (Model 1.108 of M/s GRIMM Aerosoltechnik, GmbH, Germany), Sequential Mobility Particle Sizer+Condensation Particle Counter (SMPS+C) (Model:5.401 and 5.403, M/s GRIMM Aerosoltechnik, GmbH, Germany) and “MASTERSIZER” (M/s Malvern, UK), based on ensemble diffraction technique, were used. The aerosol dust monitor and SMPS+C are connected through 1:100 dilutors (Model 1.159 of M/s GRIMM Aerosoltechnik, GmbH, Germany) to the aerosol chamber with the help of nozzles and they measure particle concentration up to 10^{15} particles m^{-3}. Electrical Low Pressure Impactor (ELPI) (Marjamaki et al., 2000) is used for the measurement of charge size distribution. Since our measurements are mainly on electrical charges acquired by the aerosols, the measurements of charges acquired by the aerosols using ELPI is only described here (other instruments are described in elsewhere; Baskaran et al., 2009).

ELPI (Model 97 2E, M/s Dekati Ltd., Finland) is a 13 stage cascade impactor with cut sizes between 30 nm and 10 μm. The impactor stages are electrically insulated and the current signal from each impactor stage is measured with sensitive electrometers. ELPI has 12 of these electrometers, the uppermost impactor stage acts as a pre-cut but has no electrical detection. The particle number concentration in each size class (impactor stage) can be calculated from the measured current signals when the particle charging efficiency is known. The ELPI operates at a flow rate of 10 lpm and integrated with aerosol chamber through 25 mm sampling head. The instrument is provided with dilutor 1:100 and provision is available to sample the aerosols with and without connecting the dilutor. The ELPI measures count-size distribution when the instrument is operated with charger ON condition where the particles are charged by corona charger before entering into the classifier. The instrument measures the charge-size distribution of aerosols when the instrument is operated with charger OFF condition, i.e. the charges associated with particles before entering into the sampler (i.e. in the generation process) will be measured as charge-size distribution. For the charge-size distribution measurement there exists an in-built macros, which calculates both count-size distribution and charge-size distribution, for which the equipment must be operated with equal sampling time for charger ‘ON’ and charger ‘OFF’ condition. The salient feature of ELPI in (i) charging

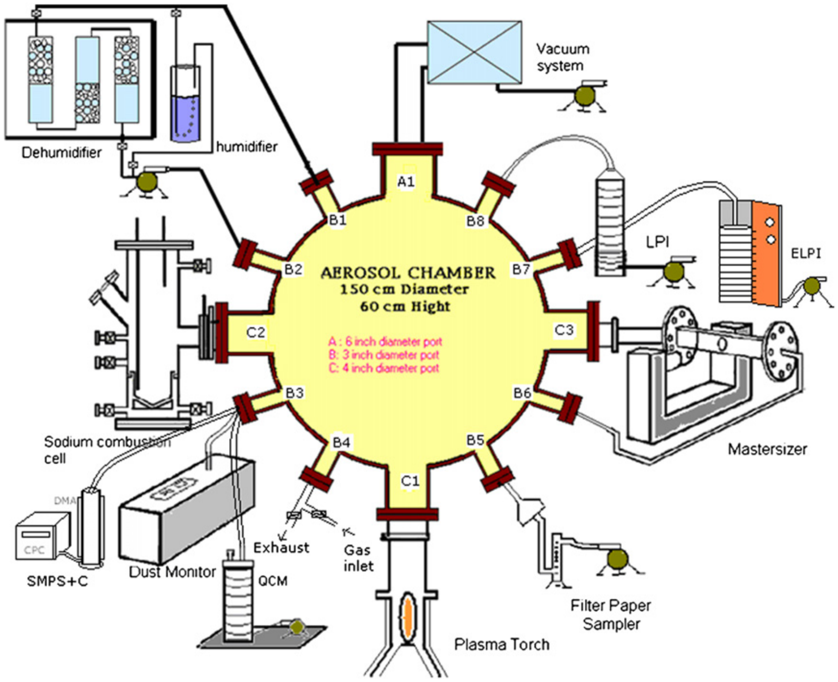

Fig. 1. A schematic diagram of the aerosol test facility.

efficiency function, (ii) measurement of number concentration (iii) measurement of uncertainty in the charge measurement and (iv) measurement of number-size distribution for bi-polarly charged aerosols in particular to positively charged aerosols are briefed in Appendix A (Marjamaki et al., 2000; ELPI User Manual, 2007; Virtanen et al., 2001).

3.3. *Aerosol generation*

3.3.1. *Generation of non-radioactive fission product aerosols*

SrO_2 aerosols are generated using the plasma torch (Subramanian et al., 2009a). A known weight of SrO_2 powder (procured from M/s ACROS Organics, USA) is palletized. Typical weight of the pellets was 5 ± 0.2 g. The pellets were rigidly fixed in to the wire feeder tube and kept in front of the plasma flame. The pellet melts and the molten vapors after leaving the flame zone condense to produce aerosols, i.e. at a particular point the vapor pressure exceeds the saturated vapor pressure of the condensed phase and nucleation of the condensed phase occurs. At the same time the vapors are flown into the aerosol chamber (distance between plasma flame and the chamber is 50 cm) along with the sheath gas (Nitrogen) (flow rate ~40 lpm) used in the plasma torch. The vapor is diluted and re-condenses to produce aerosols in the chamber by homogeneous nucleation or by heterogeneous nucleation on air molecules (Young and Pfender, 1985). The gate valve on the plasma torch side of the aerosol chamber is closed after plasma torch is switched off.

3.3.2. *Generation of sodium compound aerosols*

The sodium combustion cell is isolated, flushed and filled with argon gas, up to a pressure of 10–20 kPa excess over atmosphere. About 5–10 g of sodium is placed in a crucible and mounted on a heater. The sodium is heated up to a required temperature (say 550 °C, the temperature of the primary sodium in the fast reactor). The hot sodium is ignited by exposing it to air, after flushing out the argon. By combustion, sodium oxide aerosols are formed in the combustion cell. The gate valve is opened and the aerosol chamber and the diagnostic ports are get filled in with aerosols immediately. The pressure inside the cell rises up to 70–80 kPa excess over the atmosphere (before opening the gate valve) helps to fill the aerosol chamber and its diagnostic ports with sodium aerosols. The cell is isolated after 2 min so that sodium aerosols are bottled-up inside the aerosol chamber (Subramanian et al., 2009).

3.3.3. *Generation of polystyrene latex aerosols by atomization*

DOP poly-dispersed and mono-dispersed Polystyrene latex particles ($d = 1.3\ \mu m$ obtained from M/s Polyscience Inc., USA) are generated by using aerosol generator (Model No:7.811, M/s Grimm aerosol generator, GmbH, Germany). Atomization is carried out in de-ionized water to which few drops of DOP or polystyrene latex particles are added. After the atomization, the aerosols are made to pass through a condenser (cooling the transport line on a thermostat filled with ice cubes) followed by line heater (heating the transport line by using heating coil wounded over the line) and finally transported to the aerosol chamber. The interference of moisture condensing on aerosols and consequent perturbation on charge measurements were eliminated by cooling and heating techniques. The ratio of aerosol solution and dispersant is maintained about 1.6:100, which is proved to give good number concentration of aerosols generated by atomization processes. Thus the aerosols are pumped into the chamber and they are made to suspend in a chamber where charge measurements are carried out (Amit et al., 2010).

4. Sampling

To begin with aerosol chamber is kept in the ambient atmospheric condition prevailed in Kalpakkam site, i.e. atmospheric pressure ~101 kPa and ~65% RH. During the experiments the aerosol chamber is bottled-up with aerosols and samples are drawn through horizontal ports to avoid bias due to gravitational and settling properties. The sample heads are designed and installed in such a way to fulfill the Davies criteria (William, 1982). The sample heads are having diameter of 8.0, 13 and 25 mm to connect various diagnostic equipments according to their flow rates and inlet nozzles. By running ELPI with corona charger 'OFF' and 'charger 'ON' condition for a constant time say 100 s or 60 s, the charges associated with generation process of aerosols along with number-size distribution can be measured. The results are derived by repeating the measurement for the next 100 s or 60 s and taking average value. [Since the average charge acquired by aerosols significantly differs, due to change in number concentration of aerosols, when the measurements are continued further.] By using charge-size distribution, number-size distribution, the flow rate of the instrument, total charge measured and by taking the elementary charge value, the average number of charges associated with the aerosols is determined. The experiments are repeated by exposing the aerosol chamber volume panoramically with gamma radiation source, Cs-137,[4] of 0.5 TBq. The source is mounted on top of the chamber on the center axial line and it was fixed at a position such that it gives desired dose rate inside the chamber. The dose rate inside the chamber was measured using Teletector (Model 6112, M/s Automation Uno Mentechnik, Germany).

5. Results and discussion

The charge-size distribution (average number of charges in particular size ranges) of background aerosols (in the chamber) without and with gamma field (40 mGy/h) and its number-size distribution measured simultaneously by using ELPI, are given in Fig. 2(a) and (b), respectively. As expected, it is observed that number of elementary charges acquired in all sized aerosols is found to be more in the presence of gamma radiation field. The mean number of charges $\langle j \rangle$ (for the whole distribution), as described by Eq. (2), for without and with gamma field is found be -1.4 and $+2$ units respectively. This is calculated by drawing frequency distribution with number of particles in each cut-off size versus total number of charges in fC (femto Coulomb) measured in that size range and then finding arithmetic mean value. Typical calculation of arithmetic mean charge for the charge distribution of background aerosols (without gamma field) is given in Table 1. Then the chamber is filled with poly-dispersed SrO_2 and DOP aerosols and charge-size distributions are measured with and without the presence of gamma radiation field and the results are presented in the Fig. 2. The charge-size distribution and number-size distributions for poly-dispersed SrO_2 aerosols are given in Fig. 2(c) and (d) respectively. Similarly, the results of the DOP aerosols are shown in Fig. 2(e) and (f) respectively. It is observed from the figures [Fig. 2(c) and (d)], there is a significant reduction of average number of charges when the particle concentration above 10^6 particles cm^{-3} ($0.32\ \mu\text{m} \leq \text{ECD} \leq 3.21\ \mu\text{m}$, where ECD-Effective cut-off diameter). The mean charge over the distribution of aerosols with and without gamma field is found to be $+0.5$ and -0.15 units respectively. In the case of DOP aerosols ($N_{\max} = 10^5\ \text{cm}^{-3}$) generated via atomization route has significant reduction of charges in the presence of gamma radiation, i.e. charge neutralization is taking place. The average number of charges in each size range during generation process is more than that of gamma radiation field ($n = 10^6\ \text{cm}^{-3}$). The mean number of charges for whole distribution of DOP aerosols with and without gamma field is found be $+0.5$ and $+2.5$ respectively. The variation in the magnitude of charge seen in the charge-size distribution is due to (i) the aerosols are poly-dispersed and the larger sized particles could have wider charge distribution while the smaller sized particles could have singly or doubly charged and (ii) the normalized data (charge/particle) is presented in the graph (Clement & Harrison, 1992), accordingly the average charge decreases when the number of particles in those size ranges increases.

The measurement of mean charge for the whole distribution gives the weighted average distribution because; it has influence on number of aerosols in that particular size range. But, in order to investigate the phenomena of aerosol charging by the excess ionpairs generated due to gamma radiation; we have conducted experiment by generating mono-dispersed aerosols. The measured average charge acquired by the aerosols in the generation process is compared with the additional charge acquired, if any, by the same aerosols, by applying gamma radiation field (10^7 ionpairs/cm^3). Table 2 gives, the charge acquired 'abs $\langle j \rangle$' by the mono-dispersed polystyrene-latex aerosols of size 1.3 μm (diameter), mono-dispersed sodium combustion aerosols of 1.0 μm (diameter) and 1.29 μm (diameter) sized SrO_2 aerosols with and without the presence of gamma radiation field. The reason for selecting the size is that, initial size distribution of sodium

---

[4] The ^{137}Cs decays into ^{137}Ba* through beta decay, ${}_{55}\text{Cs}^{137} \rightarrow {}_{56}\text{Ba}^{137*} + {}_{-1}\text{e}^{0} + \overline{\gamma}$ (514 keV), which in-turn decays through gamma decay, ${}_{56}\text{Ba}^{137*} \rightarrow {}_{56}\text{Ba}^{137} + \gamma$ (662 keV)

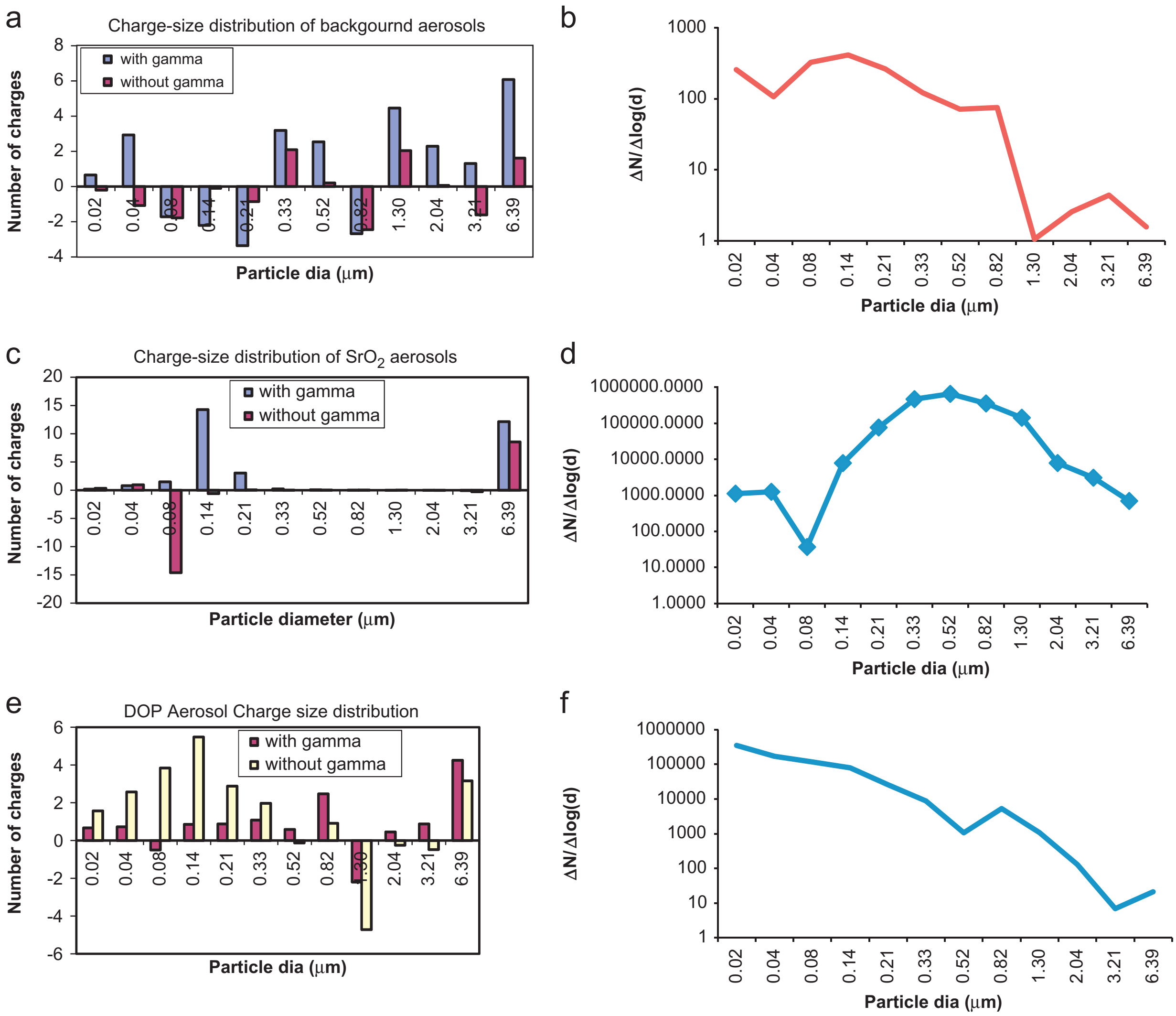

Fig. 2. Charge-size distribution and their number concentrations of background aerosols, poly-dispersed SrO_2 and DOP aerosols.

combustion aerosols at 50%RH is 1.0 μm, (Subramanian & Baskaran, 2007), hence polystyrene latex particles of 1.3 μm is used for atomization technique, while in the case of SrO_2 aerosols, vaporization and condensation route produce poly-dispersed aerosols, of which, particles corresponding to 1.29 μm (ECD) is chosen for this study. Table 3 gives the magnitude of average charge obtained by theoretical calculation using Eq. (4)—under steady state condition, Eq. (5)—under recombination limit and Eq. (6)—under attachment limit.

The particle charging phenomena is described as follows for both the situations, i.e. in the generation process and when the gamma field is applied:

In the generation process: In the case of combustion route, the particles are formed generally as a solid by condensation of sodium fumes. The condensation produces little or no charge on the aerosols but these aerosols acquire charges by Brownian collision with omnipresent air ions and attain Boltzmann equilibrium. In vaporization and condensation route, particle charging is significant as evaporation produce significant number of high mobility ions. Hence charge-associated with these aerosols also attain Boltzmann equilibrium. In the atomization process of polystyrene latex particles, it is observed that average-number of charges associated with these aerosols are maximum. Since polystyrene is a dielectric liquid associated with surface charges, during the atomization the charged surface gets disrupted hence the aerosols acquire charges by spray electrification. Thus the average number of charge acquired by the polystyrene latex particles is found to be more than other two aerosols.

In the presence of excess ion pairs (*with gamma field*)*:* Aerosols are injected into the sea of ionpairs. The ion pair concentration is of the order of $10^8/cm^3$. Since it is a gamma interaction, and the dose rate obtained is steady (40 mGy/min) the number of positive ions and negative ions become equal. The aerosols begin to get charges, then, as time progresses the aerosol charging would be a steady state charging and attain Boltzmann equilibrium. As the time further progresses,

Table 1
Mean charge $<j>$ associated with background aerosols without gamma field.

Stokes diameter (D_p) μm [1]	**No of particles/cm^3(Nj) [2]**	**No. of particle collected by sampler [3]**	**Charge measured (Coulomb) [4]**	**No. of ions [5]**	**Average number charges (j) [6]**	**Frequency number $j \times N_j$ [7]**
0.021	1320	220,064	2.30E–14	143,921	0.65	858
0.043	1200	200,107	9.38E–14	586,314	2.93	3516
0.082	2251	375,257	−1.03E−13	645,443	−1.72	−3871.72
0.137	6447	1,074,625	−3.79E−13	2,374,921	−2.21	−14,247.9
0.214	4007	667,944	−3.59E−13	2,244,295	−3.36	−13,463.5
0.329	1268	211,385	1.07E−13	674,318	3.19	4044.92
0.516	87	14,636	5.94E−15	37,175	2.54	220.98
0.817	449	74,846	−3.20E−14	200,588	−2.68	−1203.32
1.299	26	4455	3.17E−15	19,870	4.46	115.96
2.042	9	1621	5.94E−16	3712	2.29	20.61
3.208	2	380	7.97E−17	498	1.31	2.62
6.388	1	242	2.53E−16	1587	6.54	6.54
ΣN_j	17,067				$\Sigma j \times N_j$	−23,987.09
			Mean charge $\langle j \rangle =$	$\Sigma j \times Nj/\Sigma Nj = -1.4$		

Column [1], [2] and [4] are obtained from the instruments.
Stokes diameter is obtained by taking geometric mid-point for the successive stages and density.
Flow rate of the instrument is 10 lpm and duration of the sampling is 60 s.
Column [3] is calculated as $(N_j \times 10 \times 1000)/(60)$, the number of particles per second.
Column [5] is obtained by dividing column [4] by 1.6×10^{-19} the elementary charge value.
Column [6] is obtained by dividing column [5] by column [3].
Column [7] is obtained by multiplying column [6] and column [2].
An arithmetic mean value is determined as −1.4.

Table 2
Average number of charge 'abs $<j>$' acquired by the aerosols in three generation mechanism with and without the presence of gamma radiation field (40.0 mGy/min).

Generation method	**Aerosol material**	**Number concentration (cm^{-3})**	**Particles diameter (μm)**	**Average number of charges abs $\langle j \rangle$**	
				Without gamma field	**Ion conc. 1.4×10^8 ionpair/cm^3/s**
Combustion	Sodium aérosols	10^6	1.0	1.8	3.4
Vaporization and condensation	SrO_2	10^6	1.29	0.4	3.02
Atomization	Polystyrène latex particules	10^5	1.3	4.53	5.1

Table 3
Theoretical estimation of magnitude of average number of charges $\bar{J}$ acquired by the aerosols.

Particle radius (μm)	**N (cm^{-3})**	**q (ions cm^{-3} s^{-1})**	**Theoretical value**		
			Under steady state condition	**Recombination limit**	**Attachment limit**
0.5	10^6	10^8	8.2	4.3	8.1
0.5	10^5	10^8	9.2	8.2	9.1

aerosols with higher number of charges begin to appear, caused by multiple charging of the aerosols and the spread become wider, and hence, the magnitude of average charge gets increased in the presence of given additional ionpairs due to gamma radiation than background field (Table 2). This charging phenomenon with additional ion pair condition is theoretically approached, by considering equal ion properties, which cause the ion-asymmetry factor tends to be unity and assumes the logarithm is small in Eqs. (4)–(6). Table 3 gives the theoretically calculated value of average charge $\bar{j}$, for the particle of 0.5 μm (radius), with particle concentration $N = 10^6$ cm^{-3} and $N = 10^5$ cm^{-3} at ion pair concentration[5] $q = 10^8$ ions cm^{-3} s^{-1}. The

---

[5] 1 Rontgen $= 10$ mGy $= 1$ SC/cm$^3 = 3.33 \times 10^{-10}C/cm^3 = 3.33 \times 10^{-10} \times [1$ ion$/1.6 \times 10^{-19}$C$] = 3.33 \times 10^9/1.6 = 2.08 \times 10^9$ ionpair/cm^3; 40.0 mGy/h $= 2.2 \times 10^6$ ionpair/cm^3/s; 400.0 mGy/h $= 2.2 \times 10^7$ ionpair/cm^3/s.

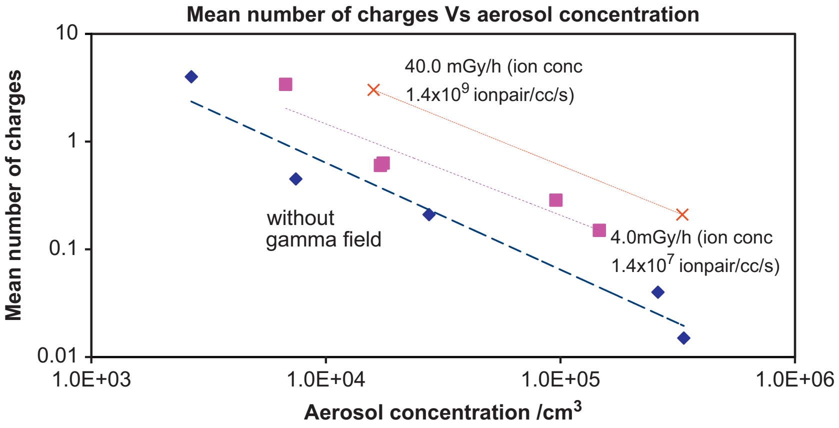

Fig. 3. Mean charge acquired by the distribution of aerosols vs number concentration for the two cases with and without gamma field and two gamma dose rates (4.0 mGy/h and 40.0 mGy/h).

result obtained from the theoretical calculation (Table 3) is compared with the experimental values (Table 2). It is observed that with $N=10^5$, the theoretical value for all the condition is found to be 9 while the experimental value is found to be 5.1, which is in same order and nearly close to theoretical value. Similarly, with $N=10^6$, the value under steady state condition and attachment condition is found to be 8, while at recombination limit it is found to be 4.2. But the experimental value is found to be 3.2, which is again a very close to theoretical value. Results on mean charge calculated in each limiting conditions show small variation because ion-asymmetry factor is not considered. Further, as the concentration of aerosols 'N' is two orders less than 'q', so there will be enough ions available for the attachment on the aerosols. The situation follows the condition as stated by Harrison (1992), $N\,(10^6 \text{ or } 10^5) > \sqrt{(\alpha q)/\beta}(10^4)$.

The above condition is being explained with (i) the situation described by Davies (1966), when $n/N^2 > 10^{-5}$ (applicable here) and with (ii) Boltzmann's equilibrium mean charge described in Eq. (3). It is also the same equation for the average charge developed by Harrison (1992) (Eq. (4)). The average value $\bar{j}$ calculated by Eq. (3) is 9.2. The values calculated using Eq. (4) under steady state charging condition ($n_+ = n_-$; and the value of n is taken as q); for the two situations $N=10^5$ and $n=10^7$ ($n/N^2 > 10^{-5}$) and $N=10^6$ and $n=10^7$ ($n/N^2 = 10^{-5}$) are 9.2 and 8.2 respectively (Table 3). It is observed that, the values are very close. The condition as stated by Davies that $n/N^2 < 10^{-7}$ warrants $N > n$ which, does not exists here. It is also observed that, since N is in denominator, i.e. when the difference between N and q gets increased, the magnitude of charge attached with aerosols is also getting increased; and further, when N decreases for a given ionpair concentration, $\bar{j}$ increases; and it follows that, when N tends to zero, the charge become maximized (Chapter 5, Harrison,1992).

Our next investigation is to vary both the particle number concentration and number of ionpair concentration and to measure the average charge acquired on the aerosols. The experiments are conducted by generating poly-dispersed DOP aerosols of various concentrations and exposing the chamber with two dose rates. The mean charge abs $\langle j \rangle$ acquired by the distribution of aerosols versus number concentration of aerosols ($N\,\mathrm{cm}^{-3}$) for the two dose rates condition (40 mGy/h and 400 mGy/h), i.e. in the presence of excess ion pairs condition are given in Fig. 3. Fig. 3 also includes abs $\langle j \rangle$ value for the same distribution of aerosols when there is no gamma field. It is observed that mean number of charges $\langle j \rangle$ (abs $\langle j \rangle$) acquired for the distribution of aerosols decreases with increase of number concentration of aerosols 'N', for a particular ionpair concentration 'n' for all the three situations. It is also observed that, with increase in the value of ionpair concentration 'n' for a given value of aerosol number concentration 'N', the mean charge 'abs $<j>$' value increases. It is ascertained that, the prediction made by Clement and Harrison on the attachment of charges on the aerosols, when there is difference between N and n increases, the charging increases, and it is experimentally verified.

6. Summary

In this paper, we studied the charge acquired by the aerosols on the generation process. We have also presented experimental results of the electrical charging of non-radioactive aerosols with and without the presence of additional ionpair concentration and compared the results with some of the modeling equations developed by Clement and Harrison and condition stated by Davies. It is evident that, charge acquired in the generation process has a significant role. In the case of polystyrene latex aerosols, the charge neutralization effect (when polarity is considered) was seen when the aerosols are exposed to gamma radiation; whereas slight increase in the average charge acquired by the aerosols generated by other route say: combustion and vaporization and condensation. The result on the average charge obtained by theoretical and experimental values are compared by considering ion-asymmetry to be 1, and found to be nearly same. It is observed that, the magnitude of charge on aerosols in a confined environment in the presence of gamma radiation increases. Further, as stated in the introduction, the reasonable number of charges acquired on the aerosols can be obtained by varying with number concentrations and ionpair concentrations accordingly.

Appendix A. ELPI measurement feature

A.1. ELPI charging efficiency function

ELPI charging is carried out by Corona discharge, which produces a high number of ions and it is controlled by adjusting the corona current to a predefined values. As a result of the charging process, particles will have a known positive charge state that is stable during different operation conditions and high enough to ensure a good detection limit.

The charger efficiency function is a three-part power fit and it is a result of calibration values P, n and constants e and Q. where P—charger penetration (factory set), n—average charge per particle, e—elementary charge (1.6×10^{-19}C) and Q—calibration flow rate (10 lpm).

The charging efficiency is obtained by drawing a graph between PneQ and Di (particle diameter), which is three part power fit. The ELPI calculates conversion vector X from current to number and it is given as

For $\mathrm{Di} < 0.095$; $X(\mathrm{Di}) = 4.8 \times \mathrm{Di}^{1.9087}$
For $0.095 < \mathrm{Di} < 1.196$; $X(\mathrm{Di}) = 1.293 \times \mathrm{Di}^{1.381}$
For $\mathrm{Di} > 1.196$; $X(\mathrm{Di}) = 1.3529 \times \mathrm{Di}^{1.1308}$

The example calculation is as follows:

Let $\mathrm{Di_s} = 0.029$ then $X(\mathrm{Di_s}) = 4.8 \times 0.029^{1.9087} \times$ flow rate where $\mathrm{Di_s}$—stokes diameter. Once $X(\mathrm{Di_s})$ is calculated, then number concentration is$=(1/X \times 1/d \log D_p) = dN/d \log D_p$where D_p is particle diameter. Simply, conversion factors were evolved for all stages of impactor. Then taking into density value for $\mathrm{Di_s}$, the number-size distribution will be determined.

A.2. ELPI measurement of number concentration

In ELPI readout, the measurement of charge is accomplished by the particle entering in to that stage and the sampled current values from each stage (each stage is considered as ELPI electrometer) to form a current vector (c_i). All stages are measured simultaneously. The current vector of each stage is an average value and as a result of a sample. The amount of averaging is defined in the ELPI program console. Then, these current values vectors are multiplied with conversion vectors to get the particle distribution. If the change in concentration is seen, the current vector of the particular stage or multiple stages would vary and accordingly distribution will be drawn. Thus, the averaging the value of current vectors helps to minimize the uncertainty in the measurement of particle number distribution. [ELPI-user manual pages A-9 and A-18, Fig. A, and B, measurement of ideal response and real induced currents M. Marjamaki, TUT report 8-95].

A.3. ELPI measurement of uncertainty

ELPI is calibrated to show correct particle number concentration. In ELPI the particles are measured by the charge they carry, so the accuracy of the concentration measurement is the accuracy of the current measurement. According the manual, diffusion is the biggest source of error in the impactor, which would be made correct in gravimetric measurements. However, since ELPI uses charge measurement, the effect can be significant due to better sensitivity of the charge measurement. To overcome this uncertainty, an algorithm is being used to correct the ELPI readings, as the losses have been measured along with stage efficiency curves. The algorithms fails, if the particles are seen below the detection level of the instrument, i.e. < 10 nm.

ELPI is provided with a feature called 'Zeroing'. Zeroing is needed to adjust the measured current for the electrometers' bias current. Different bias current would be caused by different operating condition like ambient temperature, humidity, etc. Zeroing has to be done before ELPI is used for measuring. If the measurement period is long, zeroing should be checked regularly. After successful zeroing, the current values (noise levels) should not exceed some fixed values stipulated in the manual. The accuracy of current measurement in ELPI on a single collection stage is 1.5 fA=1.5 fC/s The current measurement ranges are as high as 400,000 fA with the time constant of 2 s. The experiments are conducted taking care of all these precautions into account.

A.4. Measurement of number-size distribution for bi-polarly charged aerosols

In most of the cases the original charge of the particles does not affect the ELPI results. If the charger is turned off, the readings indicate the original charge state of the aerosols. When the charger is ON (during corona is ON) and if the original particles are negative (unipolar), ELPI charger produces a sufficient amount of positive ions to first neutralize and then charge the particles normally. If the original charge of the particles is positive, in some cases there might be a need to neutralize the particles before they enter into ELPI when the positive charge is high. If the charge level is more than 50% of the charge produced by the ELPI charger, use of neutralizer is recommended. This means that, if the current reading with charger OFF is more than 50% of the current reading with charger ON, a neutralizer is required. The ELPI can be used with four measurement range for the current reading viz. 10,000 fA, 40,000 fA, 100,000 fA and 400,000 fA. We have operated the instrument with 100,000 fA and 400,000 fA ranges and so we have not observed the current reading crossing 50% of our measurement range when corona is OFF.

References

Abbey F., & Silberberg M. (1979). Resolving aerosol safety for LMFBR's—an international consensus. In: *Proceedings of International Meeting on Fast Reactor Safety Technology*, Seattle, Washington, pp. 884–893.

Amit, Kumar, Subramanian, V., Baskaran, R., Misra, J., & Chellapandi, P. (2010). A study on aerosol charging in generation mechanism. IASTA-2010 March, 2010, Bose Institute, Darjeeling. *IASTA Bulletin*, *19*(1–2), 277–279.

Baskaran, R., Selvakumaran, T.S., & Subramanian, V. (2004). Aerosol test facility for fast reactor safety studies. *Indian Journal of Pure and Applied Physics*, *42*, 873–878.

Baskaran, R., Subramanian, V., & Indira, R. (2007). Aerosol issues in fast reactor. IASTA-2007 Nov.2007, NPL, Delhi. *IASTA Bulletin*, *18*(1-2), 222–224.

Baskaran, R., Subramanian V., Misra J., Indira R., Chellapandi P., & Baldev Raj (2009). Aerosol characterization and measurement techniques towards SFR safety studies. *ANIMMA-2009, International Conference in Advancements in Nuclear Instrumentation, Measurement Method and their Application*, Marseille, CEA, France, June 7–10, 2009. 〈http://ieeexplore.ieee.org〉 (24 August 2011).

Clement C.F., & Harrison R.G. (1991a). Charge distribution on aerosols. In: B.C. O'Neill (Eds.), *Proceedings of 8th International Electrostatics Conference*, Oxford, Institute of Physics Conference Series, Vol. 118, pp. 275–280.

Clement, C.F., & Harrison, R.G. (1991b). *Criteria for aerosol charging*. *Proceedings of Vth Annual Conference*. The Aerosol Society: Loughborough. pp. 149–154.

Clement, C.F., & Harrison, R.G. (1992). Charging of radioactive aerosols. *Journal of Aerosol Science*, *23*, 481–504.

ELPI User Manual Ver.4.02 (2007). Dekati Ltd.: Finland.

Fuchs, N.A. (1964). *The Mechanics of Aerosols*. Pergamon: New York.

Gensdarms, F., Boulaud, D., & Renoux, A. (2001). Electrical charging of radioactive aerosols-comparison of the Clement–Harrison model with new experiments. *Journal of Aerosol Science*, *32*, 1437–1458.

Harrison R.G. (1992). *Aerosol Charging and Radioactivity*. Ph.D. Thesis, University of London.

Hautanen, J., et al. (1995). Brownian agglomeration of bipolarly charged aerosol particles. *Journal of Aerosol Science*, *26*(Suppl.1), S21–S22.

Indira R., Baskaran R., & Subramanian V. (2006). Source term studies for prototype fast breeder reactor. *Seventh Meeting of AERB-VSNRC Nuclear Safety Cooperation Programme on Severe Accident Analysis, Severe Accident Management and Standard Problem Exercises*, Mumbai, March, 2006.

Konstantines Barbranis. (2009). *Bipolar Diffusion Charging: Experimental and Theoritical Evaluation of the Parameters Affecting the Charge Distribution of Nano-Particles in the Size Range 10–100 nm*. M.S. Dissertation, University of Aegean, Greece.

Lee, Hye Moon, Kim, Chan Soo, Shimada, Manabu, & Okuyama., Kikuo (2005). Bipolar diffusion charging for aerosol nanoparticle measurement using a soft X-ray charger. *Journal of Aerosol Science*, *36*, 813–829.

Marjamaki, Marko, Keskinen, Jorma, Chen, Da-Ren, & Pui, David Y.H. (2000). Performance evaluation of the electrical low-pressure impactor (ELPI). *Journal of Aerosol Science*, *31*(*2*), 249–262.

Park, S.H., Lee, K.W., Shimada, M., & Okuyama, K. (2005). Coagulation of bipolarly charged ultrafine aerosol particles. *Journal of Aerosol Science*, *36*, 830–839.

Subramanian, V., & Baskaran, R. (2007). Initial size distribution of sodium combustion aerosol. *Nuclear Technology*, *160*, 308–313.

Subramanian, V., Baskaran, R., & Indira, R. (2008). Experimental study on enhanced Brownian coagulation of sodium compound aerosol in the presence of gamma field. *Journal of Aerosol Science*, *39*, 814–818.

Subramanian, V., Baskaran, R., & Krishnan, H. (2009a). Thermal plasma synthesis of iron oxide aerosols. *Aerosol and Air Quality Research*, *9*(*2*), 172–186.

Subramanian, V., Sahoo, P., Malathi, N., Anathanarayanan, R., Baskaran, R., & Saha, B. (2009b). Studies on chemical speciation of sodium aerosols produced in sodium fire. *Nuclear Technology*, *165*, 257–269.

Subramanian V., Baskaran R., & Venkatraman B. (2011). Studies on sodium aerosol characteristics in the presence of gamma radiation field. In: *Proceedings of the Seventh Asian Aerosol Conference*, Xi'an, China, 17–21 August 2011, pp. 545–551.

Virtanen, A., Marjamaki, M., Ristimaki, J., & Keskinen, J. (2001). Fine particle losses in electrical low-pressure impactor. *Journal of Aerosol Science*, *32*, 389–401.

William, C.Hinds (1982). *Aerosol Technology*. John Wiley & Sons, Inc.: Boston.

Williams, M.M.R., & Loyalka, S.K. (1991). *Aerosol Science Theory and Practice*. Pergamon: Oxford.

Young, R.M., & Pfender, E. (1985). Generation and behaviour of fine particles in thermal plasmas—a review. *Plasma Chemistry and Plasma Processing*, *5*(*1*), 1–37.

Zebel, G. (1966). Coagulation of aerosols. In: C.N. Davies (Ed.), *Aerosol Science*. Academic Press: London.

Aerosol and Air Quality Research, 14: 1534–1541, 2014
Copyright © Taiwan Association for Aerosol Research
ISSN: 1680-8584 print / 2071-1409 online
doi: 10.4209/aaqr.2013.07.0256

Technical Note

Development and Validation of a Methodology for Characterization of Sodium Aerosols in Cover Gas Region

Amit Kumar[1], Venkatesan Subramanian[1], Ramakrishnan Baskaran[1*], Subramanian Krishnakumar[2], Sivasubramanian Chandramouli[2], Balasubramanian Venkatraman[1]

[1] Radiological Safety Division, Indira Gandhi Centre for Atomic Research, Kalpakkam - 603 102, India
[2] Device Development and Rig Services Division, Indira Gandhi Centre for Atomic Research, Kalpakkam -603 102, India

ABSTRACT

This paper describes an experimental methodology developed in an Aerosol Test Facility (ATF) for sampling and analysis of sodium aerosol (metal vapour) from the cover gas region of a fast rector, and details of the validation of the methodology in an experimental sodium loop. The methodology involves; (i) sampling of sodium aerosols by drawing them without exposure to the atmosphere, (ii) trapping them in paraffin oil medium, and (iii) analyzing the paraffin oil for the determination of mass concentration by the conductivity method and size distribution by using a Mastersizer. Validation of the methodology is carried out in a sodium loop called the SILVERINA facility. The aerosol size distribution is found to vary from 1 to 12 µm, with the Mass Median Diameter (MMD) around 4.0 µm ($\sigma_g = 1.5$), and the mass concentration is found to be ~9.50 g/m^3. The experimental results agree with the values found in the literature.

Keywords: Fast reactor; Cover gas region; Sodium aerosol; Size distribution; Mass concentration.

INTRODUCTION

Major energy resources that are being exploited for electricity generation at present are coal, natural gas, hydro, renewable energy resources and nuclear. In order to bridge the growing energy demand, the contribution from nuclear energy is inevitable and it can provide an environmentally clean, sustainable and secured energy (Bhoje, 2003). The development of nuclear reactor began in 1950, which resulted in commercial thermal fission reactors called first generation reactors. The thermal fission reactors can only use a very small fraction of the total energy available in Uranium and rest of the energy resource in U^{238} is not utilized. The fast reactor provides a method of converting the non fissile U^{238} into fissionable Pu^{239} isotopes i.e., allowing the possibility of breeding. (The breeding ratio is the ratio of the number of fission nuclei produced to the number consumed) (Raj and Rajan, 2006). The reactor design evolved further into generation IV type reactors, which addresses compact core, thermal and fast neutron spectra, and closed and open fuel cycles. The generation IV type reactor systems are (i) Very high temperature gas reactor (VHTR), (ii) Sodium cooled fast reactor (SFR), (iii) Super critical water-cooled reactor (SCWR), (iv) Gas cooled Fast Reactor (GFR) and (v) Molten salt reactor (MSR) (http://www.gen-4.org/PDFs/GIF_Overview.pdf & http://mragheb.com/NPRE%20402%20ME%20405%20Nuclear%20Power%20Engineering/Fourth%20Generation%20Reactor%20Concepts.pdf). Another development of generation IV reactor system is Integral Fast Reactor (IFR). The IFR is a closed nuclear power system that recycles its own waste, so that, the elements that are radioactive for tens of thousands of years are all consumed and converted into electricity and waste elements with short half-lives. So it essentially solves the nuclear waste problem (http://large.stanford.edu/courses/2013/ph241/waisberg1/docs/archambeau.pdf).

India's fast reactor program started with 40 MWt/13.2 MWe Fast Breeder Test Reactor (FBTR) which is presently in operation. As a logical follow-up of FBTR, a 500 MWe Prototype Fast Breeder Reactor (PFBR) is being constructed at Kalpakkam, INDIA. The PFBR is a pool type, liquid metal (sodium) cooled fast breeder reactor (LMFBR) (http://www.iaea.org/Publications/Magazines/Bulletin/Bull206/20604782938.pdf). It uses mixture of PuO_2-UO_2 as a fuel. The major components like the core, intermediate heat exchanger, primary coolant pumps lie submerged in a large pool of sodium and housed inside a Reactor Containment Building (RCB). The core of the reactor is compact which

---

[*] Corresponding author.
Tel.: 0091 44 27480062; Fax: 0091 44 27480235
E-mail address: rb@igcar.gov.in

results in a very high power density. For efficient removal of heat, liquid sodium is used as a coolant. The advantage of using liquid sodium includes high thermal conductivity, high boiling point and low fast neutron absorption and scattering cross-section. Liquid sodium has low viscosity and high electrical conductivity allowing it to be easily pumped. Also, it is compatible with the structural materials. The sodium is made to run in two loops, the primary loops takes away the heat generated in the core of the reactor and the secondary loops takes the heat from the primary loop and transfers the heat in the boiler circuit for the generation of steam. Argon is used as cover gas which serves as a blanket for sodium above the reactor core in the reactor vessel.

In the normal operating condition of LMFBR or PFBR, evaporation of sodium vapor from the hot pool surface and subsequent condensation of vapors results in the formation of sodium aerosol within cover gas space (Ford *et al.*, 1993). (The space above the pool surface and below the roof slab of reactor vessel and it is filled with Argon). These aerosols will absorb and scatter the heat radiation coming out from the pool surface and modify the total heat transfer to the cooled roof structure and side wall. Further, the mass transfer occurs due to condensation of sodium vapor on the cooler surface like annular gaps, roof top, control plug, rotating plug and fuel handling machine resulting deposition of aerosols, which hinders the rotational movement of rotating plug, and operation of fuel handling machine (Robert *et al.*, 1995). The sodium aerosols are also affecting the operation of cover gas purification system and reduce its efficiency (flow through cold trap circuit). The aerosols with sufficient concentration reduce the visibility of cover gas region [Core inspection facility in RAPSODIE, France and Fast Breeder Test Reactor (FBTR), India]. To understand the above issues, it is necessary to know the spatial variation of aerosol concentration and size distribution in the cover gas region.

Studies on aerosol characteristics were carried out by various groups. It is observed form the literature, sodium aerosol size ranges from 1–16 µm and mass concentration ranges from 1–40 g/m^3 (Himeno and Takahashi, 1980; Himeno and Yamagishi, 1982; Frukawa *et al.*, 1984; Glockling *et al.*, 1991; Minges and Schutz, 1991; Yamamoto *et al.*, 1991; Ford *et al.*, 1993; Jackson *et al.*, 1993; Minges and Schutz, 1993; Newson *et al.*, 1993; Robert *et al.*, 1995). In general, the sodium aerosol mass concentration increases with the increasing of difference between roof to pool temperatures whereas, there is no definite correlation of aerosol size distribution with the variation of pool and roof temperatures. It is to be noted here that, there were several techniques used for the characterization of sodium aerosol size and mass distribution viz: Andersen Impactor, laser light based techniques, sodium ionisation detector, and SS mesh filter. But, it is important to adopt suitable method by drawing aerosols from the cover gas region and trap them in a suitable medium without exposing them to the atmosphere, to determine the characteristics of the sodium aerosols. Jackson *et al.* (1993), Minges and Schutz (1991, 1993) and Yamamoto *et al.* (1991) in their studies, used Andersen multistage Impactor and determined the mass-size distribution cumulatively over a period of time. By using stainless steel wire mesh filter (filtration technique), Himeno and Takahashi (1980), Himeno and Yamagishi (1982), Frukawa *et al.* (1984), Yamamoto *et al.* (1991) and Newson *et al.* (1993) determined the size distribution based on sieve size. In the above methods, measurements were conducted by keeping the sampling unit/system in the atmospheric condition. Glockling *et al.* (1991) used Malvern 2600C (based on Franhofer diffraction) and Dantec particle dynamic analyzer for characterizing sodium aerosols in the cover gas region, but the results obtained in both techniques were found different for the same experimental condition. Laser mist concentration meter and sintered stainless steel filter were used for sodium aerosol mass concentration measurements by Himeno and Takahashi (1980) and Himeno and Yamagishi (1982). In the above three investigations, the methodologies adopted in their measurements were not dealt in details. Roberts *et al.* (1995) used a technique to collect the sodium aerosol and measured the mass concentration by using atomic absorption spectroscopy and size distribution by using laser scattering technique. He observed that, the sodium aerosol characteristics in cover gas region are strongly dependent on the geometric dimension (diameter of the sodium pool surface, height of the argon cover gas and shape of roof top) of the cover gas system.

It is inferred from the literature that, sodium aerosol characteristics were studied in various experimental facilities but none of them in the reactor environment. It is important to note that in the reactor environment, sodium aerosols are immersed in the sea of bi-polar charges (generated by gamma radiation) and get charged upon interaction with ions. The aerosol properties (size and mass concentration, coagulation coefficient & deposition rate etc.) would get modified due to enhanced coagulation of charged sodium aerosols (Subramanian *et al.*, 2008; Kumar *et al.*, 2010; Subramanian *et al.*, 2012). Thus, it is important to characterize sodium aerosols in cover gas region with and without the presence of gamma radiation. In order to characterize the sodium aerosols, it is required to have in-situ sampling and suitable analysis technique. In this paper, methodology for characterization of sodium aerosols developed in Aerosol Test Facility (ATF) and validation of methodology in SILVERINA Loop are presented. The methodology includes, sampling technique and determination of concentration and size distribution of sodium aerosols. This paper also includes brief description of SILVERINA loop, sampling arrangements and the experimental results obtained in SILVERINA Loop.

METHODOLOGY

The methodology for characterization of sodium aerosols is developed in Aerosol Test Facility (ATF) (Baskaran *et al.*, 2007; Misra *et al.*, 2012). The methodology involves: (i) aerosols are drawn from the region above sodium pool and allowed to get trapped in liquid paraffin oil medium without exposing them to atmosphere, (ii) determination of mass concentration by using conductivity measurement technique and (iii) determination of size distribution by using Malvern Mastersizer.

Sampling Technique

A schematic diagram of sodium aerosol sampling system in ATF is shown in Fig. 1. About 5 g of sodium is taken in a crucible and heated in the sodium combustion cell under Argon environment. The temperature is raised upto 500°C and maintained, which results in formation of sodium vapour above the pool surface. The sodium vapour along with argon is made to bubble through a gas washing bottle filled with liquid paraffin oil (250 mL) kept at room temperature, at a flow rate of 2 L/min for about 10 minutes. Condensation of sodium vapor and solidification of aerosol particle would occur as the vapour passes through the paraffin oil while argon escapes out (Singh *et al.*, 2011). The second bottle is used to trap the sodium aerosols if any, escaped from the first bottle. Line heaters are used to prevent solidification of aerosols in the sampling lines.

Characterization of Sodium Aerosols

The measurement of sodium aerosol size distribution is carried out by using Mastersizer (M/s Malvern Instruments, UK). The Mastersizer uses the principle of ensemble diffraction technique. The Mastersizer measures the volume-size distribution of particles in the laden volume of liquid medium from 0.05–900 µm. Sodium aerosol trapped in the liquid parafin is made to circulate in the liquid flow cell and the volume-size distribution and its Mass Median Diameter (MMD) of the sodium aerosols are determined. The volume size distribution of sodium vapor is given in Fig. 2. It is observed from the Fig. 2, that the particles size range is from 5.68–12.20 µm with MMD of 7.72 µm.

The methodology adopted for determination of sodium aerosol mass concentration is explained as follows: The mass of sodium aerosols trapped in the liquid paraffin oil is measured by transferring them into a water medium (to become NaOH) and then measure the conductivity of the NaOH solution. The conductivity measurement of NaOH solution is carried out by using conductometer (M/s Metrohm, 856 conductivity module, Switzerland). The calibration of the

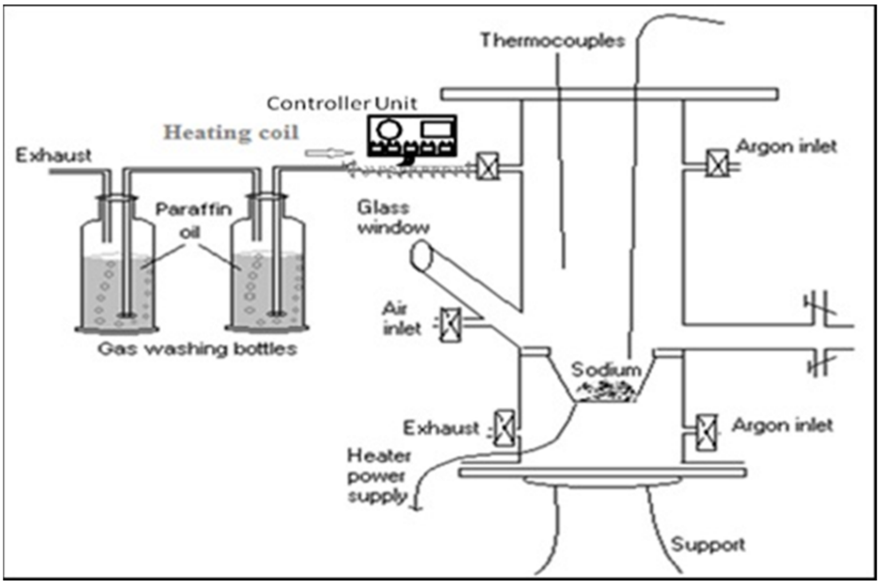

Fig. 1. A schematic diagram of sodium aerosols sampling system in ATF.

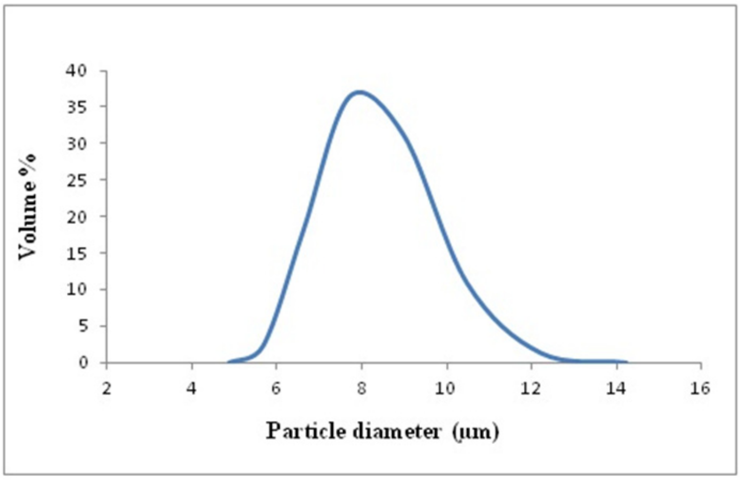

Fig. 2. Volume – size distribution of sodium vapor.

conductometer is verified before each set of measurements with standard KCl reference solution supplied with the instrument. Sodium mass concentration is estimated by using a pre-established calibration graph between conductivity versus concentration of NaOH (http://myweb.wit.edu/sandinic/Research/conductivity%20v%20concentration.pdf, May 2013) and it is shown in Fig. 3.

The experimental procedure is as follows: 200 mL of liquid paraffin oil (trapped with sodium aerosols) is mixed with same amount of water (1:1 ratio) in a separating funnel and vigorously shook for few hours to transfer the sodium into the water medium (to become NaOH). Out of 200 mL solution, 100 mL solution is taken for the conductivity measurement. The conductivity of NaOH is determined after subtracting the background conductivity of DM water (1 µS/cm). From the calibration graph, the trapped sodium mass in the paraffin oil is determined and the sodium aerosol mass concentration in the combustion cell is calculated by taking into account of flow rate and sampling time. The sodium aerosols mass concentration in the combustion cell is found to be around 0.173 g/m^3. The measured value is verified with the standard procedure. For that, the remaining solution is subjected to Pulsating Conductometric Titration (Subramanian *et al.*, 2009) method. An aliquot of the sample is titrated against HCl reactant, added in small steps and simultaneously measuring the change in conductivity. Conductivity variation as a function of the volume of HCl is obtained. It is found that, the sodium aerosols mass concentration in combustion cell is 0.18 g/m^3, and the error is found to be nearly 4.0% from the conductivity measurement (Kumar *et al.*, 2012).

VALIDATION OF CHARACTERIZATION TECHNIQUE IN SILVERINA LOOP

After developing methodology for characterization of sodium aerosols in ATF, the experiments are conducted in SILVERINA Loop for validating the methodology. The details of SILVERINA sodium loop is described in Chandramouli *et al.* (2006). SILVERINA sodium loop was constructed and commissioned at Engineering Hall-I, FRTG, IGCAR to conduct various experiments related to Prototype Fast Breeder Reactor (PFBR) and general Sodium Technology. The loop consists of three cylindrical test pots namely Test Pot-1(TP-1), Test Pot-2 (TP-2) and Test Pot-3(TP-3). This is a dynamic sodium loop with an electromagnetic pump, cold trap, plugging indicator, sodium sampler, heater vessel, interconnecting pipe lines, bellows sealed valves, flow meters and cover gas circuit. Sodium is filled in to the loop from a storage tank (capacity of 1300 kg). The sodium aerosol characterization experiments are carried out in TP-1. The height and internal diameter of the TP-1 are 2235 and 750 mm respectively and the height of the cover gas region is 820 mm. The total volume and quantity of sodium holdup in the TP-1 are 1.04 and 0.512 m^3 respectively. The top flange of TP-1 is provided with three nozzles for sodium level indication (low, middle and high levels) and a spare nozzle. The internal diameter of spare nozzle is 60.3 mm. The features of SILVERINA Loop are as follows: (i) the loop consists of a sodium tank in which liquid sodium could be maintained at various temperatures from 200–550°C and it simulates the reactor pool condition, (ii) the region above the sodium pool is filled with cover gas (Argon) and the cover gas height equals to that of FBTR, IGCAR.

Experiments have been carried out in SILVERINA loop by designing and fabricating a sampling system. The integrated view of aerosol sampling system with TP-1 is shown in Fig. 4. The aerosol sampling system (Fig. 4) consists of (a) Aerosol sampling tube, (b) Aerosol sampling bottle, (c) Line heaters and controller and (d) Aerosol flow controlling device. The sampling tubes are inserted in the spare nozzle with suitable arrangement.

(a) *Aerosol Sampling Tube*: The sampling tube is divided into two parts. One part of the sampling tube is inside the TP-1 and other part is outside. Both the parts are connected with a flange. The sampling tube which goes inside the TP-1 has been fabricated with three different lengths (300 mm, 500 mm and 700 mm) to enable the sampling at three different heights. Before starting the experiment the required length tube is attached with the flange and inserted into the TP-1. The aerosol sampling tube is made of SS316 with

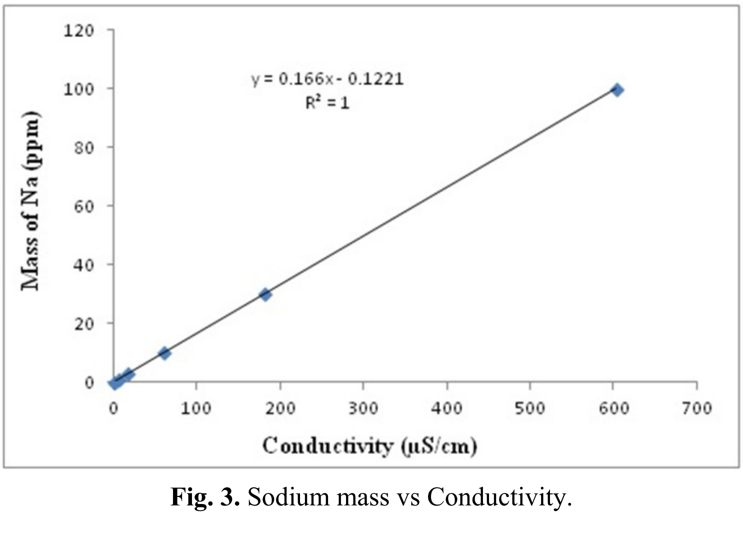

Fig. 3. Sodium mass vs Conductivity.

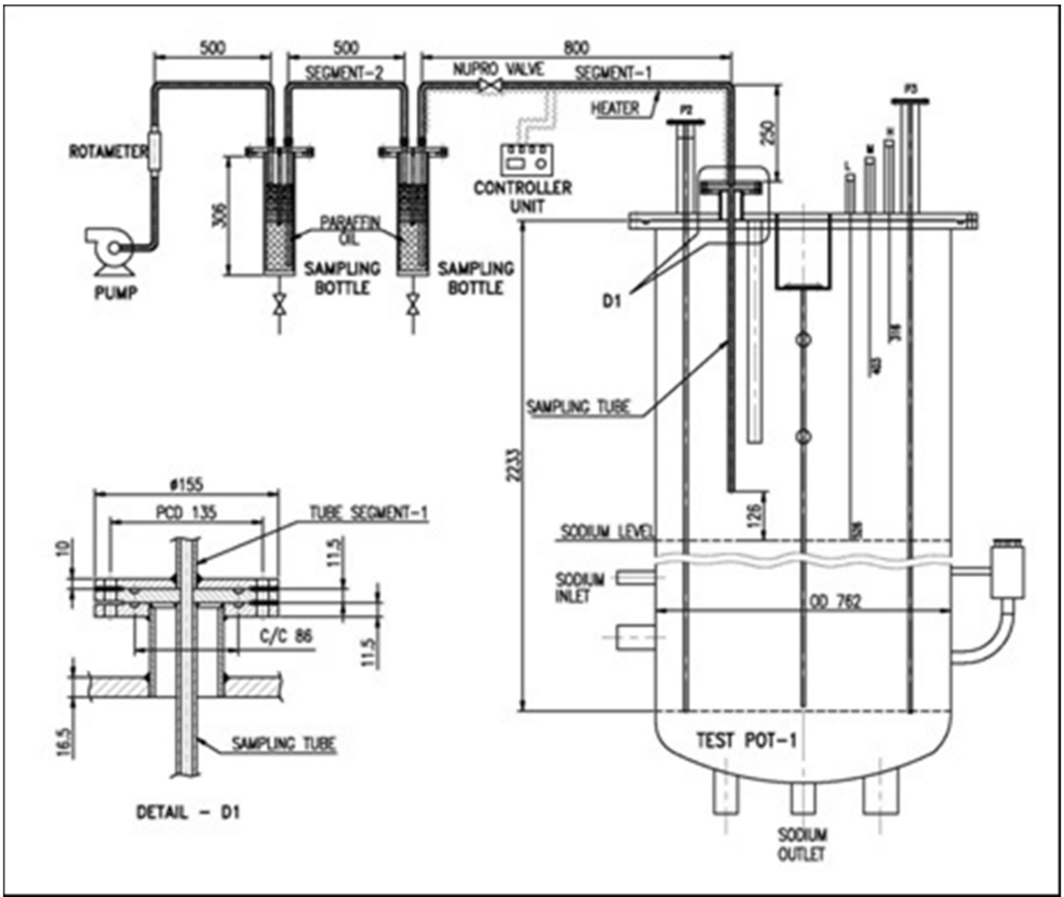

Fig. 4. The integrated view of aerosol sampling system with TP-1.

internal diameter of 10 mm (1.5 mm wall thickness), to avoid wall deposition by impaction for a flow rate of 2 L/min. The maximum particle diameter that can be collected without bias due to particle settling is 20 µm (Hinds, 1982).

(b) *Aerosol Sampling Bottle:* The schematic diagram of the sampling bottle is shown in Fig. 5. The capacity of the sampling bottle is 1.0 liter (height: 306 mm; diameter: 80 mm) and made of Perspex. The bottle is closed on top side with Perspex flange arrangement. The flange is provided with two opening for the insertion of inlet and outlet tubes. The inlet tube inserted upto bottom and it is connected to sampling tube by means of KF coupling and ball valve/gate valve. The paraffin oil will be drained by using a tube and needle valve arrangement at the bottom.

The sampling bottle is filled with paraffin oil (~700 mL) and maintained at ambient temperature. The sodium aerosol laden cover gas is made to pass through the bottle, thus condensation of sodium vapour and solidification of aerosol particle would occur as the cover gas enters into the paraffin oil. The residence time of the cover gas is increased due to baffle arrangement, which ensures that all sodium aerosols get trapped from the cover gas before it goes out of the bottle. The cover gas coming out from the sampling bottle – 1 is made to pass through sampling bottle – 2 so as to remove aerosols escaped, if any, from the 1st bottle. The sample bottles are removed from the loop and paraffin oil is drained for the analysis.

(c) *Line Heaters and Controller:* To prevent sodium vapour condensation and aerosol solidification within the sampling tube during experimental measurements, the wall temperature of the sampling tube is maintained at 110°C. The heating coils are wound on the sampling tube along with insulation and the current through the heating coils is controlled by using PID (proportional-integral-derivative) controller. The temperature along the sampling tube is monitored by 2 thermocouples. In order to have a redundancy in heating, a spare heater is also provided. The heater controller set-up consists of a panel board mounted with one PID controller, temperature display units, 3 pole rotary switch for double heaters, allied PCBs etc.

(d) *Aerosol Flow Control Device:* The cover gas is drawn from the TP-1 and made to bubble through the paraffin bottle at a specified flow rate using a rotameter. The flow rate is metered in such a way that (i) it takes into account of positive pressure of the cover gas inside the TP-1 and (ii) sufficient flow up to the second bottle. It is optimized that, for the pressure in the cover gas region 0.35 kg/cm^2 and flow rate of 2 L/min, sufficient flow up to the second bottle is achieved.

The pressure holdup test of sampling tube and gate valve has been carried out by pressurizing TP-1 up to 0.5 kg/cm^2. The functioning of surface heaters, PID temperature controller and thermocouples has been checked by heating the heater up to 110°C. The photograph of the sodium

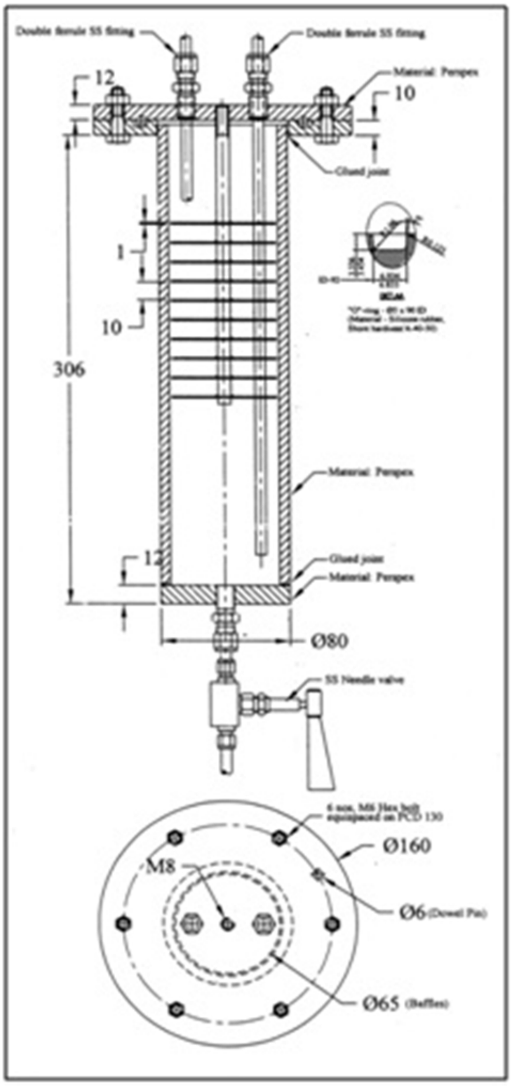

Fig. 5. Schematic diagram of the sampling bottle.

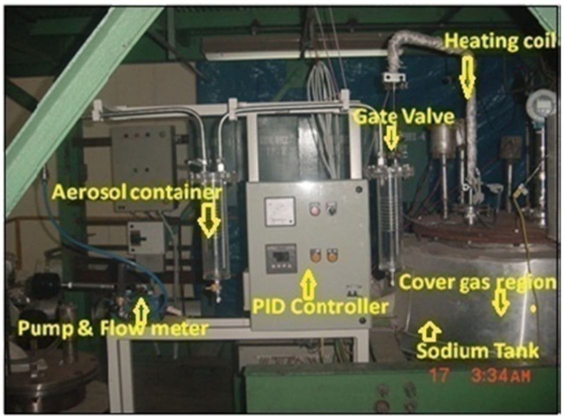

Fig. 6. Photograph of the sampling arrangement.

aerosol sampling system in SILVERINA loop is shown in Fig. 6. The sampling time and flow rate are kept such that the mass of sodium aerosol in the bottle is optimum for measurement of size distribution and mass concentration. Test runs showed that up to a trapped sodium aerosol mass of 50 mg in the bottle, the coagulation of aerosols in the sampling bottle was not noticed before analyzing with Mastersizer (within 20 minutes).

The sampling tube is inserted at the middle level of cover gas region (415 mm from the top). Sodium cover gas height and pressure were kept as 820 mm and 0.35 kg/cm^2 respectively. The sodium pool temperature was maintained at 550°C. Cover gas is made to bubble through liquid paraffin oil at a flow rate of 2 L/min for 15minutes. After sampling, the paraffin oil is analyzed using Mastersizer and the aerosol size distribution is found to vary from 2 to 12 µm with MMD around 4.0 µm ($\sigma_g = 1.5$) (Fig. 7). The mass of trapped sodium aerosol in the bottle was estimated and then the mass concentration of sodium aerosol in cover gas region of SILVERINA loop is determined to be 9.50 g/m^3. The mass collected in the second bottle was negligible (< 1% of the first bottle).

SUMMARY

Experimental methodology for characterization sodium aerosols in cover gas region is developed and evaluated. The experimental results agree with the values found in the literature. The design of sampling system in SILVERINA Loop is found very useful and similar one is being fabricated by taking into account of appropriate dimension of reactor vessel of FBTR, for next phase of experiments.

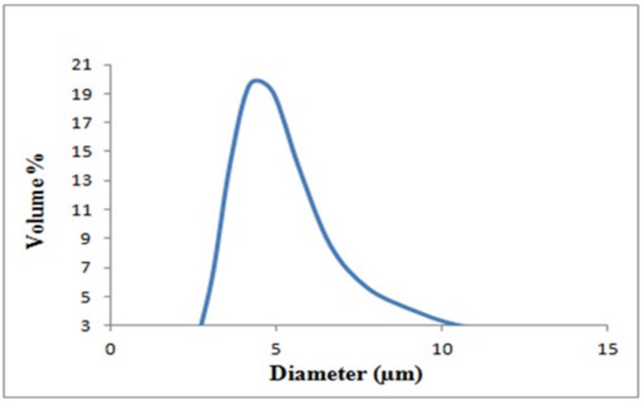

Fig. 7. Sodium aerosol size distribution in SILVERINA Loop.

ACKNOWLEDGEMENT

Shri K.K. Rajan, Director FRTG and Shri S.A.V. Satyamurthy, Director EIRSG are acknowledged for their support and constant encouragement for carrying out this work. FRTG control room staffs of Loop -1 are acknowledged for their help in conducting the experiments. The authors are thankful to the colleagues of IIS, RTSD for Conductometric titration.

REFERENCES

Baskaran, R., Selvakumaran, T.S. and Subramanian, V. (2004). Aerosol Test Facility for Fast Reactor Safety Studies. *Indian J. Pure Appl. Phys.* 42: 873–878.

Bhoje, S.B. (2003). Status of Fast Reactor Development in India, International Conference on Nuclear Power Technologies with Fast Neutron Reactors, Obnisk, Japan, December.

Chandramouli, S., Sakthivel, S., Vijayamohana Rao, P., Gurumoorthy, K., Rajan, K.K., Kalyanasundaram, P. and Vaidyanathan, G. (2006). Commissioning and Operation of SILVERINA Sodium Loop, OPENUPP-2006, Nov. 13-15, BARC, Mumbai, Proceedings of National Conference on Operating Experiences of Nuclear Reactors and Power Plants, p. 203–209.

Clement, C.F. and Julian Dolias, M. (1987). Sodium Aerosol Formation in Argon Flow over Hot Sodium. Theoretical Physics Division, Harwell Laboratory, Oxfordshire OX11 ORA. AERE R 12489.

Ford, I.J. (1993). Sodium Aerosol Formation and Removal Mechanisms in the Fast Reactor Cover Gas Space. *J. Aerosol Sci.* 24: 237–253.

Frukawa, O., Furutani, A., Hattori, N. and Iguchi, T. (1984). Experimental Study of Heat and Mass Transfer through the Cover Gas in the Liquid Metal Fast Breeder Reactor (LMFBR), Proceeding of the Third International Conference on Liquid Metal Engineering and Technology, ISBN0-7277-0209-2, The British Nuclear Societ*y* 1: 451–458.

Glockling, J.L.D. (1991). Heat and Mass Transfer in Specific Aerosol System, PhD Thesis, Department of Chemical Engineering. South bank University, London.

Himeno, Y. and Takahashi, J. (1980). Sodium Mist Behavior in Cover Gas Space of LMFBR. *J. Nucl. Sci. Technol.* 17: 404–412.

Himeno, Y. and Yamagishi, Y. (1982). Effect of Barriers on Sodium Mist Deposition on LMFBR Components. *J. Nucl. Sci. Technol.* 19: 837–844.

Hinds, W.C. (1982). *Aerosol Technology: Properties, Behavior, and Measurement of Airborne Particles*, John Wiley & Sons.

http://large.stanford.edu/courses/2013/ph241/waisberg1/docs/archambeau.pdf.

http://mragheb.com/NPRE%20402%20ME%20405%20Nuclear%20Power%20Engineering/Fourth%20Generation%20Reactor%20Concepts.pdf.

http://myweb.wit.edu/sandinic/Research/conductivity%20v%20concentration.pdf, May 2013.

http://www.gen-4.org/PDFs/GIF_Overview.pdf.

http://www.iaea.org/Publications/Magazines/Bulletin/Bull206/20604782938.pdf.

Jackson, J.D., Sanchis Pei An, .J.F. and Alamar A. (1993). Closing Report of the MUSAC 3A Project. Department of Nuclear Engineering, University of Manchester, Manchester.

Kumar, A., Subramanian, V., Baskaran, R., Misra, J. and Chellapandi, P. (2010). A Study on Aerosol Charging in Generation Mechanism, IASTA-2010 Bose Institute, Darjeeling, IASTA Bulletin, p. 277–279.

Kumar, A., Subramanian, V., Misra, J., Baskaran, R. and Venkataraman, B. (2012). Standardization of Sodium Aerosols Characterisation Techniqes, IASTA-2012, Navi Mumbai, IASTA Bulletin, p. 441–445.

Minges, J. and Schutz, W. (1991). Experiments to Characterize the Sodium Aerosol System in the Cover Gas of the European Fast Reactor EFR. *J. Aerosol Sci.* 22 1: S761–S764.

Minges, J. and Schutz, W. (1993). Experiments on the Enrichment of Cesium in the Cover Gas Aerosol of the European Fast Reactor (EFR). *Nucl. Eng. Des.* 147: 17–22.

Misra, J., Subramanian, V., Amit Kumar, Baskaran, R. and Venkatraman, B. (2012). Investigation of Aerosol Mass and Number Deposition Velocity in a Closed Chamber. *Aerosol Air Qual. Res.* 13: 680–688.

Newson, I.H., Dawoson, R.W., Wade, C.D., Moul, A.N. and Finch, J.E. (1993). Studies of Caesium-134 Transfer through Argon and Helium Cover Gases above Hot Sodium Pool in the Hawell Active mass Transfer Loop (AMTL), AEA Industrial Technology Report number AEA-In Tec-1220.

Raj, B. and Rajan, M. (2006). India's Fast Reactor Program in the Context of Environment Sustainability. *Int. J. Environ. Stud.* 64: 729–747.

Roberts, D.N. (1995). Heat and Mass Transfer Studies in Sodium – Argon Filled Enclosures, PhD thesis, South bank University, London.

Singh, V.P., Gupta, T., Tripathi, S.N., Jariwala, C. and Das, U. (2011). Experimental Study of the Effects of Environmental and Fog Condensation Nuclei Parameters on the Rate of Fog Formation and Dissipation Using a New Laboratory Scale Fog Generation Facility. *Aerosol Air Qual. Res.* 11: 140–154.

Subramanian, V., Baskaran, R. and Indira, R. (2008). Experimental Study on Enhanced Brownian Coagulation of Sodium Compound Aerosols in the Presence of Gamma Field. *J. Aerosol Sci.* 32: 814–818.

Subramanian, V., Amit Kumar, Baskaran, R., Misra, J., and Venkatraman, B. (2012). An experimental study on the Charging of Non-radioactive aerosols with and without the Presence of Gamma Radiation. *J. Aerosol Sci.* 52: 98–108.

Subramanian, V., Sahoo, P., Malathi, N., Anathanarayanan, R., Baskaran, R. and Saha, B. (2009). Studies on Chemical Speciation of Sodium Aerosols Produced in Sodium Fire. *Nucl. Technol.* 165: 257–269.

Yamamoto, H., Sakai, T. and Murakami, N. (1991). Analytical Study on Mass Concentration and Particle

Size Distribution of Sodium Mist in Cover Gas Phase of LMFBR. Reactor Vessel. *J. Aerosol Sci.* 22: S713–S716.

Received for review, July 25, 2013
Accepted, November 24, 2013

Aerosol and Air Quality Research, 15: 2270–2276, 2015

ISSN: 1680-8584 print / 2071-1409 online
doi: 10.4209/aaqr.2015.03.0150

Size Evolution of Sodium Combustion Aerosol with Various RH%

Amit Kumar, Venkatesan Subramanian*, Ramakrishnan Baskaran, Balasubramanian Venkatraman

Radiological Safety Division, Indira Gandhi Centre for Atomic Research, Kalpakkam - 603 102, India

ABSTRACT

Studies on sodium aerosol characteristics are very important for fast reactor safety. Physical and chemical changes that occur at various times at various atmospheric conditions to sodium aerosols would results particles in various diameters. In this context, a study has been conducted in Aerosol Test Facility, Radiological Safety Division, in which sodium combustion aerosols were generated in a controlled manner and made to hover in a confined volume. The particle diameter (Mass Median Diameter - MMD) is measured on-line with progress of time by using Mastersizer. The experiments are conducted by generating aerosols in two different mass concentrations viz. 3.0 g m^{-3} and 0.5 g m^{-3} and in three different relative humidity conditions viz. 20%, 50% and 90% to show the influence of relative humidity on the particle diameter. A theoretical simulation of particle growth due to coagulation is drawn and compared with the experimental value. It is observed that sodium combustion aerosols size grow due to absorption of moisture (hygroscopic growth) in the initial period of times say in first 20 minutes followed by Brownian coagulation. An empirical relation is determined based on the difference between coagulation growth and experimental observation and applied to match experimental observation of particle diameter. A detailed experimental procedure, theoretical simulation and comparison of results of particle growth between experimental observation and theoretical simulation are presented in this paper.

Keywords: Sodium combustion; Aerosol size; Growth; Relative humidity.

INTRODUCTION

In sodium cooled fast reactors (SFR), the leakages in the secondary sodium pipes lead to sodium fires, which are classified as Pool fire, Spray fires and Column fire. The hot sodium burns in air and gives rise to aerosols. The aerosols are mainly sodium oxide (Na_2O) or higher oxides of sodium (Na_2O_2 and NaO_2) depending upon the ratio of sodium to oxygen available during the onset of fire. Since these oxides are highly reactive, they are further converted to sodium hydroxide, sodium carbonate and sodium bi-carbonate upon reaction with water vapour and carbon dioxide present in the environment (Clough and Garland, 1971). These sodium aerosols pose serious problems such as chemical toxicity, corrosion of building materials and equipments. Sodium peroxide and harmful corrosive nature of soda (NaOH) are responsible for chemical attack. The Threshold Limiting Value (TLV) by American Conference of Governmental industrial Hygienists (ACGIH), for the atmospheric concentration of soda is 2 mg m^{-3} for humans (http://www.osha.gov/). Hence several studies have been initiated in Aerosol Test Facility (ATF), Radiological Safety Division (RSD), Indira Gandhi Centre for Atomic Research (IGCAR) related to physical and chemical characterization of sodium aerosols which help in hazard evaluation of Sodium cooled Fast Reactors with respect to sodium fire and dispersion of sodium aerosols.

The vapour phase combustion of the sodium, results in the generation of sodium oxide aerosols in the flame zone (Newman, 1974). The physical and chemical changes of sodium oxide aerosols after leaving the flame zone are very important to understand the sodium oxide aerosol process. Hence, the particle size after leaving the flame zone is an important factor for the aerosol process. In our earlier studies, the initial size distribution of aerosols was studied by varying ignition temperature for a confined pool and by varying relative humidity of the surroundings. It is reported that, higher the humidity the bigger will be the initial size of the aerosols (Subramanian and Baskaran, 2007) and the species would be fully sodium hydroxide. Cooper, 1980, studied the initial radius of the aerosol formed under relative humidity condition varying from 35–90% and derived an empirical relation as

$$r\ (initial\ radius) = (r_0\ (dry\ particle\ radius) \times 0.87)/(1 - RH)^{1/3} \quad (1)$$

---

[*] Corresponding author.
Tel.: 0091 44 27480062; Fax: 0091 44 27480235
E-mail address: vsn@igcar.gov.in

and showed that by considering r_0 equal to 0.5 µm, the initial particle size increases with increase of relative humidity. The bigger sized particle is formed, at higher humidity conditions, until the partial pressures of the water vapour inside the particle become equal to saturated water vapour of the surroundings (Newman, 1983; Cooper, 1989; Malet, 1996). At this juncture, the carbon dioxide prevailed in the atmosphere diffuses into the particle and converting the species as carbonate. When the initial particle diameter is large, i.e., at high humidity conditions (at 90% RH), the particles have larger surface area, the particle is nothing but the solution of hydroxide, which enhance the diffusion of CO_2 into the particle, resulting carbonate conversion (total conversion) in lesser time (Ramsdale *et al.*, 1989). An experimental investigation was carried out to determine the chemical speciation of aerosols with progress of time and reported that carbonation is faster in higher humidity condition (Subramainian *et al.*, 2009; Ananthanarayanan *et al.*, 2015). The carbonation of sodium aerosols is studied and a phenomenological modeling is carried out based on shrinking core model by considering of diffusion of CO_2 into a particle of hydroxide formed at various RH conditions i.e., shrinking of hydroxide core with progress of time as carbonation progress from the surface (Gilardi *et al.*, 2013). In addition to all these studies, the particle size is important to be considered for the settling phenomena, as the aerosols are formed inside a confined environment undergo coagulation followed by gravitational settling (Misra *et al.*, 2010; Subramanian *et al.*, 2011).

Hence, the size of the sodium aerosols, formed at given humidity condition and suspended in a confined environment, changes by (i) accumulation of water vapour over particle followed by chemical conversion (Sitarski, 2012) and (ii) coagulation by physical process. Hence an experimental investigation was conducted by generating aerosols in a closed chamber and on-line measurement of particle size (Mass Median Diameter - MMD) with progress of time is carried out. The enlargement of particle size observed in the experimental study is compared with enlargement of particle size simulated due to Brownian coagulation and the comparison would yield the extent of hygroscopic growth. Since the initial particle size is different for different RH conditions, experiments are conducted by keeping the atmosphere in 20%, 50% and 90% RH conditions. Further, the initial particle size and hygroscopic growth is independent of initial concentration, while the coagulation is dependent on concentration, hence, experiments conducted in two different initial mass concentrations in order to differentiate the particle enlargement measured by experimental study and by theoretical simulation. In addition to the above, an empirical relation is derived and applied in the model in order to match the hygroscopic growth condition. In this paper, the generations of sodium combustion aerosol, aerosol sampling system, measurement of aerosol size with evolution of time, theoretical simulation of change in particle size with time and comparison of results are presented.

THEORETICAL SIMULATION

Sodium aerosols are formed by combustion process by exposing the hot sodium into the ambient atmosphere. As the combustion is progressing, the sodium aerosols are in the form of sodium oxide in flame zone and they are converted into sodium hydroxide immediately after leaving the flame zone. When these aerosols are suspended in a confined volume, these aerosols are removed from the suspended space continuously by several mechanisms i.e. concentration is reduced by gravitational settling, wall plating, and ventilation if there. Since, all the removal mechanisms are dependent on particle size, a theoretical model is developed using standard mass and number concentration decay equation by including initial mass concentration and various removal mechanisms. A first order differential equation is formulated to predict the decay of mass and number concentration of sodium aerosols in closed chamber with progress of time. Taking initial size of the aerosols as an input from the experimental results obtained from ATF, the equilibrium aerosol size is evolved by solving rate equation of mass concentration and number concentration numerically by finite difference method. In this model, the inputs parameters are (i) initial sodium aerosol mass concentration, (ii) geometry of the vessel (diameter and height of the vessel) and (iii) initial radius of sodium aerosol. The rate equations for mass concentration, number concentration and inter-relating equation of mass and number concentration of the aerosols are given below:

$$\frac{dc}{dt} = -\lambda c \tag{2}$$

$$\frac{dN}{dt} = -\lambda N - KN^2 \tag{3}$$

$$c = \frac{4}{3}\pi r^3 \rho N \tag{4}$$

where N – Number concentration (cm^{-3})
c – Mass concentration (g cm^{-3})
λ – Decay rate (gravitational, wall plating and ventilation) (s^{-1})
K – Coagulation rate (s^{-1})
ρ – Particle density (g cm^{-3})
r – Radius of particle (cm)

The initial conditions are taken as: the initial mass concentration $c = c_0$ obtained from the experimental value (for two different concentrations) and initial particle size is taken from the empirical relation derived from the previous experimental results conducted in ATF, (Subramanian and Baskaran, 2007) in which Cooper's relation (Cooper, 1980) is modified by taking an empirical constant as 0.97 and dry particle radius (r_0) = 0.45 measured in ATF at RH% of 20. The initial radius at various RH% is modified as

$$r\ (initial\ radius) = r_0 \times 0.97)/(1 - RH)^{1/3} \tag{5}$$

By taking initial sodium aerosol radius from the modified Cooper relation, the parameters λ, and K are calculated.

Using these values, equations are solved for next time step and the process continued till the convergence of size is reached.

MATERIALS AND METHODS

Aerosol Chamber

The experiments reported in this work were conducted in ATF (Baskaran *et al.*, 2004). The schematic of the experimental set up is presented in Fig. 1. The major components of ATF are (i) combustion cell made of SS-304 L, in which, sodium will be heated using electrical bunsen burner under Argon environment, (ii) aerosol chamber (having volume 1 m^3 with height = 60 cm and diameter = 150 cm), (iii) auxiliary systems such as pneumatic control system, data acquisition system for temperature, pressure and RH during experiments, (iv) filter paper samplers to collect samples for the measurement of mass concentration, and (v) Mastersizer for the measurement of real time particle size distribution and MMD. The aerosol chamber is maintained with ambient temperature (25–30°C) and required RH% and CO_2 content, before injection of aerosols.

AEROSOL DIAGNOSTIC EQUIPMENT

Mastersizer

In our studies, for the real-time measurement of sodium aerosol volume –size distribution, a laser based aerosol measurement instrument called Mastersizer (M/s Malvern, UK) is used. The instrument is working on ensemble diffraction technique. The Mastersizer integrated with the aerosol chamber with a help of an aerosol flow cell. Aerosol flow cell is a hallow stainless steel pipe with rectangular cross section of 14.3 mm width (standered length for optical path specified by Mastersizer) and 103 mm breath and it has a length of 730 mm. suitable opening are made in side plates of the flow cell and laser window are connected. The aerosols are drawn through the aerosol flow cell whose optical window is aligned with the laser path of Mastersizer (within ± 0.1 deg.). A constant air flow (~0.5 L min^{-1}) from the aerosol chamber is maintained by a pump to avoided turbulence and giving laminar flow of the aerosol in flow cell. Performance test of the aerosol flow cell was carried out with polystyrene latex particles of diameter 2.799 µm and methylene blue aerosols (Baskaran *et al.*, 2006).

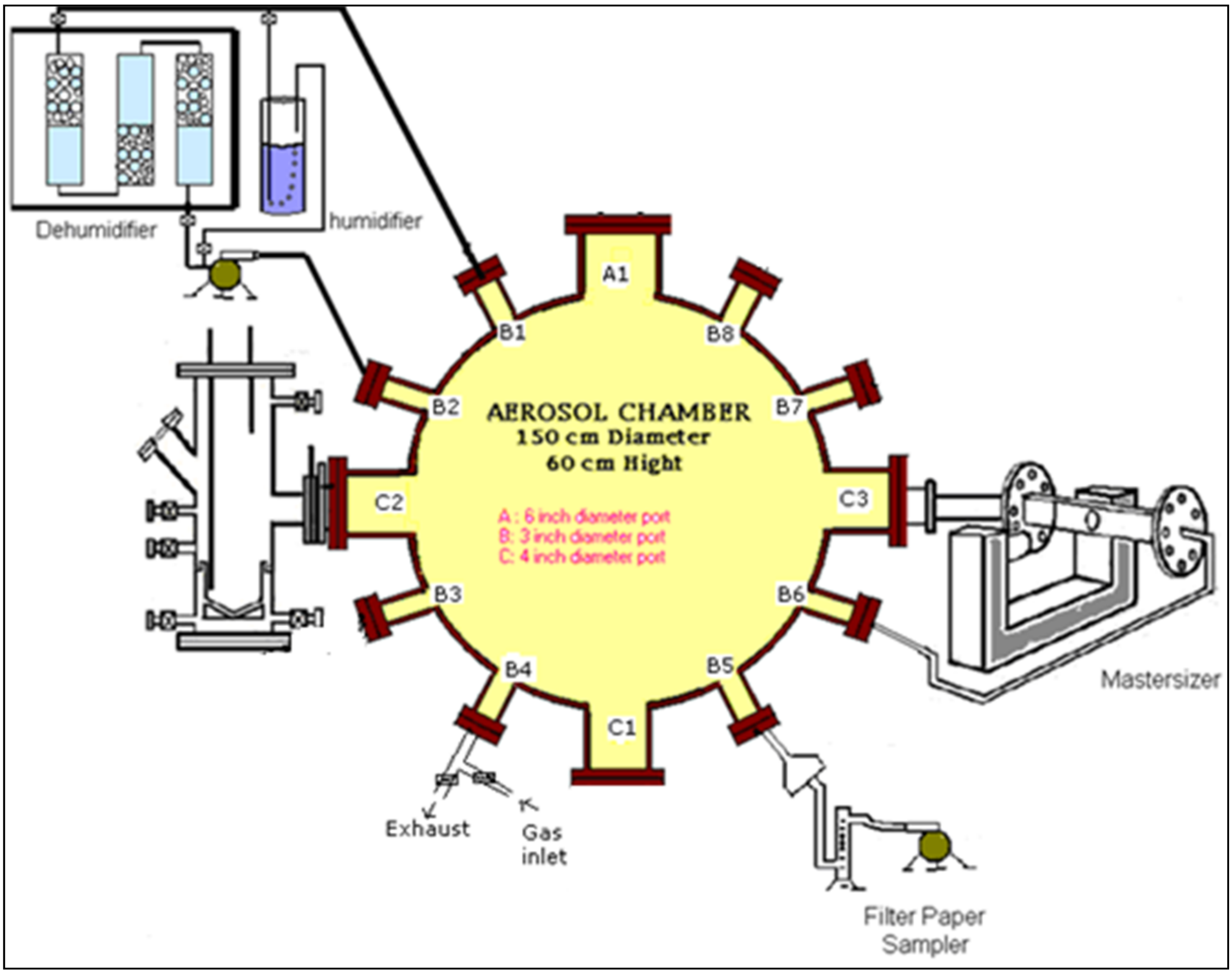

Fig. 1. An integrated view of the aerosol chamber, the sodium combustion cell, Filter paper sampler and Mastersizer.

Filter Paper Sampler

This technique is used to determine the aerosol mass concentration by gravimetric analysis. A closed face type filter paper sampler (47 mm) and a non-lubricant rotary vane pump with a capacity of 20 L min^{-1} coupled with rotameter were used for the measurement of mass concentration. An analytical balance with an accuracy of 0.1 mg (Model No.GR 200, M/s AND Corporation, Japan) was used for the gravimetric analysis. Aerosol sampling was carried out for 1minute at a flow rate of 10 L min^{-1}. The cumulative experimental errors associated with measurement in time, flow rate and mass is nearly ± 10%. Glass fiber filters (M/s Whatman) are used for the present experimental study.

SAMPLING

About 10 g of sodium was heated upto 550°C (the temperature of the sodium in primary loop of fast reactor) in the sodium combustion cell under argon environment. The hot sodium was ignited by exposing it to compressed air, after letting out the argon gas. By combustion, the sodium oxide aerosols were formed in the combustion cell. Immediately, the valve separating the aerosol chamber and combustion cell was opened and the aerosols get filled into the chamber. Since the initial pressure at the combustion cell was at 50–70 kPa excess over atmospheric pressure, it helps to fill the aerosol into the chamber and its diagnostic port immediately. The combustion last for about two minutes and the cell is isolated by closing the gate value. Immediately, the real time measurement of particle size measurement is carried out by using Mastersizer. The sodium aerosol size is measured continuously for about 1 hour. The experiments on sodium aerosol size evolution were conducted at three relative humidity conditions viz. 20%, 50% and 90%. The required relative humidity of aerosol chamber is maintained with the use of humidity controller. At the same time, the suspended aerosol mass concentration inside the chamber is measured by using filter paper sampling in the first minute and it is taken as initial mass concentration of aerosols. The desired initial mass concentration is obtained by optimizing the parameters viz. quantity of sodium, combustion time, rate of injection of air etc.

RESULT AND DISCUSSION

The initial volume - size distribution of sodium combustion aerosol for various RH% is shown in Fig. 2. It is observed from Fig. 2, that the initial size distribution is mono model with MMD 0.98, 1.1 and 1.8 µm for 20%, 50% and 90% RH respectively, for the initial mass concentration of 3 g m^{-3}. The particle size distribution and corresponding MMD is measured continuously with progress of time (every minute). The experimentally measured particle size (MMD) with progress of time for 50% RH is shown in Fig. 3(a) (for 3 g m^{-3}). It is observed from Fig. 3(a), the measured initial particle size is 1.1 µm and size enlarges upto 1.56 µm in 20 minutes and thereafter, the size enlarges to reach a saturated value around 1.7 µm in about 60 minutes. The theoretically simulated particle size with progress of time due to coagulation is included in Fig. 3(a). In the case of theoretical simulation, the particle size enlarges progressively from 1.1 µm and in 20 minutes it increases around 1.4 µm then slowly increases to the saturation value of 1.7 µm at about 80 minutes. It is evidenced in the Fig. 3(a), the difference in the particle size at 20 minutes is about 12% and it would be due to hygroscopic growth. The rate of growth in both theoretical simulation and experimental observation is nearly same after 40 minutes. But within 30 minutes, the particle size enlarges upon absorption of moisture. In order to distinguish the hygroscopic growth in sodium aerosols, the experiment is conducted with initial mass concentration of 0.5 g m^{-3} by burning 2 g of sodium. Fig. 3(b) shows that particle size growth with progress of time observed in the experimental measurement and theoretical simulation for the case of initial mass concentration of 0.5 g m^{-3} and RH at 50%. It is observed from the experimental measurement, the initial particle size is 1.1 µm and it enlarges to 1.55 µm in 20 minutes and increases to 1.6 µm in 80 minutes. But in the case of simulated particle size due to coagulation, the initial particle size is also 1.1 µm and it increases marginally in 80 minutes reaching 1.15 µm only. It is noted from Figs. 3(a) and 3(b), the measured initial particle size is same

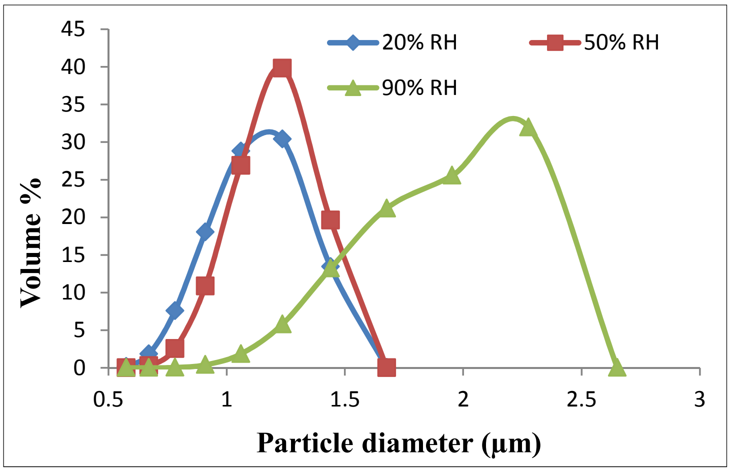

Fig. 2. Initial volume – size distribution of sodium combustion aerosol for various RH%.

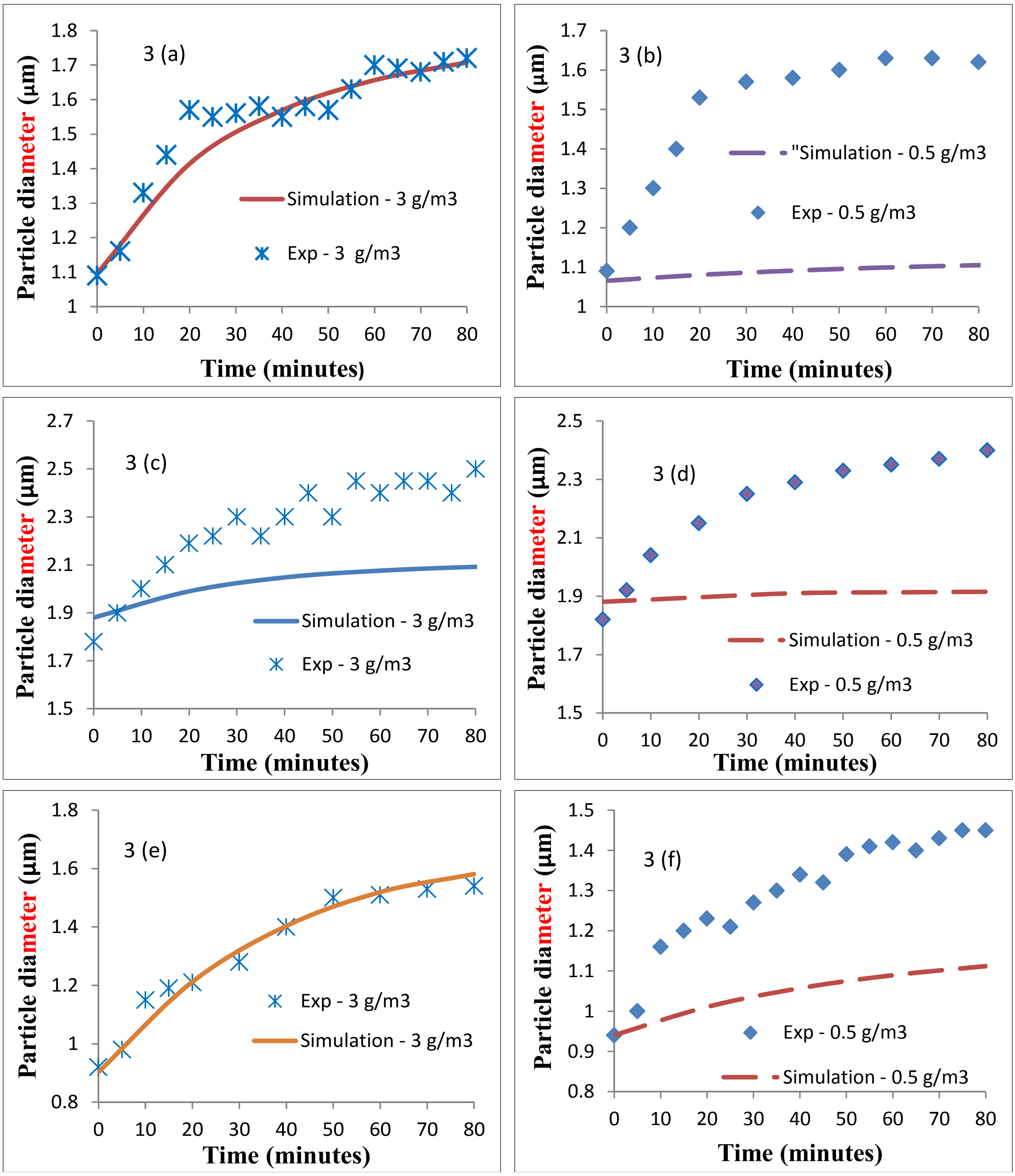

Fig. 3. Growth of particle size with time (experimental observation and simulation due to coagulation) for various conditions (a) 50%, - 3.0 g m^{-3} (b) 50%, - 0.5 g m^{-3} (c) 90%, - 3.0 g m^{-3} (d) 90%, - 0.5 g m^{-3} (e) 20%, - 3.0 g m^{-3} and (f) 20%, - 0.5 g m^{-3}.

(~1.1 µm) for the both mass concentrations, which shows that initial particle size is independent of mass concentration. In the case of 0.5 g m^{-3}, the hygroscopic growth of sodium aerosols is clearly evidenced from the difference in particle size between measurement and theoretical simulation. It is to be noted here that, the experimental observation includes hygroscopic, chemical and coagulation changes. The difference in particle size in the first 20 minutes between measurement and theoretical simulation is attributed to hygroscopic growth and chemical conversion.

Fig. 3(c) shows the particle size with progress of time for both experimental observation and theoretical simulation for 90% RH condition with initial concentration of 3 g m^{-3}. The measured initial particle size is 1.8 µm and enlarges to reach about 2.4 µm (saturated value), whereas the simulated particle size is found always well below the experimental value (in the range of 2.0 µm) (saturated value) and found to have 20% deviation. The growth rate after 40 minutes is found to be similar for both experimental and theoretical values (slope) but with different starting size. The same experiment is repeated with initial mass concentration 0.5 g m^{-3}. Fig. 3(d) shows the particle enlargement in both theoretical and experimental observations. The measured initial particle size for 0.5 g m^{-3} condition is again 1.8 µm, which is found to be independent of initial mass concentration and reaches about 2.35 µm. The simulated curve for 0.5 g m^{-3} is also found to have values below the experimental observations (in the range of 1.9 µm). The difference between experimental values and the simulated values (for both mass concentrations) is attributed to hygroscopic growth due to presence of more moisture content in the chamber than 50% RH case (all values found above the theoretical prediction).

The experiment is conducted by keeping aerosol chamber at 20% RH condition. Fig. 3(e) shows the experimental and theoretical simulated particle size with progress of time in the case of initial mass concentration of 3.0 g m^{-3}. The initial particle is found at 0.9 µm. The particle size enlarges to reach 1.2 µm in 15 minutes with deviation of about 5% found between experimental and theoretical prediction (due to less moisture content when compared to 50% case). Thereafter, from 20 minutes, the measured values and simulated values of particle size is found to be almost same. Fig. 3(f) represents the particle size with progress of time in the case 0.5 g m^{-3} condition. The initial particle size is found to be in the range of 0.9 µm. The deviation in the particle size in the 15th minute is about 21%. However, the growth rate after 20 minutes for both experimental and theoretical simulation is almost same from the different starting size at 20 minutes.

It is observed from Figs. 3(b), 3(d) and 3(f), in the case initial mass concentration of 0.5 g m^{-3}, there exists definite demarcation between the experimental observation and theoretical simulation by coagulation growth. In order to match the experimental observation, an empirical equation of 2nd polynomial is derived based on the difference between the two curves (between coagulation growth and experimental observation) for 50%RH condition and it is given as follows:

$$d' = -0.00006 \times t^2 + 0.0079 \times t + 1.0466 \qquad (6)$$

where d' – particle diameter (µm) and t – time in minutes.

Upon multiplying the value of "d" obtained by simulation due to coagulation effect with above polynomial equation for d', the resultant value D (the final particle diameter determined experimentally) for any time would be obtained. The value of D includes particle diameter due to coagulation, chemical conversion and hygroscopic growth. The value of D obtained for various times for the three Relative Humidity conditions along with experimental observation is shown in Fig. 4. It is to be noted here that, the above equation for d' is valid only for the mass concentration of 0.5 g m^{-3}. The variation in d′ for all the three RH%, is very less, such that, d' for 50% RH case is taken. The resultant D would found to have deviation of about 10%.

SUMMARY

It is determined clearly that, initial particle size of sodium aerosols (after coming out of flame zone) is independent of mass concentration. It is clearly observed that the size of the sodium aerosols undergo hygroscopic growth due to adhesion of moisture over the solid particle of sodium oxide released out of flame zone. The coagulation growth is dominant for higher mass concentration (3.0 g m^{-3}) condition, whereas, the hygroscopic growth is dominant in the lower mass concentration (0.5 g m^{-3}) condition. Higher the RH%, the particle enlargement is also found higher. If we compare the rate of enlargement in size after the initial period of time say 20 minutes, both theoretical growth and experimental growth are almost same but only with the difference of particle radius at 20 minutes (say starting diameter). Further, the growth of particle size is also included with chemical speciation of particle with time, as conversion of sodium oxide to sodium hydroxide and further to sodium carbonate. The saturated value of the particle measured experimentally

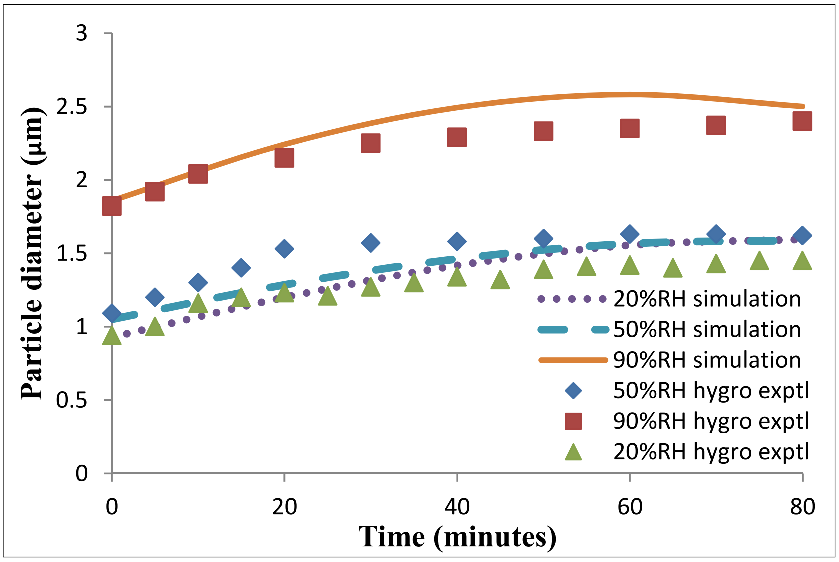

Fig. 4. Growth of particle size with progress of time (experimental observation and theoretical simulation due to coagulation and hygroscopic) for 0.5 g m^{-3}.

in both concentration regions is found to have only less variation, showing seizure of moisture absorption and chemical transformation (The final chemical composition would be $NaHCO_3$). Further experiments are in progress to correlate the chemical speciation with respect to particle size at various times.

ACKNOWLEDGEMENT

Shri S.A.V. Satya Murty, Director EIRSG acknowledged for his support and constant encouragement for carrying out this work.

REFERENCES

Anantha Narayanan, R., Subramanian, V., Sahoo, P., Misra, J., Kumar, A., Baskaran, R., Venkatraman, B. and Murali, N. (2015). Experimental Investigations on Carbonation of Sodium Aerosol Generated from Sodium Fire in the Context of Fast Reactor Safety. *Ann. Nucl. Energy* 80: 188–194.

Bamford, G.J., Ketchell, N. and Dunbar, I.H. (1992). Aerosol Mass Deposition: The Important of Gravitational Agglomeration. *J. Aerosol Sci.* 23: S1: S79–S82.

Baskaran, R., Selvakumaran, T.S. and Subramanian, V. (2004). Aerosol Test Facility for Fast Reactor Safety Studies. *Indian J. Pure Appl. Phys.* 42: 873–878.

Baskaran, R., Subramanian, V. and Selvakumaran, T.S., (2006). Real Time Measurement of Aerosol Size Distribution Using MASTERSIZER. *Indian J. Pure Appl. Phys.* 44: 576–580.

Clough, W.S. and Garland, J.A. (1971). The Behaviour in the Atmosphere of the Aerosol from a Sodium Fire. *J. Nucl. Eng.* 25: 425–435.

Cooper, D.W. (1980). Prediction of the Rate of Chemical Transformation of Sodium Fire Aerosols. Douglas, Harvard School of Public Health Boston, Massachusetts, U.S.A.

Cooper, D.W. (1989). Predictions of the Rates of Chemical Transformation of Sodium Fire Aerosols. Proc. CSNI-Specialists Meeting on Nuclear Aerosol in Reactor Safety, April 15–17, Gatlinburg, Tennessee, USA.

Gillardi, T., Chassery, A., Perrais, C., Letge, C., Baskaran, R. and Subramanian, V. (2013). Modleing of the Chemical Behavior of Sodium Fire Aerosols during Atmospheric Dispersion. IAEA-CN- 199/196.

http://www.osha.gov/dts/chemicalsampling/data/CH_267700.html

Malet, J.C. (1996). Ignition and Combustion of Sodium–Fire Consequences Extinguishments and Prevention. IWGFR/92, Technical Committee Meeting on Evaluation of Radiative Materials Release and sodium Fires in Fast Reactors, November 11–14, O-arai, Ibaraki, JAPAN.

Misra, J., Subramanian, V., Kumar, A., Baskaran, R. and Venkatraman, B. (2010). Investigation of Aerosol Mass and Number Deposition Velocity in a Closed Chamber. *Aerosol Air Qual. Res.* 13: 680–688.

Newman, R.N. (1974). The Vapour Phase Combustion of Sodium, RD/B/N2965, Research Department, Berkeley Nuclear Laboratory, Central Electricity Generating Board, USA. April 1974.

Newman, R.N. (1983). The Ignition and Burning Behaviour of Sodium Metal in Air. *Prog. Nucl. Energy* 12:119–147.

Ramsdale, S.A. (1989). The Chemical Conversion and Dispersion of Toxic Sodium Fire Aerosol in the Atmosphere. *J. Aerosol Sci*. 20: 1401–1404.

Schnell, M., Chung, C.S. and Leung, C.W. (2006). Investigation on the Coagulation and Deposition of Combustion Particles in an Enclosed Chamber with and without Stirring. *J. Aerosol Sci.* 37: 1581–1595.

Sitarski, M.A. (2012). Brownian Coagulation of Knudsen Particles on Evaporating/Condensing Aerosol Droplet; Modeling of Capture of Soot Particles by Marine Fog. *Aerosol Air Qual. Res.* 12: 1189–1199.

Subramanian, V. and Baskaran, R. (2007). Initial Size Distribution of Sodium Combustion Aerosols. *Nucl. Technol.* 160: 308–313.

Subramanian, V., Sahoo, P., Malathi, N., Ananthanarayanan, R., Baskaran, R. and Saha, B. (2009). Studies on Chemical Speciation of Sodium Aerosols Produced in Sodium Fire. *Nucl. Technol.* 165: 257–269.

Subramanian, V., Baskaran, R., Misra, J. and Indira, R., (2011). Experimental Study on the Behviour of Suspended Aerosols of Sodium and Fission Products in a Closed Vessel. *Nucl. Technol.* 176: 83–92.

Received for review, March 7, 2015
Revised, May 13, 2015
Accepted, May 15, 2015

Aerosol and Air Quality Research, 15: 1813–1822, 2015
Copyright © Taiwan Association for Aerosol Research
ISSN: 1680-8584 print / 2071-1409 online
doi: 10.4209/aaqr.2014.09.0193

Characterisation of Sodium Aerosol in Cover Gas Region of SILVERINA Loop

Amit kumar[1], Venkatesan Subramanian[1*], Subramanian Krishnakumar[2], Ramakrishnan Baskaran[1], Sivasubramanian Chandramouli[2], Balasubramanian Venkatraman[1]

[1] *Radiological Safety Division, Indira Gandhi Centre for Atomic Research, Kalpakkam - 603 102, India*
[2] *Device Development and Rig Services Division, Indira Gandhi Centre for Atomic Research, Kalpakkam -603 102, India*

ABSTRACT

Sodium aerosols are continuously being generated in the cover gas region of Sodium cooled Fast Reactor (SFR) from the hot sodium pool and they play major role in heat and mass transfer to the roof top plug and side walls. In order to characterize the sodium aerosols, a study has been initiated by conducting experiments in one of the sodium loop facility SILVERINA of IGCAR. This paper describes design and installation of aerosol sampling system in SILVERINA loop, results and analysis of sodium aerosol characteristics, measurement of temperature profile of cover gas region, theoretical simulation of sodium aerosols mass concentration for the given pool (loop) condition and validation of the model with experimental results.

The sodium aerosol size distribution in cover gas region is found to be mono-model. The Mass Median Diameter (MMD) of sodium aerosol is found to be varying from 1.5–11.5 µm as a function of sodium pool temperature and found to increase linearly with increase of sodium pool temperature. The sodium aerosol mass concentration is found to be varying from 0.026–35.6 g m^{-3} as a function of sodium pool temperature and it is found to follow 3rd order polynomial regression with increase of sodium pool temperature. The sodium aerosol mass concentration and MMD are found to be higher near the sodium pool compared to middle of the cover gas region and near the roof top. A theoretical simulation has been carried out to predict the sodium aerosol mass concentration with respect to pool temperature for a given geometry of the vessel and the theoretical and experimental mass concentration of sodium aerosols found to have good agreement.

Keywords: Fast Reactor; Cover gas region; Sodium aerosol; Size distribution; Mass concentration.

INTRODUCTION

In the pool type Sodium cooled Fast Reactor (SFR), the pool design has an argon gas blanket (cover gas region) sandwiched between the surface of hot sodium pool and the roof structure of the reactor vessel (Sinai *et al.*, 1993). In the normal operating condition of SFR, the temperature difference between the sodium pool and the bulk gas temperature leads to considerable evaporation of sodium from the pool surface and subsequent condensation results in the formation of sodium aerosol within the cover gas region (Ford *et al.*, 1993) either by heterogeneous nucleation or self-nucleation (homogeneous nucleation). When these aerosols have sufficient concentration, would modify the total heat transfer to the cooled roof structure by absorption and scattering mechanisms. Further, the mass transfer occurs due to condensation of sodium aerosols on the cooler surfaces like annular gaps, roof top, control plug, rotating plug and fuel handling machine resulting deposition of aerosols, which hinders the rotational movement of rotating plug and operation of fuel handling machine (Robert *et al.*, 1995). The aerosol mass concentration influences the operation of cover gas purification system and reduces its efficiency (flow through cold trap circuit). The aerosols with sufficient concentration reduce the visibility of cover gas region [Core inspection facility in RAPSODIE, France and Fast Breeder Test Reactor (FBTR), India].

The designer of the roof structure need to know heat and mass transfer rate to the roof in order to assess cooling requirements, thermal stress within the structure and the possible influence of sodium aerosol deposition (Sinai *et al.*, 1993). In the reactor design, necessary care (conservative estimate - without taking into account of aerosols) has been taken to account for the heat and mass transfer phenomena. However, it is at most important to know the aerosol concentration and aerosols size distribution in order to predict effectively the heat and mass transfer phenomena, which may get changed due to interaction of thermal radiation with aerosols and mass transfer due to condensation of aerosols. At this juncture, in order to account for the role

---

[*] Corresponding author.
Tel.: 0091 44 27480062; Fax: 0091 44 27480235
E-mail address: vsn@igcar.gov.in

of aerosols, it is important to consider the sodium aerosol properties, which would get modified due to (i) temperature difference between the sodium pool surface and bottom of the roof top plug, (ii) spatial variation of aerosol mass concentration and size distribution in cover gas region, (iii) effect of geometric dimension (diameter of the sodium pool surface, height of the argon cover gas and shape of roof top) of the cover gas system, and (iv) possible enhanced coagulation of sodium aerosols upon interaction with gamma radiation, resulting increase in sizes (It is important to note that in the reactor environment, sodium aerosols are immersed in the sea of bi-polar charges (generated by gamma radiation) and get charged upon interaction with ions. The aerosol properties (size and mass concentration, coagulation coefficient and deposition rate etc.) would get modified due to enhanced coagulation of charged sodium aerosols (Subramanian *et al.*, 2008, 2012)). Hence, information on mechanism of aerosol formation, the kinetics and its characteristics is needed in the design of reactor top shield and to help in eliminating the potential operating problem caused by aerosols during steady state reactor operation.

The determination of sodium aerosols characteristics from a cover gas region requires special sampling procedure, in which sampling is to be carried out without exposing the aerosols to atmosphere (the sodium aerosols undergo chemical changes and properties would get modified when exposed to atmosphere). In some of the earlier studies, sampling of sodium aerosols from the cover gas region was carried out by using Andersen multistage Impactor, which gives mass-size distribution cumulatively over a period of time (Yamamoto *et al.*, 1991; Minges and Schutz, 1991, 1993; Jackson *et al.*, 1993). In another experiment, stainless steel wire mesh filter (kept in the open atmosphere) was used, which gave size distribution based on sieve size (Himeno and Takahashi, 1980; Himeno and Yamagishi, 1982; Frukawa *et al.*, 1984; Yamamoto *et al.*, 1991; Newson *et al.*, 1993). It is to be noted here that, the sodium aerosols undergo reaction with atmospheric constituents (oxygen, moisture and CO_2) to form various compounds like oxide, hydroxide and carbonate resulting changes in both physical and chemical characteristics. Hence, the measurement in open atmosphere could not be a true evaluation of sodium aerosol characteristics in the cover gas region. Glockling *et al.* (1991) used Malvern 2600C (based on Franhofer diffraction) and Dantec particle dynamic analyzer for characterizing sodium aerosol in the cover gas region, but the results obtained in both techniques were found different for the same experimental condition. Laser mist concentration meter and sintered stainless steel filter were used for sodium aerosol mass concentration measurements (Yoshiaki and Takahashi, 1980, Yoshiaki and Yamagishi, 1982). The methodologies adopted in their measurements were not dealt in details. In one of the experiment, atomic absorption spectroscopy was used for measurement of mass concentration and laser scattering technique was used for determination of size distribution of sodium aerosols (Roberts *et al.*, 1995). In our earlier work, a suitable technique has been developed and sodium aerosols were characterized using Mastersizer (M/s Malvern, UK). The sampling of sodium aerosols is accomplished by (i) drawing aerosols from the cover gas region, (ii) trap them in a suitable medium without exposing them to the atmosphere, and (iii) analyze the trapped aerosols for its characteristics (Amit *et al.*, 2014). The technique has been qualified in Aerosol Test Facility (Baskaran *et al.*, 2004; Misra *et al.*, 2012) and validated in SILVERINA loop facility.

It was observed from the literature survey, the size distribution of aerosols ranges from 1–16 µm and mass concentration ranges from 1–40 g m^{-3} (Yoshiaki and Takahashi, 1980; Yoshiaki and Yamagishi, 1982; Frukawa *et al.*, 1984; Glockling *et al.*, 1991; Yamamoto *et al.*, 1991; Minges and Schutz, 1991, 1993; Ford *et al.*, 1993; Jackson *et al.*, 1993; Newson *et al.*, 1993; Robert *et al.*, 1995). It is further noted from the literature, the sodium aerosol mass concentration increases with the increasing of difference between roof to pool temperatures whereas, there is no definite correlation of aerosol size distribution with the variation of pool and roof temperatures. Taking into consideration of all the above aspects and towards ongoing SFR program of our country, we are involved in the characterization of sodium aerosols in the cover gas region from one of the sodium loop facility, called SILVERINA Loop, in Fast Reactor Technology Group (FRTG), IGCAR. The characterization of sodium aerosols includes experimental determination of aerosol characteristics and theoretical modeling to predict the aerosol mass concentration in the cover gas region. The theoretical simulation is carried out with the purpose that, it can be useful and extended to the reactor geometry and serves as input in the reactor design.

In this paper, the design, fabrication and installation of aerosol sampling system and temperature profiling system for the cover gas region of SILVERINA loop, experimentation, results and analysis of sodium aerosol characteristics, theoretical simulation of sodium aerosols mass concentration for the given pool temperature and geometry and validation of the model with experimental results are presented.

THEORETICAL SIMULATION

In the cover gas space, aerosol particles are formed by a single source term (evaporation and condensation) and removed continuously by several mechanisms (gravitational, wall plating, and ventilation). Since, all the removal mechanisms are dependent on particle size, a theoretical model is developed using mass and number concentration decay equation by including the effect of continuous source term and various removal mechanisms (Sheth *et al.*, 1975). A first order differential equation is formulated to predict the equilibrium mass and number concentration of the aerosols in cover gas region over a period of time. Taking initial size of the aerosols as an input from the experimental results, the equilibrium mass concentration is evolved by solving rate equation of mass concentration and number concentration numerically by finite difference method. In this model, the inputs parameters are (i) temperature of sodium pool surface, bottom surface of roof top and bulk cover gas, (ii) geometry of the vessel (diameter of the pool surface and height of the cover gas region) and (iii) initial radius of aerosol. The rate equations for mass concentration, number concentration and inter-relating equation of mass and number concentration of the aerosols are given below:

$$\frac{dC}{dt} = -\lambda C + \delta C + Se \tag{1}$$

$$\frac{dN}{dt} = -\lambda N - KN^2 + Sn \tag{2}$$

$$C = \frac{4}{3}\pi r^3 \rho N \tag{3}$$

where
C - Mass concentration (g cm^{-3})
λ- Decay rate (gravitational, wall plating and ventilation) (1 s^{-1})
δ - Convective source rate (1 s^{-1})
S$_e$ - Evaporative source term (g cm^{-3} s^{-1})
N - Number concentration (1 cm^{-3})
S$_n$ - Source term for number concentration (no. of particles cm^{-3} s^{-1})
K - Coagulation rate (1 s^{-1})
ρ - Particle density (g cm^{-3})
r - Radius of particle (cm)
t - Time (s)

The correlation λ, δ and K are given below:

$$\lambda = \lambda 1 + \lambda 2 + \lambda 3 \tag{4}$$

where
λ1- Decay rate due to gravitational (1 s^{-1})
λ2- Decay rate due to wall plating (1 s^{-1})
λ3- Decay rate due to ventilation (1 s^{-1})

$$\lambda 1 = \frac{2 \times r^2 \times \rho \times g}{9 \times H \times \eta}\varphi \tag{4a}$$

$$\lambda 2 = \frac{k \times Tm \times Aw}{6 \times \pi \times \eta \times r \times \Delta \times V}\varphi \tag{4b}$$

$$\lambda 3 = \frac{Q}{V} \tag{4c}$$

$$\delta = 0.63\frac{\rho c \times Dem}{r \times H \times \rho}\left(\frac{g \times \Delta T \times H^3 \times \rho c}{Tm \times \eta \times Dem}\right)^{0.25} \times \left(\frac{Pp \times M}{Rg \times Tp \times \rho c \times Pp * M}\right) \tag{5}$$

$$K = \frac{4 \times k \times Tm}{3 \times \eta}\varphi \tag{6}$$

where
g - Gravitational constant (cm^2 sec^{-1})
H - Height of cover gas region (cm)
η- Viscosities of argon cover gas (g cm^{-1} sec^{-1})
φ - Cunningham correction factor
k - Boltzmann's constant (erg K^{-1})
Tm - Bulk Cover gas temperature (K)
Aw - Area of walls (cm^2)
Δ - Wall platting parameter
V - Volume of cover gas region (cm^3)
Q - Ventilation Rate (cm^3 sec^{-1})
ρc - Density of cover gas (g cm^{-3})
Dem - Diffusion coefficient of sodium vapour (cm^2 sec^{-1})
ΔT - temperature difference between sodium pool surface to roof surface (K)
Pp - Partial Pressure of sodium vapor (Torr)
M - Sodium molecular weight
R$_g$ - Gas Constant (Torr cm^3 K^{-1} mol^{-1})
Tp - Sodium pool temperature (K)

Due to evaporation of sodium vapour from the sodium pool, the concentration of sodium vapour is more near the pool boundary than bulk cover gas region. The flux of sodium vapour across the sodium pool is written as:

$$j = -D_{em}\frac{dCe}{dx} \tag{7}$$

where Ce - Sodium vapour concentration (g/cm^3) and x- Thickness of pool boundary layer (cm)

$$D_{em} = 0.424\left(\frac{Tp}{642.83}\right)^{1.823} \tag{8}$$

$$Ce = \left(\frac{Pp \times M}{Rg \times Tp}\right) \tag{9}$$

The source term due to evaporation (S$_e$) is defined as: Se = J × A$_p$/V, where, A$_p$ - Surface area of sodium pool (cm^2)

$$Se = 0.424\left(\frac{Tp}{642.83}\right)^{1.823}\left(\frac{Pp \times M}{Rg \times Tp}\right)\left(\frac{Ap}{Q \times V}\right) \tag{10}$$

The source term for number concentration (S$_n$) is calculated by using S$_e$, density and volume of particle

$$Sn = \frac{3Se}{4\pi r^3 \rho} \tag{11}$$

In our modeling, to begin with the concentrations C and N are set to zero. The initial particle radius is fed from the experimental results. In the next time step, for the initial particle radius, the convection source rate (δ), the collision kernel rate K (coagulation), the particle decay rate constant λ are calculated. Then for these conditions the mass concentration C and the number concentration N are calculated. In the next time step from the calculated value of C and N, the new particle radius is calculated. The particle radius in this step is different from the initial radius. Subsequently all parameters are calculated until the convergence of mass concentration value is reached. At this time, the mass and number concentrations reached steady state value, while the particle radius also reaches steady state value. Hence, the measured mass concentration and the theoretically calculated mass concentrations are equilibrium values.

MATERIALS AND METHOD

Descriptions of SILVERINA Loop

SILVERINA sodium loop was constructed and commissioned at Engineering Hall-I, FRTG, IGCAR to conduct various experiments related to Prototype Fast Breeder Reactor (PFBR) and general Sodium Technology (Chandramouli *et al.*, 2006). The loop consists of three cylindrical test pots namely Test Pot-1(TP-1), Test Pot-2 (TP-2) and Test Pot-3(TP-3). This is a dynamic sodium loop with an electromagnetic pump, cold trap, plugging indicator, sodium sampler, heater vessel, interconnecting pipe lines, bellows sealed valves, flow meters and cover gas purification circuit. Sodium is filled in to the loop from a storage tank (capacity of 1300 kg). The sodium aerosol characterization experiments are carried out in TP-1. The height and internal diameter of the TP-1 are 2235 mm and 750 mm respectively and the height of the cover gas region is 820 mm. The total volume and quantity of sodium holdup in the TP-1 are 1.04 m^3 and 0.512 m^3 respectively. The top flange of TP-1 is provided with three nozzles for sodium level indication (low, middle and high levels) and a spare nozzle. The internal diameter of spare nozzle is 60.3 mm which is used for the experiments. The salient features of SILVERINA Loop are as follows: (i) the loop consists of a sodium tank in which liquid sodium could be maintained at various temperatures from 200–550°C and it simulates the reactor pool condition, (ii) the region above the sodium pool is filled with cover gas (Argon).

Sampling System

A schematic diagram of sodium aerosol sampling system installed in TP-1 is shown in Fig. 1. The aerosol sampling system consists of (a) Aerosol sampling tube, (b) Aerosol sampling bottle, (c) Line Heaters and controller and (d) Aerosol flow controlling device.

(a) Aerosol sampling tube: The sampling tube is divided into two parts. One part of the sampling tube is inside the pot TP-1 and other part is outside. Both the parts are connected with a flange. The sampling tube which goes inside TP-1 has been fabricated with three different lengths

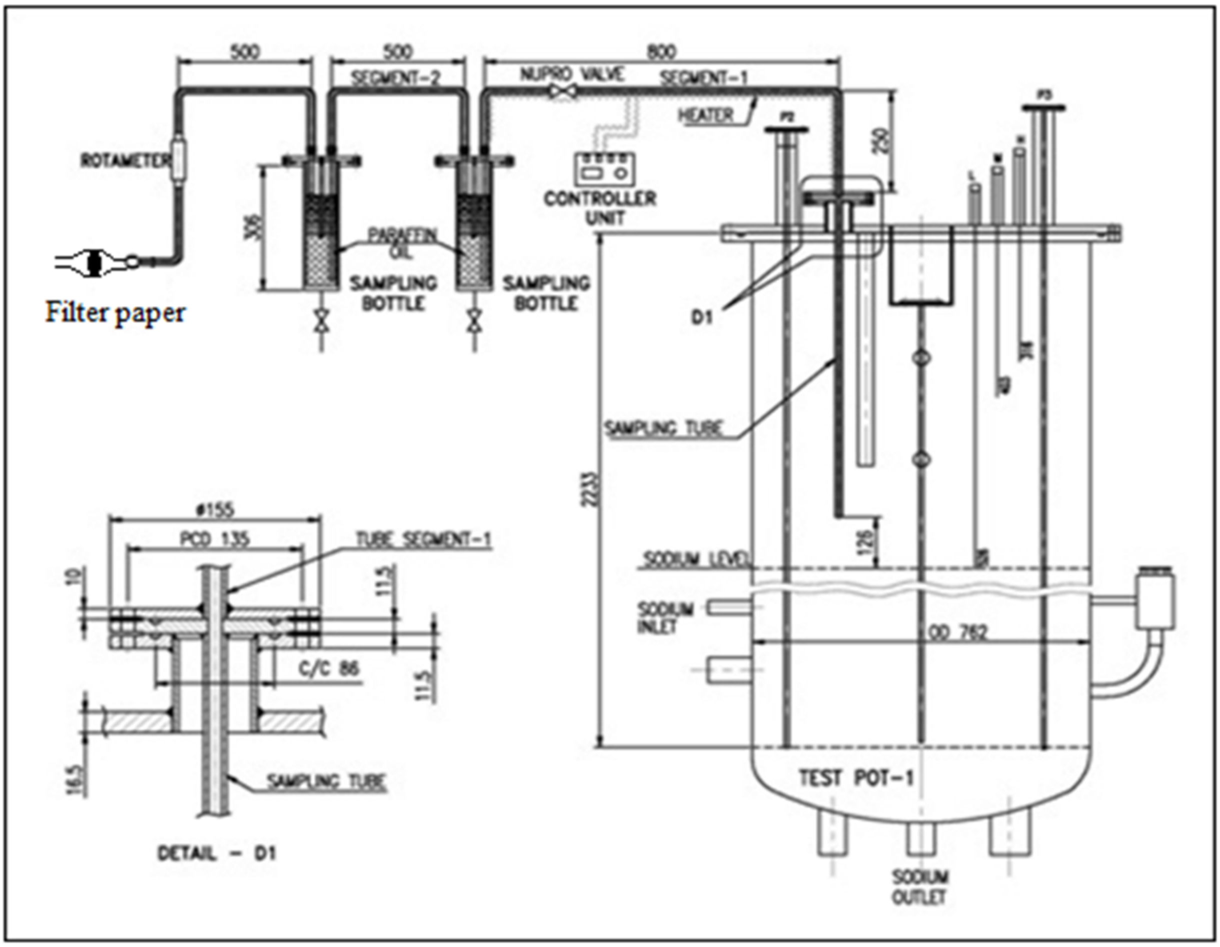

Fig. 1. A schematic diagram of sodium aerosol sampling system installed in TP-1 of SILVERINA loop.

(215, 415 and 715 mm) to enable the sampling at three different levels. Before starting the experiment the required length tube is attached with the flange and inserted into the TP-1. The aerosol sampling tube is made of SS316 with internal diameter of 10 mm (1.5mm wall thickness). The maximum particle diameter that can be collected is 20 µm, without having bias due to wall deposition by impaction for a flow rate of 2 L min^{-1} (Hinds, 1982).

(b) Aerosol sampling bottle: The schematic diagram of sodium sampling bottle is shown in Fig. 2. The capacity of the sampling bottle is 1.0 L and made of Perspex. The height and diameter of the bottle are 306 and 80 mm respectively. The bottle is closed on top side with perspex flange arrangement. The flange is provided with two opening for the insertion of inlet and outlet tubes. The inlet tube is inserted upto bottom and it is connected to sampling tube by means of KF coupling and ball valve/gate valve. The paraffin oil will be drained by using a tube and needle valve arrangement at the bottom.

The sampling bottle is filled with paraffin oil (~600 mL) and maintained at ambient temperature. The sodium aerosol laden cover gas is made to pass through the bottle, thus solidification of aerosol particles would occur as the cover gas enters into the paraffin oil. The residence time of the cover gas is increased due to baffle arrangement, which ensures that all sodium aerosols get trapped from the cover gas before it goes out of the bottle. The cover gas coming out from the sampling bottle #1 is made to pass through sampling bottle #2 so as to remove aerosols escaped if any, from the 1st bottle. After sampling, the sample bottles are removed from the loop and paraffin oil is drained for analysis.

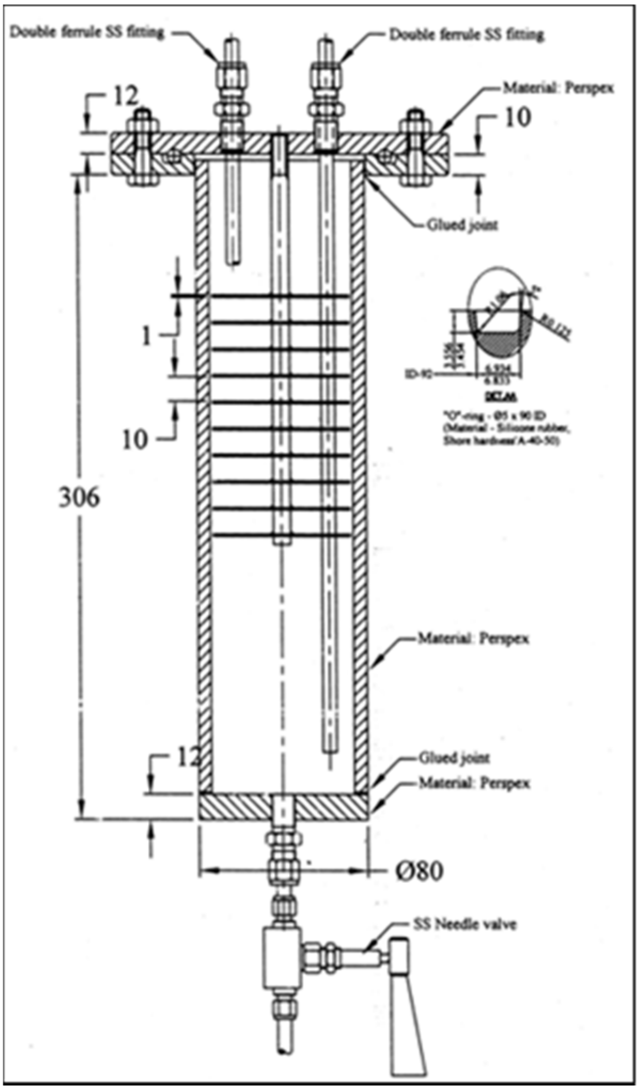

Fig. 2. A schematic diagram of sodium aerosol sampling bottle.

(c) Line heaters and controller: To prevent sodium aerosol solidification within the sampling tube during experimental measurements, the wall temperature of the sampling tube is maintained at 110°C. The heating coils are wound on the sampling tube along with insulation and the current through the heating coils was controlled by using PID (proportional-integral-derivative) controller. The temperature along the sampling tube was monitored by 2 thermocouples. In order to have a redundancy in heating, a spare heater is also provided. The heater controller set-up consists of a panel board mounted with one PID controller, temperature display units, 3 pole rotary switches for double heaters and allied PCBs.

(d) Aerosol flow control device: In order to regulate the gas flow through the sampling bottles a rotameter is connected after the 2nd bottle followed by a filter paper holder (25 mm diameter). The pressure of the cover gas region is maintained at 34 kPa above atmosphere. The cover gas is drawn from the cover gas space of TP-1 and made to bubble through the paraffin bottles. The cover gas flow rate was maintained at 2 L min^{-1} using the rotameter and found to be maintained upto 30 minutes. A glass fiber filter of 25 mm was used to prevent aerosols escaped, if any, after the 2nd bottle.

Before the experiment, pressure holdup test for sampling tube and gate valve has been carried out by pressurizing TP-1 up to 50 kPa above atmosphere. The functioning of surface heaters, PID temperature controller and thermocouples has been checked by heating the heater up to 110°C.

Temperature Measurement System

The pool, roof and cover gas temperature are important parameters for the theoretical simulation of aerosol mass concentration in cover gas region of SILVERINA loop. A temperature measurement system has been fabricated, installed in top flange of SILVERINA loop TP-1 (spare nozzle) and measurements were carried. A schematic diagram of the temperature measurement system is shown in Fig. 3. The system consists of matched top flange for the aerosol port, a vertical cylindrical shaft welded below the top flange and six grooves to insert 6 thermocouples which are terminated at six different heights. Temperature was measured by using chromel-aluminium K-type thermocouples at the six locations in the cover gas region. The material used for the fabrication of cylindrical soft and flange is SS316. The diameter and length of the cylindrical shaft is 60 mm and 820 mm respectively. Proper O-ring arrangements were made to prevent leakage of cover gas through thermocouple holes. The temperature measurement locations from the top of flange are (i) the pool surface (820 mm), (ii) near to the

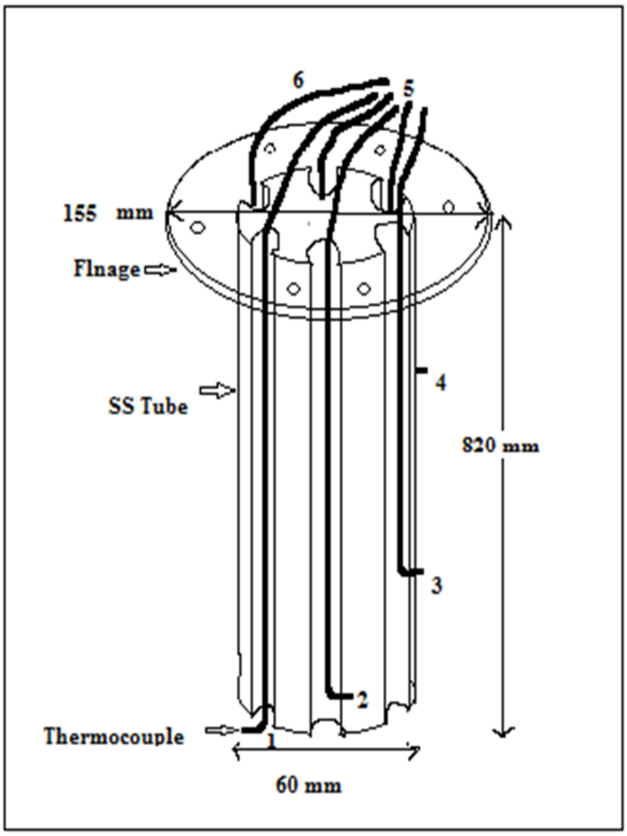

Fig. 3. A schematic diagram of the temperature measurement system.

pool (790 mm), (iii) two locations on the middle of the cover gas region with 300 mm difference in height (400 mm and 100 mm). (iv) near to the roof surface (20 mm) and (v) roof surface (0 mm). Accordingly, the thermocouples were terminated at 820 mm, 790 mm, 400 mm, 100 mm, 20 mm, and 0 mm from bottom surface of the top flange. Each thermocouple is connected with 3½ - digit digital indicator.

Sampling and Analysis

The pot is filled with sodium up-to a particular level before starting the experiment. The argon is filled above the sodium surface at pressure 34 kPa above the atmosphere. The temperature of the sodium is raised by heater and monitored continuously by using thermocouples. There is no ventilation path other than sampling line. Aerosols are drawn from the cover gas region and allowed to get trapped in liquid paraffin oil medium without exposing them to atmosphere. After isolating the bottles from the system the sampling bottles were taken for analyzing the samples. The size distribution of sodium aerosols is determined by using Mastersizer (M/s Malvern Instruments, UK). The instrument measures the particle size distribution (sodium aerosol) hovered in a liquid dispersant (paraffin oil) by using ensemble diffraction technique. The measurement of sodium aerosol mass concentration is carried out by conductivity method (M/s Metrohm, 856 conductivity module, Switzerland). The mass of sodium aerosols trapped in the liquid paraffin is measured by transferring them into a water medium (to become NaOH) and measuring the change in conductivity of the NaOH solution. The sodium aerosol mass concentration is estimated by using a pre-established calibration graph between changes in conductivity as a function of concentration of NaOH (Amit *et al.*, 2014).

The sodium pool temperature was varied from 250–550°C. The cover gas (argon gas) is made to bubble through liquid paraffin oil at a flow rate of 2 L min^{-1}. The sampling time is varied from 20 minute to 2 minute according to sodium pool temperature. Since the sodium aerosol mass concentration increases with increase of sodium pool temperature and in order to avoid coagulation of aerosol trapped in the paraffin oil, the sampling time was kept for 20 minutes for the pool temperature 250°C and progressively reduced to 2 minutes when pool temperature is 550°C. The maximum volume of sample would be 40 L when the sodium pool temperature is 250°C and the minimum volume of sample is 4 L when sodium pool temperature is 550°C. The total volume of cover gas is 500 L at 34 kPa pressure inside the cover gas region. The maximum pressure drop in the cover gas region is from 34 kPa to 25 kPa during 40 L sampling. Test runs showed that, up to 50 mg of trapped sodium aerosol mass in the bottle, the coagulation of aerosols was not noticed for next 24 hrs after sampling. It is observed that, total sampled aerosol mass is found to get trapped in the first bottle itself for the sampling temperature upto 350°C, while, for the temperature of 400–550°C, there exists trapping of aerosols mass in the second bottle upto a maximum of 10% of the first bottle. There is no trapping of aerosol is observed in filter paper in all the runs.

RESULTS AND DISCUSSION

Temperature Profile: The temperature profile of cover gas region in SILVERINA loop was measured by varying sodium pool temperature from 250–550°C. The temperature profiles of the cover gas region with cover gas height for various pool temperatures are shown in Fig. 4. It is observed that, temperature profile is found to follow a similar pattern as found in the literature (Roberts *et al.*, 1995). The temperature started decreasing from the pool surface (820–790 mm) - region C, then has uniform temperature region (790–20 mm) for about 770 mm height - region B, and decreases towards roof temperature (20–0 mm) - region A. The temperature of the roof top found to vary from 90 to 150°C for the sodium pool temperatures from 250 to 550°C respectively. The decrease of temperature in the region A varies according to the temperature of the bottom surface of the roof top from bulk gas temperature.

Size Distribution: The liquid paraffin oil sampled after each measurement is analyzed and mass-size distribution and MMD were determined. The size distribution and MMD were obtained for all the three sampling heights (probe length) and for all the pool temperatures. A typical steady state size distribution at middle region of cover gas for 400°C pool temperature is shown in Fig. 5. It is observed from Fig. 5, that particles are found in the range of 1 to 16 µm with MMD around 7.0 µm ($\sigma_g = 1.5$). The MMDs obtained for three different sampling levels for

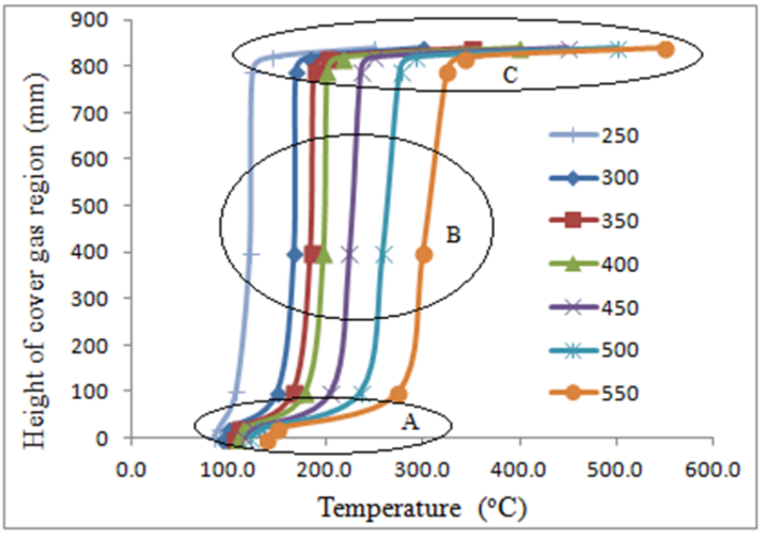

Fig. 4. The variation of temperature in cover gas region with cover gas height for various pool temperatures.

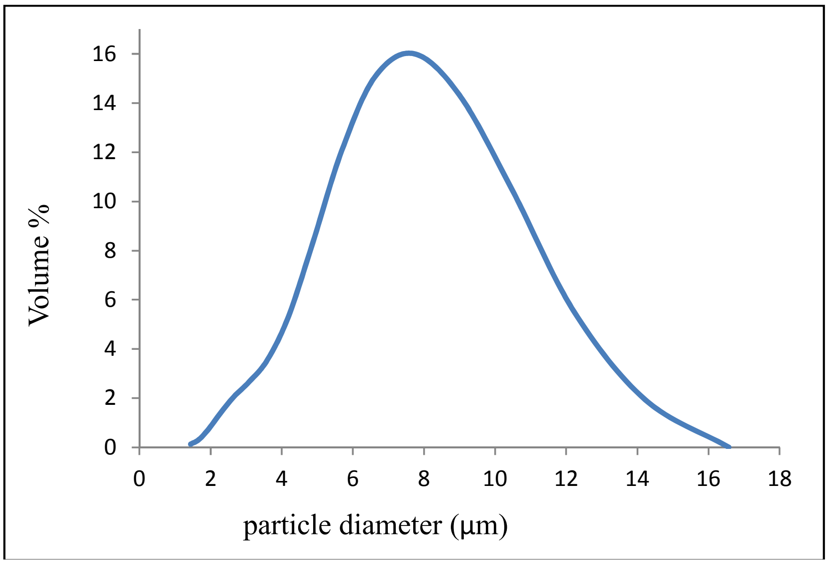

Fig. 5. Volume – size distribution of sodium aerosol at the middle level of cover gas region for 400°C pool temperature.

various pool temperatures are shown in Fig. 6. It is observed from Fig. 6, that, MMD found to increase linearly with increase of sodium pool temperature. It is also noted from the figure, for all the pool temperatures, the value of MMD is found to be higher near the pool surface (715 mm) when compared with that of near the roof (215 mm) and middle level of cover gas region (415 mm).

Mass concentration: The mass of trapped sodium aerosols in the bottles for all the samples was determined and found to vary from 0.026–35.6 g m^{-3}. The variation of sodium aerosol mass concentration for various pool temperatures is shown in Fig. 7. It is observed that, the mass concentration increases with increase of sodium pool temperature and found to fit in 3rd order polynomial regression. It is also observed from the figure, for all the pool temperatures, the sodium aerosol mass concentration is higher near the pool than that of near the roof and middle level of cover gas region.

Theoretical simulation: Fig. 8 shows the MMD of sodium aerosols measured in the middle region of cover gas for various pool temperatures along with fitted equation (linear regression). This fitted equation is used as an input for calculating mass concentration of the sodium aerosols for various pool temperatures in the cover gas region. Since sodium aerosols are continuously generated in the pool when rising the pool temperature, to calculate the mass concentration of aerosols for a particular temperature, the initial particle size is taken for the temperature below that particular temperature by using the fitted equation. For example, if we want to calculate the mass concentration at pool temperature of 300°C, the initial radius is taken from fitted equation at 290°C. It is observed that, the mass concentrations predicted for pool temperature of 250°C and 300°C did not show significant difference when the initial particle size is taken for the temperature difference of more than 10°C, but it shows significant variation

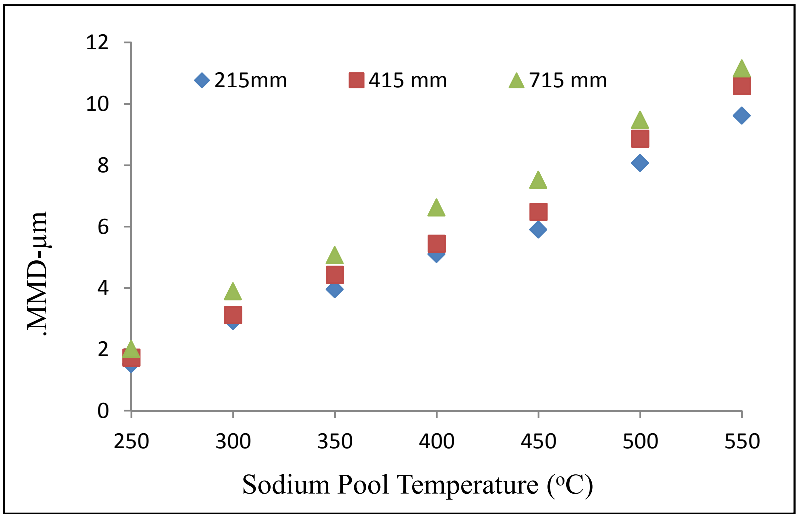

Fig. 6. Mass Median Diameter (MMD) of sodium aerosol for various pool temperatures.

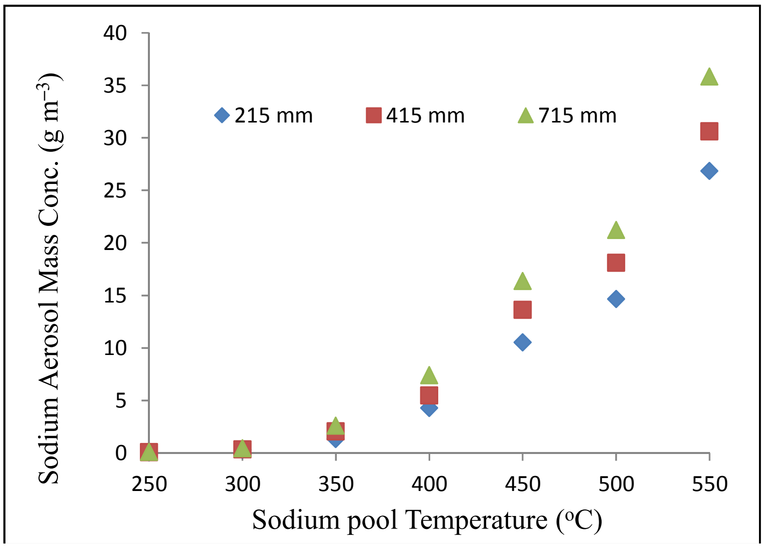

Fig. 7. Sodium aerosol mass concentration for various pool temperatures.

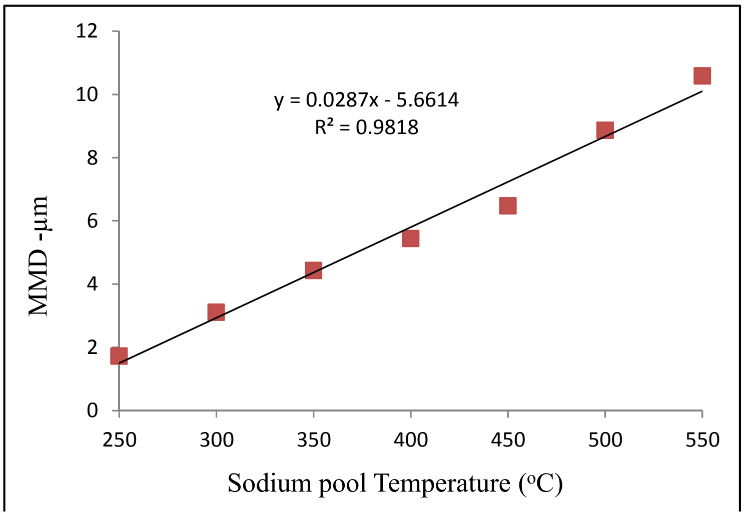

Fig. 8. Experimental variation of MMD of sodium aerosol for various pool temperatures at the middle level of cover gas region.

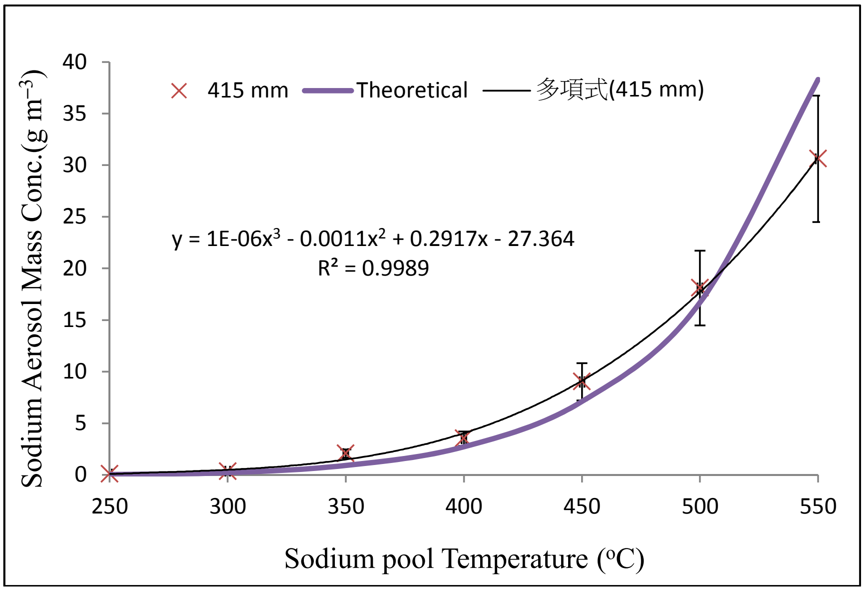

Fig. 9. Theoretical and experimental comparison of sodium aerosol mass concentration.

(> 15%) in the range of 400°C and above. (It is to be noted that aerosol mass concentration is very less in 250°C and 300°C, when compared with 400°C and above).

Fig. 9 shows the simulated and experimentally measured mass concentration for various pool temperatures at the middle level of the cover gas region. It is noted from the figure that, mass concentration predicted by the simulation is found to be underestimated by 10–15% with experimental value for the temperatures between 250°C and 450°C. Afterwards the trend begins to change and at 550°C the mass concentration is overestimated by 15%. The variation of 10–15% in the lower temperature region (250–450°C) is attributed to the spatial variation of concentration in the actual scenario, whereas, it is assumed to be uniform in the theoretical estimation. As the evaporation rate increases with increase of temperature, the mass concentration as well as MMD gets increased. Due to higher concentration, the higher sized particles undergo cloud settling resulting the difference in the measured concentration by about –15% from the predicted value for 550°C; whereas, the simulation deals with individual particle settling. It is to be noted here that, similar trend is observed between the predicted mass concentrations and measured concentrations for other two levels (lower and upper cover gas regions). The experimental error associated due to flow rate, sampling time and analysis is 7–10%.

The role of aerosols in the cover gas region: The thermal radiation from the pool surface is scattered by the presence of aerosols in the cover gas region and it reduces the heat flux reaching the bottom of the roof top. The modified Stephan's law for heat transfer including aerosols between two surfaces is given below:

$$\varphi' = \frac{\sigma \times Ap \times \left(Tp^4 - Tr^4\right)}{\left(\dfrac{1}{\varepsilon p} + \dfrac{1}{\varepsilon r} - 1 + \tau\right)} \qquad (12)$$

where σ- Stefan-Boltzmann constant;
εp- Emissivity of sodium pool surface;
εr- Emissivity of roof bottom surface;
Tr- Roof bottom surface temperature.

$$\text{Optical thickness - } \tau = \kappa \times L \qquad (13)$$

where κ- extinction coefficient of aerosol = C × Kc, where Kc is the mass extinction coefficient and to be determined experimentally by conducting experiments for the absorption of black body radiation for a various known concentration C;
L - Height of cover gas region.

It is further observed that, particle size plays important role in the forward scattering (Mie Scattering) of thermal radiation. It is noted that, the thermal radiation transfer is unique feature to a particular geometry (Roberts *et al.*, 1995).

It is observed in literature, the mass transfer occur mainly due to condensation of aerosol reaching the bottom of roof surface. The mass transfer rate found to increase with increase of roof temperature with corresponding decrease in bulk to roof temperature difference upto 100°C. At higher roof temperature, the mass transfer rate decreases and mass deposited on the roof bottom surface also begin decrease. It is noted that, the sodium aerosols begin to condense in the bulk gas region before reaching the roof surface.

SUMMARY

The sodium aerosol size distribution is found to be mono-model. Both, MMD and mass concentration of sodium aerosols increases with increase of sodium pool temperature. The sodium aerosol mass concentration and MMD are found to be higher near the sodium pool compared to middle of the cover gas region and near the roof top. The simulated and experimental measured mass concentration of sodium aerosol in cover gas region is found to have good agreement.

The modeling is found useful in predicting the sodium aerosol mass concentration for a given geometry and pool temperature.

ACKNOWLEDGEMENT

Shri K.K. Rajan, Director FRTG and Shri S.A.V. Satyamurthy, Director EIRSG are acknowledged for their support and constant encouragement for carrying out this work. FRTG control room staffs of SILVERINA loop are acknowledged for their help in conducting the experiments.

REFERENCE

Amit Kumar, Subramanian, V., Baskaran, R., Krishnakumar, S., Chandramouli, S. and Venkatraman, B. (2014). Development and Validation of a Methodology for Characterization of Sodium Aerosols in Cover Gas Region. *Aerosol Air Qual. Res.* 14: 1534–1541.

Baskaran, R., Selvakumaran, T.S. and Subramanian, V. (2004). Aerosol Test Facility for Fast Reactor Safety Studies. *Indian J. Pure Appl. Phys.* 42: 873–878.

Chandramouli, S., Sakthivel, S., Vijayamohana Rao, P., Gurumoorthy, K., Rajan, K.K., Kalyanasundaram, P. and Vaidyanathan, G. (2006). Commissioning and Operation of SILVERINA Sodium Loop. OPENUPP-2006, Nov. 13–15, BARC, Mumbai. Proceedings of National Conference on Operating Experiences of Nuclear Reactors and Power Plants, pp. 203–209.

Clement, C.F. and Julian Dolias, M. (1987). Sodium Aerosol Formation in Argon Flow over Hot Sodium. Theoretical Physics Division, Harwell Laboratory, Oxfordshire OX11 ORA. AERE R 12489.

Ford, I.J. (1993). Sodium Aerosol Formation and Removal Mechanisms in the Fast Reactor Cover Gas Space. *J. Aerosol Sci.* 24: 237–253.

Frukawa, O., Furutani, A., Hattori, N. and Iguchi, T. (1984). Experimental Study of Heat and Mass Transfer through the cover Gas in the Liquid Metal Fast Breeder Reactor (LMFBR). Proceeding of the Third International Conference on Liquid Metal Engineering and Technology. ISBN0-7277-0209-2, British Nuclear Medicine Society. 1: 451–458.

Glockling, J.L.D. (1991). Heat and Mass Transfer in Specific Aerosol System. PhD Thesis, Department of Chemical Engineering. South bank University, London.

Himeno, Y. and Takahashi, J. (1980). Sodium Mist Behavior in Cover Gas Space of LMFBR. *J. Nucl. Sci. Technol.* 17: 404–412.

Himeno, Y. and Yamagishi, Y. (1982). Effect of Barriers on Sodium Mist Deposition on LMFBR Components. *J. Nucl. Sci. Technol.* 19: 837–844.

Hinds, W.C. (1982). *Aerosol Technology*, John Wiley and Sons.

Jackson, J.D., Sanchis, An P.J.F. and Alamar, A. (1993). Closing Report of the MUSAC 3A Project. Department of Nuclear Engineering, University of Manchester, Manchester.

Minges, J. and Schutz, W. (1991). Experiments to Characterize the Sodium Aerosol System in the cover Gas of the European Fast Reactor EFR. *J. Aerosol Sci.* 22: S761–S764.

Minges, J. and Schutz, W. (1993). Experiments on the Enrichment of Cesium in the cover Gas Aerosol of the European Fast Reactor (EFR). *Nucl. Eng. Des.* 147: 17–22.

Misra, J., Subramanian, V., Kumar, A., Baskaran, R. and Venkatraman, B. (2012). Investigation of Aerosol Mass and Number Deposition Velocity in a Closed Chamber. *Aerosol Air Qual. Res.* 13: 680–688.

Newson, I.H., Dawoson, R.W., Wade, C.D., Moul, A.N. and Finch, J. E. (1993). Studies of Caesium-134 transfer through Argon and Helium Cover Gases above Hot Sodium Pool in the Hawell Active Mass Transfer Loop (AMTL). AEA Industrial Technology Report number AEA-In Tec-1220.

Roberts, D.N. (1995). Heat and Mass Transfer Studies in Sodium - Argon Filled Enclosures. PhD Thesis, South Bank University, London.

Sheth, A. (1975). Parametric Study of Sodium Aerosols in the Cover Gas-Space of Sodium-Cooled Reactors. Argonne National Laboratory, ANL-75-11.

Sinai, Y.L., Ford, I.J., Barrett, J.C. and Clement, C.F. (1993). Prediction of Coupled Heat and Mass Transfer in the Fast Reactor Cover Gas: the C-GAS Code. *Nucl. Eng. Des.* 140: 159–192.

Subramanian, V., Kumar, A., Baskaran, R., Misra, J. and Venkatraman, B. (2012). An Experimental Study on the Charging of Non-Radioactive Aerosols with and without the Presence of Gamma Radiation. *J. Aerosol Sci.* 52: 98–108.

Subramanian, V., Baskaran, R. and Indira, R. (2008). Experimental Study on Enhanced Brownian Coagulation of Sodium Compound Aerosols in the Presence of Gamma Field. *J. Aerosol Sci.* 32: 814–818.

Yamamoto, H., Sakai, T. and Murakami, N. (1991). Analytical Study on Mass Concentration and Particle Size Distribution of Sodium Mist in Cover Gas Phase of LMFBR Reactor Vessel. *J. Aerosol Sci.* 22: S713–S716.

Received for review, September 3, 2014
Revised, May 22, 2015
Accepted, June 16, 2015

Aerosol and Air Quality Research, 16: 1832–1840, 2016

ISSN: 1680-8584 print / 2071-1409 online
doi: 10.4209/aaqr.2016.01.0010

Studies on Geometrical Effect on Sodium Aerosol Characteristics in Cover Gas Region

Amit Kumar[1], Venkatesan Subramanian[2*], Subramanian Krishnakumar[3], Ramakrishnan Baskaran[1], Sivasubramanian Chandramouli[3], Balasubramanian Venkatraman[1]

[1] *Radiological Safety Division, Indira Gandhi Centre for Atomic Research, HBNI, Kalpakkam - 603 102, India*
[2] *Radiological Safety Division, Indira Gandhi Centre for Atomic Research, Kalpakkam - 603 102, India*
[3] *Device Development and Rig Services Division, Indira Gandhi Centre for Atomic Research, Kalpakkam -603 102, India*

ABSTRACT

Sodium aerosol characteristics in the cover gas region of sodium cooled fast reactor is important for determining the heat and mass transfer phenomena from the hot sodium pool surface to the roof slab of the reactor vessel. In this study, experiments are carried out in the Test Pot-3 (TP-3) of SILVERINA loop and sodium aerosol characteristics are compared with that of Test Pot-1 (TP-1) carried out in our earlier work and with previous similar type of work available in the literature to understand the geometrical effect of sodium aerosol characteristics. The bulk cover gas temperature and sodium aerosol diameter are required as input parameters for the theoretical simulation of sodium aerosol mass concentration. An empirical relation for bulk cover gas temperature is derived and validated with our experimental results and used for other geometries. Similarly, an empirical relation for sodium aerosol diameter is arrived based on our experimental results and available published works. The theoretical model developed earlier for the prediction of sodium aerosol mass concentration is used for calculating the aerosol mass concentration for various geometries, by incorporating new relation for particle diameter and bulk cover gas temperature. The simulated mass concentration of sodium aerosol in cover gas region of various studies showed good agreement with the experimental results. The sodium aerosol mass concentration and Mass Median Diameter (MMD) increases with increase of sodium pool temperature. However, the values are strongly dependent on the aspect ratio (L/D) of cover gas geometry. It is also observed that MMD of sodium aerosols increases with increase of aspect ratio (L/D) while mass concentration increases with decrease of aspect ratio of the cover gas region. The modeling is found useful in predicting the sodium aerosol mass concentration for similar type of geometries and pool temperature.

Keywords: Sodium aerosol characteristics; Cover gas region; Geometrical effect; Particle radius and bulk cover gas temperature.

INTRODUCTION

In pool type sodium cooled fast reactor (SFR), reactor core, primary sodium pumps, intermediate heat exchange systems, decay heat exchangers etc. are immersed in sodium pool in the reactor vessel. Argon is used as cover gas, which serves as blanket above the sodium pool in the reactor vessel. The reactor vessel is closed by using a top shield above the cover gas region. The sandwiched region between the surface of hot sodium pool and the top shield (called as roof slab) of the reactor vessel is called as cover gas region (Sinai *et al.*, 1993). The schematic diagram of cover gas region (cylindrical in shape) is shown Fig. 1. Fig. 1 describes diameter of the sodium pool (D) and height of the cover gas region (L) having boundary on the bottom side with sodium pool, on top side with roof slab and at the side with wall of the reactor vessel. The temperatures of the corresponding regions are described as Tp, Tr, Tm and Tw as sodium pool temperature, bottom of roof slab temperature, bulk cover gas temperature and wall temperature respectively. In the cover gas region, there exist pool boundary layer near the sodium pool and roof boundary layer near the roof slab due to temperature gradient near the sodium pool and roof slab respectively. The roof slab supports, rotatable plugs, control plug, in-vessel fuel handling machine, primary sodium pumps, intermediate heat exchangers, and decay heat removal systems. In the normal operating condition of SFR, the temperature difference between the sodium pool and the bulk gas temperature leads to considerable evaporation of sodium from the pool surface and subsequent condensation results in the formation of sodium aerosol within the cover gas region (Ford *et al.*, 1993) either by heterogeneous

---

[*] Corresponding author.
Tel.: 0091 44 27480062; Fax: 0091 44 27480235
E-mail address: vsn@igcar.gov.in

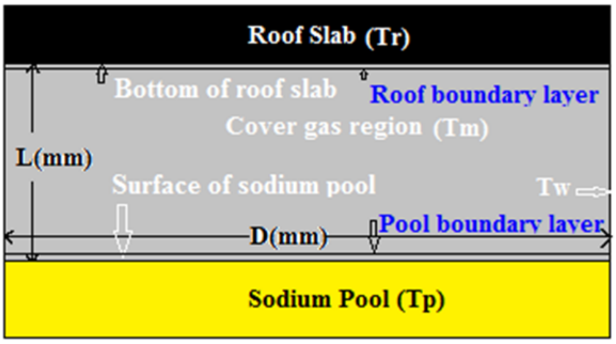

Fig. 1. Schematic diagramme of cover gas region, sodium pool and roof top.

nucleation or self-nucleation (homogeneous nucleation). When these aerosols have sufficient concentration, they would modify the total heat transfer to the cooled roof structure by absorption and scattering mechanisms. Further, the mass transfer occurs due to condensation of sodium aerosols on the cooler surfaces like annular gaps, roof top, control plug, rotating plugs and fuel handling machine resulting deposition of aerosols, which hinders the rotational movement of rotating plug and operation of fuel handling machine (Roberts, 1995). The aerosol mass concentration influences the operation of cover gas purification system and reduces its efficiency (flow through cold trap circuit). Also, the aerosols with sufficient concentration reduce the visibility of cover gas region [Core inspection facility in RAPSODIE, France and Fast Breeder Test Reactor (FBTR), India].

In the reactor design, conservative approach without taking into account of aerosols characteristics has been considered for the heat and mass transfer phenomena. However, it is at most important to know the aerosol mass concentration and aerosols size distribution in order to predict effectively the heat and mass transfer phenomena, which may get changed due to interaction of thermal radiation with aerosols and mass transfer due to condensation of aerosols. Towards this, as a part of aerosol studies related to fast reactor program, characterization of sodium aerosols in the cover gas region has been initiated in Radiological Safety Division (RSD) Indira Gandhi Center for Atomic Research (IGCAR), India. The studies are performed in one of the sodium test pot (TP-1) of sodium loop facility called SILVERINA loop in Fast Reactor Technology Group (FRTG), IGCAR (Chandramouli *et al.*, 2006) and significant results have been obtained. The study began by sampling metal aerosol without exposing to atmosphere in Aerosol Test Facility (ATF) and characterization techniques is validated in SILVERINA Loop (Kumar *et al.*, 2014), followed by, experimentation in TP-1 of SILVERINA loop to determine sodium aerosol mass concentration and size distribution for various pool temperatures (250–550°C). The salient results of the experiments are summarized as: (i) the mass concentration in cover gas region is found to vary in the range of 0.026–35.6 g m^{-3} and the MMD is found to vary in the range of 1.5–11.5 µm for pool temperature 250–550°C respectively, (ii) the sodium aerosol mass concentration increases with increase of sodium pool temperature according to polynomial function and the MMD of sodium aerosol increases linearly with increase of sodium pool temperature, (iii) the mass concentration and MMD of sodium aerosol is found to be larger near the pool surface than near the top flange and middle region of cover gas (Kumar *et al.*, 2015a). The temperature profile of the cover gas region was measured at various heights viz. 0, 10, 35, 100, 300, 700, 800 and 820 mm from the top flange. The temperature profile is found to follow similar pattern in accordance with available literature. A theoretical simulation has been developed to predict the sodium aerosol mass concentration in cover gas region by taking input from experimental value of sodium aerosol diameter and dimension of cover gas region of TP-1. A good agreement has been observed for the sodium aerosol mass concentration between theoretical prediction and experimental measurements (Kumar *et al.*, 2015a).

At this juncture, it is inferred from the literature that, the dimension of cover gas region influences the aerosol characteristics. It is observed from the studies by Himeno and Takahashi (1980), Himeno and Yamagishi (1982), Frukawa *et al.*, (1984), Glockling (1991), Minges and Schutz (1991), Yamamoto *et al.* (1991), Minges and Schutz (1993), Newson *et al.* (1993) and Roberts (1995), the sodium aerosol characteristics (size distribution and mass concentration) are different for different geometries. The variation of sodium aerosol characteristics in the cover gas region for different geometries for different pool and roof temperatures are shown in Table 1. It is noted from the Table 1 that, the sodium aerosol characteristics depend on geometry of the vessel (L/D ratio, where L - height of cover gas region and D - diameter of sodium pool), in addition to the pool and roof temperatures. To confirm the above experimental observations, experiments have been carried out in another Test Pot (TP-3) of SILVERINA loop and sodium aerosols characteristics are determined. The L/D ratio of TP-3 is 1.875, which is higher than that of TP-1 (1.075) i.e., smaller vessel than TP-1. (The description of TP-3 given in Materials and Methods section). Further, in this work, an empirical relation is derived from our experimental results of TP-1 and TP-3 to predict the temperature of the bulk cover gas region and applied for predicting the bulk cover gas temperature for other studies. The sodium aerosol diameter (MMD) is arrived through an empirical relation based on our experimental results of TP-1 and TP-3 of SILVERINA loop and for the available published work by Himeno and Takahashi (1980),

Table 1. Variation of sodium aerosol characteristics in the cover gas region for different geometries.

	L/D	Pool Temp. (°C)	Roof Temp. (°C)	MMD (µm)	Mass Conc. (g m^{-3})
TP-1	1.076	250–550	85–140	1.5–11.5	0.6–30.6
Yoshiaki	4.516	300–550	120	6.0–26.0	0.2–20.0
Glockling	2.333	300–550	150	3.3–13.5	0.5–36.5
Minges	0.55	350–550	120	3.5–8.5	1.5–40.0

Glockling (1991) and Minges and Schutz (1991). It is to be noted that all the above experiments were carried out by varying sodium pool temperature only. In this paper, the details of the experimental results obtained from TP-3 of SILVERINA loop, the empirical relations for bulk cover gas temperature and the sodium aerosol diameter are presented. The validation of our theoretical simulation on aerosol mass concentration with the experimental results of TP-1, TP-3 and the experimental results published by Himeno and Takahashi (1980), Glockling (1991) and Minges and Schutz (1991) are also presented.

MATERIALS AND METHODS

A detailed description on SILVERINA Loop system with test pot-1 (TP-1), sampling system and experimental procedure are described in our earlier work (Kumar *et al.*, 2015a). In this paper, a brief note on test pot-3 (TP-3), sampling system and experimental procedure pertaining to current experiments are given in the following section.

Test Pot (TP-3) of SILVERINA Loop

SILVERINA loop is a dynamic sodium loop facility with an electromagnetic pump, cold trap, plugging indicator, sodium sampler, heater vessel, interconnecting pipe lines, bellows sealed valves, flow meters and cover gas purification circuit. Sodium is filled in to the loop from a storage tank with a capacity of 1300 kg (Chandramouli*et al.*, 2006; Kumar *et al.*, 2014). A schematic diagram of sodium aerosol sampling system installed in TP-3 along with TP-3 vessel is shown in Fig. 2. The vessel is made with SS316. Sodium heating is provided by four number of Expanded Cold Region (ECR) heaters fixed on the surface of vessel to keep the sodium in liquid state. In this vessel two heaters will be in service and two will be spares. The height and internal diameter of the TP-3 vessel are 1600 mm and 400 mm respectively and the height of the cover gas region is 750 mm. The total volume and quantity of sodium holdup in TP-3 are 0.208 m^3 and 0.11 m^3 respectively. The top flange of TP-3 is provided with three nozzles for sodium level indication (low, middle and high levels) and a spare nozzle. The spare nozzle is used for aerosol measurement.

Sampling System

The aerosol sampling system consists of (a) Aerosol sampling tube, (b) Aerosol sampling bottle, (c) Line Heaters and controller and (d) Aerosol flow controlling device. [The detailed description of the above systems is described in our earlier work (Kumar *et al.*, 2015a)]. In the present experimental set-up, the portion of the sampling tube which goes inside TP-3 has been fabricated with a length of 385 mm to enable the sampling at the middle level. Before starting the experiment the sampling tube is attached with the flange and inserted into TP-3. The aerosol sampling tube is made of SS316 with internal diameter of 10 mm (1.5 mm wall thickness). The maximum particle diameter that can be collected is 20 µm, without having bias due to wall deposition by impaction for a flow rate of 2 L min^{-1} (Hinds, 1982).

The sampling bottle is filled with paraffin oil (~600 mL) and maintained at ambient temperature. The sodium aerosol laden cover gas is made to pass through the bottle, thus solidification of aerosol particles would occur as the cover gas enters into the paraffin oil. The residence time of the cover gas is increased due to baffle arrangement, which ensures that all sodium aerosols get trapped from the cover gas before it goes out of the bottle. The cover gas coming out from the sampling bottle # 1 is made to pass through sampling bottle # 2 so as to remove aerosols escaped if any, from the 1st bottle. After sampling, the sample bottles are removed from the loop and paraffin oil is drained for analysis. To prevent sodium aerosol solidification within the sampling tube during experimental measurements, the wall temperature of the sampling tube is maintained above 110°C. The gas flow through the sampling bottles is regulated by using a rotameter. A glass fiber filter of 25mm was used to prevent aerosols escaped, if any, after the 2nd bottle.

Before the experiment, pressure holdup test for sampling tube and gate valve has been carried out by pressurizing TP-3 up to 0.5 kg cm^{-2} above atmosphere. The functioning of surface heaters, temperature controller and thermocouples (fitted in the sampling line) has been checked by heating the heater up to 150°C.

Temperature Measurement System

A photograph of the sampling system along with temperature measurement system is shown in Fig. 3. The pool, roof and bulk cover gas temperatures are important parameters for the theoretical simulation of aerosol mass concentration in cover gas region of SILVERINA loop. Hence a similar type of temperature measurement system as described in Kumar *et al.* (2015a) for TP-1, has been fabricated with matched top flange for the aerosol port. It consists of vertical cylindrical shaft welded below the top flange with six grooves to insert 6 thermocouples which are terminated at six different heights. Temperature was measured by using chromel-aluminium K-type thermocouples at the six locations in the cover gas region. The temperature measurement locations from the top of flange are (i) roof surface (0 mm), (ii) one location near to the roof surface (90 mm), (iii) three locations on the middle of the cover to gas region (200 mm, 300 mm and 500 mm) and (iv) one

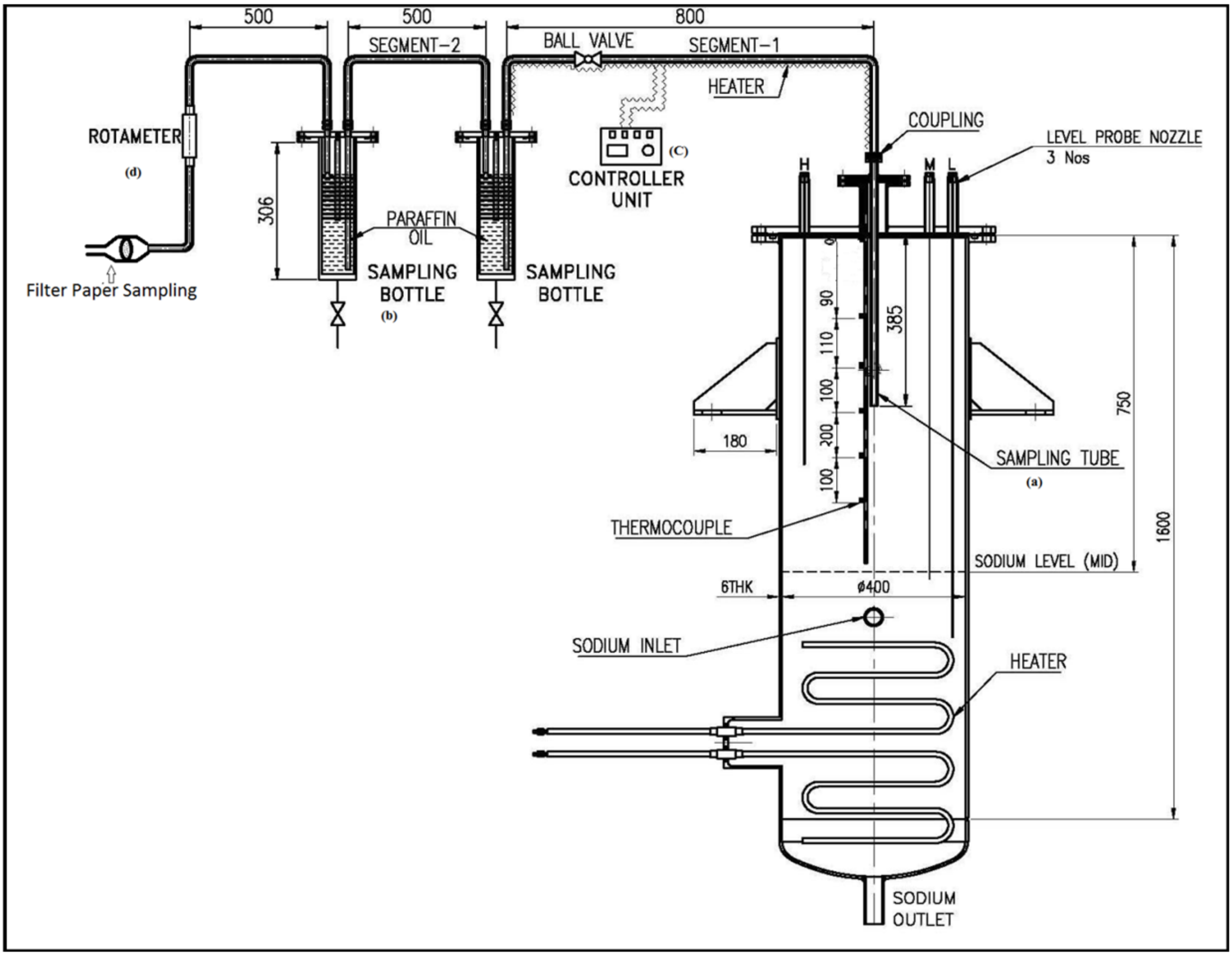

Fig. 2. A schematic diagram of sodium aerosol sampling system installed in TP-3 of SILVERINA loop.

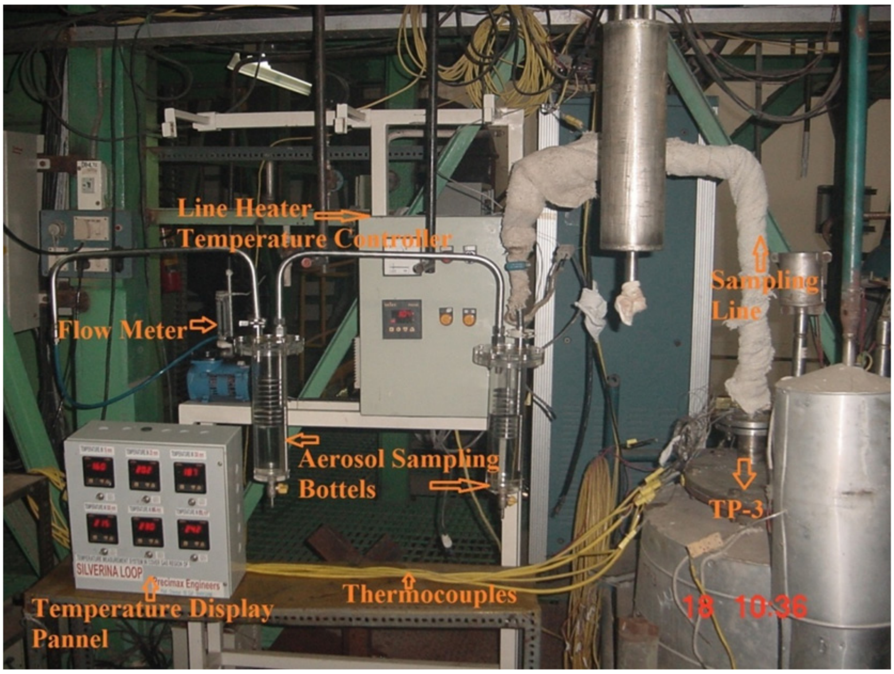

Fig. 3. A photograph of the aerosol sampling system along with temperature measurement system.

location near the sodium pool surface (600 mm). Sodium pool temperature is measured separately. Accordingly, the thermocouples were terminated at 600 mm, 500 mm, 300 mm, 200 mm, 90 mm, and 0 mm from bottom surface of the top flange. Each thermocouple is connected with 3½ - digit digital indicator.

SAMPLING AND ANALYSIS

Aerosols are drawn from the cover gas region and allowed to get trapped in liquid paraffin oil medium without exposing them to atmosphere. After isolating the bottles from the system the sampling bottles were taken for analyzing the samples. The size distribution of sodium aerosols is determined by using Mastersizer (M/s Malvern Instruments, UK). The measurement of sodium aerosol mass concentration is carried out by conductivity method (M/s Metrohm, 856 conductivity module, Switzerland). The details are described in Kumar *et al.* (2014).

The sodium pool temperature was varied from 250–550°C in step of 50°C. The cover gas (argon gas) is made to bubble through liquid paraffin oil at a flow rate of 2 L min^{-1}. The sampling time is varied from 10 minute to 2 minute according to sodium pool temperature. Since the sodium aerosol mass concentration increases with increase of sodium pool temperature and in order to avoid coagulation of aerosol trapped in the paraffin oil, the sampling time was kept for 10 minutes for the pool temperature 250°C and progressively reduced to 2 minutes when pool temperature is 550°C. Test runs showed that, up to 50 mg of trapped sodium aerosol mass in the bottle, the coagulation of aerosols was not noticed for next 24 hrs after sampling.

RESULTS AND DISCUSSION

Temperature Profile in TP-3

The temperature profile in TP-3 of cover gas region is measured by varying sodium pool temperature from 250–550°C. The temperature profiles of the cover gas region with cover gas height for various pool temperatures are shown in Fig. 4. It is observed that, temperature profile is found to follow a similar pattern as found in the literature (Roberts, 1995) and the results obtained in TP-1 (Kumar *et al.*, 2015a). The temperature started decreasing from the pool surface (750–600 mm) - region C, then has almost uniform temperature region (600–90 mm) for about 500 mm height - region B, and decreases towards roof temperature (90–0 mm) - region A. The temperature of the roof top found to vary from 90 to 160°C for the sodium pool temperatures from 250 to 550°C respectively.

Determination of Bulk Cover Gas Temperature

Bulk cover gas temperature is an important parameter for theoretical prediction of aerosol mass concentration. In order to arrive bulk cover gas temperature, an empirical relation is derived based on area and temperatures of sodium pool, roof and wall surface and it is given as:

$$Tm = \left(\frac{Tp \times Ap + Tr \times Ar + Tw \times Aw}{(Ap + Ar + Aw)} \right) \tag{1}$$

where Tm - is the bulk cover gas temperature,
Tp, Tr and Tw are the sodium pool, roof and wall surface temperatures respectively,
Ap, Ar and Aw are the area of sodium pool, roof and wall surface respectively.

The above empirical relation is validated with the experimentally measured temperature from 250–50°C of the cover gas region of TP-1 and TP-3 and it is given in Table 2. It is noted from Table 2 that, the predicted cover gas temperature is always higher compared to the experimentally measured cover gas temperature for TP-1 and TP-3. The variation in the experimental and estimated bulk cover gas temperature is well within 10%. Since, the bulk cover gas temperature is not available in the published other works,

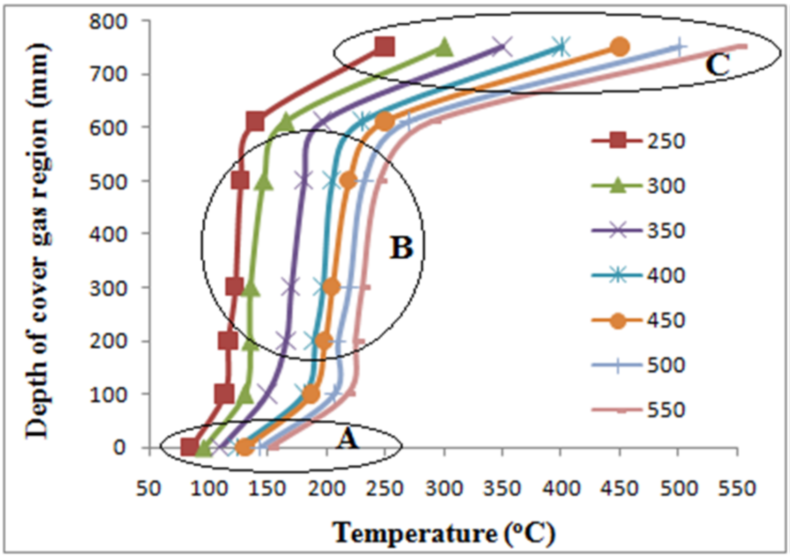

Fig. 4. The variation of temperature in cover gas region with cover gas height for various pool temperatures for TP-3.

Table 2. Comparisons of predicted and experimentally measured cover gas temperature (Tm) for various pool temperatures of TP-1 and TP-3.

Tp (°C)	TP-1				TP-3			
	Tr (°C)	Tw (°C)	Tm (°C) Exp.	Tm (°C) Estimated	Tr (°C)	Tw (°C)	Tm (°C) Exp.	Tm (°C) Estimated
250	85	120	120	135	85	120	120	130
300	95	160	160	172	95	140	140	152
350	105	180	180	195	110	170	170	182
400	110	200	200	217	125	190	190	205
450	120	230	230	247	130	210	210	226
500	130	270	270	284	145	230	230	249
550	140	330	330	335	160	260	260	279

this empirical relation [Eq. (1)] is used for predicating the bulk cover gas temperature for the geometry of other works.

Aerosol Characteristics in TP-3

The MMD obtained for middle level of cover gas region for various pool temperatures of TP-3 is shown in Fig. 5 and it is found to vary from 2.1 to 16 µm. It is observed from Fig. 5 that, MMD found to increase linearly with increase of sodium pool temperature. Fig. 5 also includes linear fitted equation for MMD with temperature of the sodium pool for TP-3. The mass concentration of the sodium aerosols is found to vary from 0.04–21.98 g m^{-3}. The variation of sodium aerosol mass concentration for various pool temperatures is shown in Fig. 6. It is observed that, the mass concentration increases with increase of sodium pool temperature and found to fit polynomial regression.

In the cover gas region, there exists convection current due to thermal gradient between hot pool surface and bottom of the roof slab. The aerosols, formed due to evaporation of vapor for a particular temperature of the pool surface, are carried by the convection current, undergo coagulation and reaches steady state value. Further, the cover gas region is being maintained at a positive pressure of 0.5 kg cm^{-2} before starting of every sampling. The positive pressure ensures the uniform distribution of aerosols through-out the region and sampling flow rate of 2 L min^{-1} without any pump. Besides, aerosol deposition does occur on colder roof slab when the particles enter into the upper boundary layer. We have noticed in our experiment in TP-1 and TP-3, for a given difference in temperature between pool surface and roof slab, the steady state condition is reached in about 20–30 minutes. The measured values of concentration and diameter are after this period. Hence, hydrodynamic condition in cover gas region viz., convection current, aerosol deposition and sampling flow rate are taken care once steady state values are reached.

Theoretical Simulation

A theoretical simulation for the aerosol mass concentration in the cover gas region is formulated in our earlier work (Kumar *et al.*, 2015a, b) using mass and number concentration decay equation by including the effect of continuous source term and various removal mechanisms (Sheth *et al.*, 1975). A first order differential equation is formulated to predict the equilibrium mass and number concentrations of the sodium aerosols in cover gas region. In this model, the input parameters are (i) temperature of sodium pool surface, roof and bulk cover gas, (ii) geometry of the vessel (diameter of the pool surface and height of the cover gas region) for a given cover gas region and (iii) initial radius of aerosol. In our earlier work, the initial radius is taken from the linearly fitted equation derived from the actual measurement in that cover gas region. This approach requires sampling of sodium aerosol from the cover gas region.

To improve theoretical modeling for predicting the sodium aerosol characteristics in cover gas region for different geometry, an empirical relation has been derived to predict the particle size of aerosols and validated with the experimental results obtained from our works in TP-1 and TP-3 (Himeno and Takahashi, 1980; Glockling, 1991; Minges and Schutz, 1991). The empirical relation includes variation of L/D ratio and sodium pool temperatures. The empirical relation for aerosol radius is arrived as:

$$R = \left(\frac{Ro}{2}\right) \times \left(0.5046 \times \frac{L}{D} + 1.0634\right) \times \left(\frac{Tp}{\mathrm{Tpi}}\right)^{2.5} \tag{2}$$

where R - radius of aerosol at Tp (µm),
Ro - 1.0 µm, (radius of aerosol at Tpi)
L- height of cover gas region (mm),
D - diameter of the sodium pool (mm),
Tp - Sodium pool temperature (°C),
Tpi - Temperature at which measurable aerosol mass concentration is observed which is 250°C.

It is observed in our study (in TP-1 and TP-3), sodium aerosol mass concentration is measurable at sodium pool temperature of 250°C. The average aerosol diameter (MMD) measured is around 2.0 µm. Hence, we have taken radius R_0 as 1.0 µm. By using this empirical relation, the sodium aerosol radius is estimated for any geometry and for all pool temperatures (250°C–550°C). The estimated and experimentally measured sodium aerosol diameter (MMD) for various pool temperatures of TP-1, TP-3 (Himeno and Takahashi, 1980; Glockling, 1991; Minges and Schutz, 1991) are given in Table 3. The variation of MMD versus sodium pool temperature for various L/D ratios for both experimentally determined values and empirically fitted equation is shown in Fig. 7. It is observed from Fig. 7 that, for a given pool temperature the value of MMD is found to

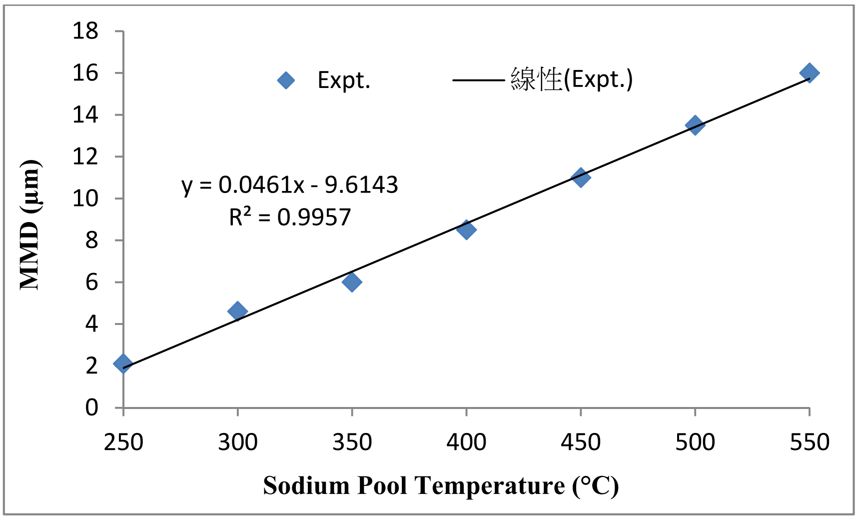

Fig. 5. MMD of sodium aerosol in the middle region of the cover gas of TP-3 for various pool temperatures.

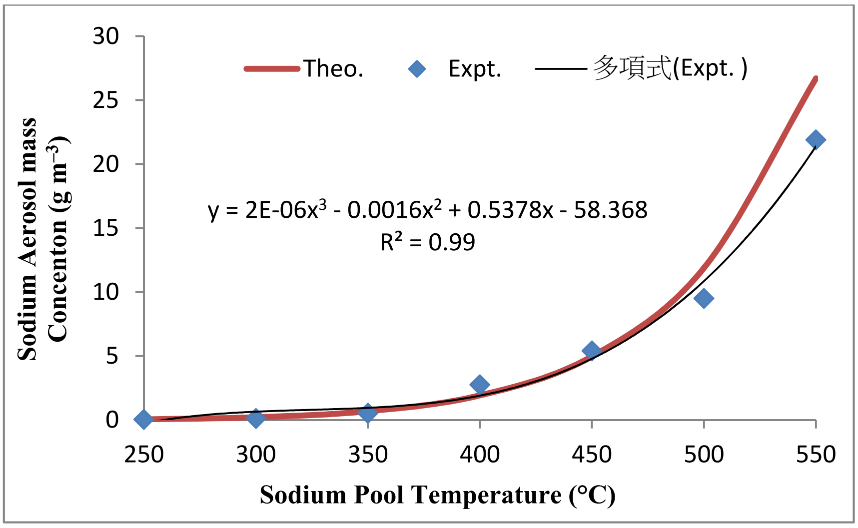

Fig. 6. Sodium aerosol mass concentration (simulated and expt.) in the middle region of cover gas of TP-3 for various pool temperatures.

Table 3. Comparison of estimated and experimentally measured sodium aerosol diameter (MMD) for various pool temperatures of TP-1, TP-3 (Himeno and Takahashi, 1980; Glockling, 1991; Minges and Schutz, 1991).

Pool Temperature (°C)		250	300	350	400	450	500	550
Minges (L/D-0.55)	Exp. MMD (µm)			3.5	4.5	6	7.2	8.5
	Theo. MMD (µm)			3.11	4.34	5.83	7.58	9.63
	Variation (%)			11.14	3.55	2.83	5.27	13.29
TP-1 (L/D-1.076)	Exp. MMD (µm)	1.5	2.89	4.33	5.44	6.47	8.86	11.5
	Theo. MMD (µm)	1.61	2.53	3.73	5.2	6.98	9.09	11.53
	Variation (%)	7.33	12.45	13.85	4.41	7.88	2.59	0.26
TP-3 (L/D-1.875)	Exp. MMD (µm)	2.11	3.95	5.62	7.59	10.81	12.85	15.79
	Theo. MMD (µm)	2.01	3.17	4.66	6.51	8.75	11.37	14.43
	Variation (%)	4.73	19.74	17.08	14.22	19.08	11.51	8.61
Glockling (L/D-2.333)	Exp. MMD (µm)		3.43	6.45	8.58	9.72	11.24	13.55
	Theo. MMD (µm)		3.53	5.19	7.25	9.73	12.67	16.07
	Variation (%)		2.91	19.53	15.5	0.1	12.72	18.59
Yoshiaki (L/D-4.516)	Exp. MMD (µm)		6	7.9	11	14.6	19.5	26
	Theo. MMD (µm)		5.27	7.75	10.82	14.53	18.91	23.99
	Variation (%)		12.16	1.89	1.63	0.47	3.02	7.73

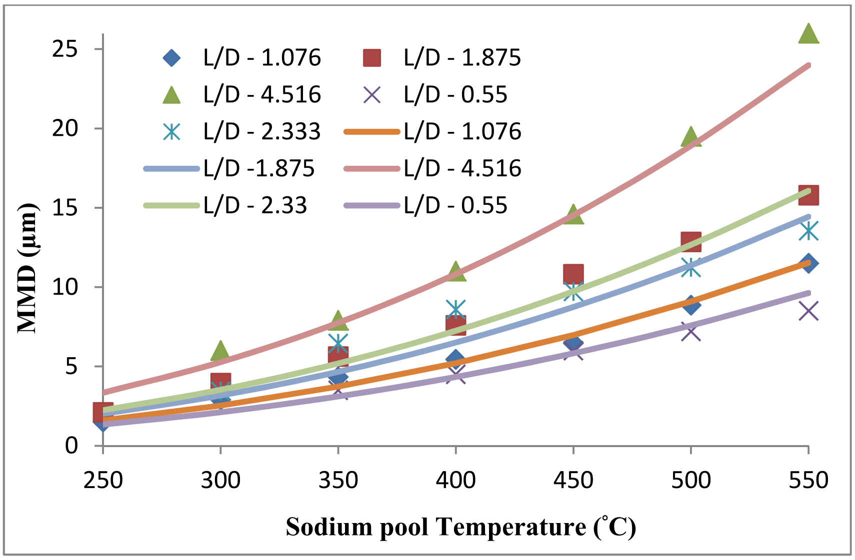

Fig. 7. Variation of MMD (Expt. and Theo.) with sodium pool temperature for various L/D ratio.

Table 4. Comparison of theoretically predicted and experimentally measured sodium aerosol mass concentration for of TP-1, TP-3 (Himeno and Takahashi, 1980; Glockling, 1991; Minges and Schutz, 1991).

Pool Temperature (°C)		250	300	350	400	450	500	550
Minges (L/D-0.55)	Exp. C (g m^{-3})			1.52	5.39	11.86	20.39	40
	Simulated C (g m^{-3})			1.31	3.73	8.72	18.02	33.39
	Variation (%)			13.81	30.79	26.47	11.62	16.52
TP-1 (L/D-1.076)	Exp. C (g m^{-3})	0.06	0.33	1.85	4.95	12.02	18.12	30.62
	Simulated C (g m^{-3})	0.06	0.33	1.31	3.75	9.59	17.89	34.11
	Variation (%)	0	0	29.18	24.24	20.21	1.26	11.39
TP-3 (L/D-1.875)	Exp. C (g m^{-3})	0.04	0.17	0.69	2.01	5.12	11.97	21.98
	Simulated C (g m^{-3})	0.05	0.21	0.89	2.61	6.45	14.46	28.67
	Variation (%)	25	23.52	28.98	29.85	25.97	20.8	30.43
Glockling (L/D-2.333)	Exp. C (g m^{-3})		0.47	1.24	5.22	11.12	22.41	36.13
	Simulated C (g m^{-3})		0.34	1.39	3.83	8.92	18.33	33.87
	Variation (%)		27.65	12.09	26.62	19.78	18.2	6.25
Yoshiaki (L/D-4.516)	Exp. C (g m^{-3})		0.21	1.39	2.45	6.51	12.14	20
	Simulated C (g m^{-3})		0.26	0.98	2.52	5.79	11.51	20.89
	Variation (%)		23.8	29.49	2.85	11.05	5.18	4.45

increase with increase in L/D ratio. Moreover, the MMD is found to increase with increase of pool temperature for a given geometry (L/D) of the cover gas region and found to follow super-linear pattern with increase of L/D value, i.e., for smaller diameter vessel. The large MMD value and super-linearity can be the result of enhanced coagulation of the aerosols during convection motions in the smaller cover gas region. It is also observed from Fig. 7, for L/D ratio of 0.55, the MMD follows linear pattern. The condition of super-linearity is observed for L/D values of 2.33 and 4.516. Hence, empirical relation is formulated with exponent 2.5 to accommodate the increment of size with increase of pool temperature for different geometry starting from 0.55 to 4.516. It is noted from the Table 3 that, the deviation of estimated and experimentally measured sodium aerosol size (MMD) is within ± 20% for all cases. The empirical relation is found useful in predicting all the conditions satisfactorily.

Once we know the radius of aerosol, temperature of the sodium pool, roof, and wall and geometry of cover gas region (diameter of the sodium pool and height of cover gas region), the sodium aerosol mass concentration in the cover gas region is estimated using the theoretical model developed earlier. Based on the theoretical formulation, sodium aerosol mass concentration is predicted for our experiment TP-3 and it is included in Fig. 6. Further the theoretical simulation for mass concentration is carried out for our works in TP-1, TP-3 and from available in literature i.e., works from Himeno and Takahashi (1980), Himeno and Yamagishi (1982), Glockling (1991) and Minges and Schutz (1991, 1993) and it is given in Table 4. It is noted from the Table 4 that, the maximum variation of theoretically simulated sodium aerosol mass concentration and experimentally measured aerosol mass concentration is found to be ± 30%. The theoretical modelling is found useful to predict the sodium aerosol mass concentration with respect to pool temperature for a given geometry of the vessel. The present study helps to predict the aerosol mass concentration for any similar geometry.

SUMMARY

A new set of experiments are carried out in TP-3 of SILVERINA loop and compared with results of TP-1 (our earlier study) and with published literature works to understand the geometrical effect on sodium aerosol characteristics. The bulk cover gas temperature and sodium aerosol diameter are used as an input parameter for theoretical simulation of sodium aerosol mass concentration. An empirical relation for bulk cover gas temperature is derived and validated with our experimental results and used for other geometry. Similarly, an empirical relation for sodium aerosol diameter is derived based on our experimental results and from available published works. The theoretical model developed earlier is used for predicting the sodium aerosol mass concentration in which, the particle radius and bulk cover gas temperatures are replaced with present empirical relation for calculating particle radius and bulk cover gas temperature taking in to account of aspect ratio (L//D) and area of the cover gas region respectively. The simulated mass concentration of sodium aerosols in cover gas region of various studies showed good agreement with the experimental results. The sodium aerosol mass concentration and MMD increases with increase of sodium pool temperature. However, the values strongly depend on the aspect ratio (L/D) of cover gas geometry. It is also observed that MMD of sodium aerosols increases with increase of aspect ratio (L/D) while mass concentration increases with decrease of aspect ratio of the cover gas region. The modeling is found useful in predicting the sodium aerosol mass concentration for any similar type of geometry and pool temperature.

ACKNOWLEDGEMENT

Shri K. K. Rajan, Director FRTG and Shri S.A.V. Satyamurthy, Director EIRSG are acknowledged for their support and constant encouragement for carrying out this work. FRTG control room staffs of SILVERINA loop are acknowledged for their help in conducting the experiments.

REFERENCE

Chandramouli, S., Sakthivel, S., Vijayamohana Rao, P., Gurumoorthy, K., Rajan, K. K., Kalyanasundaram, P., and Vaidyanathan, G. (2006). Commissioning and Operation of SILVERINA Sodium Loop. OPENUPP-2006, Nov. 13–15, BARC, Mumbai. In Proceedings of National Conference on Operating Experiences of Nuclear Reactors and Power Plants, pp. 203–209.

Frukawa, O., Furutani, A., Hattori, N. and Iguchi, T. (1984). Experimental Study of Heat and Mass Transfer through the Cover Gas in the Liquid Metal Fast Breeder Reactor (LMFBR). In Proceeding of the Third International Conference on Liquid Metal Engineering and Technology. ISBN0-7277-0209-2, British Nuclear Medicine Society, Vol. 1, pp. 451–458.

Glockling, J.L.D. (1991). Heat and Mass Transfer in Specific Aerosol System. PhD Thesis, Department of Chemical Engineering. South bank University, London.

Himeno, Y. and Takahashi, J. (1980). Sodium Mist behavior in cover gas space of LMFBR. *J. Nucl. Sci. Technol.* 17: 404–412.

Himeno, Y. and Yamagishi, Y. (1982). Effect of barriers on sodium mist deposition on LMFBR components. *J. Nucl. Sci. Technol.* 19: 837–844.

Hinds, W.C. (1982). *Aerosol Technology*, John Wiley & Sons, 1982.

Kumar, A., Subramanian, V., Baskaran, R., Krishnakumar, S., Chandramouli, S. and Venkatraman, B. (2014). Development and validation of a methodology for characterization of sodium aerosols in cover gas region. *Aerosol Air Qual. Res.* 14: 1534–1541.

Kumar, A., Subramanian, V., Krishnakumar, S., Baskaran, R., Chandramouli, S. and Venkatraman, B. (2015a). Characterisation of sodium aerosol in cover gas region of SILVERINA loop. *Aerosol Air Qual. Res.* 15: 1813–1822.

Kumar, A., Subramanian, V., Baskaran, R. and Venkatraman, B. (2015b). Size evolution of sodium combustion aerosol with various RH%. *Aerosol Air Qual. Res.* 15: 2270–2276.

Minges, J. and Schutz, W. (1991). Experiments to characterize the sodium aerosol system in the cover gas of the European Fast Reactor EFR. *J. Aerosol Sci.* 22: S761–S764.

Minges, J. and Schutz, W. (1993). Experiments on the enrichment of cesium in the cover gas aerosol of the European Fast Reactor (EFR). *Nucl. Eng. Des.* 147: 17–22.

Newson, I.H., Dawoson, R.W., Wade, C.D., Moul, A.N. and Finch, J.E. (1993). Studies of Caesium-134 Transfer through Argon and Helium Cover Gases above Hot Sodium Pool in the Hawell Active Mass Transfer Loop (AMTL). AEA Industrial Technology, Report number AEA-In Tec-1220.

Roberts, D.N. (1995). Heat and Mass Transfer Studies in Sodium – Argon Filled Enclosures. PhD Thesis, South Bank University, London.

Sheth, A. (1975). Parametric Study of Sodium Aerosols in the Cover Gas-space of Sodium-cooled Reactors. Argonne National Laboratory, ANL-75-11.

Sinai, Y.L., Ford I.J., Barrett J.C. and Clement C.F. (1993). Prediction of coupled heat and mass transfer in the fast reactor cover gas: The C-GAS code. *Nucl. Eng. Des.* 140: 159–192.

Yamamoto, H., Sakai, T. and Murakami, N. (1991). Analytical study on mass concentration and particle size distribution of sodium mist in cover gas phase of LMFBR reactor vessel. *J. Aerosol Sci.* 22: S713–S716.

Received for review, January 11, 2016
Revised, June 2, 2016
Accepted, July 12, 2016